NASA Contractor Report 3509

Numerical Analysis and FORTRAN Program for the Computation of the Turbulent Wakes of Turbomachinery Rotor Blades, Isolated Airfoils and Cascade of Airfoils

C. Hah and B. Lakshminarayana

GRANT NSG-3012
FEBRUARY 1982

NASA

NASA Contractor Report 3509

Numerical Analysis and FORTRAN Program for the Computation of the Turbulent Wakes of Turbomachinery Rotor Blades, Isolated Airfoils and Cascade of Airfoils

C. Hah and B. Lakshminarayana
The Pennsylvania State University
University Park, Pennsylvania

Prepared for
Lewis Research Center
under Grant NSG-3012

National Aeronautics
and Space Administration

**Scientific and Technical
Information Branch**

1982

TABLE OF CONTENTS

NOMENCLATURE

B_r	Constant in equation (1)
B_n, B_{n+1}	Constants in wake mean-velocity decay law in equation (5)
b	Normal distance (Figure 31)
C	Chord length of the blade
C_ε, C_ε, $C_{\varepsilon 2}$	Universal constants in the modelling of the transport equation of the rate of turbulent kinetic energy dissipation
C_s	Universal constants in the modelling of the turbulent kinetic energy equation
$C_{\phi 1}$	Universal constant in the modelling of the Reynolds stress transport equation
C_1	Constant which relates the convection and diffusion effects collectively to the production of turbulent kinetic energy
g_{ij}, g^{ij}	Covariant and contravariant fundamental metric tensor
i	Incidence of inlet flow with a single airfoil, airfoils in cascade, and rotor blades
K	Constant in equation (1)
k	Turbulence kinetic energy
L.S.	Leading surface
n	Normal distance, n = 0 at the wake centerline (Figure 3)
P	Production rate of turbulent kinetic energy ($-\overline{u_i u_j}$, $U^i{}_j$)
P.S.	Pressure side of the wake
p	Static pressure
P*	Reduced pressure ($\rho - \frac{e}{2}\Omega^2 r^2$)
p'	Fluctuating component of static pressure
R_i	Gradient Richardson number in equation (5)
R_s	Radius of curvature due to the streamline curvature on the cylindrical surface (Figure 2)
R_β	Radius of curvature due to the change in the outlet angle Figure 2)
r	Radial distance (Figure 3)
r_t	The radial distance at the blade tip
r,θ,z	Cylindrical polar coordinate system fixed in the compressor rotor. Radial, tangential, and axial directions each
S	Blade spacing in a cascade and a rotor
s	Streamwise distance (s = 0 at the trailing edge).
s'	Fluctuating shear rate in equation (57)
S.S.	Suction side of the wake
s,n,r	Streamwise, normal, and radial directions (Figure 3)
T.S.	Trailing surface (Figure 1)
U,V,W	Contravariant streamwise, normal, and radial velocity components
U^i, u^i	Contravariant mean and fluctuating velocity components (U, V, W, u, v, w in s, n, r coordinates)
U_i, u_i	Covariant mean and fluctuating velocity components (U*, V*, W*, u*, v*, w* in s, n, r coordinates in equations 34, 35 and 36)
v_s	Velocity scale in the wake
$\overline{u^i u^i}$	Turbulence intensity with components $\overline{u^2}$, $\overline{v^2}$, $\overline{w^2}$ in s, n, r coordinates

$\overline{u^2}$, $\overline{v^2}$, $\overline{w^2}$	Streamwise, normal, and radial turbulence intensity
$\overline{-uv}$, $\overline{-vw}$, $\overline{-uw}$	Streamwise, radial, and normal Reynolds shear stress
$\overline{-u^i u^j}$	Reynolds shear stress with components $\overline{-uv}$, $\overline{-vw}$, $\overline{-uw}$ in s, n, r coordinates
x, y, z	Cartesian coordinates (Figure 3)
α	Relative streamline angle with respect to blade camber line
β	Angle between streamwise direction and machine axis of the rotor
γ	Constant in the modelling of the Reynolds stress transport equation
γ_R	Constant in equation (1)
ν	Kinematic viscosity of fluid
ν_{eff}	Effective eddy viscosity of turbulent flow
ε	The rate of turbulent kinetic energy dissipation
ε_{ijk}, ε^{ijk}	Alternating tensor in covariant and contravariant tensor form
ρ	Density
ϕ	Flow coefficient
$\Gamma_{i,j,k}$	Christoffel symbol of first kind
Γ^i_{jk}	Christoffel symbol of second kind
Ω	Rotor speed of rotation
δ_{ij}	Kronecker delta
δ	Displacement thickness
θ	Momentum thickness
Δs	Finite-difference mesh size in s direction
Δn	Finite-difference mesh size in n direction
Δr	Finite-difference mesh size in r direction

Subscripts

c	Values at wake centerline
s,n,r	Values in s, n, and r directions, respectively
x,y,z	Values in x, y, and z directions, respectively
ℓ	Sensor of the probe
m	The maximum value across the wake
t	Values at blade tip
1	Condition at inlet flow
2	Condition at outlet flow
i,j,k, etc.	Tensor indices
∞	Values at free stream

Superscript

$\overline{\quad}$	Averaged values
~	Instantaneous value

NUMERICAL ANALYSIS AND FORTRAN PROGRAM FOR THE COMPUTATION OF THE TURBULENT WAKES OF TURBOMACHINERY ROTOR BLADES, ISOLATED AIRFOILS AND CASCADE OF AIRFOILS

C. Hah and B. Lakshminarayana

Department of Aerospace Engineering
The Pennsylvania State University
University Park, Pennsylvania 16802

SUMMARY

Turbulent wakes of turbomachinery rotor blades, isolated airfoils, and a cascade of airfoils were investigated both numerically and experimentally. The study was confined to low subsonic and incompressible wake flows. A finite difference procedure was employed in the numerical analysis utilizing the continuity, momentum, and turbulence closure equations in the rotating, curvilinear, and non-orthogonal coordinate system. A non-orthogonal curvilinear coordinate system was developed to improve the accuracy and efficiency of the numerical calculation.

Three turbulence models were employed to obtain closure of the governing equations. The first model was comprised of transport equations for the turbulent kinetic energy and the rate of energy dissipation, and the second and third models were comprised of equations for the rate of turbulent kinetic energy dissipation and Reynolds stresses, respectively. The second model handles the convection and diffusion terms in the Reynolds stress transport equation collectively, while the third model handles them individually. All three models were modified for the effect of streamline curvature. The rotation-originated redistribution terms were added in the transport equation of Reynolds stresses of the second and third models. This is the first reported attempt to modify Reynolds stress model for the effect of the streamline curvature and rotation. The turbulent wakes of an isolated airfoil and a cascade of airfoils are handled as simpler cases of the general rotating three-dimensional wake. The numerical results demonstrate that the second and third models provide accurate predictions, but the computer time and memory storage can be considerably saved with the second model. The experimental data are utilized to compare various turbulence closure models for the effect of streamline curvature.

INTRODUCTION

In the study of modern aerodynamics, turbulence behind turbomachinery rotor blades is a significant factor in the establishment of improved design criteria. Accurate information on the characteristics of this flow field is also indispensable in predicting noise level and determining vibration characteristics.

Several experimental investigations and approximate analyses have contributed to the understanding of these flow phenomena, although there has been no theoretical analysis. The rotor wake is highly complex and three-dimensional due to centrifugal and Coriolis forces in the shear layers; blade geometry, density, and pressure gradients in radial direction; and other effects. Velocity and pressure fluctuate periodically as well as randomly. In addition, the turbulence structure is affected by streamline curvature and machine rotation.

The rotor wake has different characteristics as compared to the wake of a single airfoil or a cascade of airfoils. Its velocity profile and decay characteristics vary in all the three coordinate directions. The analytical technique and correlation for a single airfoil cannot be used for prediction of the rotor wake, and the cascade does not represent the rotor wake's actual flow situation.

Direct measurement of the rotor wake could provide the data necessary for a theoretical analysis of the flow field, but is very expensive and time-consuming. Also, there are many parameters which influence the development of the rotor wake: blade geometry, solidity, hub-to-tip ratio, speed of rotation, inlet turbulence level, three-dimensional pressure gradient, and inlet swirl. Therefore, the correlation method of modelling the wake can be used only if ample experimental data, including all the important parameters, are available.

The numerical scheme with a suitable turbulent flow model can be considered as another promising way of analyzing the rotor wake. However, the literature survey (described later) on numerical analysis of two- and three-dimensional turbulent wakes indicates that most of the efforts have been concentrated on simple, two-dimensional flow fields without streamline curvature and rotation.

To provide the turbomachinery aerodynamicist or acoustician with an accurate method of determining the rotor wake development, or in understanding the complex features of the flow, a fully numerical scheme which utilizes suitable turbulence closure models is developed in this report. Also, its correlation with all the existing rotor wake data and related approximate analysis is presented.

Objectives and Method of Investigation

The following objectives were pursued during the investigation of the turbulent rotor wake reported in this paper:

1. To develop a numerical scheme that can predict the characteristics of the rotor wake accurately, with reasonable computing time and computer memory storage.

2. To establish a proper turbulence closure model that accounts for the effects of streamline curvature and rotation.

3. To predict the development of turbulent wakes of a single airfoil and cascade of airfoils with the developed numerical scheme.

The problem of predicting the flow field behind rotor blades is formulated using the equations of continuity, mean momentum, and turbulence closure.

In the analysis of complex flow problems, the judicious choice of the coordinate system and simplification in the governing equations are prerequisite for successful results. For the present problem, a curvilinear coordinate system, which includes streamwise, normal, and radial directions, is employed. Though this coordinate system is non-orthogonal, it provides simplicity in governing equations and in describing the boundary condition.

The existing turbulence closure models are critically reviewed for their performance in the presence of streamline curvature and rotation. Three typical turbulence closure models are considered for the present analysis. The first model is comprised of transport equations for the turbulent kinetic energy and the rate of energy dissipation. The second model makes use of the equation for the rate of turbulent kinetic energy dissipation and the Reynolds stress equation; however, the effects of convection and diffusion in the Reynolds stress transport equation were handled collectively. The third model utilizes equations of turbulent kinetic energy dissipation and Reynolds stresses in nearly exact form. All three models are modified for the effect of the streamline curvature. The effect of rotation is included in the second and third models through the rotation-originated redistribution term in the transport equation of Reynolds stress.

Bruce Reynolds and A. Ravindranath made available their experimental data for comparison purposes.

PREVIOUS INVESTIGATIONS

The term "wake" is commonly used to refer to the flow region behind a solid body, where the effect of viscosity cannot be neglected. Earlier investigations were concentrated on the wake at a low Reynolds number (laminar wake) of simple bodies (flat-plate, cylinder, and single airfoil). With the development of turbulence theories in fluid mechanics, the wake at a high Reynolds number (turbulent wake) has been widely studied for scientific and/or engineering purposes. One of the main differences between laminar and turbulent wakes is that the turbulent wake cannot be analyzed with the property of a fluid (kinematic viscosity). Hence, flow (turbulence closure) modelling is necessary for the analysis of the turbulent wake. To analyze the turbulent near wake, the scientist prefers using inner scales based on a turbulence structure at the near wake region, while the practical numerical analyst prefers an outer scale based on the far wake. This difference in approach will be discussed further later in this chapter.

In the following sections, previous work on analytical approaches, turbulence closure modelling, numerical approaches, and experimental investigation of two- and three-dimensional turbulent wakes will be comprehensively reviewed. Also a review of studies on the wakes of a single airfoil and a rotor blade by Raj and Lakshminarayana [1] and Reynolds and Lakshminarayana [2] and on the wake of a cascade inlet guide vane, and stator wake by Ravindranath and Lakshminarayana [3] will be given.

Analytical Approaches

The turbulent flow field behind a solid body can be divided into very near wake, near wake, and far wake regions depending on the evaluation of the flow. The far wake region, where the flow evolution is very slow, has been widely investigated experimentally and theoretically. The similarity solution exists at this wake region because of the slowness in evolution. Since it can be found in any standard text (Tennekes and Lumley [4]), the analytical procedure for the two-dimensional turbulent far wake is not reviewed here.

Analytical solutions for the wake downstream of the trailing edge of the flat plate and the isolated airfoil have been obtained for a laminar initial boundary layer with laminar viscous stresses in the near wake (Goldstein [5], Stewartson [6]). For the laminar near wake, the coordinate expansion solution for the inner and outer layers can be easily obtained because the flow structure is relatively simple compared to a turbulent wake.

Though numerical handling of the very near wake exists for the simple two-dimensional turbulent wake without streamline curvature, no complete analytical solution for this two-dimensional wake has been obtained. Robinson [7] obtained an analytical solution for the near wake region of a flat plate with various assumptions. His solution for the wake centerline mean-velocity defect is as follows:

$$\frac{U_c}{U_*} = \frac{1}{k}\left(\ell n g - \gamma_r\right) + B_r \qquad (1)$$

where $g(\ell n g - 1) = K^2\left(\frac{xU_*}{\nu}\right)$, U_* is the friction velocity, and k, γ_r, B_r, are constants. Although this solution is based on various assumptions on the flow structure at the near wake, it can be further refined and expanded for the general turbulent wake.

The analytical solution for the far wake of a rotor blade was derived by Lakshminarayana [8] and Raj and Lakshminarayana [9]. Lakshminarayana [8] used a cylindrical coordinate system and provided the wake centerline velocity defect and the wake width growth. Raj and Lakshminarayana [9] adopted a curvilinear coordinate system for their analytical solution of rotor wake for downstream. They indicated qualitatively the dependency of rotor wake characteristics on rotor geometry, turbulence quantity, operating condition of the rotor, and the streamline curvature. The flow characteristics of the very near wake and the near wake of a rotor blade are not well understood because the flow evolution is very fast and multiple-length scales, including the streamwise distance from the blade, strongly affect the flow development. The governing equations cannot be simplified, and remain non-linear in these flow regions.

Due to the complexity of the flow structure at the very near and the near wake of the rotor blade, no analytical or numerical solution has been tried before this study.

Turbulence Closure Modelling

With the advent of high speed digital computers, the prediction of a complex flow field, which cannot be analytically solved, has become a problem of major concern. Most interesting flow fields occur at high Reynolds numbers and contain random fluctuating components of flow characteristics. This results in more unknowns than would be the case for equations in the customary description of turbulence. To close the gap between the unknowns and the equations, various turbulence closure models have been studied.

The zero equation closure model, which uses no additional partial differential equation for the turbulence closure, has been widely studied and still applied for sophisticated practical problems. This model relates the Reynolds shear stress directly to the mean shear rate of the flow and cannot be used for the flow where multiple length and velocity dominate the problem. Prandtl [10] provided the earliest form of this model. Cebeci and Smith [11] have suggested modified forms to handle more complex turbulent flows. Their model is primarily for two-dimensional flow where only the shear stress component of the Reynolds stress tensor is important.

In an effort to reduce the empiricism required in closure modelling, models incorporating one or two partial differential equations for the transport of turbulence structural characteristics have been developed. Norris and Reynolds [12] proposed a model with the turbulent kinetic energy equation, and

Wolfstein [13] introduced a model with the transport equation for the turbulence length scale. These one-equation closure models describe the turbulent flow field more accurately than zero-equation model, but the application is restricted for the two-dimensional flow.

A two-equation model, which incorporates additional equations for the velocity scale and scalar dissipation, has been successfully applied for simple two-dimensional turbulent flows. Jones and Launder [14], Launder and Spalding [15], and Saffmann and Wilcox [16] have proposed their own versions of the two-equation model. Compared to the zero- and one-equation models, the two-equation model has less empiricism and can be used for a wider range of turbulent flows. Since the additional equation for scalar energy dissipation is derived on the basis of isotropic dissipation, the two-equation closure model does not predict individual intensity components of the Reynolds stress tensor. Even though the two-equation closure model was successful in predicting some simple three-dimensional turbulent flows, general non-isotropic three-dimensional turbulent flow fields cannot be described with two turbulence structural quantities. Mellor and Herring [17] provided an overview of one- and two-equation models, and Reynolds [18] gave a more detailed review of the two-equation model as well as other models. No major modification of the two-equation model for the effects of streamline curvature and rotation has been reported before this report.

The Reynolds stress model, which utilizes the transport equations of all the Reynolds stress components, has been investigated by Hanjalic and Launder [19], Launder, Reece, and Rodi [20], and Lumley and Khajeh-Nouri [21]. This model has been applied for relatively simple, thin shear layers. The numerical predictions using these models have been very promising. Because all the non-zero Reynolds stress components are individually estimated through the transport equations, this model is more suitable for examining the complex three-dimensional turbulent flow. For the computation of turbulent flow fields, where multiple-velocity and length scales dominate the turbulent structure, the accurate estimation of each Reynolds stress component is essential. In this situation, the Reynolds stress model works better than the one- or two-equation closure models.

Large eddy simulation, which numerically calculates the three-dimensional, time-dependent, large-eddy structure of the turbulence in addition to conventional modelling of the small-scale eddy, has been under intense development by the group at Stanford University. Large-eddy simulations are still in their infancy and, therefore, can hardly be used for the calculation of realistic problems because of the huge computing time and memory capacity required.

For the present investigation, the Reynolds stress model was modified for the effects of streamline curvature and rotation. This is the first reported attempt to modify the Reynolds stress model in this application. Also, the two-equation model was applied, and the numerical results are presented for comparison purposes.

Turbulence Closure Modelling for the Effect of Streamline Curvature

The effect of streamline curvature in a turbulent flow was first recognized by Prandtl [10], and many investigations have been carried out since then. Experimental studies of curved boundary layers have revealed that the turbulence structure as well as the mean velocity profile is changed considerably due to the effect of the streamline curvature.

Prandtl [10] demonstrated the effect of streamline curvature with the motion of a disturbed element of fluid in an inviscid and incompressible flow. According to his theory, this curvature stabilizes the flow field and, consequently, diminishes the turbulent transportation, where the angular momentum increases with the radius of streamline curvature and vice versa.

Quantitatively, the following expression can be derived for the criterion of stability due to streamline curvature (Bradshaw, [22]):

$$\omega^2 = 2 \frac{U}{r^2} \frac{d}{dr} (Ur) \qquad (2)$$

where U = tangential velocity, r = radius fo curvature, and ω = corresponding frequency. A real value of ω means stable, and an imaginary value means unstable.

Various proposals to include the effect of streamline curvature in the modelling of turbulent flow have been made. Prandtl [10] suggested a modification of mixing-length theory based on his argument of the qualitative effect of streamline curvature. A velocity scale was proposed by So [23] for curved shear flow from the simplification of Reynolds stress transport equations on a curvilinear coordinate system. Bradshaw [22] also incorporated the effect of streamline curvature by using the mixing-length concept and the analogy between buoyancy and curvature effects, in addition, Launder, Pridden, and Sharma [24] modified the two-equation closure model for this factor, and Chambers and Wilcox [25] added a singular production term in the equation of the turbulent kinetic energy to represent streamline curvature effects.

All of these approaches are based on the experimental phenomena and bear the effect of streamline curvature in various closure models qualitatively. The zero-equation model and any curvature modification based on the zero-equation model cannot be applied for the calculation of the rotor wake because the scaling laws of the turbulent rotor wake are not previously known. Also, the application of a simple modification in the two-equation turbulence closure model to the three-dimensional rotor wake is in doubt because the turbulence structure of the rotor wake is non-isotropic.

A more rational approach for the modelling of curvature effect in the turbulence closure scheme is pursued in this thesis, and the results are compared systematically.

Turbulence Closure Modelling for the Effect of Rotation

Research literature discussing the effects of rotation on flow fields is quite extensive, but very few theoretical investigations have been made that fully account for this influence. It was first recognized by Taylor [26] during his study of the stability of rotating flow. Several years later, Trefethen [27], during his investigation of the flow in a rotating long tube, recognized that the transverse pressure gradients by Coriolis acceleration could affect the process of transition by a similar mechanism of density stratification in a plane flow.

Bradshaw [28] proposed a local stability parameter for plane-rotating shear layers as a gradient Richardson number,

$$R_i = \frac{2\Omega\left(\frac{dU}{dy} - 2\Omega\right)}{\left(\frac{dU}{dy}\right)^2} \tag{3}$$

where Ω = rotational speed and $R_i > 0$ indicates the tendency for rotation to stabilize the flow. The above parameter was derived from the analogy between flows with mean streamline curvature and horizontally stratified shear layers with vertical density gradients, where centrifugal or buoyancy forces produce normal pressure gradients. A comprehensive review of the effect of rotation on the turbulent boundary layer was given by Johnston [29].

Most numerical studies (Launder, Pridden, and Sharma [24]) did not consider the effect of rotation on the turbulence structure in the computation of rotating turbulent flow. Although the total kinetic energy of turbulence is not changed by rotation, the energy is redistributed by rotation when the turbulence is not isotropic. Majumdar, Pratrap, and Spalding [30] used the conventional two-equation closure model for the calculation of the flow in a rotating duct and reported that their predictions were not quite satisfactory at high rotational speed.

The effect of rotation is substantial in the turbulent wake of rotor blades because the rotational speed is high and the turbulence structure is highly non-isotropic. Experimental investigations by Raj and Lakshminarayana [1], Reynolds et al [31], and Ravindranath and Lakshminarayana [32] have shown very high radial intensity in the rotor wake. This high radial intensity is due to the effect of rotation on the turbulence structure. Raj and Lumley [33] derived the rlative magnitudes of the turbulence quantities of the rotor wake. However, they examined a rotor wake whose streamwise direction is almost parallel to the machine axis, and their results $(\overline{u_\theta^2} > \overline{u_z^2} > \overline{u_r^2})$ do not agree with other experimental results for general configurations of the wake. A qualitative analysis of the effect of rotation on the development of the rotor wake was also given by Lakshminarayana and Reynolds [24].

Numerical Approaches

Computational fluid mechanics has rapidly developed into an important branch of fluid mechanics with the advent of faster and large computers. Numerical approaches have been used primarily for the prediction of complex flow fields where other methods do not provide reliable predictions.

To keep the numerical scheme within the capability of present-day computers, various numerical schemes have bene suggested. Patankar and Spalding [35] proposed a parabolic marching technique for three-dimensional flow. Their aim was to solve the three-dimensional flow field in a two-dimensional memory array and get the solution through a single sweep in the streamwise direction. This technique has been successful for the flow where the streamwise pressure gradient is small and no recirculating zone is involved. However, subsequent users have pointed out that an accurate pressure field cannot be obtained with the parabolic marching technique in both internal and external flows. For the complicated flow field (rotor wake, end wall flow in the compressor, etc.), the basic assumption of this technique, that the Reynolds stress acting on the plane normal to the streamwise direction is negligibly small, does not prevail. Ghia and Studerus [36] and Brilley [37] also presented their modified version of the parabolic marching technique; the basic feature of the technique is the same and the limitation of the technique is not removed.

The boundary layer assumption cannot be applied for the rotor wake because the streamwise velocity gradient is of the same order of normal velocity gradient in the near wake. Therefore, the governing equation should be solved in elliptic form to account for the streamwise diffusion of the flow quantities at the near wake region.

The governing equations can be numerically represented with the finite element or finite difference scheme. Even though the finite element scheme has some merit over the finite difference scheme for the flow whose boundary has complex geometry (Zienkiewicz [38]), its application for complex turbulent flow problems has not been extensive. Since the boundary geometry and boundary condition for the present rotor wake problem can be easily described with the employed curvilinear coordinate system, the implicit finite difference scheme was used.

To increase the efficiency and accuracy of the finite difference scheme for complex flow problems, the body-fitted coordinate system has been widely used (Thames, Thomson, and Mastin [39], Sorenson and Steger [40], and others). However, this coordinate system has been mostly applied for two-dimensional flow problems because huge computing time and memory storage is needed even for the generation of coordinate system itself (for example, about an hour for simple 3-D geometry on CDC-7600). The non-orthogonal coordinate system adopted for the present investigation provides the most merits of the body-fitted coordinate system. Also, physically important curvature terms are explicitly shown in the curvilinear coordinate system.

The finite difference equation can be solved by the alternating direction implicit (ADI) or successive over relaxation (SOR) methods. The ADI method for elliptic problems was first proposed by Peacemin and Rachford [41] and has been

widely applied for time-marching solutions for Navier-Stokes equations. For the present problem, the SOR method was used because the programming was relatively simple and the time-marching solution was not applied for the subsonic rotor wake.

Experimental Investigations

Properly correlated experimental data would provide a relatively accurate estimation of the rotor blade flow field. In previous research endeavors, many attempts have been made to find correlations for these turbulent wakes. Spence [42] derived the wake centerline velocity decay as follows, from systematic measurements of turbulent wakes of a single airfoil:

$$1 - \frac{U_c}{U_o} = 0.1265 \left(\frac{Z}{C} + 0.025\right)^{-1/2} \tag{4}$$

where C = chord at the airfoil, U_c = wake center velocity, U_o = free stream velocity, and Z = the streamwise distance from the trailing edge.

From their experimental data of the rotor wake, Raj and Lakshminarayana [9] confirmed that the streamwise velocity component has a Gaussian similarity profile at the far wake when proper length and velocity scales are introduced. In addition, they provided a correlation for the decay of streamwise and radial velocity components. Reynolds and Lakshminarayana [2] also confirmed with their measurements of fan rotor wakes that the similarity profile exists in axial and tangential velocity components. However, he found that the similarity in the velocity profile is not evident at the very near wake region. He correlated all the existing turbulent wake data with the following expression:

$$\frac{U_s - U_c}{U_\infty} = C_d^{1/4} \left[B_n \left(\frac{S}{C} - \frac{S_o}{C}\right)^{-1/2} + B_{n+1} \left(\frac{S}{C} - \frac{S_o}{C}\right)^{-1}\right] \tag{5}$$

where U_c = wake center velocity, U_∞ = free stream velocity, S_o/C = virtual origin of wake, C = chord of blade, S = streamwise distance from the trailing edge of the blade, and B_n and B_{n+1} are constants which have different values for the single airfoil, cascade, and rotor blade wakes. The experimental surveys of rotor wake at The Pennsylvania State University (Raj and Lakshminarayana [9], Reynolds et al. [31], and Ravindranath and Lakshminarayana [32]) include the measurements at the near wake region. More parameters are systematically accounted for in their investigations than in other experimental studies (Evans [43], Schmidt and Okiishi [44], Gallus [45], and Kool et al [46].

NUMERICAL ANALYSIS OF TURBULENT WAKES OF AXIAL FLOW TURBOMACHINERY ROTOR BLADES

Physical Nature of the Rotor Wake

Unlike single airfoil or cascade wakes, the rotor wake is three-dimensional (see Figure 1). The inbalance of the radial pressure gradient and the centrifugal forces in the radial direction inside the shear layers result in the radial velocity component. Furthermore, the geometry of the rotor blade and the density gradients in radial direction also contribute in generating these components. Due to the nature of these forces, therefore, the radial velocity component has an outward or inward direction.

As can be seen in Figure 1, the rotor wake develops in approximately a helix shape on the cylindrical surface (s direction), with β as the angle between the machine axis and the streamwise direction. Because a rotor blade is twisted in many cases, the outlet angle from the rotor blade and angle β both change in radial direction. One major curvature component in the three-dimensional rotor wake is due to this change of β.

The rotor wake is periodically unsteady when viewed from a stationary frame of reference, and the absolute tangential velocity components look like a jet (the maximum absolute tangential velocity occurs at the blade trailing edge). On the other hand, the rotor wake is steady if viewed from a frame rotating with the rotor blades. The rotation vector of the rotor blade has a direction parallel to the machine axis, while the streamwise component of the rotation vector varies in the radial direction.

Due to the loading on the blade, the boundary layer on the suction surface is thicker than that on the pressure surface at the trailing edge of the blade, and the rotor wake is asymmetrical.

The major components of curvature in the rotor wake is shown in Figure 2. r_m is the radius of curvature due to machine radii of the hub and annulus walls; r_β is the radius of curvature due to the change of β in the radial direction; and r_s is the radius of the streamline curvature on the cylindrical surface. The effect of streamline curvature depends on the momentum gradient in the direction of the radius of the curvature. For the turbulent wake, the fluid particles near the wake centerline are most affected by the curvature because the velocity gradient is large near the wake centerline. The effect r_m is substantial when the machine radius is relatively small and the blade is substantially twisted in the radial direction. r_β and r_s effects are dependent on the variation of outlet angles in the radial and streamwise directions, but for most practical rotor blades, the effects of these two curvature components are cancelled out because the momentum gradients have opposite signs.

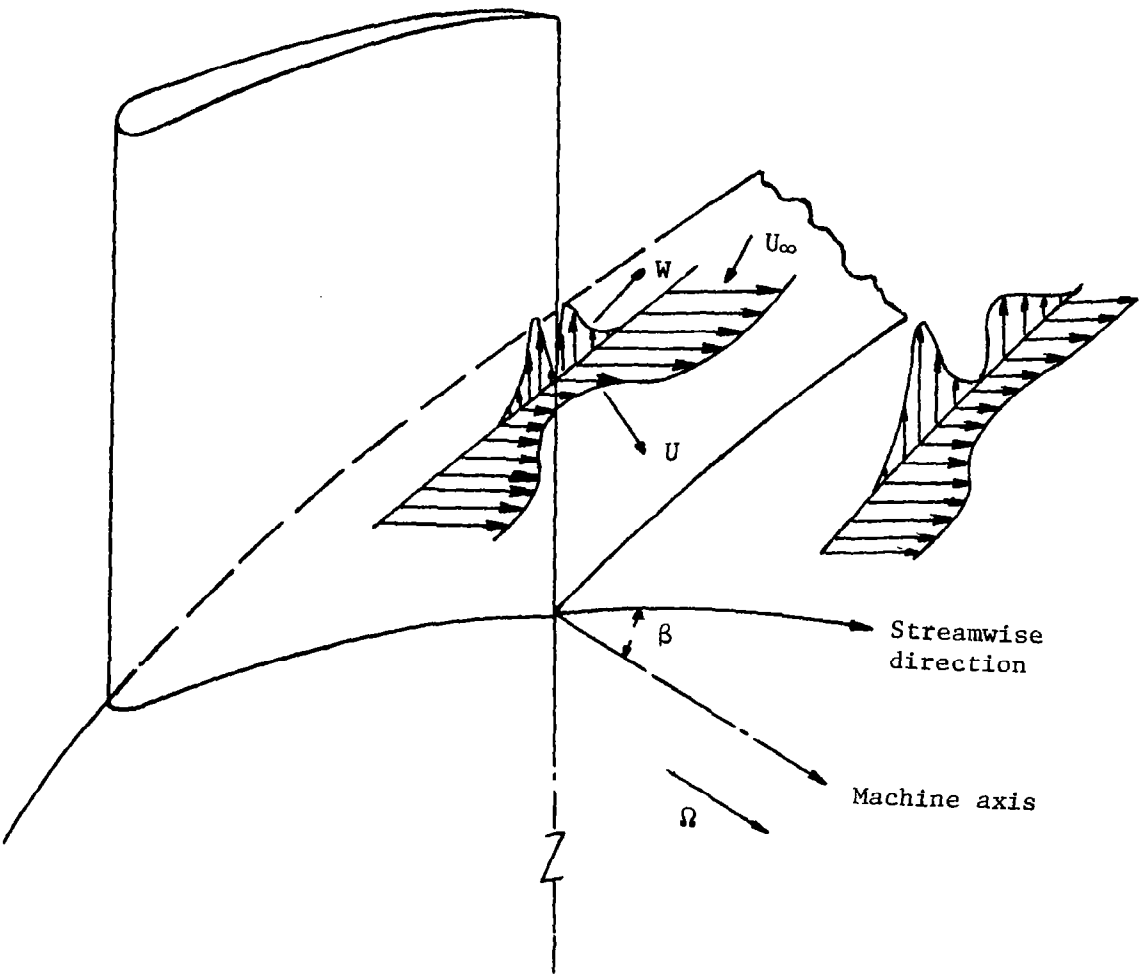

Figure 1. Characteristics of a Rotor Wake

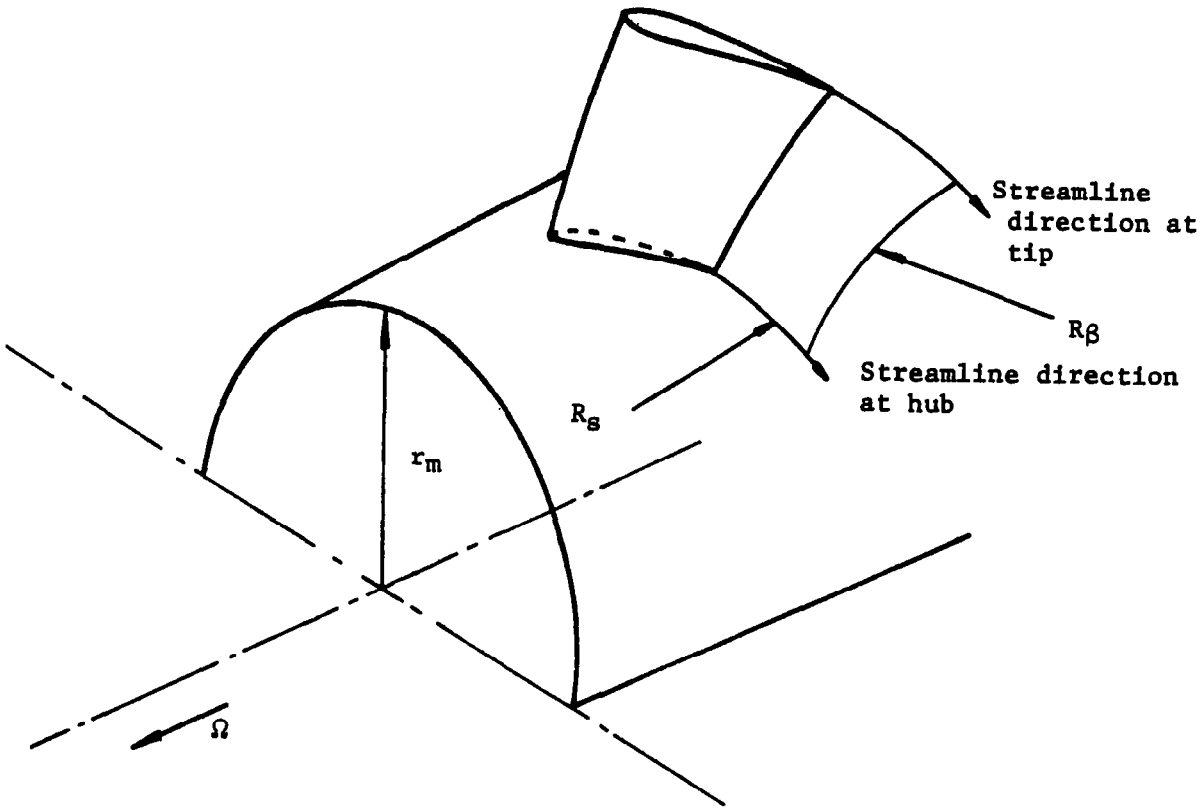

Figure 2. Major Components of Curvature in Rotor Wake

The Curvilinear Coordiante System for the Numerical Analysis of the Rotor Wake

As mentioned earlier, in the numerical analysis of complex flow problems, the judicious choice of the coordinate system and the simplification of the governing equations are prerequisites for successful results. The rotor wake develops between the annulus and hub walls, which for the present study are concentric cylinders. The fluid particles from the trailing edge of the rotor blade move approximately in a helical path whose angle varies radially. To make the governing equations simple, the streamwise direction (s) is chosen as one of the coordinates. Because the hub and annulus walls form the boundary surface, the radial direction (r) is also chosen as one of the coordinates. The third coordinate direction is chosen normal to the streamwise direction (n) on the cylindrical surface (constant radius). This physical coordinate system fixed to the rotor blade is shown in Figure 3.

This coordinate system is non-orthogonal, as will be shown later, but provides simplicity in describing governing equations and boundary conditions. The angle β between the streamwise direction and the machine axis varies radially. The variation of β in the streamwise and normal directions was not considered in the derivation of the coordinate system, since rotor wake measurements show very small changes of β in both directions.

To get the metric tensor of this coordinate system, the corresponding Cartesian coordinates system is introduced at the axis of the rotor shown in Figure 3. The y direction coincides with the axial direction of the rotor. Any arbitrary point p can be represented both in Cartesian coordinates (x,y,z) and in the curvilinear coordinates (s,n,r). The components of (s,n,r) and (x,y,z) are related as follows:

$$x = -r \sin\left(\frac{s \sin \beta + n \cos \beta}{r}\right) \tag{6}$$

$$y = s \cos \beta - n \sin \beta \tag{7}$$

$$z = r \cos\left(\frac{s \sin \beta + n \cos \beta}{r}\right) \tag{8}$$

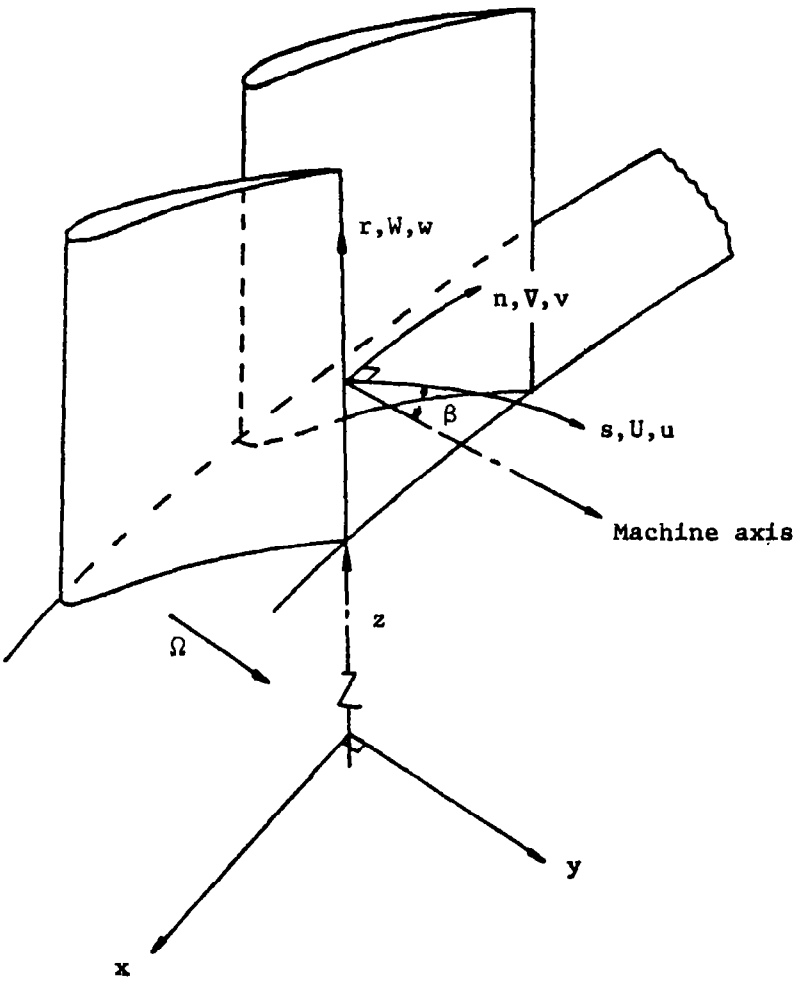

Figure 3. Curvilinear and Cartesian Coordinates Fixed on the Rotor

where s, n, and r are streamwise, principal normal, and radial directions, respectively.

The derivatives of the Cartesian coordinates with respect to the curvilinear coordinate system are as follows:

$$\frac{\partial x}{\partial s} = - \sin \beta \cos\left(\frac{s \sin \beta + n \cos \beta}{r}\right) \tag{9}$$

$$\frac{\partial x}{\partial n} = - \cos \beta \cos\left(\frac{s \sin \beta + n \cos \beta}{r}\right) \tag{10}$$

$$\frac{\partial x}{\partial r} = - \sin\left(\frac{s \sin \beta + n \cos \beta}{r}\right)$$

$$- \cos\left(\frac{s \sin \beta + n \cos \beta}{r}\right)\left[- \frac{s \sin \beta + n \cos \beta}{r} + (s \cos \beta - n \sin \beta)\frac{d\beta}{dr}\right] \tag{11}$$

$$\frac{\partial y}{\partial s} = \cos \beta \tag{12}$$

$$\frac{\partial y}{\partial n} = - \sin \beta \tag{13}$$

$$\frac{\partial y}{\partial r} = (-s \sin \beta - n \cos \beta)\frac{d\beta}{dr} \tag{14}$$

$$\frac{\partial z}{\partial s} = - \sin \beta \sin\left(\frac{s \sin \beta + n \cos \beta}{r}\right) \tag{15}$$

$$\frac{\partial z}{\partial n} = - \cos \beta \sin\left(\frac{s \sin \beta + n \cos \beta}{r}\right) \tag{16}$$

$$\frac{\partial z}{\partial r} = \cos\left(\frac{s\ \sin\beta + n\ \cos\beta}{r}\right)$$

$$- \sin\left(\frac{s\ \sin\beta + n\ \cos\beta}{r}\right)\ \left[-\ \frac{s\ \sin\beta + n\ \cos\beta}{r}\right.$$

$$\left. +\ (s\ \cos\beta - n\ \sin\beta)\frac{d\beta}{dr}\right] \qquad (17)$$

The fundamental metric tensor is obtained from the following relation:

$$g_{ij} = \frac{\partial y^{\alpha}}{\partial x^{i}}\ \frac{\partial y^{\alpha}}{\partial n^{j}}\ (\alpha = 1,2,3) \qquad (18)$$

where y^{α} = Cartesian coordinates and x^{i} = curvilinear coordinates. The resulting metric tensor in covariant components (g_{ij}) is,

$$g_{11} = 1\ ,\ g_{12} = g_{21} = 0\ ,\ g_{22} = 1$$

$$g_{13} = g_{31} = -\ \frac{s\ \sin^{2}\beta + n\ \sin\beta\cos\beta}{r} - n\ \frac{d\beta}{dr}$$

$$g_{23} = g_{32} = -\ \frac{s\ \sin\beta\cos\beta + n\ \cos^{2}\beta}{r} + s\ \frac{d\beta}{dr}$$

$$g_{33} = 1 + \frac{s^{2}}{r^{2}}\sin^{2}\beta - \frac{2s^{2}}{r}\sin\beta\cos\beta\ \frac{d\beta}{dr} + s^{2}\left(\frac{d\beta}{dr}\right)^{2} + \frac{2sn}{r^{2}}\sin\beta\cos\beta$$

$$+\frac{n^{2}}{r^{2}}\ \cos^{2}\beta + \left(\frac{2n^{2}}{r}\cos\beta\sin\beta - \frac{2ns}{r}\cos^{2}\beta\right.$$

$$\left. + \frac{2ns}{r}\sin^{2}\beta\right)\frac{d\beta}{dr} + n^{2}\left(\frac{d\beta}{dr}\right)^{2} \qquad (19)$$

and

$$|g_{ij}| = 1.0 \tag{20}$$

Then the metric tensor in contravariant components (g^{ij}) is obtained using the following relation,

$$g^{ij} = \frac{\text{Cofactor of } g_{ij} \text{ in } |g_{ij}|}{|g_{ij}|} \tag{21}$$

The resulting metric tensor in contravariant component (g^{ij}) is,

$$g^{11} = 1 + \frac{s^2}{r^2}\sin^4\beta + \frac{2sn}{r^2}\sin^3\beta\cos\beta$$

$$+ n^2 \left\{ \frac{\cos^2\beta\sin^2\beta}{r^2} + \frac{2}{r}\cos\beta\sin\beta\frac{d\beta}{dr} + \left(\frac{d\beta}{dr}\right)^2 \right\}$$

$$g^{12} = g^{21} = s^2 \left(\frac{\sin^3\beta\cos\beta}{r^2} - \frac{\sin^2\beta}{r}\frac{d\beta}{dr} \right)$$

$$+ sn \left\{ \frac{2}{r^2}\sin^2\beta\cos^2\beta - \left(\frac{d\beta}{dr}\right)^2 \right\} + n^2 \left(\frac{\sin\beta\cos^3\beta}{r^2} , \frac{\cos^2\beta}{r}\frac{d\beta}{dr} \right)$$

$$g^{13} = g^{31} = \frac{s\sin^2\beta + n\sin\beta\cos\beta}{r} + n\frac{d\beta}{dr}$$

$$g^{22} = 1.0 + s^2 \left\{ \frac{\sin^2\beta\cos^2\beta}{r^2} - \frac{2}{r}\sin\beta\cos\beta\frac{d\beta}{dr} \right.$$

$$\left. + \left(\frac{d\beta}{dr}\right)^2 \right\}$$

$$+ 2 s n \left(\frac{\sin\beta \cos^3}{r^2} - \frac{\cos^2\beta}{r} \frac{d\beta}{dr}\right)$$

$$+ \frac{n^2}{r^2} \cos^4\beta$$

$$g^{23} = g^{32} = \frac{s\sin\beta \cos\beta + n \cos^2\beta}{r} - s \frac{d\beta}{dr}$$

$$g^{33} = 1.0 \quad . \tag{22}$$

The Christoffel symbols of the first kind and the second kind are obtained using following relations,

$$\Gamma_{ijk} = \frac{1}{2} \left(\frac{\partial g_{ik}}{\partial xj} + \frac{\partial g_{jk}}{\partial x^i} + \frac{\partial g_{ij}}{\partial x^k}\right)$$

$$\Gamma^k_{ij} = g^{kl}\Gamma_{ijl} \tag{23}$$

Then the Christoffel symbols of the first kind are as follows:

$$\Gamma_{111} = \Gamma_{112} = \Gamma_{122} = \Gamma_{212} = \Gamma_{211} = \Gamma_{131} = \Gamma_{311} = 0$$

$$\Gamma_{121} = \Gamma_{221} = \Gamma_{222} = \Gamma_{232} = \Gamma_{322} = 0$$

$$\Gamma_{113} = -\frac{\sin^2\beta}{r}$$

$$\Gamma_{123} = \Gamma_{213} = -\frac{\sin\beta\cos\beta}{r}$$

$$\Gamma_{132} = \Gamma_{312} = \frac{d\beta}{dr}$$

$$\Gamma_{313} = \Gamma_{133} = \frac{s}{r^2}\sin^2\beta - \frac{2s}{r}\sin\beta\cos\beta\,\frac{d\beta}{dr} + s\left(\frac{d\beta}{dr}\right)^2$$

$$+ \frac{n}{r^2}\sin\beta\cos\beta - \left(\frac{n}{r}\cos^2\beta - \frac{n}{r}\sin^2\beta\right)\frac{d\beta}{dr}$$

$$\Gamma_{223} = -\frac{\cos^2\beta}{r}$$

$$\Gamma_{231} = \Gamma_{321} = -\frac{d\beta}{dr}$$

$$\Gamma_{233} = \Gamma_{323} = \frac{s}{r^2}\sin\beta\cos\beta + \frac{n}{r^2}\cos^2\beta$$

$$+ \left(\frac{2n}{r}\cos\beta\sin\beta - \frac{s}{r}\cos^2\beta + \frac{s}{r}\sin^2\beta\right)\frac{d\beta}{dr}$$

$$+ n\left(\frac{d\beta}{dr}\right)^2$$

$$\Gamma_{331} = -n\frac{d^2\beta}{dr^2} - s\left(\frac{d\beta}{dr}\right)^2$$

$$\Gamma_{332} = -s\frac{d^2\beta}{dr^2} - n\left(\frac{d\beta}{dr}\right)^2$$

$$\Gamma_{333} = s^2\left[-\frac{\sin^2\beta}{r^3} + \frac{2}{r^2}\sin\beta\cos\beta\,\frac{d\beta}{dr} + \frac{(\sin^2\beta-\cos^2\beta)}{r}\left(\frac{d\beta}{dr}\right)^2\right.$$

$$- \frac{\sin\beta\cos\beta}{r} \frac{d^2\beta}{dr^2} + \left(\frac{d\beta}{dr}\right)\left(\frac{d^2\beta}{dr^2}\right) \Big]$$

$$+ s\,\eta \left[- \frac{2}{r^3} \sin\beta\cos\beta + \frac{2(\cos^2\beta - \sin^2\beta)}{r^2} \frac{d\beta}{dr} \right.$$

$$\left. + 4 \frac{\sin\beta\cos\beta}{r} \left(\frac{d\beta}{dr}\right)^2 + \frac{(\sin^2\beta - \cos^2\beta)}{r} \frac{d^2\beta}{dr^2} \right]$$

$$+ \eta^2 \left[- \frac{\cos^2\beta}{r^3} - \frac{2\sin\beta\cos\beta}{r} \frac{d\beta}{dr} + \frac{(\cos^2\beta - \sin^2\beta)}{r} \left(\frac{d\beta}{dr}\right)^2 \right.$$

$$\left. + \frac{\sin\beta\cos\beta}{r} \frac{d^2\beta}{dr^2} + \left(\frac{d\beta}{dr}\right)\left(\frac{d^2\beta}{dr^2}\right) \right] . \qquad (24)$$

and the Christoffel symbols of the second kind are

$$\Gamma^1_{11} = - \frac{s}{r^2} \sin^4\beta$$

$$\Gamma^1_{12} = - \frac{s}{r^2} \sin^3\beta\cos\beta$$

$$\Gamma^1_{22} = - \frac{s}{r^2} \sin^2\beta\cos^2\beta$$

$$\Gamma^1_{13} = - \frac{s^2}{r^3} \sin^4\beta - \frac{s^2}{r^2} \sin^3\beta\cos\beta \frac{d\beta}{dr}$$

$$\Gamma^1_{23} = \frac{s^2}{r^2} \left(\frac{\sin^3\beta\cos\beta}{r} - \sin^2\beta\cos^2\beta \frac{d\beta}{dr} \right) - \frac{d\beta}{dr}$$

$$\Gamma^1_{33} = - \frac{s^3}{r^4} \sin^4\beta - \frac{2s^3}{r^3} \sin^3\beta\cos\beta \frac{d\beta}{dr}$$

$$\Gamma^2_{13} = - \frac{s^2}{r^2} \sin^2\beta(1 + \cos^2\beta) \frac{d\beta}{dr} + \frac{s^2}{r^3} \sin^3\beta\cos\beta + \frac{d\beta}{dr}$$

$$\Gamma^2_{11} = \frac{s}{r}\sin^2\beta\,\frac{d\beta}{dr} - \frac{s}{r^2}\sin^3\beta\cos\beta$$

$$\Gamma^2_{22} = \frac{s}{r}\cos^2\beta\,\frac{d\beta}{dr} - \frac{s}{r^2}\sin\beta\cos^3\beta$$

$$\Gamma^2_{12} = \frac{s}{r}\sin\beta\cos\beta\,\frac{d\beta}{dr} - \frac{s}{r^2}\sin^2\beta\cos^2\beta$$

$$\Gamma^2_{23} = \frac{s^2}{r^3}\sin^2\beta\cos^2\beta - \frac{s^2}{r^2}\sin\beta\cos\beta\,(1+\cos^2\beta)\,\frac{d\beta}{dr}$$

$$\Gamma^2_{33} = -\frac{s^3}{r^4}\sin^3\beta\cos\beta + \frac{s^3}{r^3}\sin^2\beta(1+2\cos^2\beta)\,\frac{d\beta}{dr} + s\left(\frac{d^2\beta}{dr^2}\right)$$

$$\Gamma^3_{11} = -\frac{\sin^2\beta}{r}$$

$$\Gamma^3_{21} = -\frac{\sin\beta\cos\beta}{r}$$

$$\Gamma^3_{22} = -\frac{\cos^2\beta}{r}$$

$$\Gamma^3_{13} = \frac{s}{r^2}\sin^2\beta - \frac{s}{r}\sin\beta\cos\beta\,\frac{d\beta}{dr}$$

$$\Gamma^3_{23} = \frac{s}{r^2}\sin\beta\cos\beta - \frac{s}{r}\cos^2\beta\,\frac{d\beta}{dr}$$

$$\Gamma^3_{33} = -\frac{s^2}{r^3}\sin^2\beta + \frac{2s^2}{r^2}\sin\beta\cos\beta\,\frac{d\beta}{dr} \qquad (25)$$

For thin shear flow, n/r and $(d\beta/dr)^2$ are negligibly small for most rotors. Therefore the terms containing n/r and $(d\beta/dr)^2$ can be neglected in equation (24) and these terms are not shown in equation (25).

As was mentioned earlier, this coordinate system is not orthogonal (the off-diagonal components in the fundamental metric tensor have non-zero terms). However, the boundary conditions at the hub and annulus walls can be easily expressed with this coordinate system. Also, the governing equations can be considerably simplified for thin shear layers because the normal velocity component becomes negligibly small and streamwise variation of flow quantities becomes very small far downstream in the present coordinate system.

Horlock and Wordsworth [47] proposed an orthogonal curvilinear coordinate system for the calculation of the three-dimensional boundary layer on the rotor blade, their coordinate system can neither handle the radial variation of angle β and nor be applied for general problems like the rotor wake. Although Miyake and Fujita [48] used a non-orthogonal curvilinear coordinate system for calculation of the laminar boundary layer of a rotor blade with a specific configuration, they did not allow for any curvature component of the blade. Consequently, the application of their coordinate system is strictly restricted to a very small group of rotor configurations.

The theoretical analysis of the turbulence structure of the rotor wake can be done more easily on the physical coordinate system than on the cylindrical polar coordinate system because this system is well geared to the physical nature of the rotor wake and important curvature terms are shown in the governing equations. Also, a comparison of the rotor wake flow structure with those of single airfoil and cascade wakes can be made directly, because the physical coordinate system reduces to the Cartesian coordinates used for analysis of these latter two wakes.

Governing Equations in the Rotating Curvilinear Coordinate System

The present analysis neglects the effects of Mach number on the turbulent flow fields and confines to the incompressible, fully turbulent flow. The equations governing the incompressible, fully turbulent flow relative to a coordinate system rotating with angular velocity, Ω_i, is introduced in generalized tensor form and in the curvilinear coordinates described in the previous section.

The continuity equation for incompressible flow is

$$U^i_{,i} = 0 \quad , \quad u^i_{,i} = 0 \tag{26}$$

or

$$\frac{\partial U^i}{\partial x^i} + \Gamma^i_{i\ell}\, U^\ell = 0 \quad , \quad \frac{\partial u^i}{\partial x^i} + \Gamma^i_{i\ell}\, u^\ell = 0 \tag{27}$$

where U^i and u^i are mean and fluctuating contravariant velocity components. Using Christoffel symbols in equation (25),

$$\frac{\partial U^i}{\partial x^i} = 0 \quad , \quad \frac{\partial u^i}{\partial x^i} = 0 \ . \tag{28}$$

In the present coordinate system,

$$\frac{\partial U}{\partial s} + \frac{\partial V}{\partial n} + \frac{\partial W}{\partial r} = 0 \quad , \quad \frac{\partial u}{\partial s} + \frac{\partial v}{\partial n} + \frac{\partial w}{\partial r} = 0 \tag{29}$$

Where U, V, and W are streamwise, normal, and radial contravariant velocity components in the present curvilinear coordinate system and u, v, and w are fluctuating contravariant velocity components.

The momentum conservation equation for laminar flow is

$$U^j U^i_{,j} + 2\varepsilon^{ijk}\Omega_j U_k = - \frac{g^{ij}}{\rho} \frac{\partial p^*}{\partial x^j} + \nu g_{jk} U^i_{,jk} \tag{30}$$

and for turbulent flow,

$$U^j U^i_{,j} + \overline{u^j u^i_{,j}} + 2\varepsilon^{ijk}\Omega_j U_k = - \frac{g^{ij}}{\rho} \frac{\partial p^*}{\partial x^i} + \nu g_{jk} U^i_{,jk} \ \nu \tag{31}$$

and

$$\overline{u^j u^i_{,j}} = \overline{u^j \frac{\partial u^i}{\partial x^j}} + \overline{u^j u^k} \ \Gamma^i_{jk} = \overline{\frac{\partial u^i u^j}{\partial x^j}} + \overline{u^j u^k} \ \Gamma^i_{jk} \tag{32}$$

where ε^{ijk} is the alternating tensor, Ω_j is the angular velocity of the rotor, ρ is the fluid density, and p^* is reduced pressure ($p^* = p - \rho/2 \ \Omega^2 r^2$). At a high Reynolds number, the last term in equation (31) that represents the dissipation due to the molecular viscosity of a fluid can be neglected.

For thin shear flow in turbomachinery blade wakes,

$$V << U \quad , \quad W < U \ . \tag{33}$$

Then the components of equation (31) in the curvilinear coordinate system (Figure 3) are as follows (neglecting lower-order convection terms in the mean velocity and all the small curvature terms in Reynolds stresses):

$$U\frac{\partial U}{\partial s} + V\frac{\partial U}{\partial n} + W\frac{\partial U}{\partial r} + U^2\,\Gamma^1_{11} + W^2\,\Gamma^1_{33} + 2UW\,\Gamma^1_{13} + V^2\,\Gamma^1_{22}$$
$$+ 2UV\,\Gamma^1_{12} + 2VW\,\Gamma^1_{23} - 2\Omega W^*\sin\beta = -\frac{1}{\rho}\left[g^{11}\frac{\partial P^*}{\partial s}\right.$$
$$\left. + g^{12}\frac{\partial P^*}{\partial n} + g^{13}\frac{\partial P^*}{\partial r}\right] - \frac{\partial}{\partial s}\overline{u^2} - \frac{\partial}{\partial n}\overline{uv} - \frac{\partial}{\partial r}\overline{uw} \qquad (34)$$

$$U\frac{\partial V}{\partial s} + V\frac{\partial V}{\partial n} + W\frac{\partial V}{\partial r} + U^2\Gamma^2_{11} + W^2\Gamma^2_{33} + 2UW\,\Gamma^2_{13} + V^2\Gamma^2_{22}$$
$$+ 2UV\,\Gamma^2_{12} + 2VW\,\Gamma^2_{23} - 2\Omega W^*\cos\beta = -\frac{1}{\rho}\left[g^{21}\frac{\partial P^*}{\partial s}\right.$$
$$\left. + g^{22}\frac{\partial P^*}{\partial n} + g^{23}\frac{\partial P^*}{\partial r}\right] = \frac{\partial}{\partial s}\overline{uv} - \frac{\partial}{\partial n}\overline{v^2} - \frac{\partial}{\partial r}\overline{vw} \qquad (35)$$

$$U\frac{\partial W}{\partial s} + V\frac{\partial W}{\partial n} + W\frac{\partial W}{\partial r} + 2\Omega V^*\cos\beta + 2\Omega U^*\sin\beta + W^2\,\Gamma^3_{33} + UW\,\Gamma^3_{13} + V^2\,\Gamma^3_{22}$$
$$+ 2UV\,\Gamma^3_{12} + 2VW\,\Gamma^3_{23} + U^2\,\Gamma^3_{11} = -\frac{1}{\rho}\left[g^{31}\frac{\partial P^*}{\partial s} + g^{32}\frac{\partial P^*}{\partial n} + g^{33}\frac{\partial P^*}{\partial r}\right]$$
$$- \frac{\partial}{\partial s}\overline{uw} - \frac{\partial}{\partial n}\overline{vw} - \frac{\partial}{\partial r}\overline{w^2} - \overline{u^2}\,\Gamma^3_{11} - \overline{uv}\,\Gamma^3_{12} \qquad (36)$$

where U*, V*, and W* are covariant components and U, V, and W are contravariant components of mean velocity. The solution of these equations gives the contravariant components of mean velocity which can be transformed to physical ones.

Turbulence Closure Modelling

The Modelling of the Reynolds Stress Transport Equation

Various turbulence closure models have been proposed to simulate the behavior of real turbulent flows. The common feature of a good turbulence model is its universality to a wide range of flows and simplicity in its use. Two relatively complex turbulence closure models are utilized for the calculation

of the rotor wake which develops under the influence of curvature and rotation. A two-equation turbulence closure model, which adopts two transport equations of turbulence characteristic quantities, has been proposed by Daly and Harlow [49] and Launder and Spalding [15]. Launder, Pridden and Sharma [24] extended this model to include the effects of curvature by modifying the primary decay term in the equation for the rate of dissipation. This modification is based on the experimental data and approximately represents the effect of curvature.

To include the effects of curvature and rotation, the Reynolds stress model is used in the present analysis. This model, which utilizes approximate transport equations of Reynolds stress, has been proposed by Rotta [50] and Hanjalic and Launder [19]. Raj and Lakshminarayana [1] give the transport equation in the rotating curvilinear coordinate system, which is:

$$U_j \overline{u^i u^k}_{,j} + \overline{u^k u_j} U^i_{,j} + \overline{u^i u_j} U^k_{,j} + \overline{u^i u^k u_j}_{,j} + 2\Omega_\ell \varepsilon^{i\ell m} \overline{u_m u^k} + 2\Omega_\ell \varepsilon^{k\ell m} \overline{u_m u^i}$$

$$= -\frac{1}{\rho}\left(\overline{u^k p'}_{,i} + \overline{u^i p'}_{,k}\right) + \nu g_{\ell j}\left(\overline{u^k u_{,\ell j}} + \overline{u^i u_{,\ell j}}\right) \qquad (37)$$

where p' is the fluctuating static pressure and ν is the kinematic viscosity.

To get closure, several authors have suggested a modelled form of the above equation. All the models proposed hitherto are for non-rotating systems. Most calculations for thin shear flow assume that the convection term and diffusion term in equation (37) are equal. So [23] applied this assumption for the calculation of two-dimensional curved flow. For the present analysis, the diffusion and convection terms are considered collectively. The combined effect of the two terms are assumed to be related to the production term. The modelling of the pressure-strain correlation term is based on Rotta [50] and Naot, Shavit, and Wolfshtein [51]. Furthermore, the rate of turbulence energy production, which appears in the modelling for the mean-strain effects in the pressure-strain correlation, is replaced with the rate of dissipation. Also, a high local-turbulence Reynolds number is assumed and the scalar representation of dissipation (the contraction of the dissipation tensor) is introduced for the dissipation term of equation (37). With these models, equation (37) reduces to

$$0 = (1 + C_1)\left(-\overline{u_k u^j} U^i_{,k} - \overline{u_k u^i} U^j_{,k}\right)(1 - \gamma) - 2\left(\varepsilon^{i\ell m}\Omega_\ell \overline{u_m u^j} + \varepsilon^{j\ell m}\Omega_\ell \overline{u_m u^i}\right) - \frac{2}{3} g^{ij}\varepsilon(1 - \gamma)$$
$$- C_{\phi 1}\frac{\varepsilon}{k}\left(\overline{u^i u^j} - \frac{2}{3} g^{ij} k\right) \qquad (38)$$

where $k = 1/2\ g_{ij}\overline{u^i u^j}$, ε = the rate of energy dissipation (last term in equation 37), and $C_{\phi 1}$, C_1, and γ are constants.

These equations are still intractable unless some realistic and practical assumptions are made. Using the assumptions utilized for the simplification of the mean momentum equations, the component form of equation (38) can be expressed as follows for the coordinate system of Figure 3.

$\overline{u^2}$:

$$0 = 2(1 + C_1)(1 - \gamma)\left\{\left[-\overline{uv} - \overline{uw}\left(-\frac{s}{r}\sin\beta\cos\beta + s\frac{d\beta}{dr}\right)\right]\left(\frac{\partial U}{\partial n} + U\,\Gamma^1_{12}\right.\right.$$

$$+ W\,\Gamma^1_{23}) + [-\overline{u^2} + \overline{uw}(\frac{s}{r}\sin^2\beta)](\frac{\partial U}{\partial s} + U\,\Gamma^1_{11} + W\,\Gamma^1_{13})\}$$

$$- 4\Omega_n[-\overline{u^2}\,\frac{s}{r}\sin^2\beta + \overline{uv}(-\frac{s}{r}\sin\beta\cos\beta + s\,\frac{d\beta}{dr}) + \overline{uw}\,(1$$

$$+ \frac{s^2}{r^2}\sin^2\beta - \frac{2s^2}{r}\frac{d\beta}{dr}\sin\beta\cos\beta)] - \frac{2}{3}(1 + \frac{s^2}{r^2}\sin^4\beta)\varepsilon(1 - \gamma)$$

$$- C_{\phi 1}\frac{\varepsilon}{k}[\overline{u^2} - \frac{2}{3}(1 + \frac{s^2}{r^2}\sin^4\beta)k] \qquad (39)$$

$\overline{v^2}$:

$$0 = 2(1 + C_1)(1 - \gamma)[-\overline{v^2} - \overline{vw}(-\frac{s}{r}\sin\beta\cos\beta + s\,\frac{d\beta}{dr})](\frac{\partial V}{\partial n} + U\,\Gamma^2_{12}$$

$$+ W\,\Gamma^2_{23}) + 4\Omega_s[\overline{uv}(-\frac{s}{r}\sin^2\beta) + \overline{v^2}(-\frac{s}{r}\sin\beta\cos\beta + s\,\frac{d\beta}{dr})$$

$$+ \overline{vw}(1 + \frac{s^2}{r^2}\sin^2\beta - 2\,\frac{s^2}{r}\frac{d\beta}{dr}\sin\beta\cos\beta)] - \frac{2}{3}(1 + \frac{s^2}{r^2}\sin^2\beta\cos^2\beta$$

$$- \frac{2s^2}{r}\frac{d\beta}{dr}\sin\beta\cos\beta)\varepsilon(1 - \gamma) - C_{\phi 1}\frac{\varepsilon}{k}[\overline{v^2} - \frac{2}{3}(1 + \frac{s^2}{r^2}\sin^2\beta\cos^2\beta$$

$$- \frac{2s^2}{r}\frac{d\beta}{dr}\sin\beta\cos\beta)] \qquad (40)$$

$\overline{w^2}$:

$$0 = 2(1 + c_1)(1 - \gamma)\{-\overline{vw} - \overline{w^2}(-\frac{s}{r}\sin\beta\cos\beta + s\,\frac{d\beta}{dr})](\frac{\partial W}{\partial n} + U\,\Gamma^3_{12}$$

$$+ W\,\Gamma^3_{23}) + (-\overline{uw} + \overline{w^2}\,\frac{s}{r}\sin^2\beta)(\frac{\partial W}{\partial s} + U\,\Gamma^3_{11} + W\Gamma^3_{13})\}-4\Omega_s[\,\overline{vw}$$

$$+ \overline{w^2}\,(-\frac{2}{r}\sin\beta\cos\beta + s\,\frac{d\beta}{dr})] + 4\Omega_n(\overline{uw} - \overline{w^2}\,\frac{s}{r}\sin^2\beta)$$

$$- \frac{2}{3}\varepsilon(1 - \gamma) - C_{\phi 1}\frac{\varepsilon}{k}(\overline{w^2} - \frac{2}{3}k) \qquad (41)$$

$\overline{uv}$:

$$0 = (1 + C_1)(1 - \gamma)\{[-\overline{v^2} - \overline{vw}(-\frac{s}{r}\sin\beta\cos\beta + s\frac{d\beta}{dr})](\frac{\partial U}{\partial n} + U\,\Gamma^1_{12} + W\,\Gamma^1_{23}) + (-\overline{uv} + \overline{vw}\frac{s}{r}\sin^2\beta)(\frac{\partial U}{\partial s} + U\,\Gamma^1_{11} + W\,\Gamma^1_{13}) + [-\overline{uv} - \overline{uw}(-\frac{s}{r}\sin\beta\cos\beta + s\frac{d\beta}{dr})](\frac{\partial V}{\partial n} + U\,\Gamma^2_{12})\}$$
$$- 2\{\Omega_n[-\overline{uv}\frac{s}{r}\sin^2\beta + \overline{v^2}(-\frac{s}{r}\sin\beta\cos\beta + s\frac{d\beta}{dr}) - \overline{vw}(1 + \frac{s^2}{r^2}\sin^2\beta - \frac{2s^2}{r}\frac{d\beta}{dr}\sin\beta\cos\beta)] - \Omega_s[-\overline{u^2}\frac{s}{r}\sin^2\beta + \overline{uv}(-\frac{s}{r}\sin\beta\cos\beta + s\frac{d\beta}{dr}) + \overline{uw}(1 + \frac{s^2}{r^2}\sin^2\beta - \frac{2s^2}{r}\frac{d\beta}{dr}\sin\beta\cos\beta)]\}$$
$$- \frac{2}{3}(\frac{s^2}{r^2}\sin^3\beta\cos\beta - \frac{s^2}{r}\frac{d\beta}{dr}\sin^2\beta)\varepsilon(1 - \gamma) - C_{\phi 1}\frac{\varepsilon}{k}[\overline{uv} - \frac{2}{3}(\frac{s^2}{r^2}\sin^3\beta\cos\beta - \frac{s^2}{r}\frac{d\beta}{dr}\sin^2\beta)k] \qquad (42)$$

$\overline{vw}$:

$$0 = (1 + C_1)(1 - \gamma)\{[-\overline{v^2} - \overline{vw}(-\frac{s}{r}\sin\beta\cos\beta + s\frac{d\beta}{dr})](\frac{\partial W}{\partial n} + U\,\Gamma^3_{12} + W\,\Gamma^3_{23}) + (-\overline{uv} + \overline{vw}\frac{s}{r}\sin^2\beta)(\frac{\partial W}{\partial s} + U\,\Gamma^3_{13} + W\Gamma^3_{13}) + [-\overline{vw} - \overline{w^2}(-\frac{s}{r}\sin\beta\cos\beta + s\frac{d\beta}{dr})](\frac{\partial V}{\partial n} + U\,\Gamma^2_{12})\} - 2\{\Omega_s[\overline{v^2} + \overline{vw}(-\frac{s}{r}\sin\beta\cos\beta + s\frac{d\beta}{dr})] - \Omega_n(\overline{uv} - \overline{vw}\frac{s}{r}\sin^2\beta) - \Omega_s[-\overline{uw}\frac{s}{r}\sin^2\beta + \overline{vw}(-\frac{s}{r}\sin\beta\cos\beta + s\frac{d\beta}{dr}) + \overline{w^2}(1 + \frac{s^2}{r^2}\sin^2\beta$$

$$- \frac{2s^2}{r}\frac{d\beta}{dr}\sin\beta\cos\beta)\Big]\Big\} - \frac{2}{3}\left(\frac{s}{r}\sin\beta\cos\beta - s\frac{d\beta}{dr}\right)\varepsilon(1-\gamma) - C_{\phi 1}\frac{\varepsilon}{k}[\overline{vw}$$

$$- \frac{2}{3}\left(\frac{s}{r}\sin\beta\cos\beta - s\frac{d\beta}{dr}\right)k] \qquad (43)$$

$\overline{uw}$:

$$0 = (1 + C_1)(1-\gamma)\Big\{\Big[-\overline{vw} - \overline{w^2}\left(-\frac{s}{r}\sin\beta\cos\beta + s\frac{d\beta}{dr}\right)\Big]\left(\frac{\partial U}{\partial n} + U\,\Gamma^1_{12}\right.$$

$$\left. + W\,\Gamma^1_{23}\right) + \Big[-\overline{uw} + \overline{w^2}\frac{s}{r}\sin^2\beta\Big)\left(\frac{\partial U}{\partial s} + U\,\Gamma^1_{13} + W\Gamma^1_{13}\right)\Big[-\overline{uv}$$

$$- \overline{uw}\left(-\frac{s}{r}\sin\beta\cos\beta + s\frac{d\beta}{dr}\right)\Big]\left(\frac{\partial W}{\partial n} + U\,\Gamma^3_{12} + W\,\Gamma^3_{23}\right) + \left(-\overline{u^2}\right.$$

$$\left. + \overline{uw}\frac{s}{r}\sin^2\beta\right)\left(\frac{\partial W}{\partial s} + U\,\Gamma^3_{11} + W\,\Gamma^3_{13}\right)\Big\} - 2\Big\{\Omega_s[\overline{uv} + \overline{uw}\left(-\frac{s}{r}\sin\beta\cos\beta\right.$$

$$\left. + s\frac{d\beta}{dr}\right)] - \Omega_n[\overline{u^2} - \overline{vw}\left(-\frac{s}{r}\sin\beta\cos\beta + s\frac{d\beta}{dr}\right) - \overline{w^2}(1 +$$

$$+ \frac{s^2}{r^2}\sin^2\beta - \frac{2s^2}{r}\frac{d\beta}{dr}\sin\beta\cos\beta)]\Big\} + \frac{2}{3}\frac{s}{r}(\sin^2\beta)\varepsilon(1-\gamma)$$

$$- C_{\phi 1}\frac{\varepsilon}{k}\left(\overline{uw} + \frac{2}{3}k\frac{s}{r}\sin^2\beta\right) \qquad (44)$$

where U, V, W, u, v, and w are mean and fluctuating velocity components in s, n, and r (Figure 3) directions. Ω_s and Ω_n are the components of angular velocity in s and n directions.

A Qualitative Discussion of the Effect of Rotation and Curvature on the Turbulence Structure

The effects of rotation on the turbulence structure is qualitatively analyzed employing equations (41-44). To enable simplification, the curvature terms are neglected. The resulting equations are as follows:

$$\overline{u^2} = [\frac{2}{3} C_{\phi 1} \varepsilon - \frac{2}{3} \varepsilon(1 - \gamma) - 2 \overline{uv} \frac{\partial U}{\partial n} C_\gamma]/(C_{\phi 1} \frac{\varepsilon}{k} + 2 C_\gamma \frac{\partial U}{\partial s})$$

$$- 4\Omega_n \overline{uw}/(C_{\phi 1} \frac{\varepsilon}{k} + 2C_\gamma \frac{\partial U}{\partial s}) \quad (45)$$

$$\overline{v^2} = \frac{2}{3} \varepsilon[C_{\phi 1} - (1 - \gamma)]/(C_{\phi 1} \frac{\varepsilon}{k} + 2C_\gamma \frac{\partial V}{\partial n}) + 4\Omega_s \overline{vw}/(C_{\phi 1} \frac{\varepsilon}{k} + 2C_\gamma \frac{\partial V}{\partial n}) \quad (46)$$

$$\overline{w^2} = \frac{2}{3}[1 - (1 - \gamma)/C_{\phi 1}]k + (-2 \overline{vw} \frac{\partial W}{\partial n} - 2 \overline{uw} \frac{\partial W}{\partial s}) C_\gamma / C_{\phi 1} (\frac{\varepsilon}{k})$$

$$+ (-4\Omega_s \overline{vw} + 4\Omega_n \overline{uw})/C_{\phi 1} (\frac{\varepsilon}{k}) \quad (47)$$

$$- \overline{uv} = C_\gamma \overline{v^2} \frac{\partial U}{\partial n}/(C_{\phi 1} \frac{\varepsilon}{k} + C_\gamma \frac{\partial U}{\partial s} + C_\gamma \frac{\partial V}{\partial n}) + (2 \Omega_n \overline{vw}$$

$$- 2 \Omega_s \overline{uw})/(C_{\phi 1} \frac{\varepsilon}{k} + C_\gamma \frac{\partial U}{\partial s} + C_\gamma \frac{\partial V}{\partial n}) \quad (48)$$

$$- \overline{uw} = C_\gamma (\overline{vw} \frac{\partial U}{\partial n} + \overline{u^2} \frac{\partial W}{\partial n})/(C_{\phi 1} \frac{\varepsilon}{k} + C_\gamma \frac{\partial U}{\partial s}) + 2(\Omega_n \overline{w^2} + \Omega_s \overline{uv}$$

$$- \Omega_n \overline{u^2})/(C_{\phi 1} \frac{\varepsilon}{k} + C_\gamma \frac{\partial U}{\partial s}) \quad (49)$$

$$- \overline{vw} = C_\gamma (\overline{v^2} \frac{\partial W}{\partial n} + \overline{uv} \frac{\partial W}{\partial s} + \overline{vw} \frac{\partial V}{\partial n})/C_{\phi 1} (\frac{\varepsilon}{k}) + 2(\Omega_s \overline{v^2} - \Omega_n \overline{uv}$$

$$- \Omega_s \overline{w^2})/C_{\phi 1} (\frac{\varepsilon}{k}) \quad (50)$$

where $C_\gamma = (1 + C_1)(1 - \gamma)$

For the coordinate system shown in Figure 3, $\Omega_s = \Omega\cos\beta$, and $\Omega_n = -\Omega\sin\beta$; hence the effect of rotation is to decrease $\overline{u^2}$ and increase $\overline{w^2}$ for negative values of $\overline{uw}$, while the negative value of $\overline{vw}$ increases the radial component of intensity ($\overline{w^2}$) and decreases the normal component of intensity ($\overline{v^2}$). These effects are reversed when the correlations are positive. The wake measurements reported by Lakshminarayana and Reynolds [34] indicate that $\overline{uw}$ is negative. Thus, the overall effect of rotation is to increase the radial intensity and decrease the streamwise intensity in a compressor rotor wake. Similar comments can be made with regard to shear stresses. Negative values of $\overline{uw}$ and $\overline{vw}$ increase the streamwise shear stress ($-\overline{uv}$) through the rotation. The radial shear stress ($-\overline{vw}$) increases when $\overline{u^2} > \overline{w^2}$ and when $\overline{uv}$ is positive. The more quantitative estimation of the rotation effect can be made on the basis of order analysis. The relative magnitudes of three intensity components are $\overline{u^2} > \overline{w^2} > \overline{v^2}$ for a non-rotating flow without curvature. The rotation-related terms in equations (45), (46), and (47) contain the term $\Omega_s/\frac{\varepsilon}{k}$ or $\Omega_n/\frac{\varepsilon}{k}$, whose order is less than 1 for the present problem. The shear stress terms are one order smaller than the intensity terms. Therefore, the rotation-related terms in equations (45), (46), and (47) are one order smaller than the intensity terms. Also, neglecting smaller coefficients in equations (45), (46), and (47), the relative magnitudes of three intensity components can be represented approximately as,

$$\frac{\overline{w^2}}{\overline{u^2}} = \frac{(\overline{w^2})_n + 4\Omega\frac{k}{\varepsilon}(-\overline{uw} - \overline{vw})}{(\overline{u^2})_n + 4\Omega\frac{k}{\varepsilon}\overline{uw}} \tag{51}$$

$$\overline{v^2} = \frac{(\overline{v^2})_n + 4\Omega\frac{k}{\varepsilon}\overline{vw}}{(\overline{u^2})_n + 4\Omega\frac{k}{\varepsilon}\overline{uw}} \tag{52}$$

where subscript n represents the value with no rotation effect.

Equation (51) shows that the relative magnitude of the radial intensity as compared to the streamwise intensity is increased by the rotation effect for the case of negative values in $\overline{uw}$ and $\overline{vw}$. On the other hand, the relative magnitude of the normal intensity as compared to the streamwise intensity does not change much due to the rotation. Therefore, the relative magnitudes of three intensity components become $\overline{u^2} \geq \overline{w^2} > \overline{v^2}$ or $\overline{w^2} \geq \overline{u^2} > \overline{v^2}$, depending on the order $\Omega\ k/\varepsilon$. Similar estimation can be drawn for the shear stress components, but the effect of rotation on them is more complex. Comparison of the data for the isolated airfoil (Hah and Lakshminarayana [52]), cascade (Raj and Lakshminarayana [53]), and rotor wakes (Lakshminarayana and Reynolds [34]) provides a confirmation of the trends predicted by the qualitative argument.

The major components of the curvature in the rotor wake were shown in Figure 2. The curvature components due to the machine radius and the variation of the flow outlet angle ($d\beta/dr$) are explicitly included in the governing equations of the present curvilinear coordinate system.

The effect of streamline curvature on the turbulence structure and the performance of various turbulence closure models for the curvature effect is explained in great detail earlier.

To represent the effect of streamline curvature more accurately with the existing second-order turbulence closure schemes, the transport equation of the rate of turbulent kinetic energy dissipation should be modified. For the calculation of the rotor wake, two different terms of the energy dissipation rate equation were used and the results will be compared. An examination of equations (40) through (44) reveals that the effect of the curvature due to the machine radius is substantial for a rotor of small radius. The curvature effect due to radial variation of the outlet angle depends on β and $d\beta/dr$. Further, this component cannot be neglected for rotors with highly twisted blades. Additionally, in the present numerical scheme, the effect of curvature due to the radius r_s in Figure 2 is implicitly included when the modified term of the transport equation is used for the rate of turbulent kinetic energy dissipation.

Closure of Turbulence for the Numerical Analysis of the Rotor Wake

Continuity and momentum conservation equations governing the flow have to be solved simultaneously to get the unknown flow quantities (three mean-velocity components and static pressure) in the rotor wake. As the mean momentum equations include the Reynolds stress terms, turbulence closure equations also should be solved to get these stress terms. With the modelled transport equations of Reynolds stresses, the six components of these stresses can be calculated if the values of the turbulent kinetic energy, the energy dissipation rate, and the mean shear rates are known at a given location of the flow field.

The transport equations for the turbulent kinetic energy and the rate of turbulent kinetic energy dissipation are

$$U^k \frac{\partial \varepsilon}{\partial x^k} = S - C_{\varepsilon 2} \frac{\varepsilon^2}{k} + C_\varepsilon \left(\frac{k}{\varepsilon} \overline{u^k u^\ell} \frac{\partial \varepsilon}{\partial x^\ell} \right)_{,k} \tag{53}$$

$$U^k \frac{\partial k}{\partial x^k} = P - \varepsilon + C_2 \left(\frac{k}{\varepsilon} \overline{u^k u^\ell} \frac{\partial k}{\partial x^\ell} \right)_{,k} \tag{54}$$

where $P = -\overline{u_i u_j} U^i_{,j}$; $C_{\varepsilon 1}$, $C_{\varepsilon 2}$, C_ε, and C_s are constants; and S is the source term of the energy dissipation equation.

The following two forms of the source term in equation (53) were used for the calculation of the rotor wake:

$$S = C_{\varepsilon 1} \frac{\varepsilon}{k} (- \overline{u_i u_j} U^i_{,j}) \tag{55}$$

and

$$S = C_\ell \frac{\varepsilon^2}{k^3} (\overline{u^i u^j} - \frac{2}{3} k \delta_{ij})(\overline{u^j u^i} - \frac{2}{3} k \delta_{ji}) \tag{56}$$

The first form of the source term, equation (55), has been widely used for the calculation of thin shear flow (Hanjalic and Launder [19], Launder, Reece, and Rodi [20], Launder and Spalding [15], and others), but is considered to be mainly responsible for the poor performance in predicting curved turbulent flow. The transport equation of the rate of turbulent kinetic energy dissipation (which is defined as the contraction of the second-order dissipation tensor $\varepsilon_{ij} = \nu \frac{\overline{\partial u_i}}{\partial x_k} \frac{\overline{\partial u_j}}{\partial x_k}$ in the Cartesian tensor) for a high Reynolds number, is as follows:

$$\begin{aligned}
\frac{\partial \varepsilon}{\partial t} + U^j \varepsilon_{,j} = & -\nu [U_{i,j} (\overline{s'^{ik} u^j_{,k}}) + U_{k,j} (\overline{s'^{ik} u^j_{,i}}) + U^i_{,j} (\overline{s'_{ik} u^{j,k}}) \\
& + \overline{U^k_{,j} (s'_{ik} u^{j,i})} - \nu [\overline{s'^{ik} u^j_{,k} u_{i,j}} + \overline{s'^{ik} u^j_{,i} u_{k,j}} \\
& + \overline{s'_{ik} u^{j,k} u^i_{,j}} + \overline{s'_{ik} u^{j,i} u^k_{,j}}] - 2\nu g^{nj} g^{\ell i} g^{mk} [\overline{s'_{ik,n} s'_{\ell m,j}} \\
& + \overline{s'_{\ell m,n} s'_{ik,j}}] - (\overline{\varepsilon u^j})_{,j} - \frac{2}{\rho} \nu g^{\ell i} g^{mk} [\overline{s'_{\ell m} p'_{,ik}} + \overline{s'_{ik} p'_{,\ell m}}] .
\end{aligned} \tag{57}$$

The above exact form of the turbulent kinetic energy dissipation equation does not include the mean strain rate. Furthermore, the use of the production of turbulent kinetic energy as the source term in equation (53) does not have any theoretical basis and is probably faulty. This point will be further discussed later. The second form of the source term, equation (53), is based on the term originally suggested by Lumley and Khajeh-Nouri [21],

$$S = (u^i u^j - \frac{2}{3} k \delta_{ij})(\overline{u^j u^i} - \frac{2}{3} k \delta_{ji}) \tag{58}$$

To make the dimension correct, additional terms were multiplied. Since the derivation of this term is based on the order estimation of equation (57) and does not include any mean strain rate, it is expected to perform better for analyzing the effect of streamline curvature.

The present turbulence closure model solves two transport equations for the turbulence kinetic energy, equation (54), the rate of turbulence dissipation, equation (53), and the mean momentum and continuity equations (29, 34-36) simultaneously. The Reynolds shear stresses and the components of intensity

are calculated through the modelled form of the transport equation of Reynolds stress (equations 39-44). This procedure thus leads to simultaneous solution of U, V, W, p, k, and ε from a coupled set of equations. The components of stresses ($\overline{u^2}$, $\overline{v^2}$, $\overline{w^2}$, $\overline{uv}$, $\overline{vw}$, $\overline{uw}$) are derived from the Reynolds stress equations (uncoupled from the main program, equations 39-44). Though this model does not include the individual effects of convection and diffusion, it does fully account for the effects of rotation and curvature. Also, the consistency of this turbulence closure model is achieved through the coefficient C_1 in equation (38). Therefore, this model is efficient for the calculation of thin shear flow under strong effects of rotation and curvature with considerably less computation time and computer storage compared to the full Reynolds stress model. The numerical values for the universal constants used in this analysis are given below (Launder et al. [20] and Pope and Whitelaw [54]). A slightly higher value of $C_{\varepsilon 1}$ resulted in a better prediction in the mean velocity as well as the turbulence quantity.

C_s	$C_{\phi 1}$	C_ε	$C_{\varepsilon 1}$	$C_{\varepsilon 2}$	γ
0.1	1.5	0.15	1.45	1.9	0.6

The value of C_ℓ in equation (56) was 1.8 for all the calculations.

Numerical Technique

Solution Scheme

The continuity and the time-mean momentum equations (29, 34-36), along with turbulence model equations, were solved elliptically. At the near wake region, the streamwise velocity gradient is of the same order of magnitude as the normal velocity gradient; hence, the conventional boundary layer calculation cannot predict this region well. According to experimental data by Raj and Lakshminarayana [1], Reynolds et al. [31], and Ravindranath and Lakshminarayana [32], the Reynolds stresses acting on the nr plane are of comparable magnitude to those on the sn or sr plane. This may be due to the effects of rotation and curvature. Thus, the parabolic marching technique cannot be used. Such strong elliptic effects in the rotating flow was also pointed out by Majumdar, Pratrap, and Spalding [30]. The pressure field was first assumed to be constant on the plane of constant r and the pressure distribution in the radial direction was assumed to be the same as that at the free stream. The pressure field was corrected at each iteration using the Poisson equation derived from the continuity equation. The procedure is similar to those used by Patankar and Spalding [35] and Briley [37], but streamwise diffusion was included in the continuity equation.

The major difference between the present numerical scheme and the so-called parabolic marching technique is that the variables downstream are included in the finite difference equations and streamwise diffusion of flow quantities are included in the numerical solution scheme.

As will be shown in the following section, the parabolic marching scheme does not predict the wake decay rate accurately compared to the elliptic scheme. This is because the parabolic marching scheme neglects the streamwise diffusion of flow quantities that is of comparable magnitude to the diffusion in the normal direction at the near wake.

Initial and Boundary Conditions

As the governing equations are solved in elliptic form, a boundary condition on the whole perimeter of domain is necessary. The computing domain extended from hub to tip, one complete passage of the wake, and two chords downstream of the trailing edge. The domain of calculation is shown in Figure 4. A, B, C, and D lie on the same cylindrical surface (the annulus wall), as do E, F, G, and H (the hub wall). The boundary curves AD and BC, and EH and FG, lie on the same cylindrical surface and make the same angles with machine axis. AB and EF are part of helix, and their lengths are the same as the spacings of the blades at each corresponding radius.

Because an elliptic scheme was used to solve the governing equations, boundary conditions were specified on all boundary surfaces (ABFE, BCGF, DCGH, ADHE, ABCD, and FGHE). Due to the nature of the rotor wake, a periodic boundary condition was applied between the planes ADHE and BCGF (the distribution of flow quantities on the surface ADHE is the same as that on the surface BDGF).

The available experimental data was used for the boundary conditions on the surfaces ABFE, DCGH, ABCD, and EFGH, and extrapolation of this data was used for the unprovided conditions on the same boundary surface. The boundary value of each dependent variable on the boundary surface was obtained from the data, except for the rate of turbulent kinetic energy dissipation. Because this rate cannot be obtained from the experimental data, it was assumed that it is equal to the production of the turbulent kinetic energy at that location. Fine mesh was used in the wake center region and no wall function was utilized.

The Grid System and the Finite-Difference Equations

The typical three-dimensional mesh used for the present numerical calculation is shown in Figure 5. The turbulent kinetic energy and the rate of dissipation were handled as diffusion terms in numerical calculation and located at the same point as the streamwise velocity component and static pressure. The turbulent Reynolds stress components are computed with the turbulent kinetic energy, the rate of dissipation, and the mean velocity gradients at given points in the present turbulence closure scheme. Therefore, the link between the mean shear rate and the Reynolds stress remains strong. Furthermore instability in numerical calculation due to the absence of such a strong link (reported by Pope and Whitelaw [54] in their calculation using full Reynolds closure scheme) was not sensed in the present calculation of rotor wake. The relative dimensions of typical three-dimensional mesh were

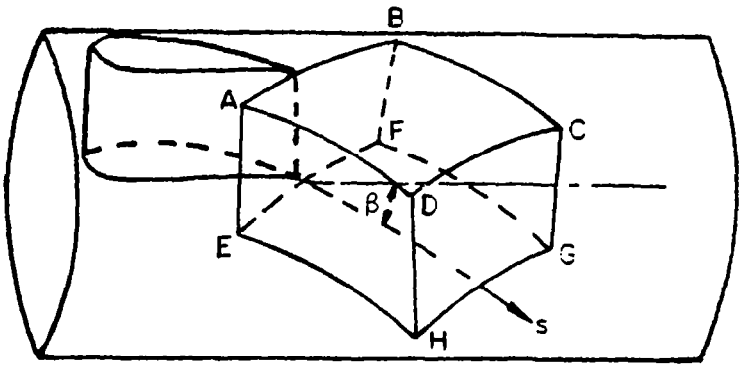

Figure 4. Calculation Domain

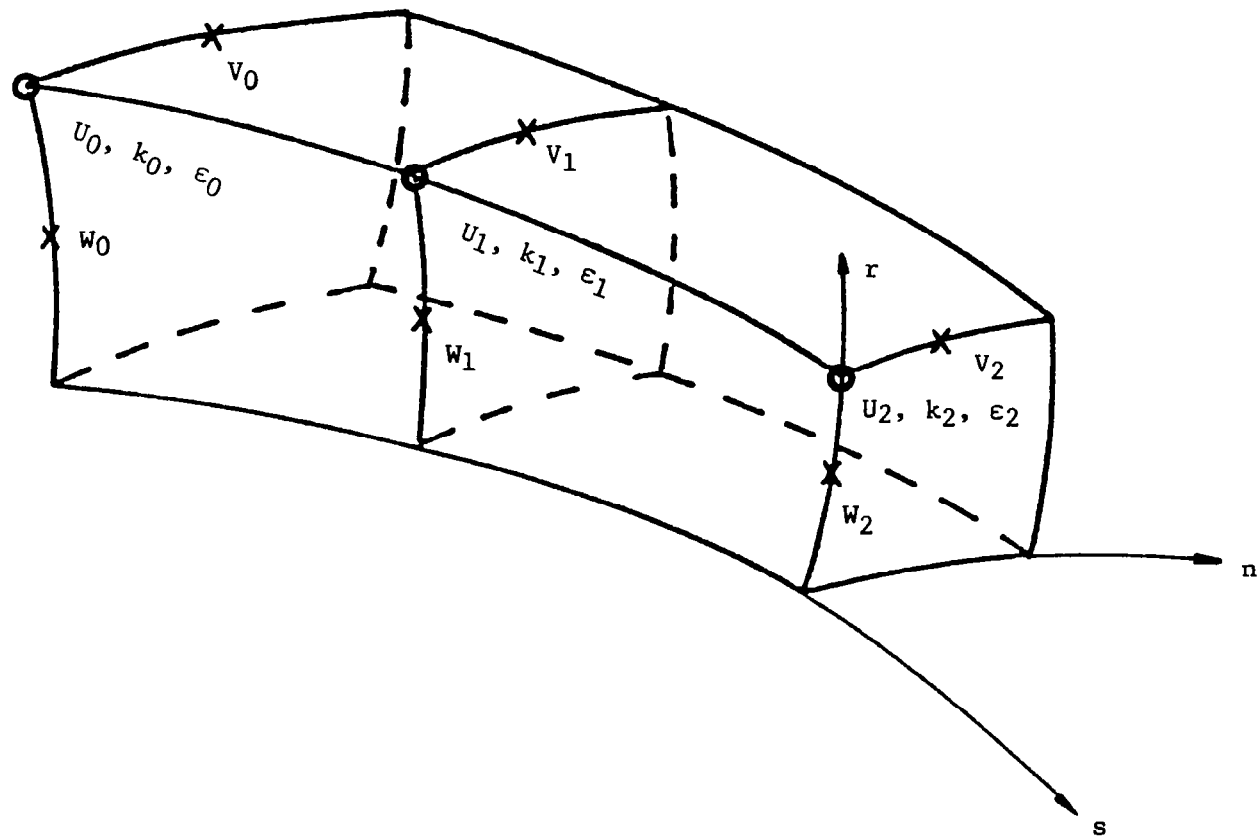

Figure 5. Typical Three-Dimensional Grid

$\Delta s/\Delta n = 1.2$, $\Delta r/\Delta n = 4$. Since the radial variation of flow quantities was mild compared to the normal and streamwise variations, relatively large distances were used between radial stations. Up to 60, 90, and 20 nodal points were used in streamwise, normal, and radial directions.

As three momentum equations are used for the calculation of three mean-velocity components, the continuity equation (29) is used to calculate the static pressure. However, since equation (29) does not include any pressure terms, it should be transformed to a more convenient form. Patankar and Spalding [35] and Briley [37] combined the momentum equations for the normal and bi-normal velocity components and the continuity equation for the static pressure. However, they did not handle the equation in its exact form and simplified the obtained Poisson equation substantially.

For the present investigation, a Poisson equation for the pressure is obtained by combining the continuity equation and the divergence of the mean momentum equations. In the rotating curvilinear coordinate system used here, the Poisson equation across the incompressible turbulent rotor wake is as follows:

$$\frac{g^{ij}}{\rho}\frac{\partial^2 p^*}{\partial x^i \partial x^j} = \nu g^{jk} U^i_{,ijk} + 2(U^1_{,1}\,U^2_{,2} + U^1_{,1}\,U^3_{,3} + U^2_{,2}\,U^3_{,3} - U^1_{,2}\,U^2_{,1} - U^1_{,3}\,U^3_{,1} - U^2_{,3}\,U^3_{,2}) - 2\,\varepsilon^{ijk}(\Omega_j\,U_k)_{,i} - \overline{u^i u^j}_{,ij} \tag{59}$$

The present rotor wake calculation in this study has neglected the viscous term in the equation (59) because the local turbulence Reynolds number is very high. The three mean momentum equations (34), (35), and (36) and Poisson equation for the pressure distribution (59) were represented in finite difference forms. All spacial derivatives were computed by second-order central differences. The velocity component part of the convection term (i.e., U^j of $U^j U^i_{;j}$) and source terms in the momentum equations were evaluated from the values of previous iteration for the convenience of the calculation.

The finite difference forms of the equations (34), (35), (36), and (59) are as follows:

$$U_{i,j,k}\frac{U_{i+1,j,k} - U_{i-1,j,k}}{2\Delta s} + \frac{V_{i,j,k} + V_{i,j+1,k}}{2} \times \frac{U_{i,j+1,k} - U_{i,j-1,k}}{2\Delta n}$$

$$+ \frac{W_{i,j,k} + W_{i,j,k+1}}{2} \times \frac{U_{i,j,k+1} - U_{i,j,k-1}}{2\Delta r} + (U_{i,j,k})^2 \times (\Gamma^1_{11})_{i,j,k}$$

$$+ \left(\frac{V_{i,j,k} + V_{i,j-1,k}}{2}\right)^2 \times (\Gamma^1_{22})_{i,j,k} + \left(\frac{W_{i,j,k} + W_{i,j,k+1}}{2}\right)^2 \times (\Gamma^1_{33})_{i,j,k}$$

$$+ 2\, U_{i,j,k} \times \left(\frac{W_{i,j,k} + W_{i,j,k+1}}{2}\right) \times (\Gamma^1_{13})_{i,j,k} + 2\, U_{i,j,k}$$

$$\times \left(\frac{V_{i,j,k} + V_{i,j-1,k}}{2}\right) \times (\Gamma^1_{1})_{i,j,k} + 2 \left(\frac{V_{i,j,k} + V_{i,j-1,k}}{2}\right)$$

$$\times \left(\frac{W_{i,j,k} + W_{i,j,k+1}}{2}\right) \times (\Gamma^1_{23})_{i,j,k} - 2\, \Omega(\sin\beta)_{i,j,k} \left(\frac{W^*_{i,j,k} + W^*_{k,j,k+1}}{2}\right) =$$

$$- \frac{1}{\rho}\Big[g^{11}_{i,j,k} \frac{P^*_{k+1,j,k} - P^*_{i-1,j,k}}{2\Delta s} + g^{12}_{k,j,k} \frac{P^*_{i,j+1,k} - P^*_{i,j-1,k}}{2\Delta n}$$

$$+ g^{13}_{k,j,k} \frac{P^*_{i,j,k+1} - P^*_{i,j,k-1}}{2\Delta r} - \frac{\overline{u^2}_{i+1,j,k} - \overline{u^2}_{i-1,j,k}}{2\Delta s} - \frac{\overline{uv}_{i,j+1,k} - \overline{uv}_{i,j-1,k}}{2\Delta n}$$

$$- \frac{\overline{uw}_{i,j,k+1} - \overline{uw}_{i,j,k-1}}{2\Delta r} \qquad (60)$$

$$\frac{V_{i+1,j,k} + V_{i+1,j-1,k} - V_{i-1,j,k} - V_{i-1,j-1,k}}{4\Delta s} + \frac{V_{i,j,k} + V_{i,j-1,k}}{2}$$

$$\times \frac{V_{i,j,k} - V_{i,j-1,k}}{\Delta n} + \frac{V_{i,j,k} + V_{i,j-1,k+1} - V_{i,j,k-1} - V_{i,j-1,k-1}}{4\Delta r}$$

$$\times \frac{W_{i,j,k} + W_{i,j,k+1}}{2} + U^2_{i,j,k} \times (\Gamma^2_{11})_{i,j,k} + \left(\frac{W_{i,j,k} + W_{i,j,k+1}}{2}\right)^2 \times (\Gamma^2_{33})_{i,j,k}$$

$$+ \left(\frac{V_{i,j,k} + V_{i,j-1,k}}{2}\right)^2 (\Gamma^2_{22})_{i,j,k} + 2\, U_{i,j,k} \times \left(\frac{W_{i,j,k} + W_{i,j,k+1}}{2}\right)$$

$$\times (\Gamma^2_{13})_{i,j,k} + \left(\frac{V_{i,j,k} + V_{i,j-1,k}}{2}\right)^2 \times (\Gamma^2_{22})_{i,j,k} + 2\, U_{,j,k}$$

$$x \left(\frac{V_{i,j,k} + V_{i,j-1,k}}{2}\right) x \left(\Gamma^2_{12}\right)_{i,j,k} - 2\,\Omega \left(\frac{W^*_{i,j,k} + W^*_{i,j,k+1}}{2}\right)\cos\beta_{i,j,k}$$

$$= -\frac{1}{\rho}\left[g^{21}_{i,j,k}\,\frac{P^*_{i+1,j,k} - P^*_{i-1,j,k}}{2\Delta s} + g^{22}_{i,j,k}\,\frac{P^*_{i,j+1,k} - P^*_{i,j-1,k}}{2\Delta n}\right.$$

$$\left. + g^{23}_{i,j,k}\,\frac{P^*_{i,j,k+1} - P^*_{i,j,k-1}}{2\Delta r}\right] - \frac{\overline{uv}_{i+1,j,k} - \overline{uv}_{i-1,j,k}}{2\Delta s}$$

$$- \frac{\overline{v^2}_{i,j+1,k} - \overline{v^2}_{i,j-1,k}}{2\Delta n} - \frac{\overline{vw}_{i,j,k+1} - \overline{vw}_{i,j,k-1}}{2\Delta r} \qquad (61)$$

$$U_{i,j,k}\,\frac{W_{i+1,j,k} + W_{i+1,j,k+1} - W_{i-1,j,k} - W_{i-1,k,k+1}}{4\Delta s} + \left(\frac{V_{i,j,k} + V_{i,j-1,k}}{2}\right) x$$

$$\left(\frac{W_{i,j+1,k} + W_{i,j+1,k+1} - W_{i,j-1,k} - W_{i,j-1,k+1}}{4\Delta n}\right) + \left(\frac{W_{i,j,k} + W_{i,j,k+1}}{2}\right) x$$

$$\frac{W_{i,j,k+1} - W_{i,j,k}}{\Delta r} + \left(\frac{W_{i,j,k} - W_{i,j,k+1}}{2}\right)^2 x \left(\Gamma^3_{33}\right)_{i,j,k}$$

$$+ 2U_{i,j,k} \left(\frac{W_{i,j,k} + W_{i,j,k+1}}{2}\right) x \left(\Gamma^3_{13}\right)_{i,j,k} + U^2_{i,j,k} \left(\Gamma^3_{11}\right)_{i,j,k}$$

$$+ \left(\frac{V_{i,j,k} + V_{i,j-1,k}}{2}\right)^2 x \left(\Gamma^3_{22}\right)_{i,j,k} + 2\,U_{i,j,k} \left(\frac{V_{i,j,k} + V_{i,j-1,k}}{2}\right) x$$

$$\left(\Gamma^3_{12}\right)_{i,j,k} + 2 \left(\frac{V_{i,j,k} + V_{i,j-1,k}}{2}\right) x \left(\frac{W_{i,j,k} + W_{i,j,k+1}}{2}\right) x \left(\Gamma^3_{23}\right)_{i,j,k}$$

$$+ 2\,\Omega\, x \left(\frac{V^*_{i,j,k} + V^*_{i,j-1,k}}{2}\right) \cos\beta_{i,j,k} + 2\,U^*_{i,j,k}\,\Omega\, x\, \sin\beta_{i,j,k} =$$

$$- \frac{1}{\rho}\Big[g^{31}_{i,j,k}\,\frac{P^*_{i+1,j,k} - P^*_{i-1,j,k}}{2\Delta s} + g^{32}_{i,j,k}\,\frac{P^*_{i,j+1,k} - P^*_{i,j-1,k}}{2\Delta n}$$

$$+ g^{33}_{i,j,k}\,\frac{P^*_{i,j,k+1} - P^*_{i,j,k-1}}{2\Delta r}\Big] - \frac{\overline{uw}_{i+1,j,k} - \overline{uw}_{i-1,j,k}}{2\Delta s}$$

$$- \frac{\overline{vw}_{i,j+1,k} - \overline{vw}_{i,j-1,k}}{2\Delta n} - \frac{\overline{W^2}_{i,j,k+1} - \overline{W^2}_{i,j,k-1}}{2\Delta v} - \overline{U^2}_{i,j,k}\,\Gamma^1_{11}$$

$$- \overline{uv}_{i,j,k}\,(\Gamma^3_{12})_{i,j,k} \qquad (62)$$

$$\frac{g^{11}_{ijk}}{\rho}\,\frac{P^*_{i+1,j,k} - P^*_{i-1,j,k}}{2\Delta s} + \frac{g^{22}_{i,j,k}}{\rho}\,\frac{P^*_{i,j+1,k} - P^*_{i,j-1,k}}{2\Delta n}$$

$$+ \frac{g^{33}_{i,j,k}}{\rho}\,\frac{P^*_{i,j,k+1} - P^*_{i,j,k-1}}{2\Delta r}$$

$$+ \frac{g^{12}_{i,j,k}}{\rho}\,\frac{P^*_{i+1,j+1,k} + P^*_{i-1,j-1,k} - P^*_{i+1,j-1,k} - P^*_{i-1,j+1,k}}{\Delta s \Delta n}$$

$$+ \frac{g^{13}_{i,j,k}}{\rho}\,\frac{P^*_{i+1,j,k+1} + P^*_{i-1,j,k-1} - P^*_{i+1,j,k-1} - P^*_{i-1,j,k+1}}{2\Delta s \Delta r}$$

$$+ \frac{g^{23}_{i,j,k}}{\rho}\,\frac{P^*_{i,j+1,k+1} + P^*_{i,j-1,k-1} - P^*_{i,j+1,k-1} - P^*_{i,j-1,k+1}}{2\Delta n \Delta r}$$

$$= 2\,(G11 \times G22 + G11 \times G33 + G22 \times G33 - G12 \times G21 - G13 \times G31$$

$$- G23 \times G32)$$

$$- \Omega\,\frac{(-W^*_{i+1,j,k} + W^*_{i-1,j,k})\,\sin\beta_{i,j,k}}{\Delta s} + \Omega\,\frac{(-U^*_{i,j,k+1} + U^*_{i,j,k-1})\sin\beta_{i,j,k}}{\Delta r}$$

$$- \Omega \frac{(V^*_{i,j,k+1} - V^*_{i,j,k-1}) \cos\beta_{i,j,k}}{\Delta r}$$

$$- \frac{\overline{u^2}_{i+1,j,k} + \overline{u^2}_{i-1,j,k} - 2\,\overline{u^2}_{k,j,k}}{\Delta sx\Delta s} - \frac{\overline{v^2}_{i,j+1,k} + \overline{v^2}_{i,j-1,k} - 2\,\overline{v^2}_{i,j,k}}{\Delta nx\Delta n}$$

$$- \frac{\overline{w^2}_{i,j,k+1} + \overline{w^2}_{i,j,k-1} - 2\,\overline{w^2}_{i,j,k}}{\Delta rx\Delta r}$$

$$- \frac{\overline{uv}_{i+1,j+1,k} + \overline{uv}_{i-1,j-1,k} - \overline{uv}_{i+1,j-1,k} - \overline{uv}_{i-1,j+1,k}}{2\Delta sx\Delta n}$$

$$- \frac{\overline{uw}_{i+1,j,k+1} + \overline{uw}_{i-1,j,k-1} - \overline{uw}_{i+1,j,k-1} - \overline{uw}_{i-1,j,k+1}}{2\Delta sx\Delta r}$$

$$- \frac{\overline{vw}_{i,j+1,k+1} + \overline{vw}_{i,j-1,k-1} - \overline{vw}_{i,j+1,k-1} - \overline{vw}_{i,j-1,k+1}}{2\Delta nx\Delta r} \qquad (63)$$

where $G11 = U^1_{,1} = \frac{\partial U}{\partial s} + U\Gamma^1_{11} + V\,\Gamma^1_{12} + W\Gamma^1_{13}$

and generally $Gij = U^i_{,j} = \frac{\partial u^i}{\partial n^i} + U^k\Gamma^i_{jk}$

Sequence of Calculation, Stability, and Accuracy

The flow chart of numerical calculation is shown in Figure 6. The following steps were used for the calculation.

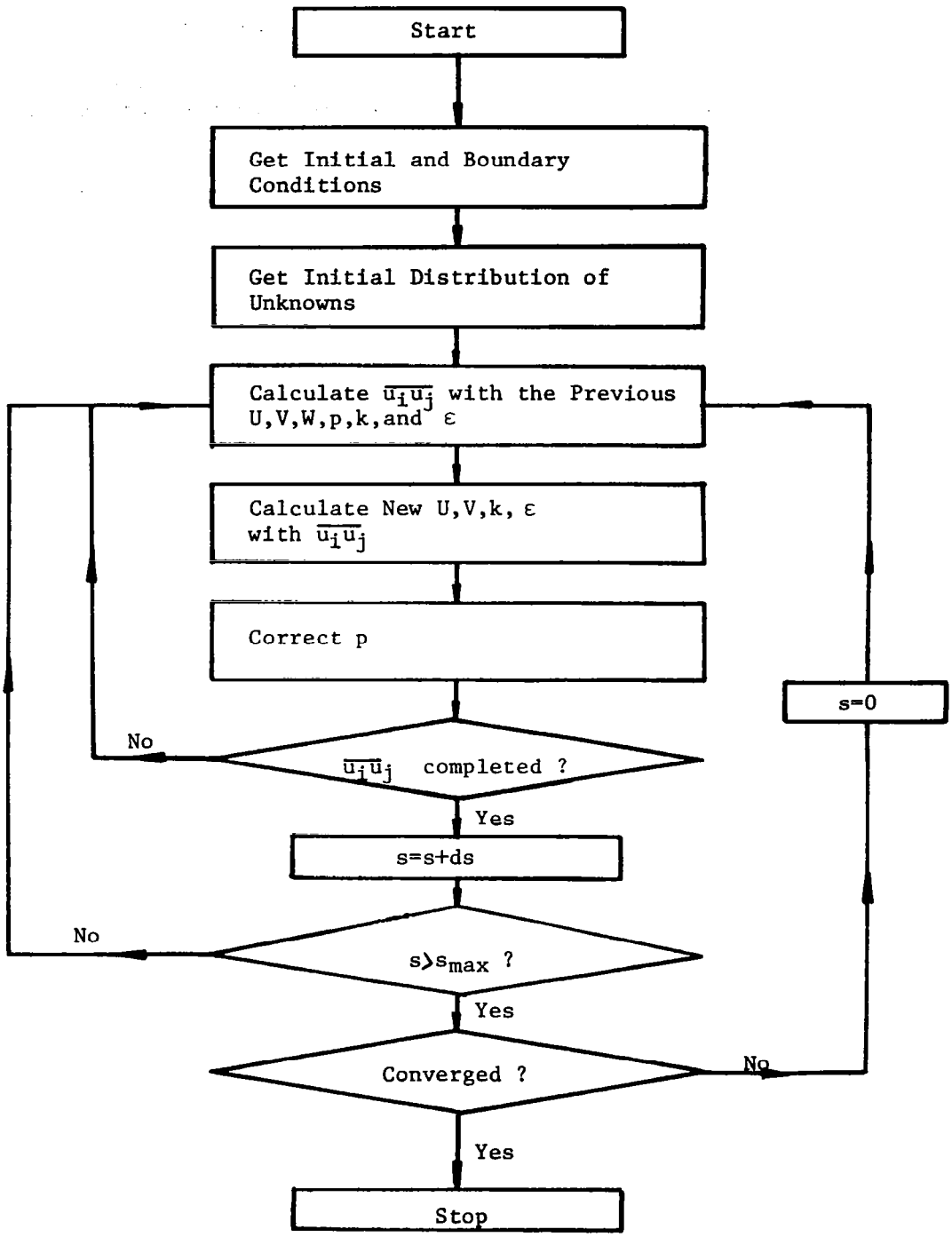

Figure 6. Flow Chart of Rotor Wake Code

1. The initial distribution of unknown variables were obtained by downstreamwise parabolic marching with the given boundary conditions.

2. At each new iteration, the Reynolds stress components were computed with the equations (39) through (44) using the previous values of mean velocity, turbulent kinetic energy, and the rate of turbulent kinetic energy dissipation.

3. Using the computed Reynolds stress and previous static pressure distribution, the momentum equations and two transport equations for the turbulent energy and the rate of dissipation were calculated for the new values of the three mean-velocity components and the turbulent kinetic energy and the rate of dissipation.

4. New static pressure distribution was obtained using the newly obtained mean velocity components and the Reynolds stress components.

5. The Reynolds stress components were newly evaluated using the new values of the mean velocity components, the turbulent kinetic energy, and the rate of turbulent kinetic energy dissipation; steps 3 and 4 were repeated.

6. The above steps 2-5 were repeated downstreamwise for the whole flow field. Since the governing equations are solved in elliptic form, the values of dependent variables on the $(i-1)$th, 1-th, and $(1+1)$th streamwise stations are used to calculate new values of dependent variables at i-th streamwise station.

7. Whenever the whole flow field is newly iterated, the convergence criteria is tested and if not converged, the whole domain is reiterated.

The algebraic equations obtained during the numerical steps were solved by SOR. Since the present numerical scheme adopts implicit finite-difference simulation of the governing equation, no specific source of instability is considered.

Because three-dimensional storage is needed for the elliptic calculation, the required memory size was up to 800 K words, which exceeds the available computer main core storage. Therefore, an auxiliary memory system was utilized for the calculation.

The computing time per each iteration of the entire field was up to four minutes using the IBM 370/3033 at The Pennsylvania State University.

In Figure 7, the calculated decay rate of wake center streamwise velocity is shown at various iterations for the rotor wake data by Ravindranath and Lakshminarayana [32]. The results in this figure show that the numerical scheme gives uniform convergence, and no oscillation is observed.

For all the calculations reported, the following criterion was used to determine the convergence of calculation:

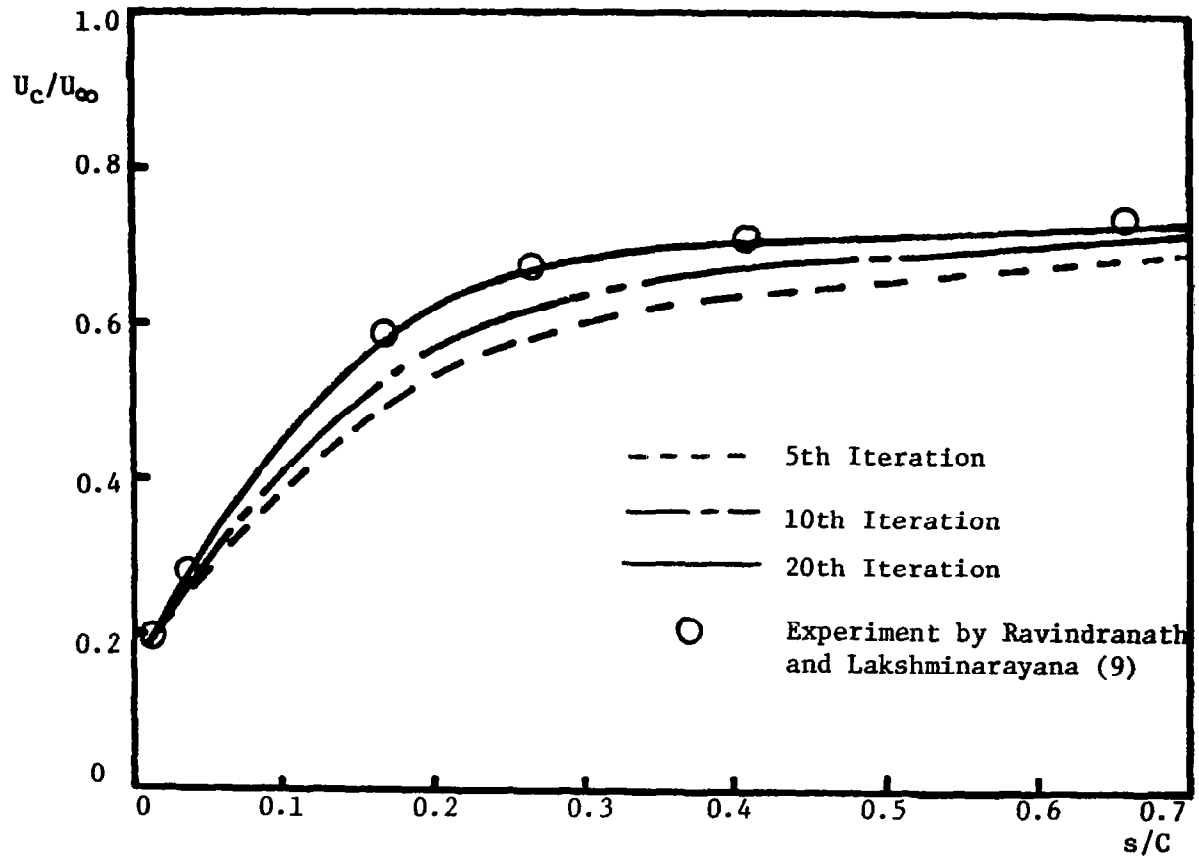

Figure 7. Wake centerline Velocity Prediction at Different Iterations

$$\sum_{i=1}^{N} \left| \frac{(U_c)_i^{n+1} - (U_c)_i^n}{(U_c)_i^n} \right| \leq 0.007 \qquad (64)$$

Where U_c = wake center streamwise velocity, subscript i = the value at i-th streamwise station, and superscript n = the value at n-th iteration. For most calculations, the convergence with the above criterion was achieved at the iterations around 20. To check the numerical behavior of computation, the streamwise mesh size was halved and the same calculation was done. With the smaller mesh size, the convergence was achieved around 14 iterations and no overall computing time was reduced. Comparisons between the numerical results and experimental data show that the convergence criteria (equation 64) provides a sufficiently accurate solution.

Table 1. Relevant Data on the Compressor and the Operating Conditions

	Raj and Lakshminarayana [1]	Reynolds et al. [31]	Ravindranath and Lakshminarayana [32]
hub/tip	0.44	0.44	0.5
R.P.M.	1010	1010	1066
number of blade	12	12	21
blade shape	symmetric	symmetric	cambered
ratio of blade chord (C) to spacing (S) at mid-radius	0.68	0.68	0.6
tip radius	0.27 m	0.27 m	0.46 m
incidence at mid-radius	0°	10°, 15°	7°
stagger angle at mid-radius	45°	45°	30°
drag coefficient (C_D) at mid-radius	0.0055	0.011	0.0116
lift coefficient (C_L) at mid-radius	0.028	0.5	0.88
experimental technique	stationary tri-axial hot wire probe	stationary tri-axial hot wire probe	rotating hot-wire probe & static pressure tube
radial stations at which measurements was taken (r/r_t)	0.488, 0.536, 0.581, 0.6281, 0.72, 0.966, 0.815 0.86	0.465, 0.535, 0.629, 0.721, 0.814, 0.860, 0.907	0.5676, 0.6581, 0.7297, 0.7973, 0.8615, 0.9329, 0.9595

COMPARISON BETWEEN ROTOR WAKE DATA AND NUMERICAL PREDICTIONS

Rotor Wake Data and Predictions with the Present Turbulence Closure Model

The present turbulence closure model and numerical scheme were used to predict turbomachinery rotor wakes, utilizing the energy dissipation equation with the conventional source term, equation (55). The results of the calculations using this equation including the modified source term equation (56), will be discussed in the following section.

Three different sets of experimental data of the rotor wake were compared with the numerical predictions. Some relevant data on the compressor and the operating conditions are given in Table 1.

For the present investigation, the hub wall and annulus wall regions, where no experimental data or flow model were available, were not considered. The boundary surfaces ABCD and EFGH in Figure 4 were cylindrical surfaces closest to the hub and annulus walls where measurements were taken. The inlet boundary surface ABFE and outlet boundary surface DCGH were the surfaces closest and farthest, respectively, from the trailing edge of the blade where measurements were made. For all three sets of experimental data, the distance between the blade trailing edge and the inlet boundary surface was less than 1/50 chord length of the blade. The outlet boundary surface was located about 2 chords downstream.

For elliptic calculation, the inlet boundary condition specified on ABFE, and the boundary conditions on ABCD, EFGH, and DCGH, were based on experimental data. Due to the nature of the flow field around rotor blades, a periodic boundary condition was specified on ADHE and BCGF. Fourth-order power laws were used for the representation of measured flow quantities to avoid the effect of scatter in the experimental data on the calculation.

Comparison Between the Numerical Predictions and the Rotor Wake Data by Raj and Lakshminarayana [1]

The comparison between the numerical predictions in this thesis and experimental data by Raj and Lakshminarayana [1] is made for the measurements at $r/r_t = 0.58$. Since the experimental data do not include the static pressure distribution, the static pressure was assumed to be constant and radial variation of the reduced static pressure due to the centrifugal force was considered during the calculation. Comparison between the predictions and the experimental data for three mean-velocity components are shown in Figure 8. The streamwise velocity component U, the normal velocity component V, and the radial velocity component W are normalized by U_∞. The turbulence intensity and Reynolds stress are plotted in Figures 9, 10, and 11, respectively. In these figures, s is the distance from the trailing edge and n is the distance from the wake center. n = s = 0 represents the blade trailing edge and S is the blade spacing. The prediction is quite accurate for the streamwise component of the mean velocity. The discrepancy in the normal velocity component may be due to inaccurate information on the boundary condition or scatter in the experimental data.

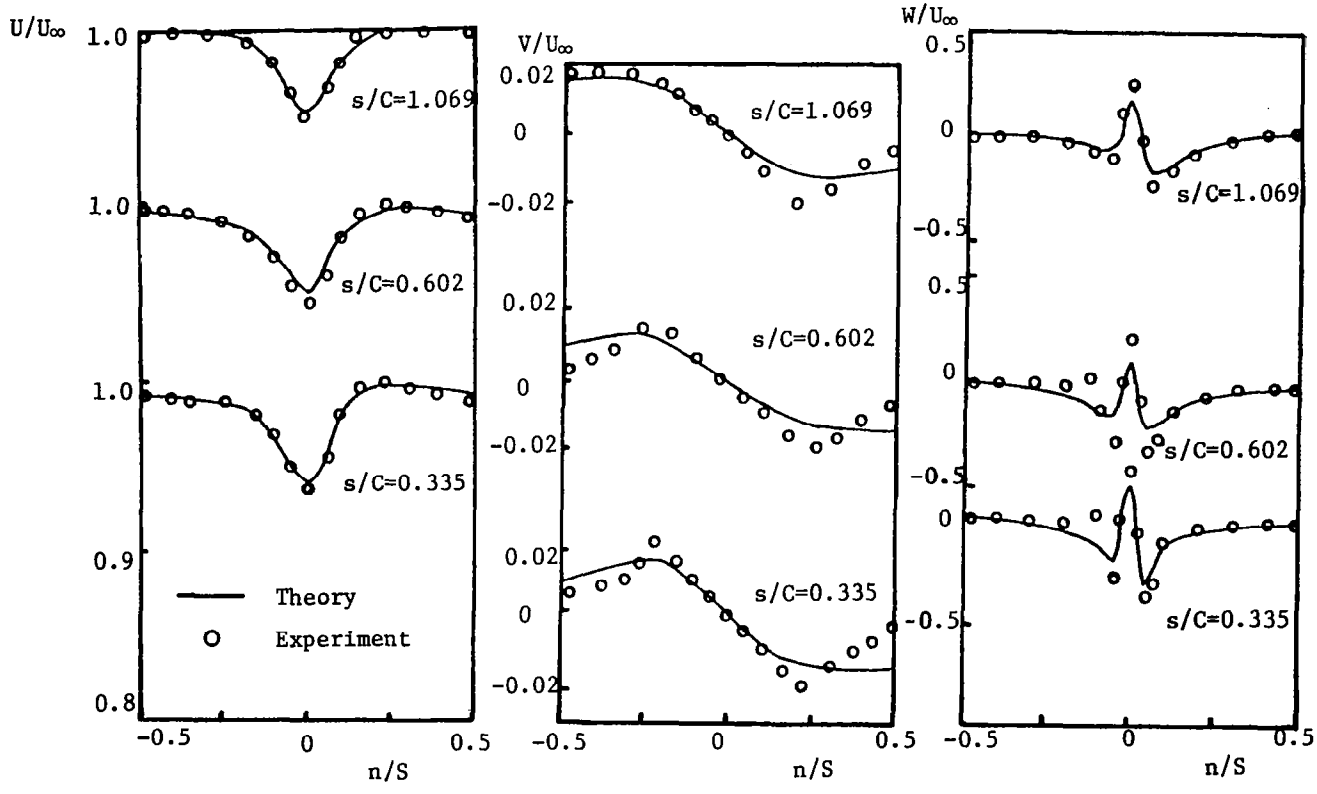

Figure 8. Profiles of Mean Velocity Components at $r/r_t=0.58$
(Data of Raj and Lakshminarayana, [9]

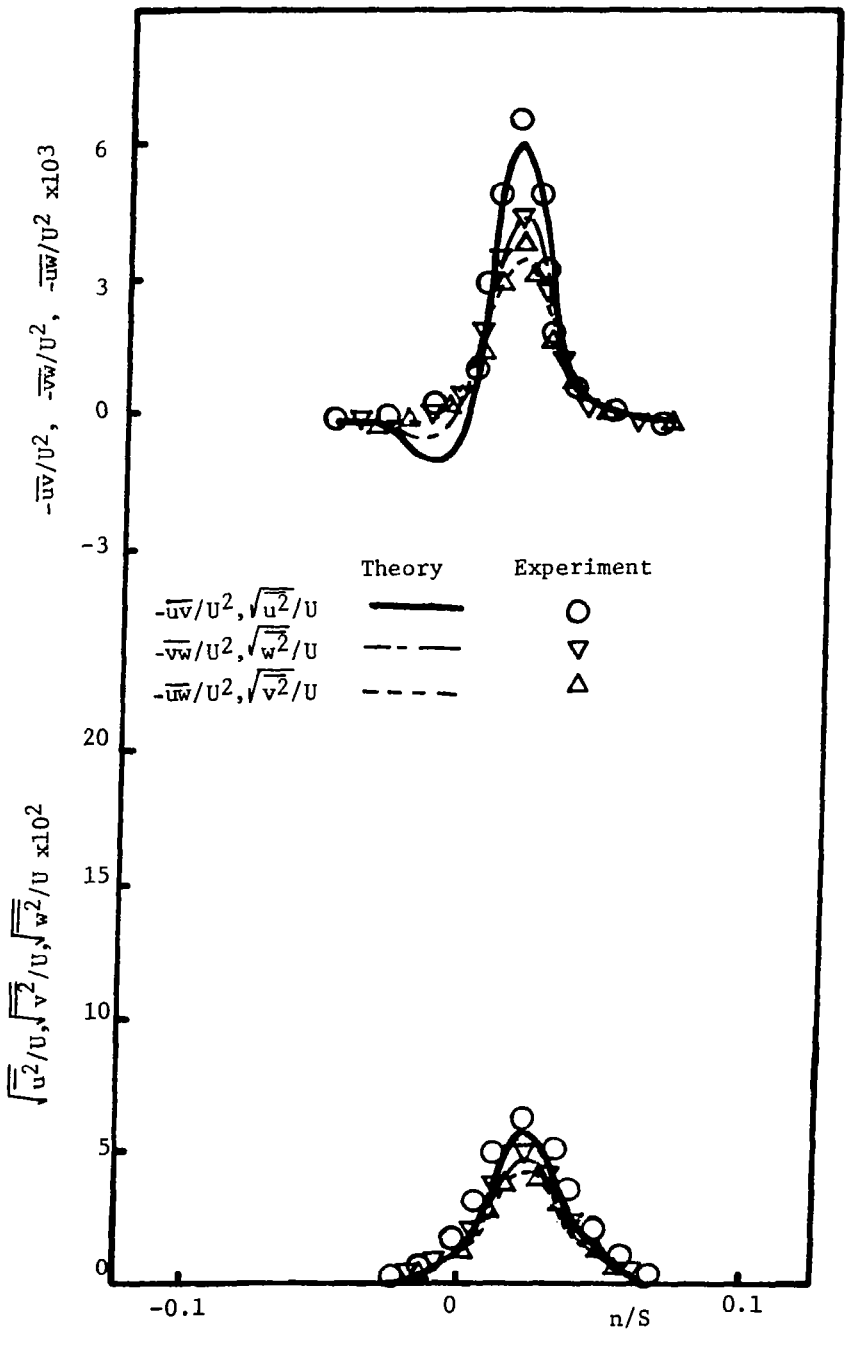

Figure 9. Reynolds Stress at r/r_t=0.58 and s/C=0.335 (Data of Raj and Lakshminarayana, [9]

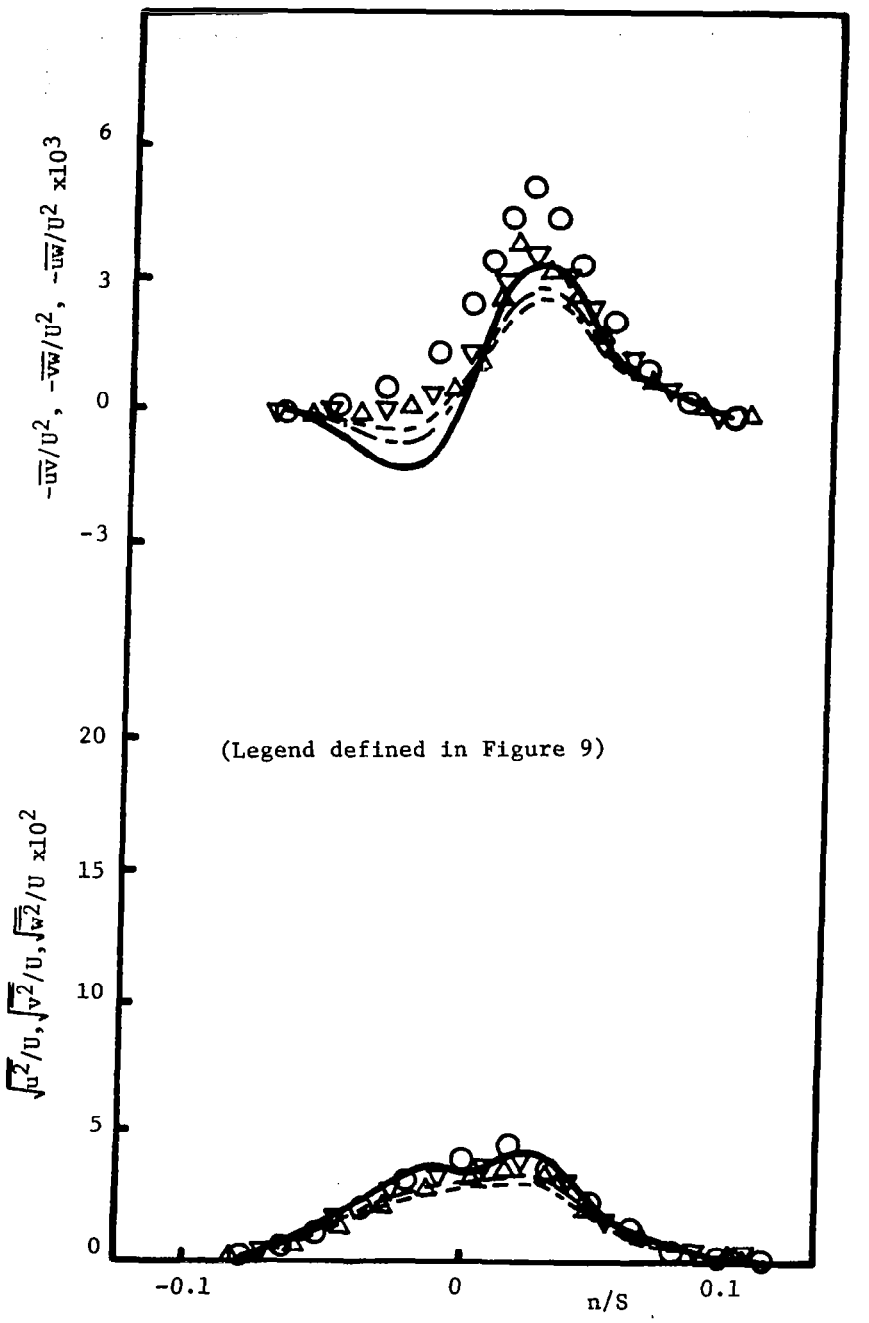

Figure 10. Reynolds Stress at r/r_t=0.58 and s/C=0.602 (Data of Raj and Lakshminarayana, [9]

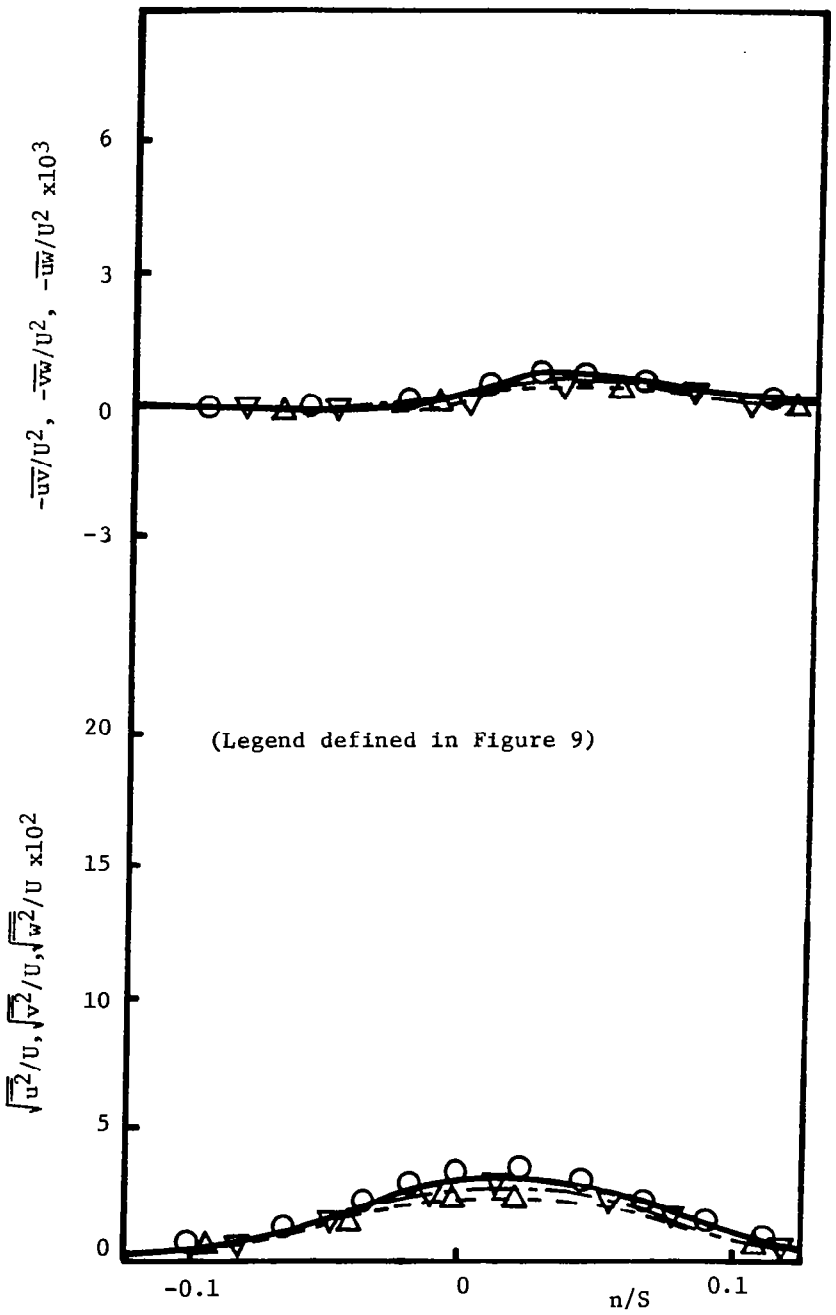

Figure 11. Reynolds Stress at r/r_t=0.58 and s/C=1.069 (Data of Raj and Lakshminarayana, [9]

The prediction of the radial velocity component shows slower decay of velocity peaks than the experimental data. This may be due to improper turbulence closure modelling or experimental error due to the finite distance between the tri-axial probe wires. The prediction of the turbulence intensity shows good agreement with the experimental data, while the prediction for the Reynolds shear stress shows considerable deviation from the reported results. The discrepancy in the Reynolds shear stress also may be due to scatter in the experimental data which were obtained with the stationary tri-axial hot-wire technique. However, overall agreement between the numerical prediction and the experimental data are quite satisfactory if the complexity of the flow field is considered.

The typical distribution of the rate of turbulent kinetic energy dissipation across the wake is shown in Figure 12.

Comparison Between the Numerical Predictions and the Rotor Wake Data by Reynolds et al. [31]

The second set of data for the comparison were obtained from Reynolds et al. [31]. They measured the wake in the same compressor as Raj and Lakshminarayana [1], but the rotor was operated with higher blade loadings. Here again, the experimental data did not include the static pressure distribution of the whole flow field, and this pressure was assumed to be constant. The radial variation of the reduced static pressure due to centrifugal force was considered during the calculation.

Comparisons of the mean-velocity, turbulence-intensity, and shear-stress profiles at various axial locations and $r/r_t = 0.72$ are shown in Figures 13 through 16. Streamwise velocity components were accurately predicted for both incidence angles. Even though some minor disagreements existed between the prediction and the experimental data, the radial and normal velocity components were well predicted. The experimental data showed that the peaks in the radial velocity distribution become wider and smaller with the increase of the incidence angle, this trend is well predicted by the numerical calculations. For the present sets of data ($i = 10°, 15°$), the boundary layers at the blade trailing edge are thicker than those of the data in the previous section ($i = 0°$), and the effects of rotation and streamline curvature are substantial compared to the first example. According to the qualitative analysis on the effect of rotation, the radial turbulence intensity is increased due to the rotation, and this is nearly equal to the streamwise intensity for the present experimental data. Again, this trend is more than adequately or, "successfully predicted" by the numerical calculations. Therefore, the present method can fully account for the rotation effect through the modelling of the Reynolds stress equation in the rotating curvilinear coordinate system. The typical distributions of the rate of turbulent kinetic energy distribution are shown in Figure 17 for the incidence angles of 10° and 15°.

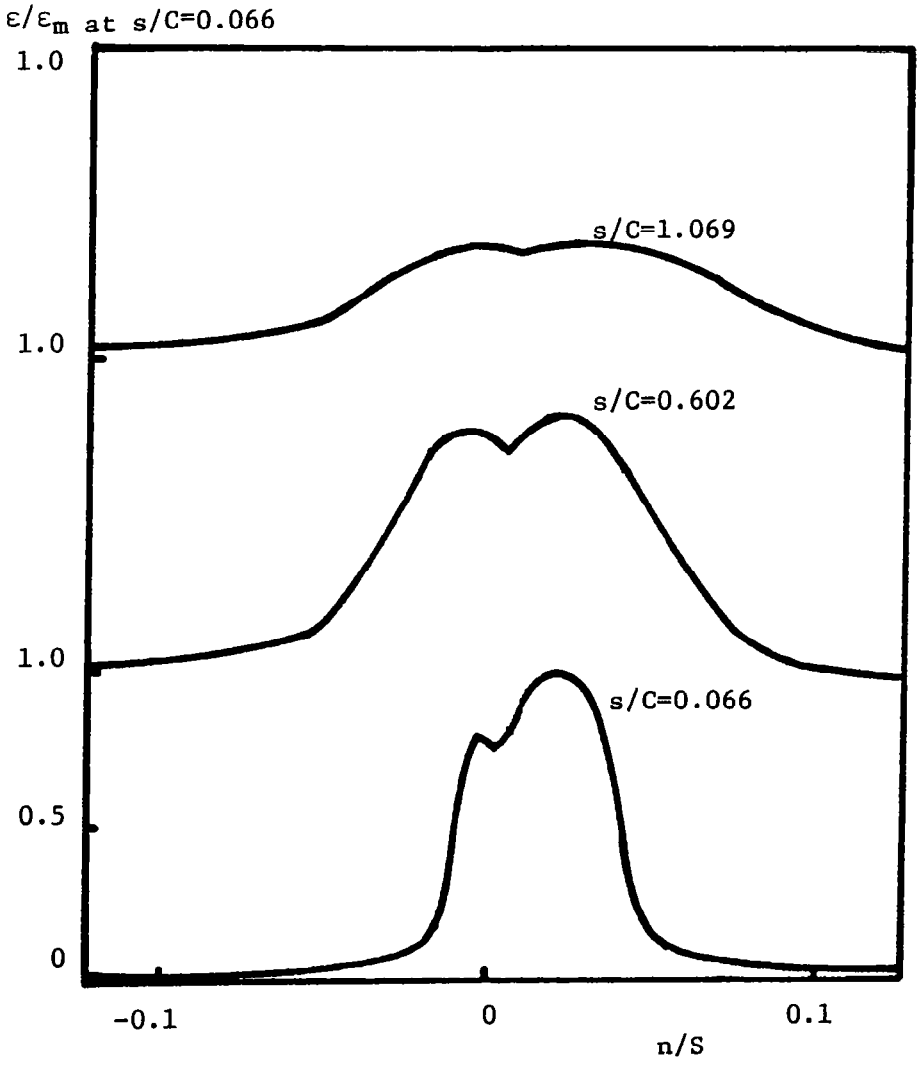

Figure 12. Energy Dissipation Rate at r/r_t=0.58

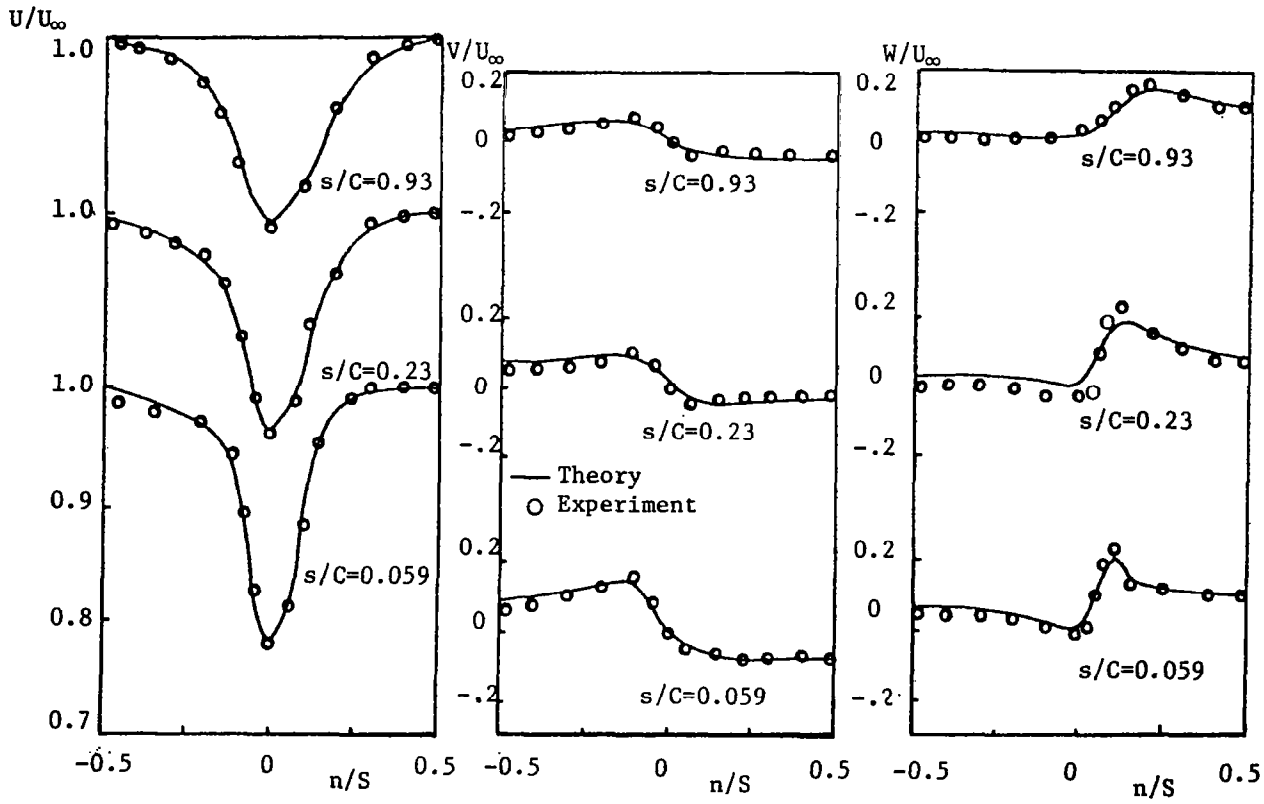

Figure 13(a). Profiles of Mean Velocity Components at $r/r_t=0.72$ and $i=10^o$ (Data of Reynolds et al., [31])

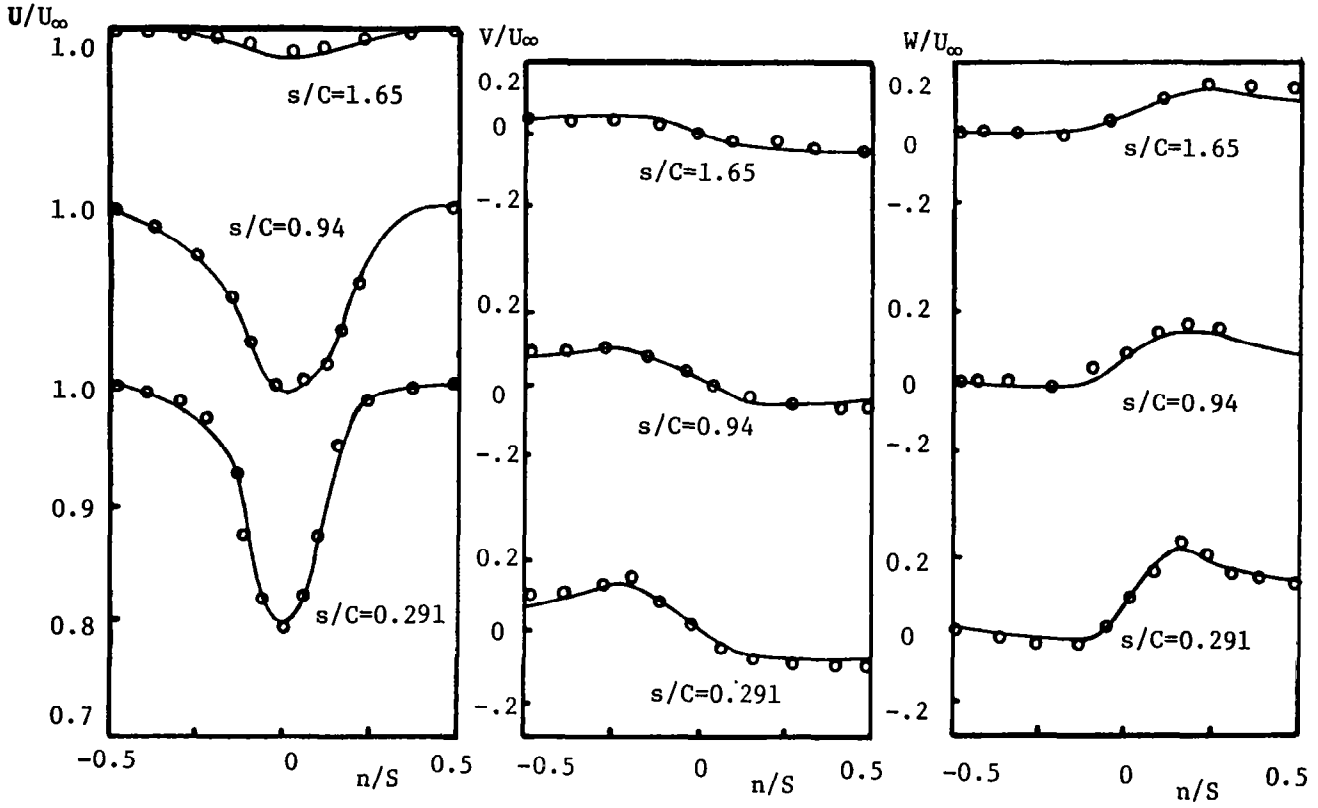

Figure 13(b). Profiles of Mean Velocity Components at $r/r_t=0.72$ and $i=15°$ (Data of Reynolds et al., [31])

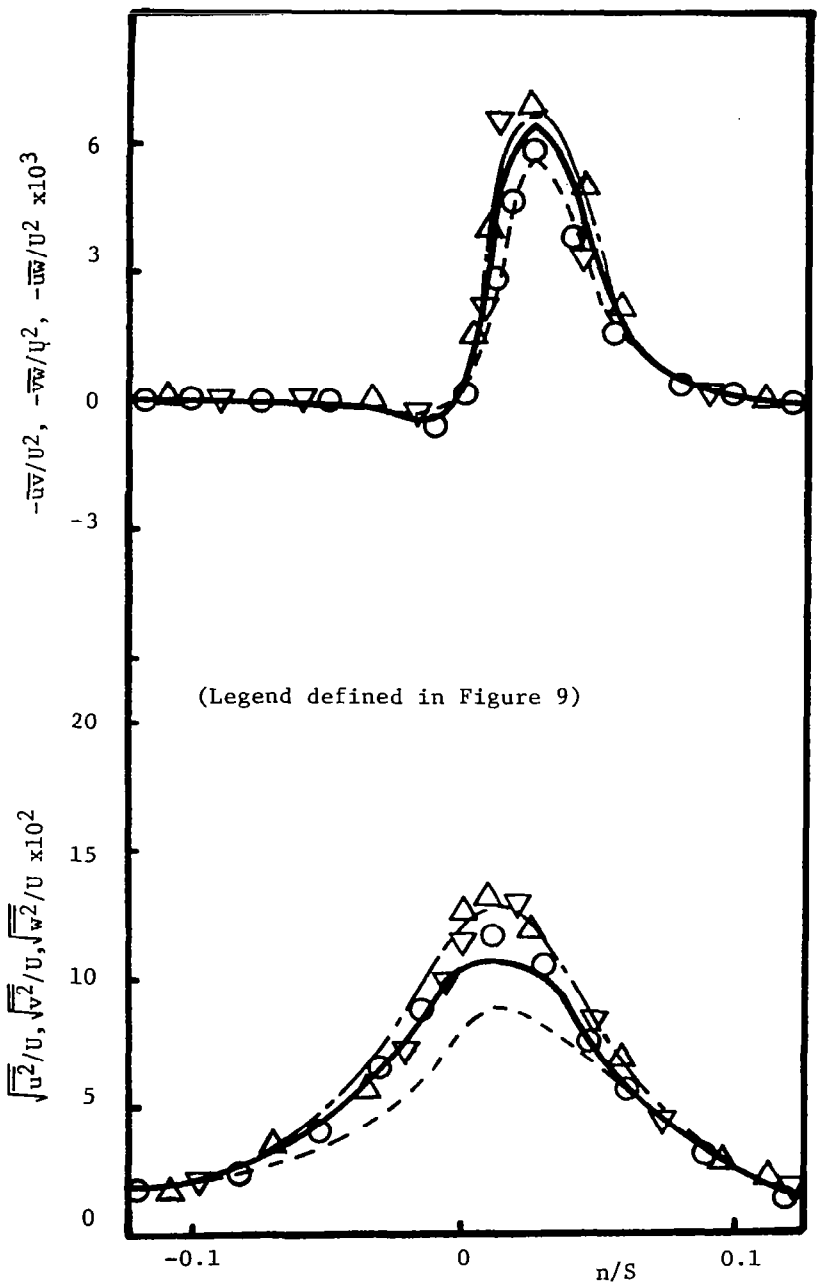

Figure 14(a). Reynolds Stress at r/r_t=0.72, s/C=0.059 and i=10° (Data of Reynolds et al., [31])

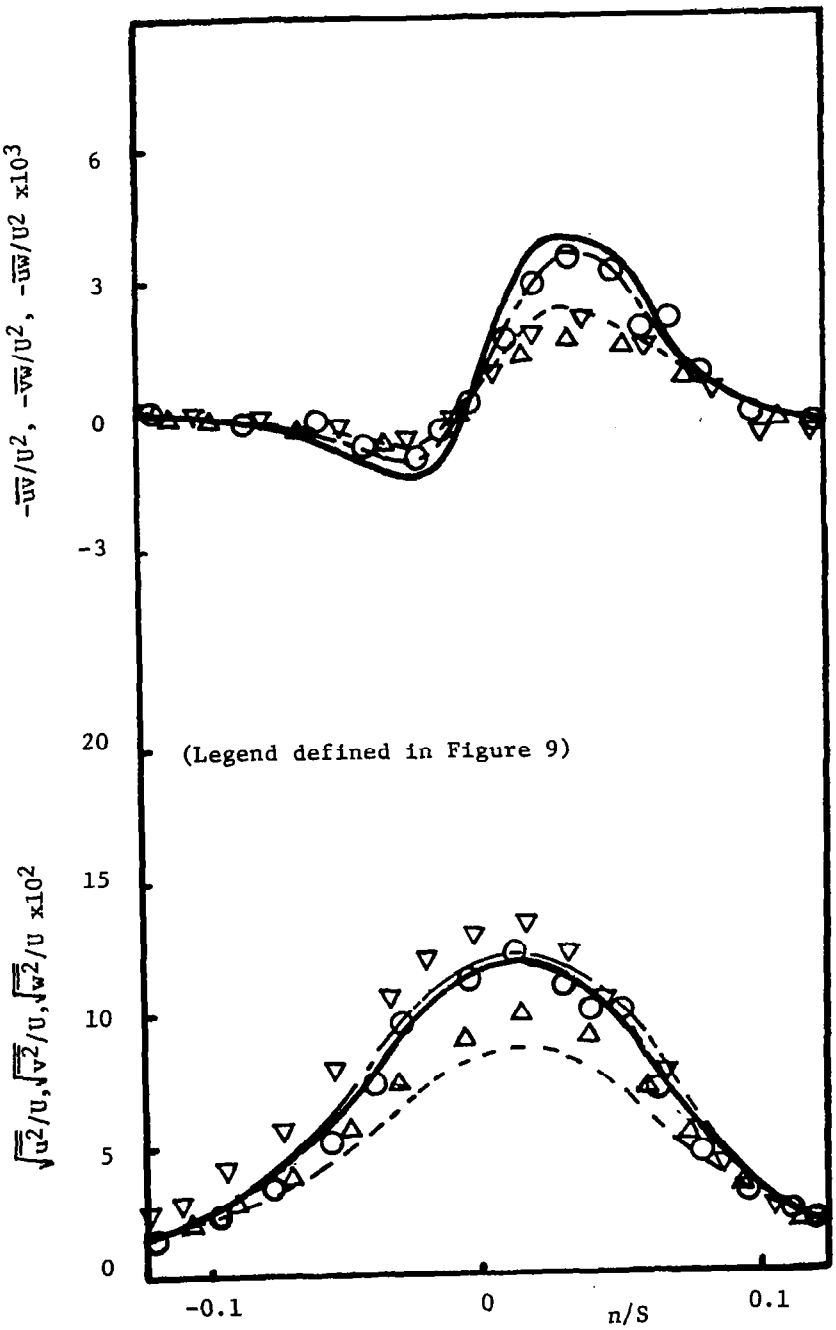

Figure 14(b). Reynolds Stress at r/r_t=0.72, s/C=0.291 and i=15° (Data of Reynolds et al., [31])

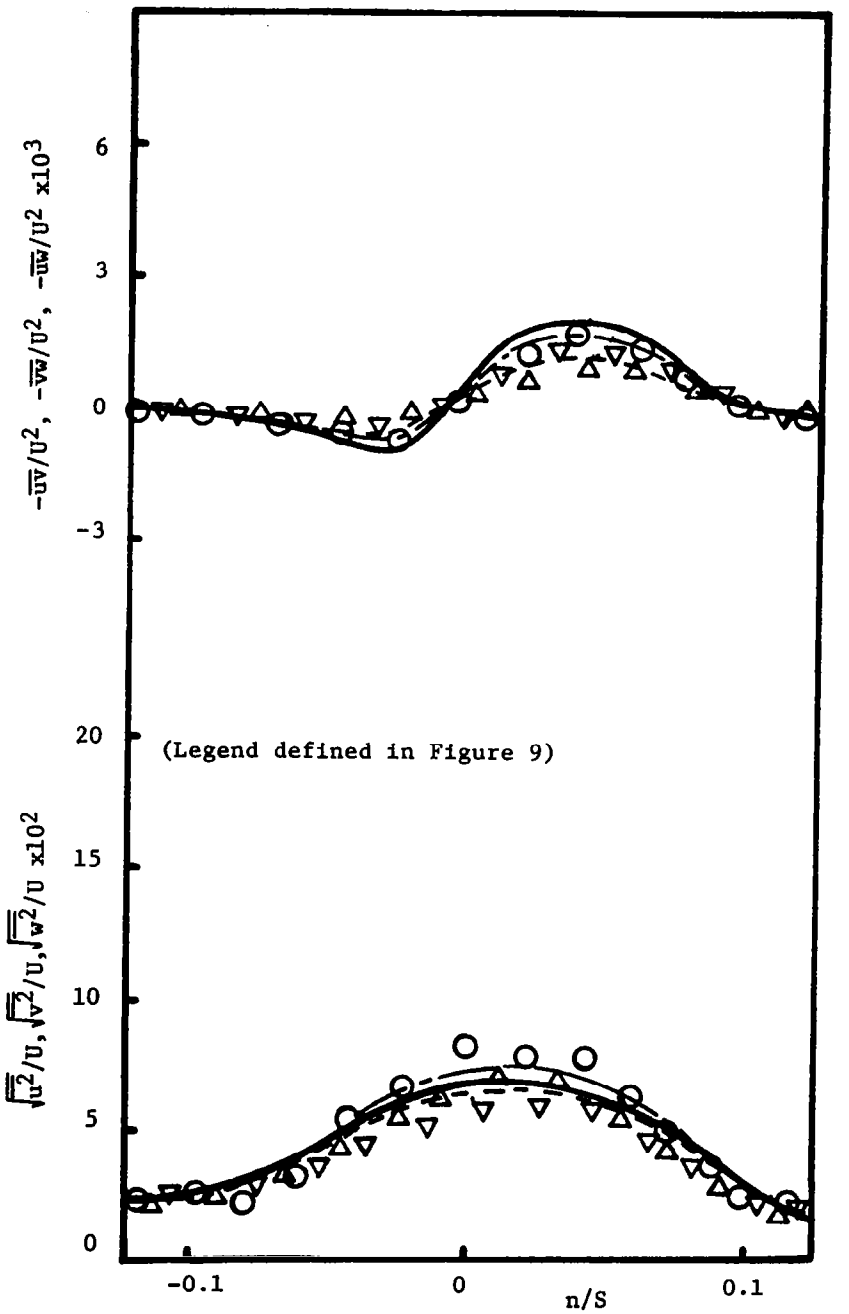

Figure 15(a). Reynolds Stress at r/r_t=0.72, s/C=0.23 and i=10° (Data of Reynolds et al., [31])

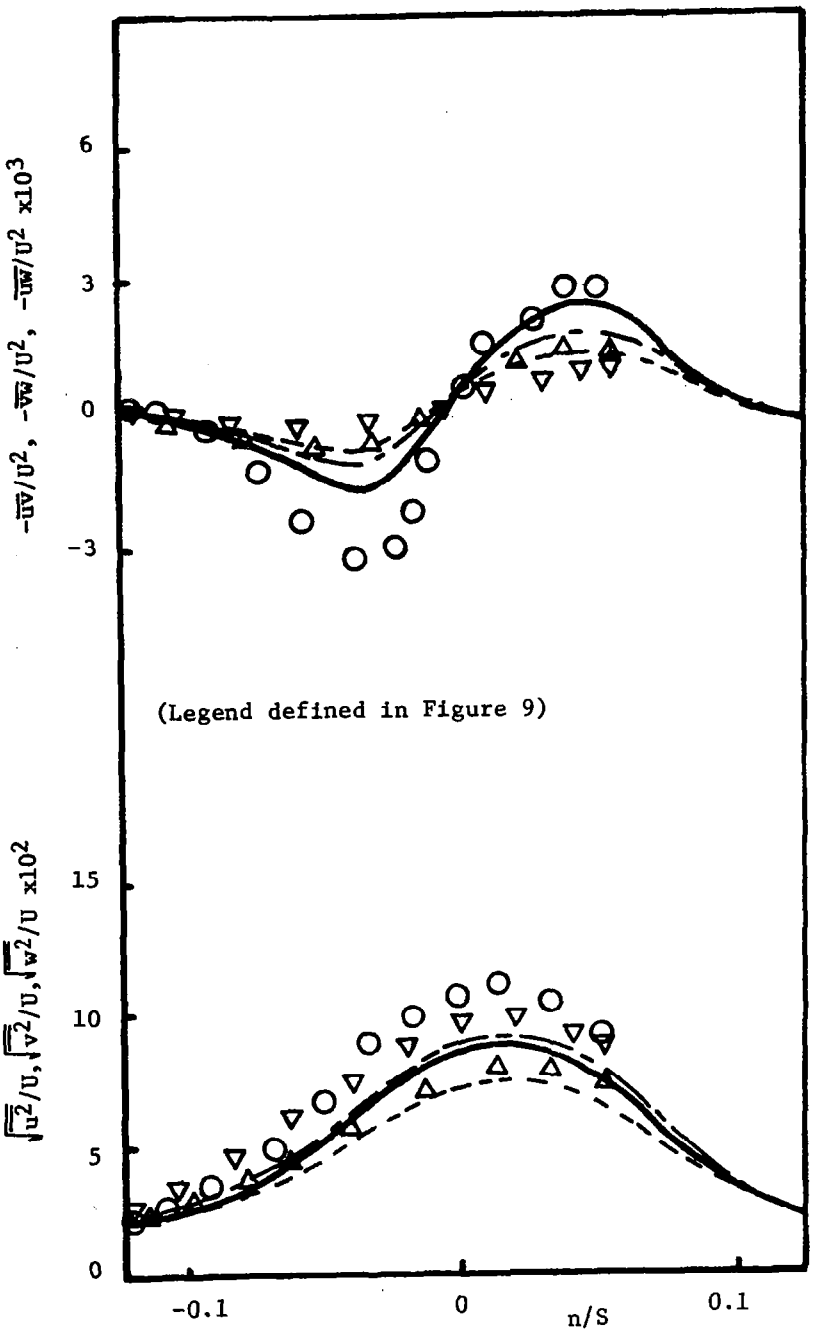

Figure 15(b). Reynolds Stress at r/r_t=0.72, s/C=0.94 and i=15° (Data of Reynolds et al., [31])

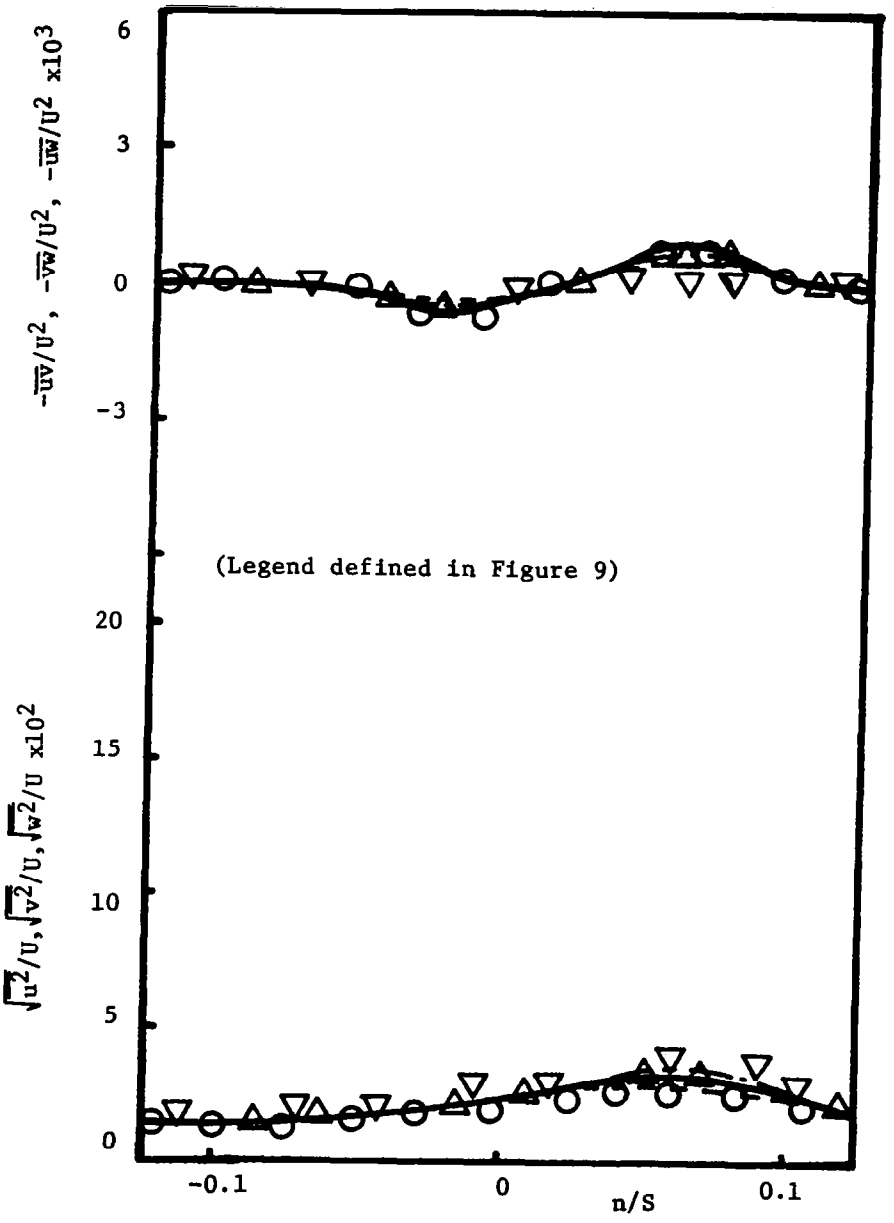

Figure 16(a). Reynolds Stress at r/r_t=0.72, s/C=0.93 and i=10° (Data of Reynolds et al., [31])

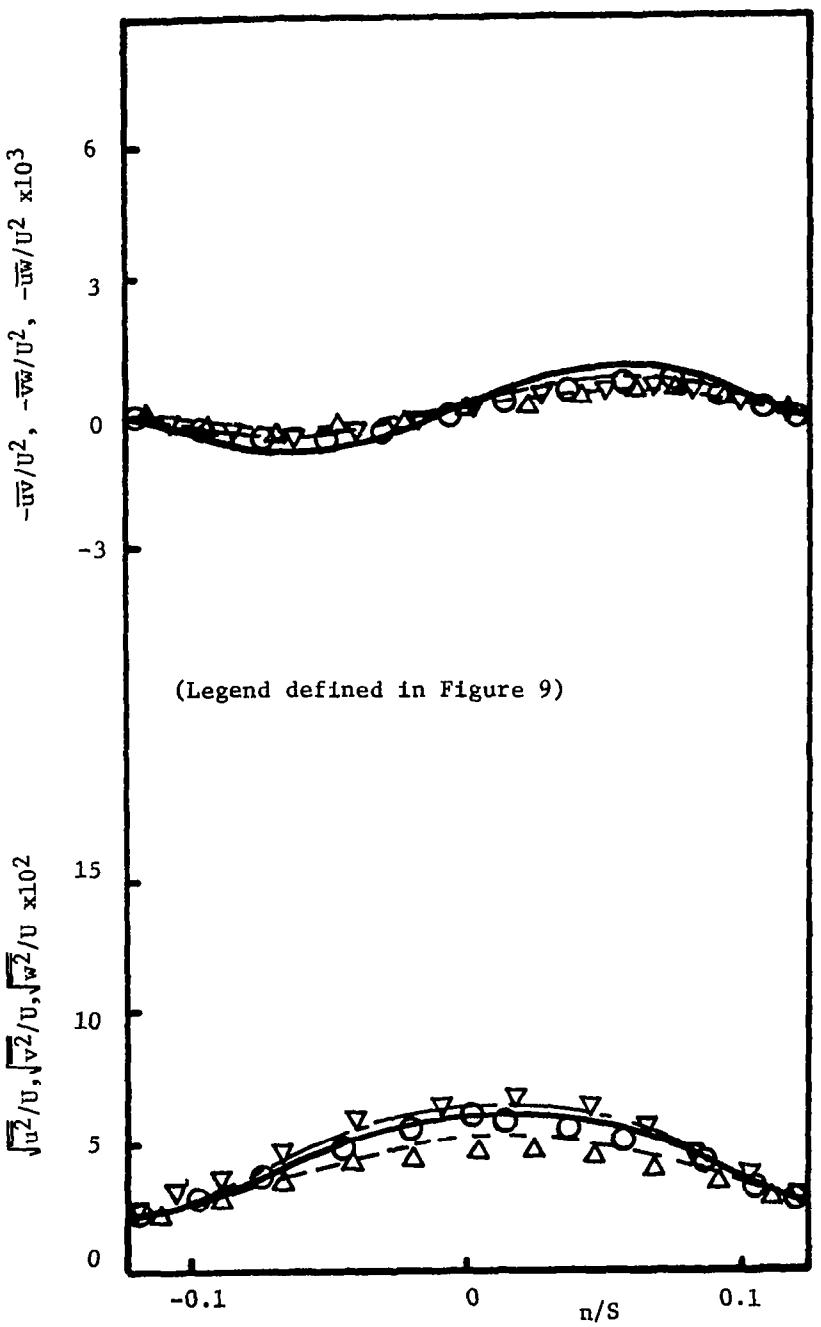

Figure 16(b). Reynolds Stress at r/r_t=0.72, s/C=1.65 and i=15° (Data of Reynolds et al., [31])

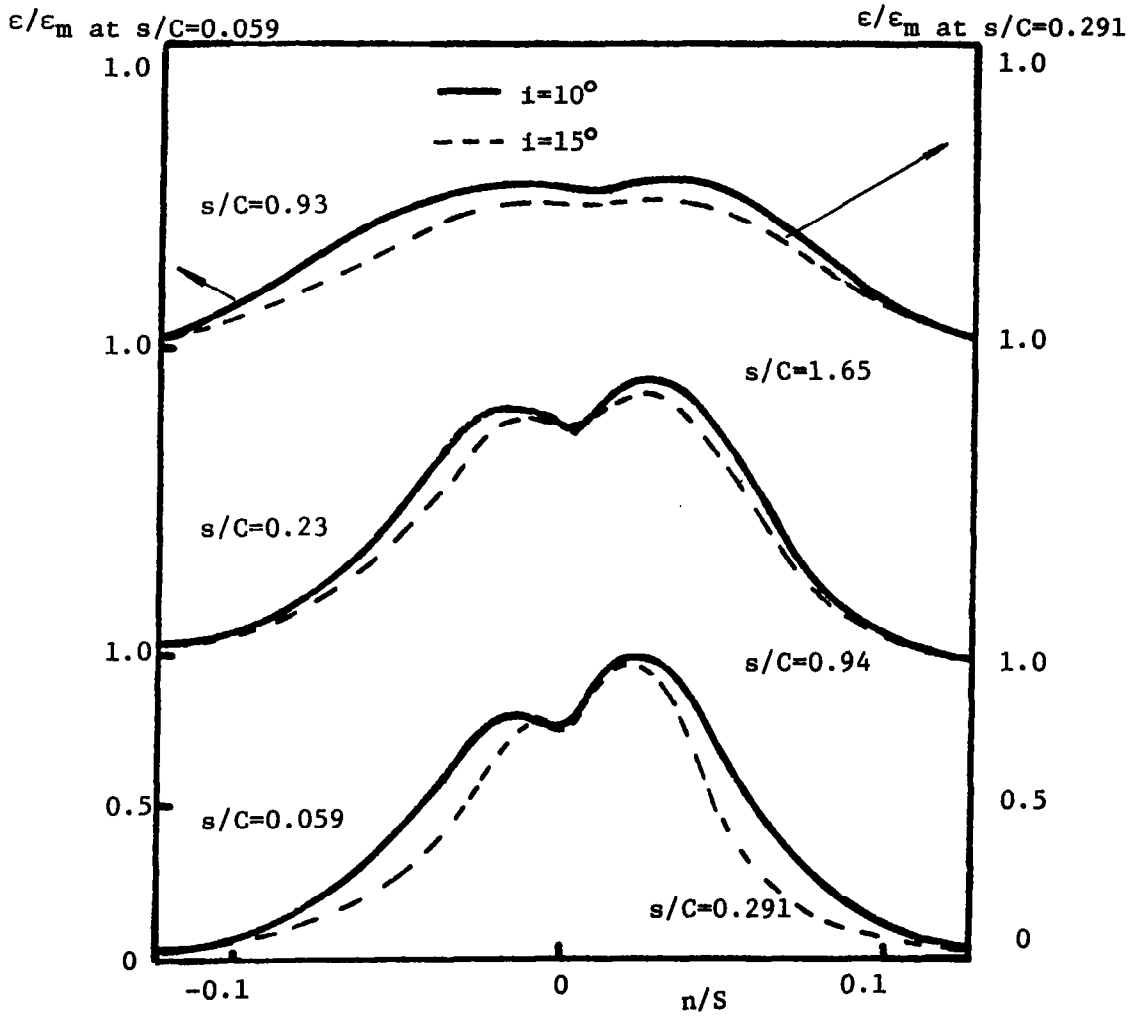

Figure 17. Energy Dissipation Rate at $r/r_t=0.72$

Comparison Between the Numerical Prediction and the Rotor Wake Data by Ravindranath and Lakshminarayana [32,3]

In the third comparison of experimental data, the findings of Ravindranath and Lakshminarayana [32,3] were used. They measured the wake in a single-stage compressor (Table 1). The rotor was non-zero camber. The experiment was done near the design condition, and the blade was moderately loaded. The data include a complete survey of the static pressure distribution across the wake at mid-radius. For the numerical calculation, the radial variation of the reduced static pressure was assumed to be dependent only on the centrifugal force. Also, the rate of turbulent kinetic energy dissipation was assumed to be equal to the production of turbulent kineticeryg.

The comparison of mean velocity is given in Figure 18. The overall agreement between the numerical prediction and the experimental data is good, although there is some discrepancy in the profiles of radial velocity components.

The comparisons of Reynolds stresses are given in Figures 19, 20, and 21. Even though the numerical results do not agree exactly with the experimental data, the overall characteristics in the local distribution of Reynolds stress are excellently predicted. The numerical prediction does accurately represent the qualitatively analyzed effect of rotation, that the radial turbulence intensity is increased and the normal turbulence intensity is decreased by the rotation. The experimental data show that the radial intensity is higher than the streamwise intensity. This relative magnitude is correctly predicted, although there exists a substantial difference in the magnitude of the individual stress component between the prediction and the experimental data.

The predicted static pressure distributions at the mid-radius are compared with the experimental data in Figure 22. As the static pressure measurement itself contains some amount of error, it is difficult to comment as to whether the deviations between the predictions and the experimental data arise from the improper turbulence closure modelling or experimental error.

The typical distribution of the rate of turbulent kinetic energy dissipation is shown in Figure 23. These results show that the magnitude the decay rate of the energy dissipation is the same order of that of the turbulent kinetic energy. This indicates that the characteristic length scale of the turbulent flow field in the rotor wake ($l \sim k^{3/2}/\varepsilon$) increases more rapidly than the rate at which the turbulent kinetic energy decreases.

Comparison of Predictions with Two Different Turbulence Closure Models

The rotor wake was also calculated with the so-called two-equation turbulence closure model (Launder and Spalding [15]) and the results were compared with those of the present turbulence closure model [modified Reynolds stress model, equations (39) through (44), (53), and (54)].

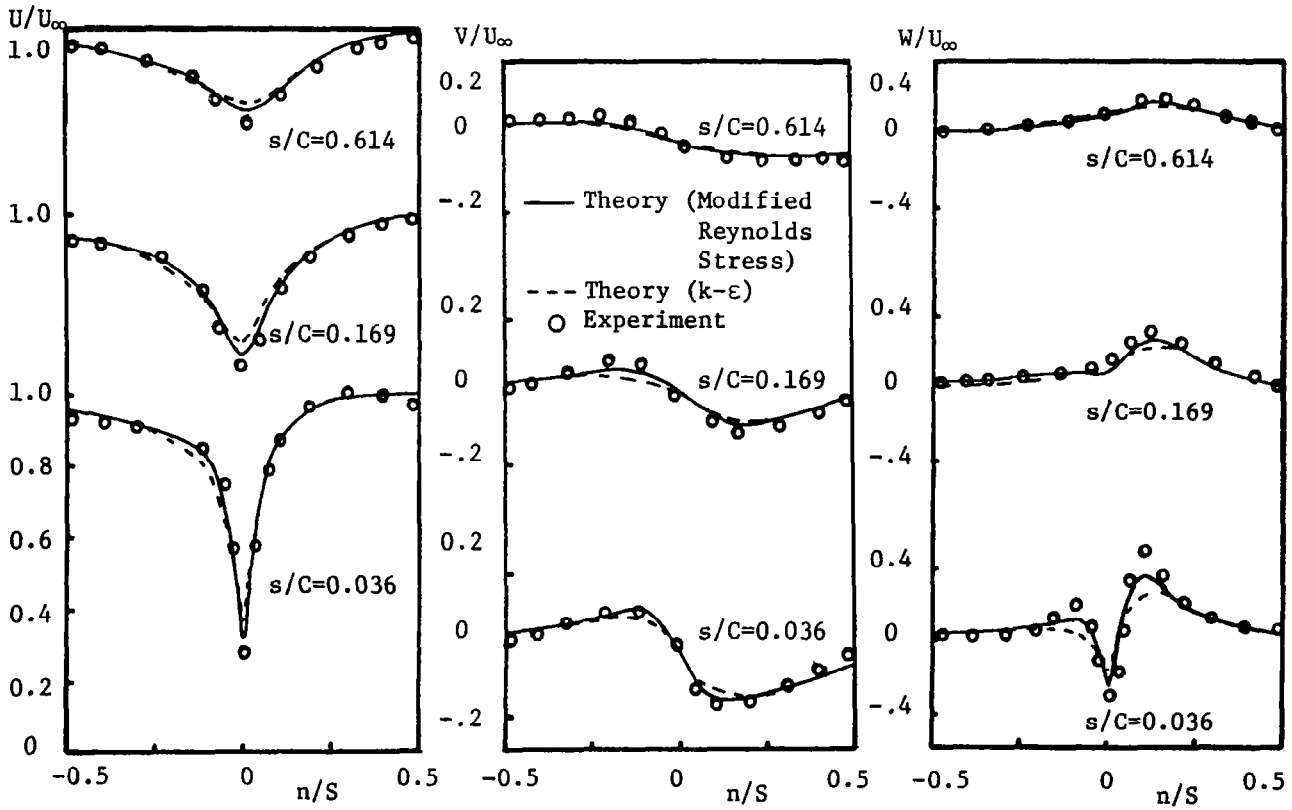

Figure 18. Profiles of Mean Velocity Components at r/r_t=0.8 (Data of Ravindranath and Lakshminarayana, [32])

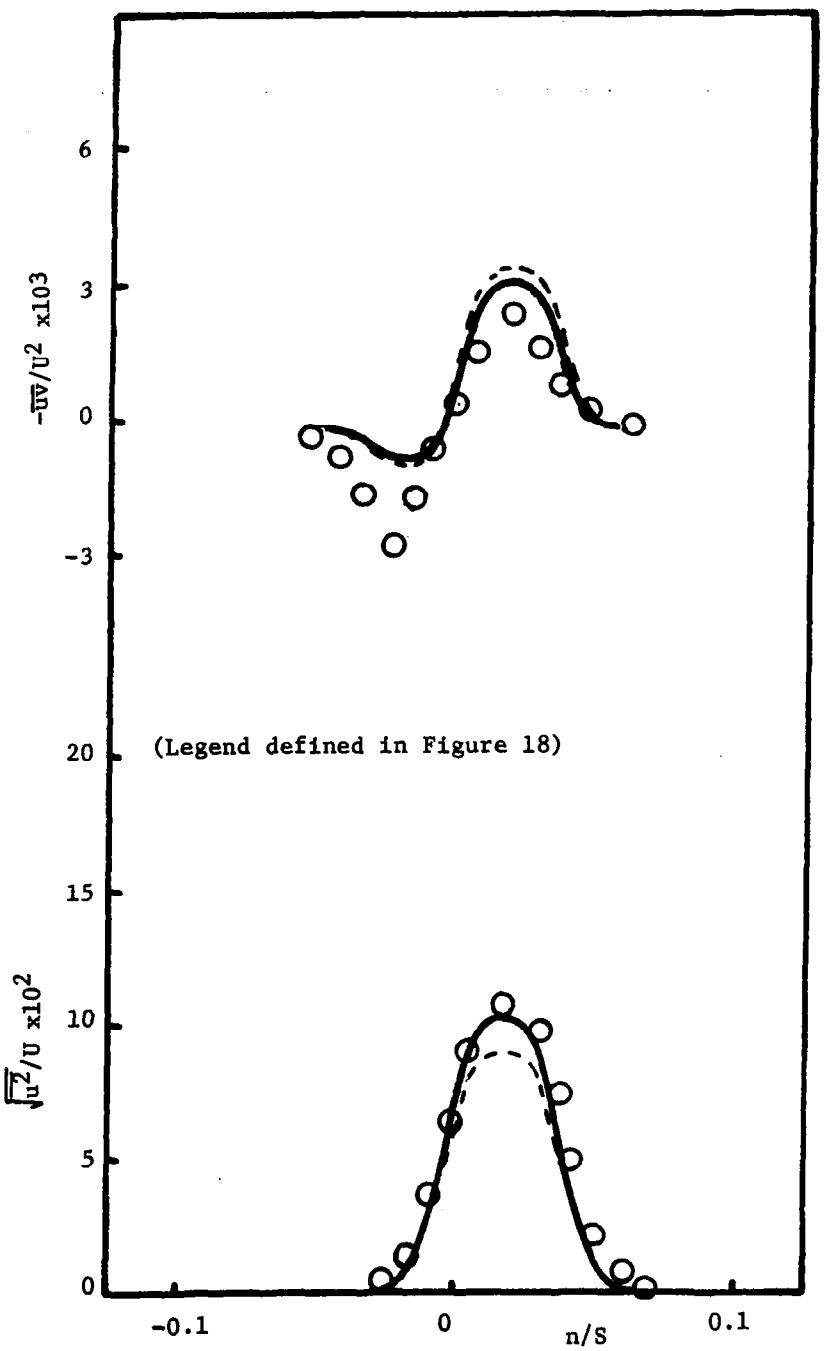

Figure 19(a). Reynolds Stress at r/r_t=0.80 and s/C=0.036 (Data of Ravindranath and Lakshminarayana, [32,3])

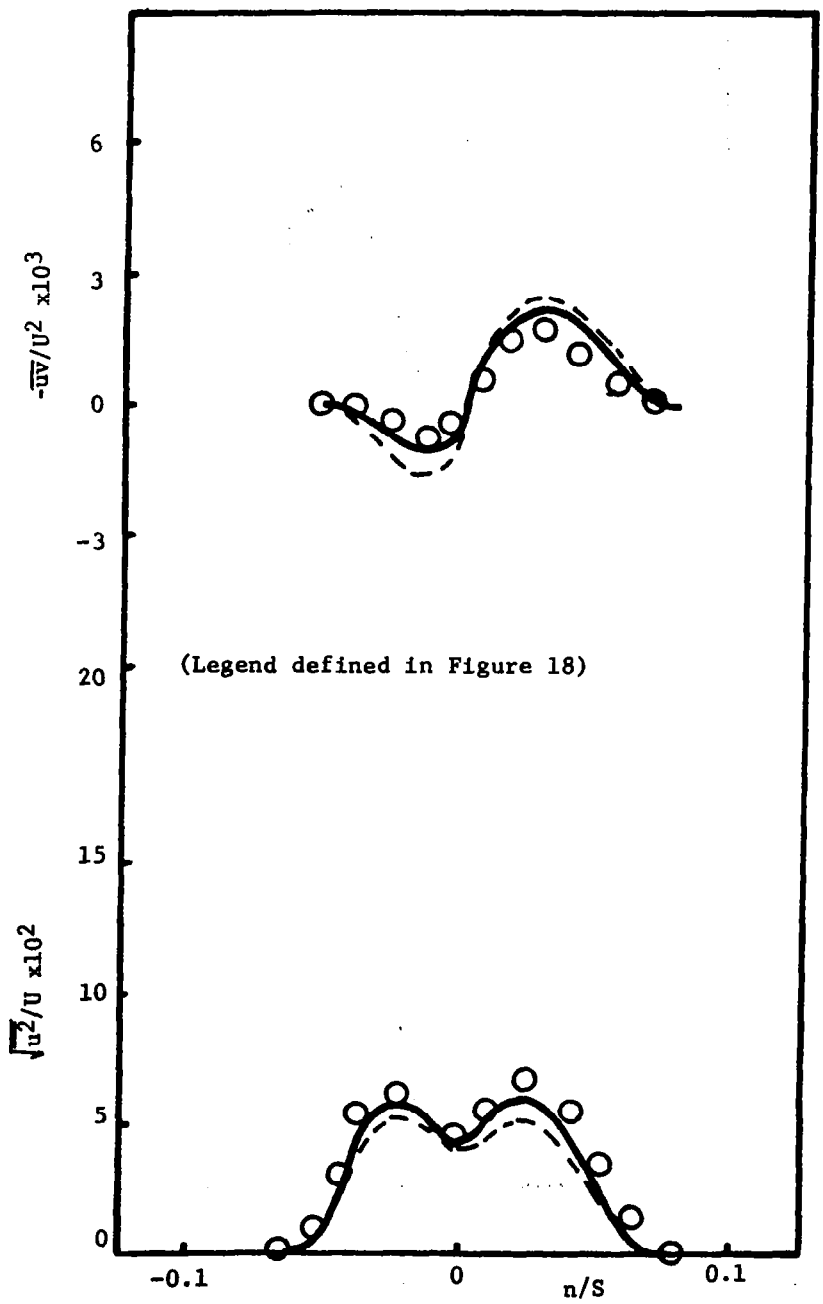

Figure 19(b). Reynolds Stress at r/r_t=0.80 and s/C=0.614 (Data of Ravindranath and Lakshminarayana, [32,3])

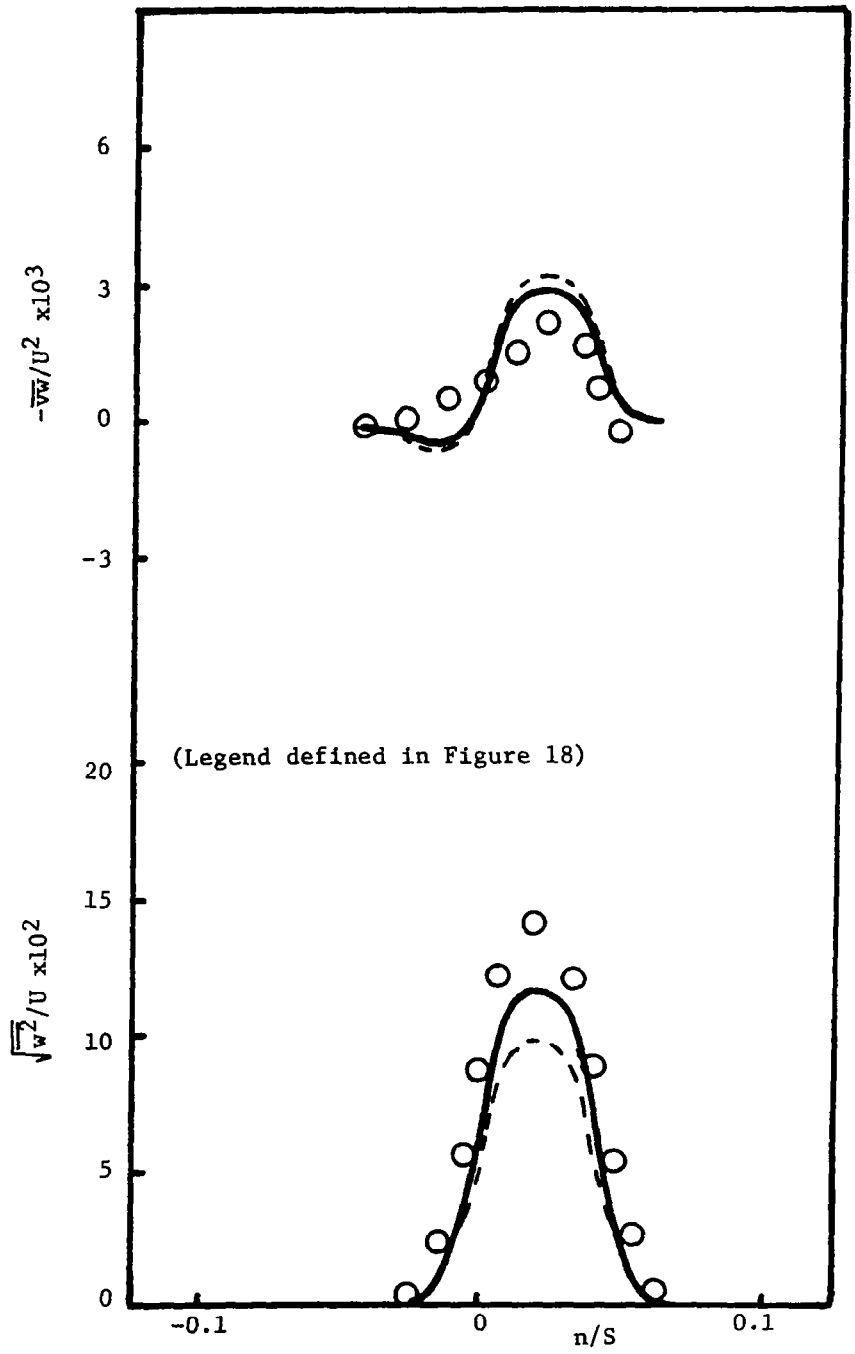

Figure 20(a). Reynolds Stress at r/r_t=0.80 and s/C=0.036 (Data of Ravindranath and Lakshminarayana, 1979)

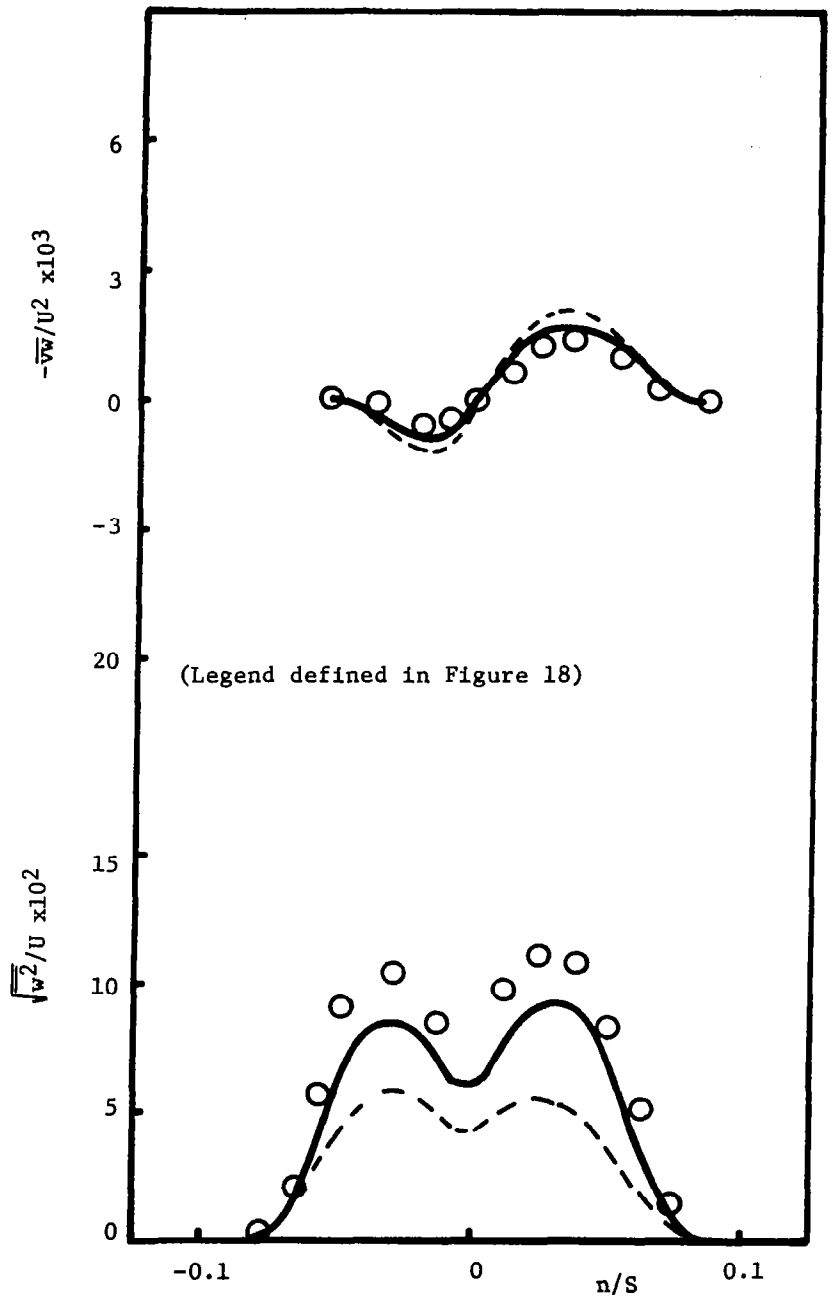

Figure 20(b). Reynolds Stress at r/r_t=0.80 and s/C=0.614 (Data of Ravindranath and Lakshminarayana, [32,3])

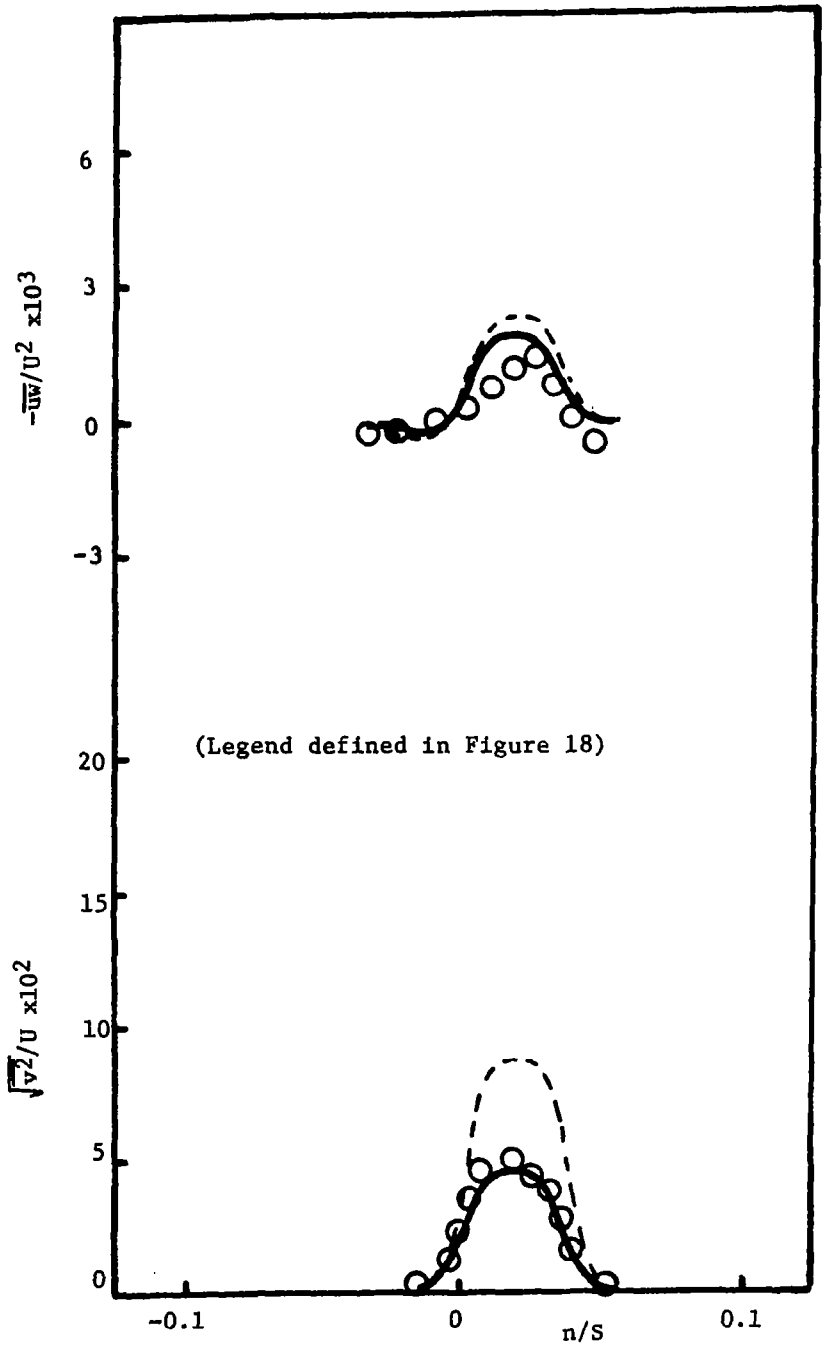

Figure 21(a). Reynolds Stress at r/r_t=0.80 and s/C=0.036 (Data of Ravindranath and Lakshminarayana, [32,3])

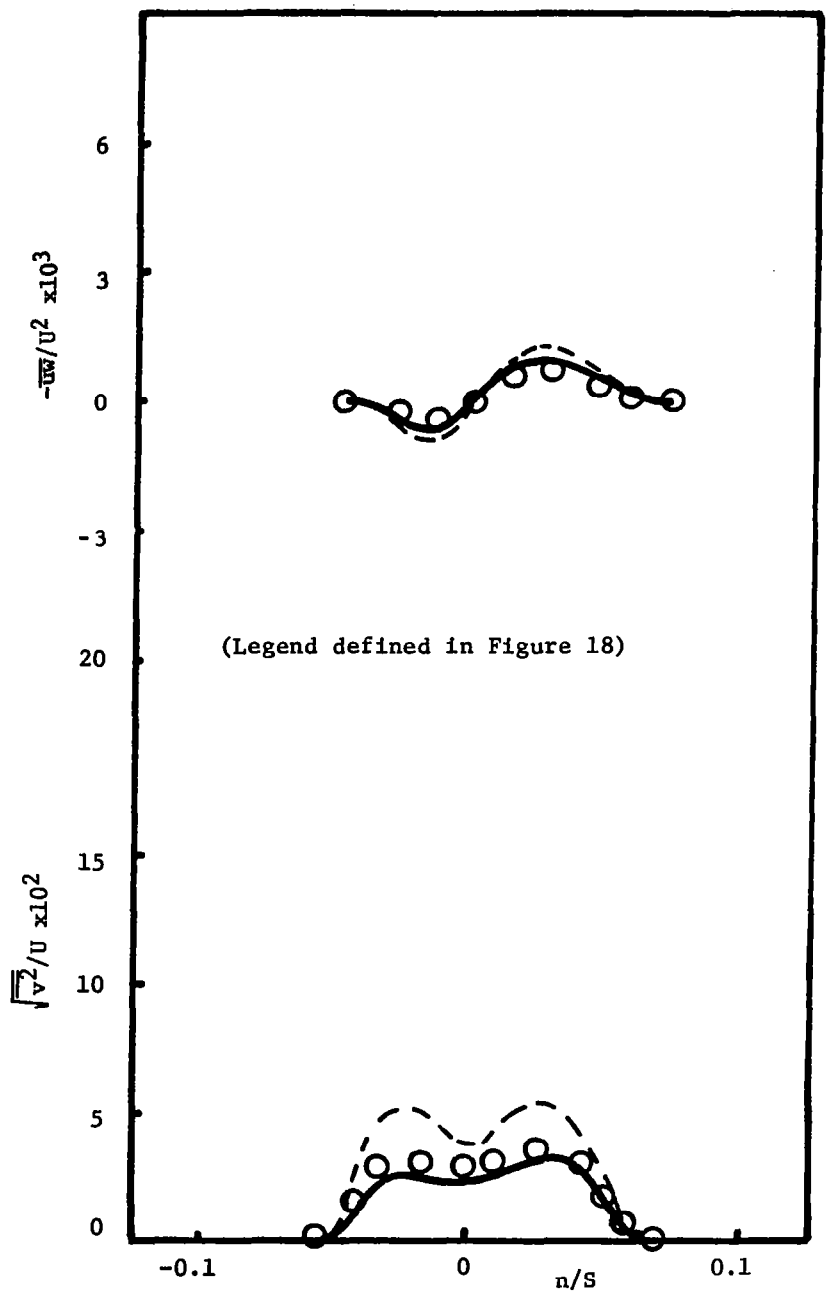

Figure 21(b). Reynolds Stress at r/r_t=0.80 and s/C=0.614 (Data of Ravindranath and Lakshminarayana, [32,3])

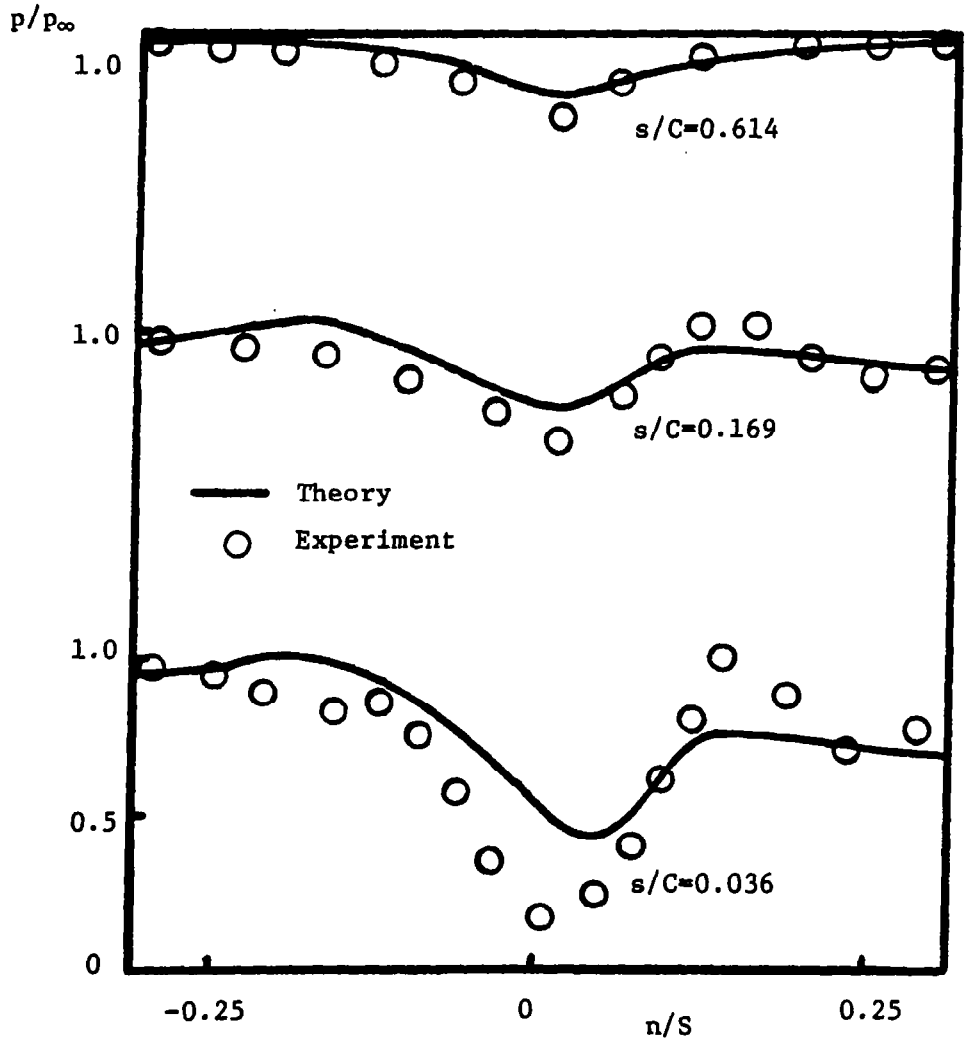

Figure 22. Static Pressure Distribution at r/r_t=0.80 (Data of Ravindranath and Lakshminarayana, [32])

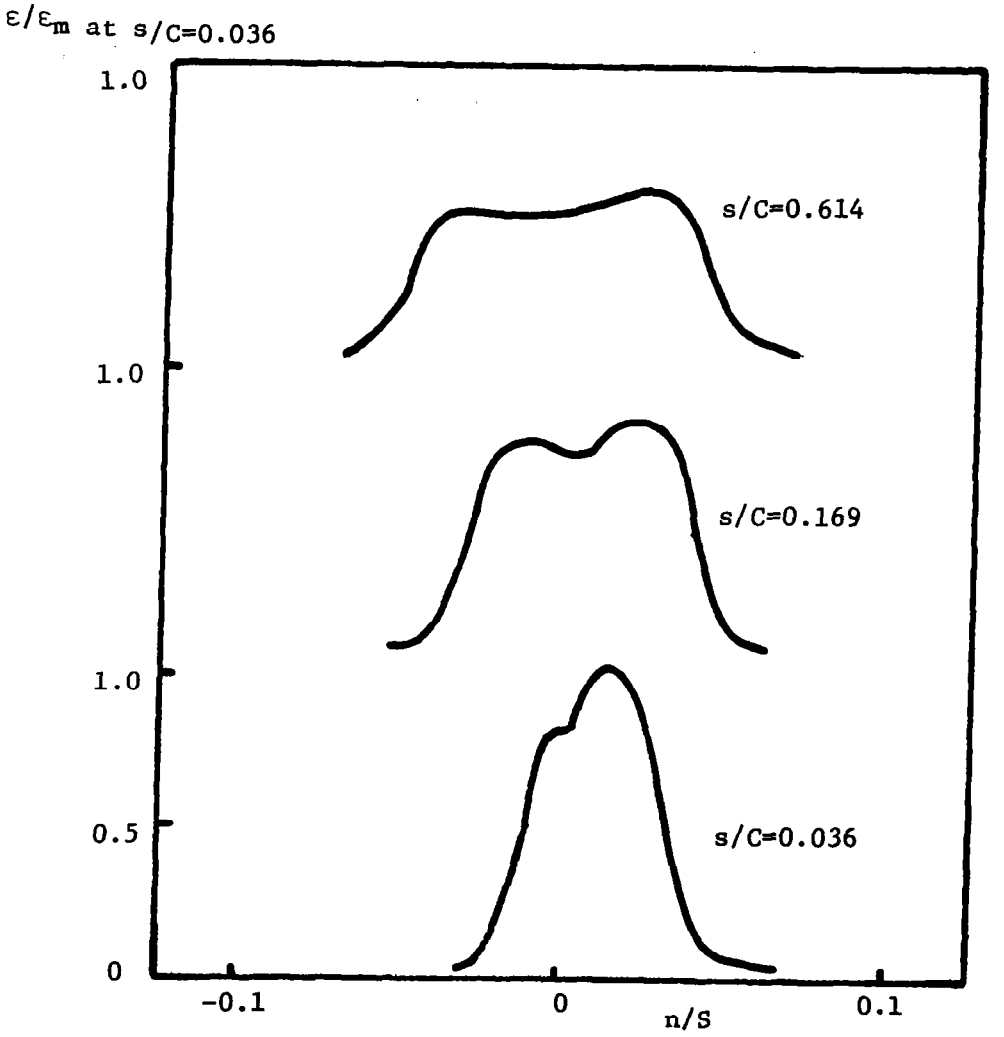

Figure 23. Energy Dissipation Rate at r/r_t=0.80

With the two-equation turbulence closure model, the local Reynolds stresses are evaluated with two local characteristic quantities of turbulence--the turbulent kinetic energy and the rate of turbulent kinetic energy dissipation. In addition, two transport equations are provided to give local values of these two quantities.

The two transport equations for the turbulent kinetic energy and the rate of turbulent kinetic energy dissipation in tensor form are as follows:

$$U^i \frac{\partial k}{\partial x^i} = \frac{\partial}{\partial x^i}\left(\frac{\nu_{eff}}{\sigma_k} \frac{\partial k}{\partial x^i}\right) + P - \varepsilon \tag{65}$$

$$U^i \frac{\partial \varepsilon}{\partial x^i} = \frac{\partial}{\partial x^i}\left(\frac{\nu_{eff}}{\sigma_\varepsilon} \frac{\partial \varepsilon}{\partial x^i}\right) + S - C_{\varepsilon 2} \frac{\varepsilon^2}{k} \tag{66}$$

where

$$\nu_{eff} = C_\mu k^2/\varepsilon \quad , \quad P = \overline{u_i u_j}\, U^i_{,j}$$

$$k = \frac{1}{2} g_{ij} \overline{u^i u^j}$$

$$-\overline{u^i u^j} = \nu_{eff}\left(U^i_{,j} + U^j_{,i}\right) - \frac{2}{3} k\, g^{ij}$$

and S is the source term in the transport equation of the rate of turbulent kinetic energy dissipation given in equation (55).

In the present curvilinear coordinate,

$$U \frac{\partial k}{\partial s} + V \frac{\partial k}{\partial n} + W \frac{\partial k}{\partial r} = \frac{\partial}{\partial S}\left(\frac{\nu_k}{\sigma_k} \frac{\partial K}{\partial s}\right) + \frac{\partial}{\partial n}\left(\frac{\nu_k}{\sigma_k} \frac{\partial K}{\partial n}\right) + \frac{\partial}{\partial r}\left(\frac{\nu_k}{\sigma_k} \frac{\partial K}{\partial r}\right) + P - \varepsilon \tag{67}$$

$$U \frac{\partial \varepsilon}{\partial s} + V \frac{\partial \varepsilon}{\partial n} + W \frac{\partial \varepsilon}{\partial r} = \frac{\partial}{\partial s}\left(\frac{\nu_k}{\sigma_k} \frac{\partial \varepsilon}{\partial s}\right) + \frac{\partial}{\partial n}\left(\frac{\nu_k}{\sigma_\varepsilon} \frac{\partial \varepsilon}{\partial n}\right) + \frac{\partial}{\partial r}\left(\frac{\nu}{\sigma_\varepsilon} \frac{\partial \varepsilon}{\partial r}\right) + C_1 \frac{\varepsilon}{k} \cdot S - C_2 \frac{\varepsilon^2}{k} \tag{68}$$

where

$$P = 2\nu\left\{\left(\frac{\partial U}{\partial s}\right)^2 + \left(\frac{\partial V}{\partial n}\right)^2 + \left(\frac{\partial W}{\partial r}\right)^2 + \Gamma^1_{11}\, U\, \frac{\partial U}{\partial s} + \Gamma^2_{21}\, U\, \frac{\partial V}{\partial n} + \Gamma^3_{31}\, U\, \frac{\partial W}{\partial r}\right\}$$

$$+ \nu_t\left\{\left(\frac{\partial U}{\partial r}\right)^2 + \left(\frac{\partial W}{\partial s}\right)^2 \cdot \left(\frac{\partial U}{\partial n}\right)^2 \cdot \left(\frac{\partial V}{\partial s}\right)^2 + \left(\frac{\partial V}{\partial r}\right)^2 + \left(\frac{\partial W}{\partial n}\right)^2 + 2\,\frac{\partial U}{\partial r}\,\frac{\partial W}{\partial s} + 2\,\frac{\partial U}{\partial n}\,\frac{\partial V}{\partial s}\right.$$

$$+ 2\,\frac{\partial V}{\partial r}\,\frac{\partial W}{\partial n} + \left(\frac{\partial U}{\partial r} + \frac{\partial W}{\partial s}\right)\left(\Gamma^1_{13}\, U + \Gamma^2_{11}\, U\right) + \left(\frac{\partial U}{\partial n} + \frac{\partial V}{\partial s}\right)\left(\Gamma^1_{12}\, U + \Gamma^2_{11}\, U\right)$$

$$\left. + \left(\frac{\partial V}{\partial r} + \frac{\partial W}{\partial r}\right)\left(\Gamma^2_{31}\, U + \Gamma^3_{21}\, U\right)\right\}$$

The experimental data by Ravindranath and Lakshminarayana [32,3] were used for the comparison of results by two different turbulence closure models. The comparison of mean velocity is given in Figure 18. The agreement between the theory and the experimental data is good for both models; however, the modified Reynolds stress model predicts better results than the two-equation model.

It should be mentioned here that the conventional k-ε model will not predict the shear stress or intensity components satisfactorily. The modified Reynolds stress model, however, can accurately provide this information. The comparison of Reynolds stresses are given in Figures 19, 20, and 21, where the present turbulence closure model shows substantial improvements in prediction of mean velocity as well as turbulent quantity.

As explained earlier, the effect of rotation is to reduce the streamwise intensity and increase the radial component of turbulence intensity. The present model, which includes this effect, correctly predicts the trend (see Figures 19, 20, and 21). The radial component of intensities predicted by the k-ε model is much lower than the measured data (Figure 20), while the author's prediction comes closer to the data.

The k-ε model predicts higher values of shear stresses in the pressure side of the wake (Figures 19, 20, and 21). The mean strain rates are very high in this side, resulting in higher shear stresses when the k-ε model is used for turbulence closure.

These comparisons seem to indicate that the present Reynolds stress closure scheme models the rotation effect correctly through the rotation-originated redistribution term in the Reynolds stress transport equations.

As explained in an earlier section, the rotor wake is highly three-dimensional and has multiple components of curvature. The transport equation of the rate of turbulent kinetic energy dissipation with the conventional source term, equation (55) is known to be responsible for the poor performance in predicting curved turbulent flows (Pope and Whitelaw [54], and Bradshaw [22]). This poor performance is reportedly caused due to inclusion of the mean shear rate in the production term. The energy dissipation equation with modified source term, equation (56) can predict curved turbulent flows better than that with the conventional source term. This point will be discussed further in the next chapter.

Comparisons of the predictions with two forms of the energy dissipation equation are made for the rotor wake data by Ravindranath and Lakshminarayana [32,3]. The comparison of mean velocity is given in Figure 24. Both turbulence closure models predict close values in mean velocity. The comparison of Reynolds stress is given in Figures 25, 26, and 27. Though there seems to be some improvement by the modified form of the energy dissipation equation, the difference is not substantial.

Most of the curvature effect is sensed by the fluid particle near the wake center line where the velocity gradient is very large. The effect of curvature is directly related to the variation of angular momentum in the radial direction of curvature. For the rotor wake, the variation of angular momentum in the direction of the machine radius is small compared to the variations in the direction of r_β and r_s (Figure 2), except for the hub wall and the annulus wall region. Furthermore the effect of curvature due to r_s is opposite to that due to r_β near the wake center line (the sign of angular momentum change in equation (4) is opposite for r_s and r_β). Therefore, the two curvature effects are cancelled and the total effect of curvature may not be substantial. The preceding argument holds only for the present case of rotor geometry and operating condition. Generally, the effect of curvature is significant. The decay of streamwise and radial velocity components predicted by the present modified Reynolds stress model with modified source term is compared with experimental data in Figure 28, where U_∞ is the streamwise velocity component in the free stream, and U_c and W_c are streamwise and radial velocity components at the center of the wake. Also, the decay of Reynolds stresses is compared in Figures 29 and 30. Where subscript m indicates the maximum value in the wake at that streamwise station. The agreement between predictions and experimental data is excellent, though some minor deviations are observed at the very near wake region. These comparisons indicate that the turbulence closure model employed in this thesis correctly models the rotation and curvature effects, through the modelled Reynolds stress transport equation.

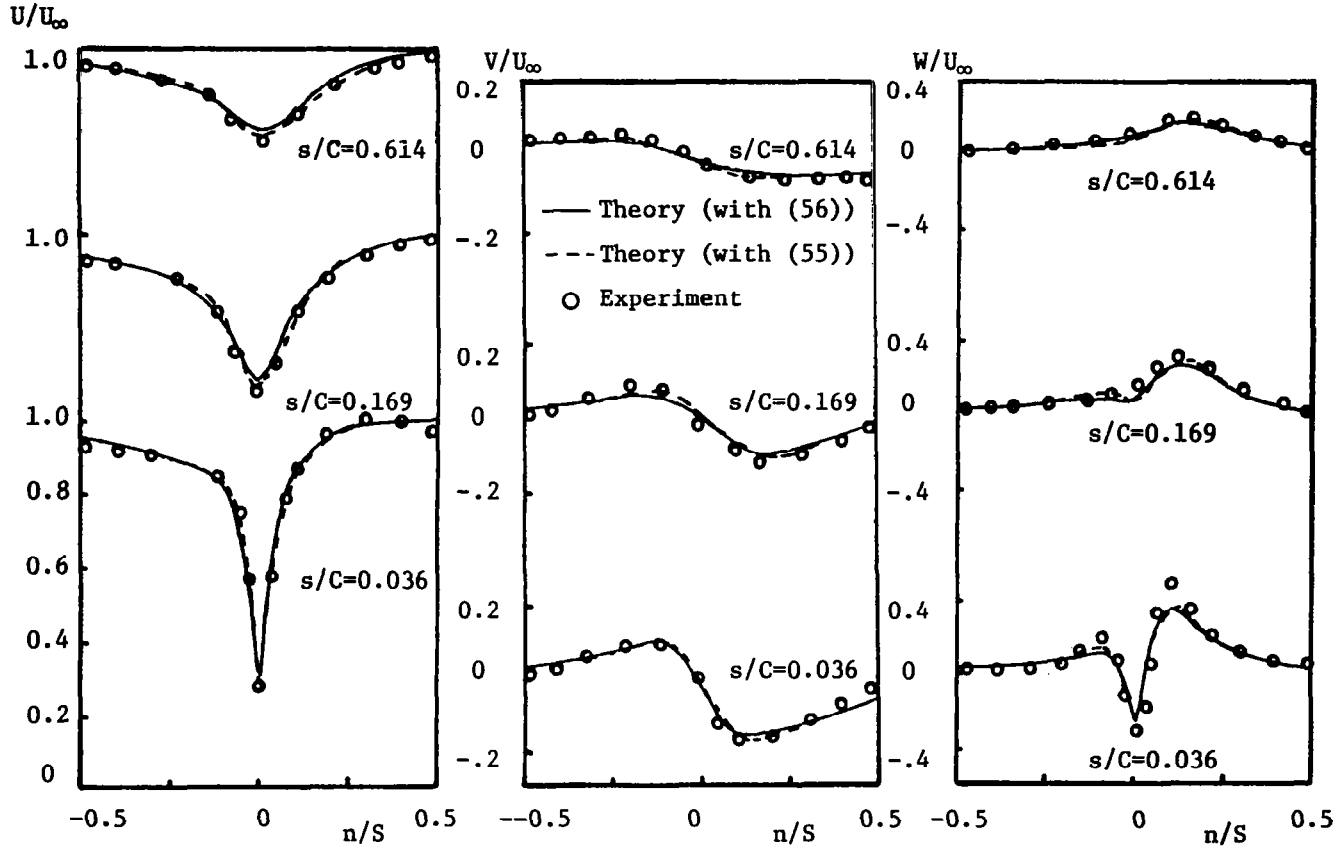

Figure 24. Profiles of Mean Velocity Components at r/r_t=0.8 (Data of Ravindranath and Lakshminarayana, [32,3])

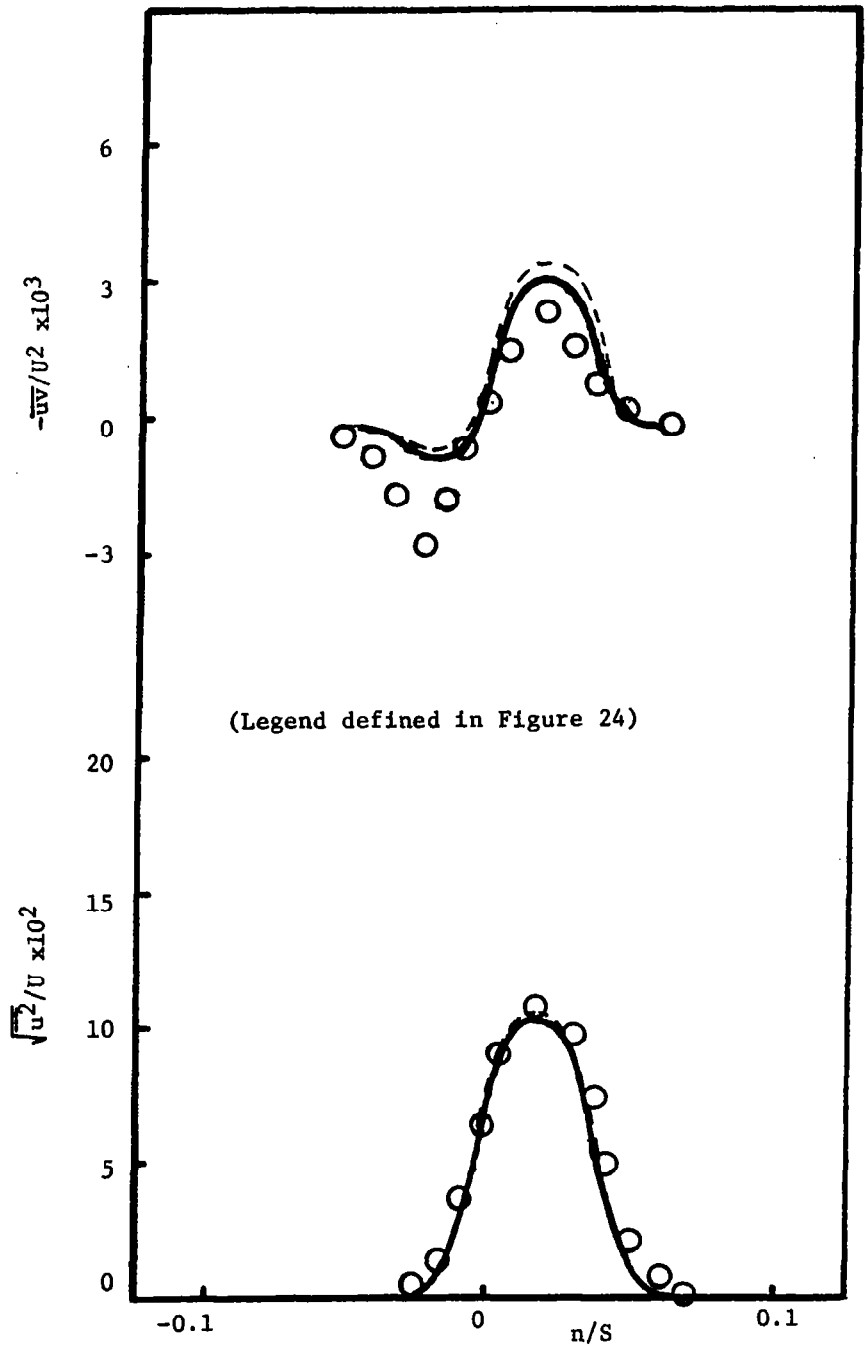

Figure 25. Reynolds Stress at r/r_t=0.80 and s/C=0.036 (Data of Ravindranath and Lakshminarayana, [32,3])

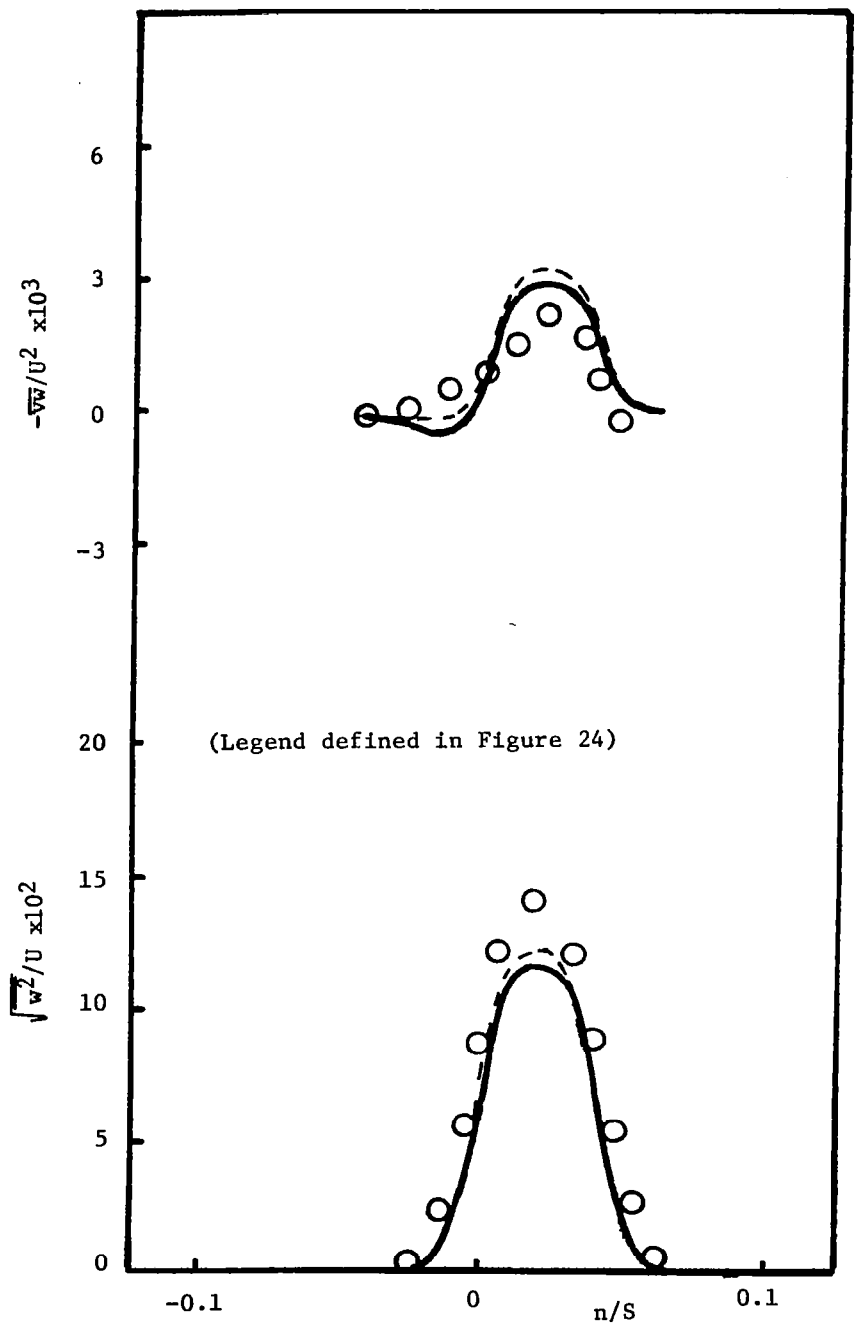

Figure 26. Reynolds Stress at r/r_t=0.80 and s/C=0.036 (Data of Ravindranath and Lakshminarayana, [32,3])

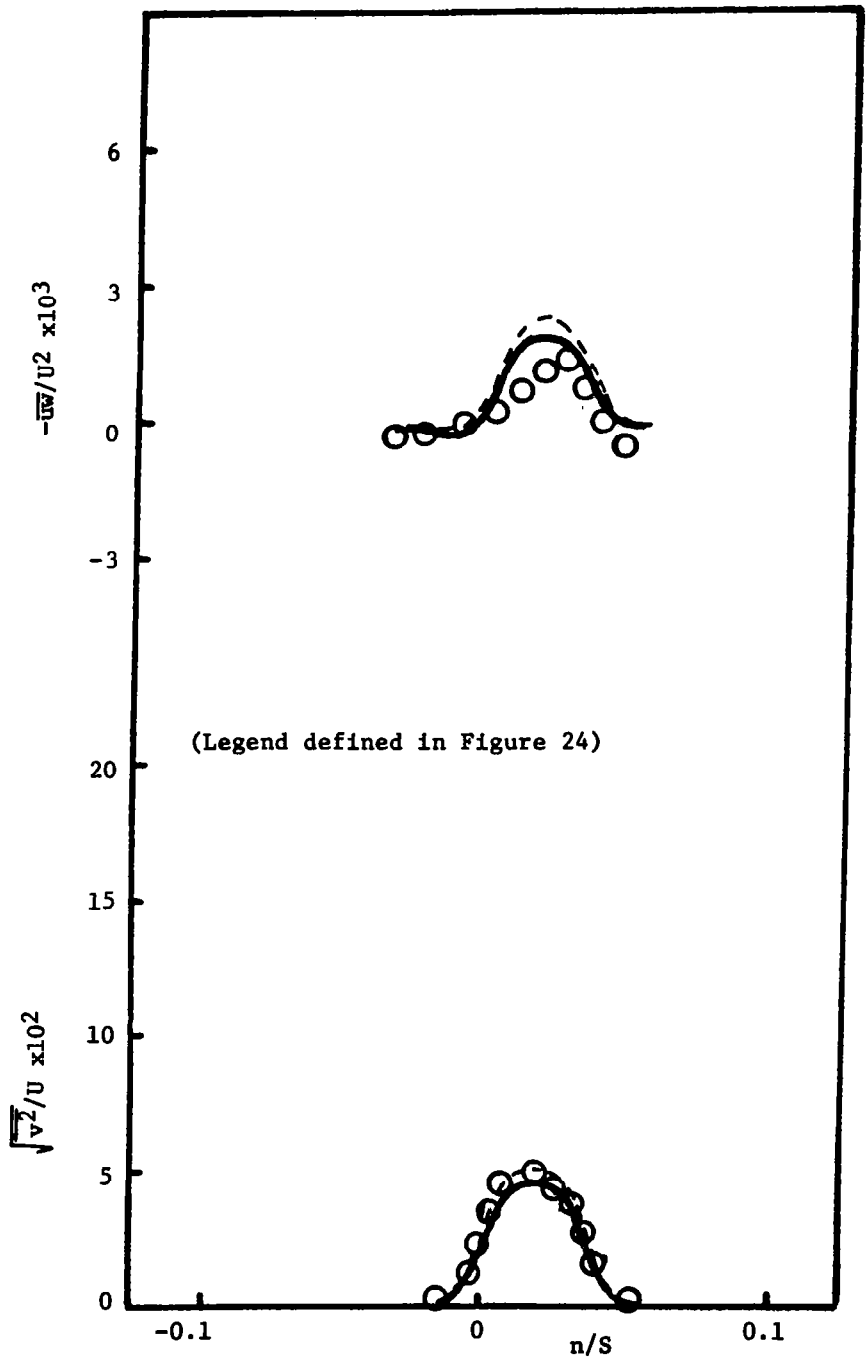

Figure 27. Reynolds Stress at r/r_t=0.80 and s/C=0.036 (Data of Ravindranath and Lakshminarayana, [32,3])

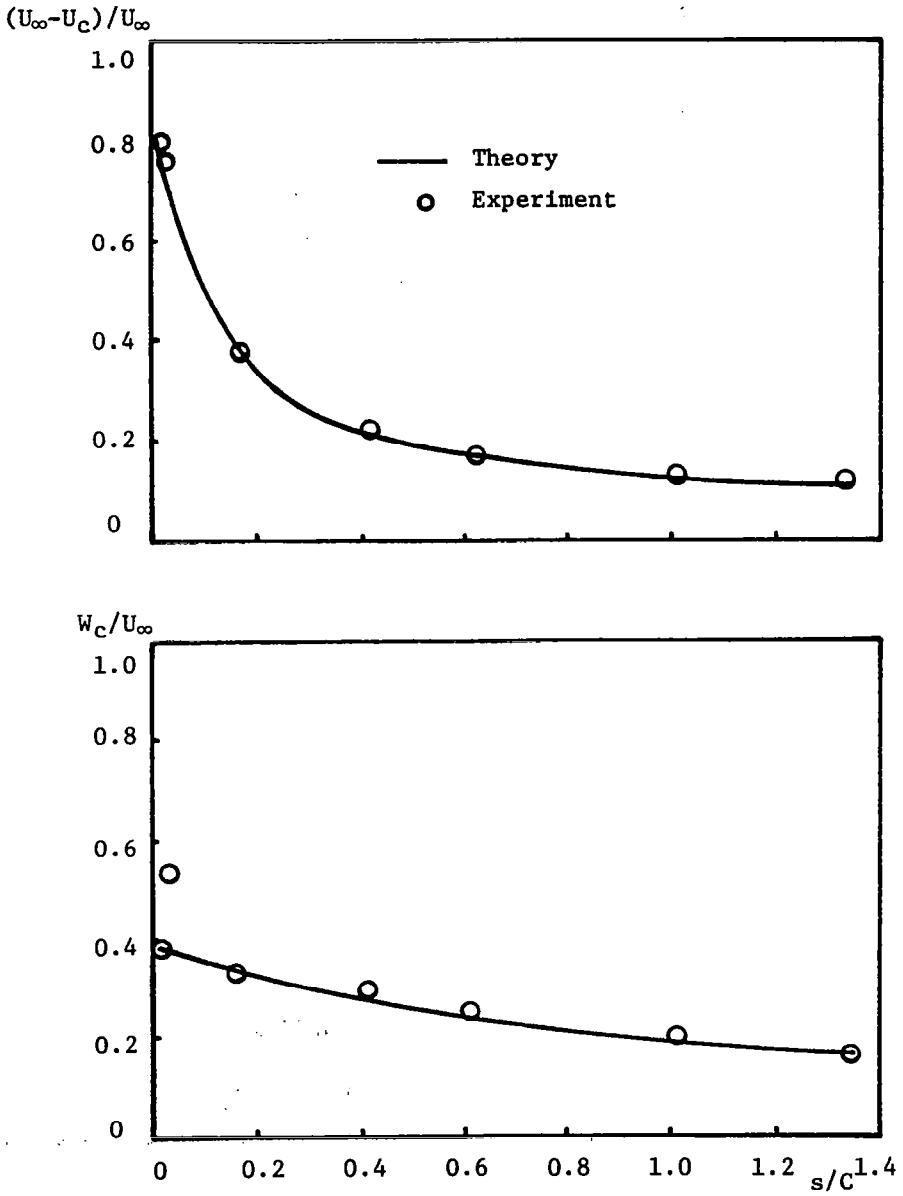

Figure 28. Decay of Wake Centerline Velocity Components (Data of Ravindranath and Lakshmanarayana, [32,3])

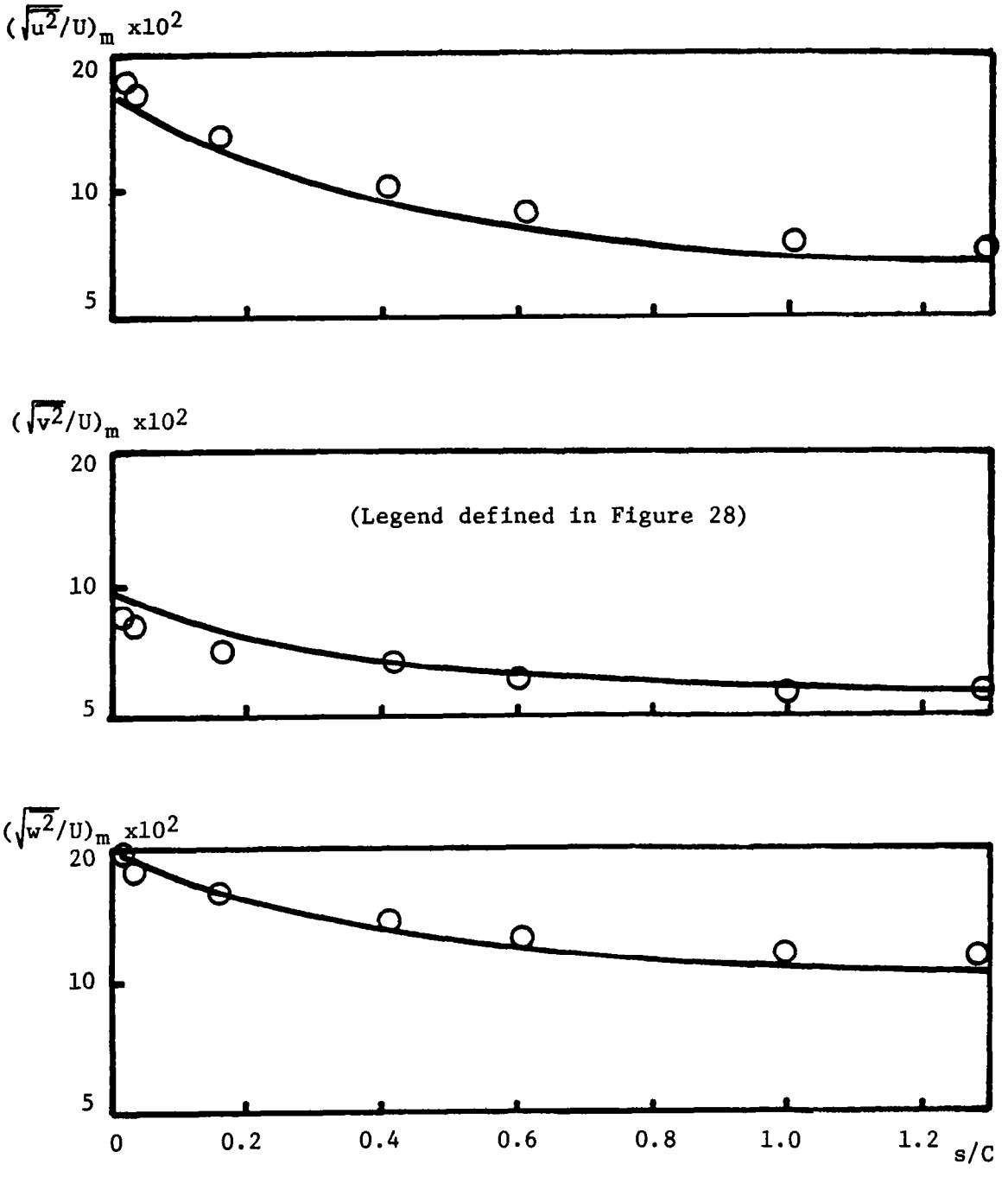

Figure 29. Decay of Maximum Turbulence Intensity (Data of Ravindranath and Lakshminarayana, [32,3])

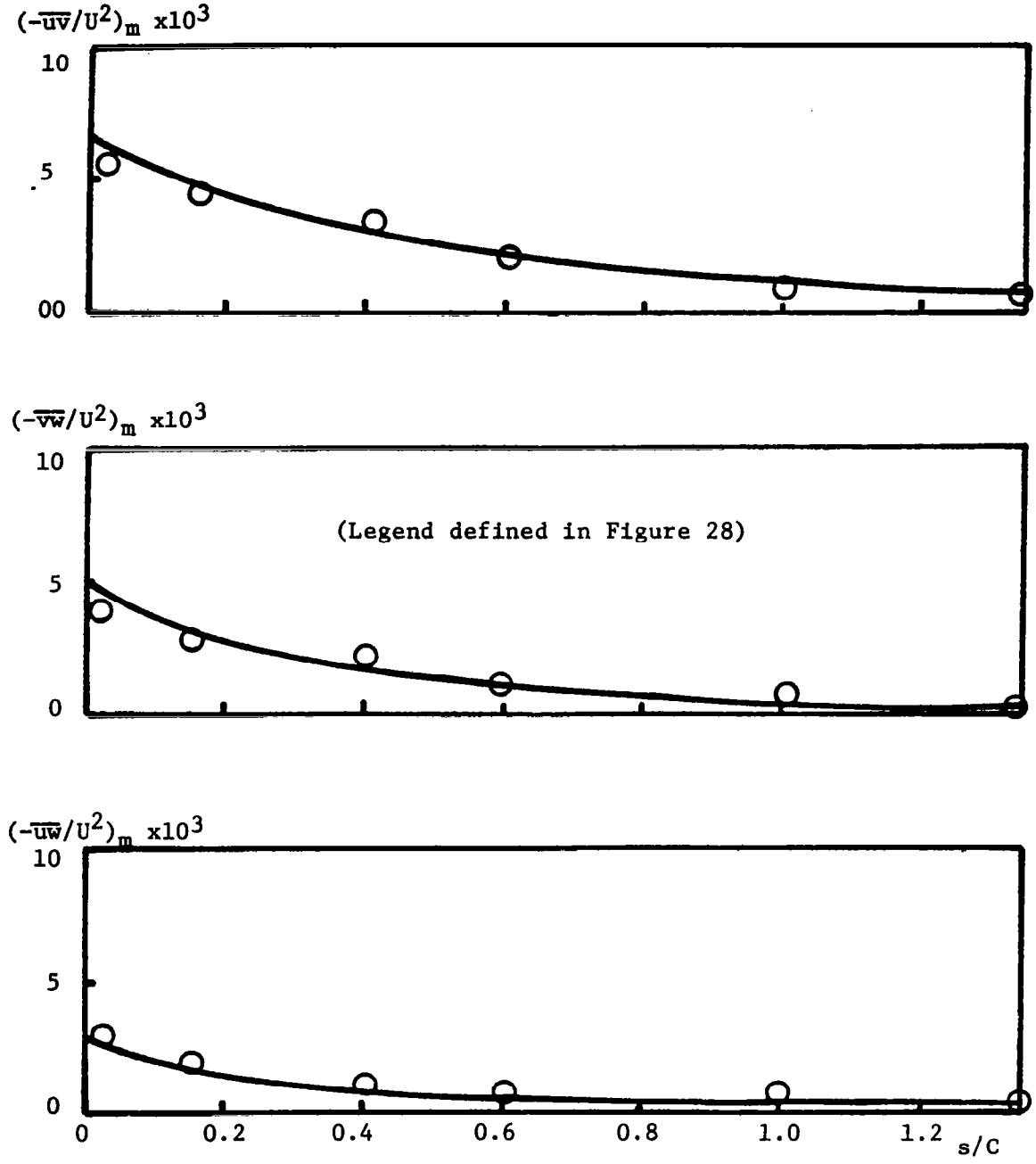

Figure 30. Decay of Maximum Shear Stress (Data of Ravindranath and Lakshminarayana, [32,3])

NUMERICAL STUDY OF ASYMMETRIC TURBULENT WAKES OF SINGLE AIRFOILS AND CASCADES OF AIRFOILS

Previous Analytical and Experimental Investigation of the Isolated Airfoil and Cascade Wake

As free shear flows, the wakes of single airfoils and of cascades of airfoils have their own physical natures. The mean velocity profiles of the single airfoil wake and the cascade wake is two-dimensional and generally asymmetric. The asymmetric nature in the wake is due to the past history of the flow. For most engineering applications, the Reynolds number, based on the chord length of the airfoil, is large enough for the boundary layer near the trailing edge to be considered fully turbulent. Therefore, the subsequent wake is also turbulent. The cascade wake has a periodic distribution of flow quantities with a period equal to the spacing of the blades. Both the single-airfoil wake and the cascade wake have an elliptic nature if the flow field very near to the trailing edge of the airfoil is considered. The static pressure change in the single airfoil wake has been reported to be mild both in normal and streamwise direction (Chevray and Kovasznay [55], and Fermin and Cook [56]). For the cascade wake, the static pressure is considered to have an adverse gradient in the streamwise direction because the edge velocity in the cascade wake decreases downstream.

The understanding of the turbulent wakes of the single airfoil and the cascade of airfoils represents not only an interesting problem in fluid mechanics, but also an important aerodynamic problem related to the prediction of lift, drag, and aerodynamic noise level of the airfoil and the cascade.

Very few experimental and theoretical studies have been made for the turbulent wakes of the single airfoil and the cascade of airfoils. Near and far wakes of a symmetrical airfoil were first investigated experimentally by Silverstein et al. [57], who provided empirical relationships for the wake decay. Preston et al. [58] carried out a systematic investigation of the characteristics of the wake behind an isolated airfoil and observed that a similarity in mean velocity profile exists close behind the airfoil. Mendelsohn [59] measured the wake of an isolated airfoil at various incidence angles. All of these measurements were concentrated on the mean velocity, and turbulence flow quantities were not measured. Chevray and Kovasznay [55] measured the mean velocity and turbulent quantities in the symmetric wake of a flat plate including the trailing edge region. Though their experimental data have been frequently referred to as the most accurate and comprehensive data for the two-dimensional turbulent wake by many investigators (Launder, Reece and Rodi [30], Bradshaw [60], etc.), the experimental data do not include the measurement of spanwise intensity. No turbulence measurements for the asymmetric wake of a single airfoil including the near wake region have been reported before this report. The turbulent structure as well as the mean velocity profile of an asymmetric turbulent wake is known to be different from that of a symmetric wake. Measurements of turbulence quantities as well as the mean velocity in an asymmetric wake of a single airfoil will be reported in the following sections.

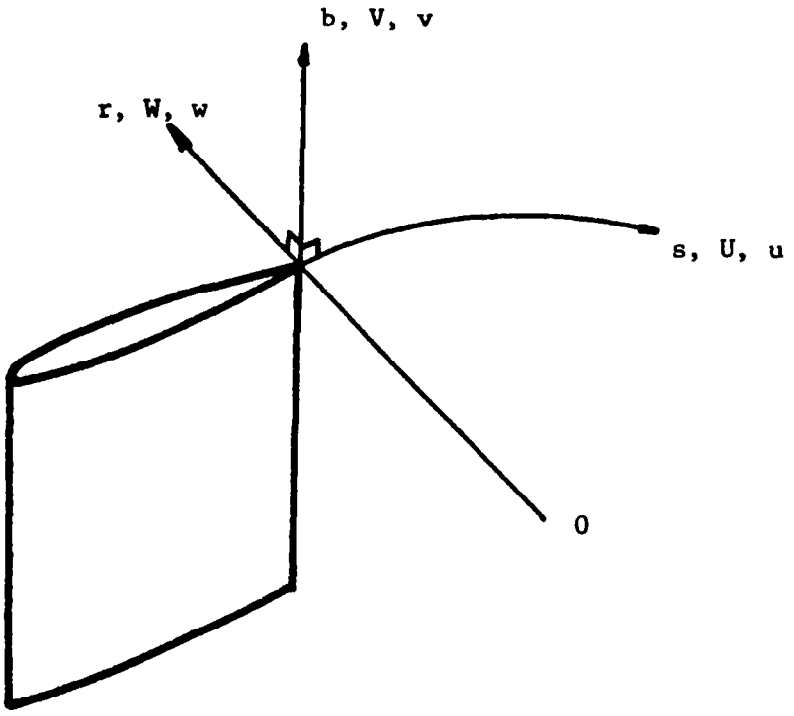

Figure 31. Coordinate System for the Single Airfoil Wake

Theoretically, most work related to the two-dimensional turbulent wakes has been confined to the far wake region. This is because the flow evolution far downstream is very slow and a subsequent similarity solution can be assumed (Tennekes and Lumley [4]). Though the similarity solution has good agreement with experimental measurements, it cannot be easily expanded to the upstream flow. The measurements in the turbulent wake of a cylinder by Townsend [61] shows the similarity in mean velocity about 80 cylinder diameters behind and the similarity in Reynolds stress beyond about 200 cylinder diameters. Furthermore, the more complicated the statistical quantity, the longer it takes to reach the region which is characterized by the similarity rule. For the near-wake region, Goldstein [5] obtained a semi-analytical solution for the symmetrical laminar wake of a flat plate. Also, the symmetric laminar near wake of a flat plate including the trailing edge region has been successfully predicted with various numerical schemes (Dennis and Dunwoody [62], Dennis and Chang [63], and Stewartson [6]). Compared to the laminar wake, the turbulent wake has a much more complicated structure at the trailing edge region. The boundary layer at the trailing edge of an airfoil has a viscous sublayer, buffer layer, inertial sublayer, and an outer layer. The transfer from the boundary layer structure at the trailing edge to the wake structure occurs in a short distance and is not well-understood.

Numerically, the symmetric turbulent wake of a flat plate has been predicted by Launder, Reece, and Rodi [20] and Pope and Whitelaw [54] with slightly different numerical schemes. As the asymmetric turbulent wake has a different turbulence structure from that of the symmetric wakes, the turbulence closure modelling for the symmetric turbulent wake is not considered to be directly applied for the predictions of asymmetric turbulent wakes. Proper modification of existing turbulence closure models for the prediction of asymmetric turbulent wakes will be discussed and the numerical results will be compared with the experimental study in this thesis.

Numerical Analysis of Turbulent Wakes of Isolated Airfoils and Cascades of Airfoils

The Curvilinear Coordinate System

As was evident from the previous flow visualization around a single airfoil, there exists streamline curvature in the near wake when the flow field is not symmetric. For calculation of the curved turbulent wakes of a single airfoil and a cascade, the curvilinear coordinate system shown in Figure 31 was introduced. In this figure, r is the distance from the origin of curvature, s is the streamwise distance on the specified path, and b is normal to s and r. With this coordinate system, the actual streamline of the wake can be closely represented. This coordinate system forms part of the coordinate system for the calculation of the wakes of the single airfoil and the cascade blade. The fundamental metric tensor, Christoffel symbols can be derived in the same way as for the curvilinear coordinate system for the rotor wake. Detailed derivations are not repeated here. The fundamental metric tensor for this coordinate system is:

$$g_{ij} = \begin{bmatrix} 1 & -\frac{s}{r} & 0 \\ -\frac{s}{r} & 1+\frac{s^2}{r^2} & 0 \\ 0 & 0 & 1 \end{bmatrix}$$

$$g^{ij} = \begin{bmatrix} 1+\frac{s^2}{r^2} & \frac{s}{r} & 0 \\ \frac{s}{r} & 1 & 0 \\ 0 & 0 & 1 \end{bmatrix} \qquad (69)$$

Christoffel symbols of the second kind are as follows:

$$\Gamma^1_{11} = -\frac{s}{r^2}$$

$$\Gamma^2_{11} = -\frac{1}{r}$$

$$\Gamma^1_{12} = -\Gamma^2_{22} = \frac{s^2}{r^3}$$

$$\Gamma^2_{21} = \frac{s}{r^2}$$

$$\Gamma^1_{22} = -\frac{s^3}{r^4} \qquad (70)$$

All other Christoffel symbols of the second kind are zero.

The Governing Equation in the Curvilinear Coordinate System

The equations governing the steady incompressible flow are introduced in generalized tensor form.

The continuity and momentum equations are, respectively,

$$U^i_{,i} = 0 \quad , \quad u^i_{,i} = 0 \tag{71}$$

$$U^j U^i_{,j} + \overline{u^j u^i}_{,j} = - \frac{g^{ij}}{\rho} \frac{\partial p}{\partial x^j} + \nu g_{jk} U^i_{,jk} \tag{72}$$

In the present coordinate system, the continuity equation is:

$$\frac{\partial U}{\partial s} + \frac{\partial W}{\partial r} = 0 \quad , \quad \frac{\partial u}{\partial s} + \frac{\partial w}{\partial r} = 0 \tag{73}$$

Where U, W are mean contravariant velocity components in the present curvilinear coordinate system and u, w are corresponding fluctuating velocity components. Two components of the equation of mean momentum conservation in the present curvilinear coordinate system, at high Reynolds number are:

$$U \frac{\partial U}{\partial s} + W \frac{\partial U}{\partial r} + U^2 \Gamma^1_{11} + W^2 \Gamma^1_{22} + 2\, UW \Gamma^1_{12} = - \frac{1}{\rho} \left[\frac{s}{r} \frac{\partial p}{\partial r} + \left(1 + \frac{s^2}{r^2}\right) \frac{\partial p}{\partial s} \right] - \frac{\partial \overline{uw}}{\partial r} - \frac{\partial \overline{u^2}}{\partial s} - \overline{u^2}\, \Gamma^1_{11} - \overline{uw} \Gamma^1_{12} - \overline{w^2} \Gamma^1_{12} \tag{74}$$

$$U \frac{\partial W}{\partial s} + W \frac{\partial W}{\partial r} + U^2 \Gamma^2_{11} + W^2 \Gamma^2_{22} + 2\, U\, W\, \Gamma^2_{12} = - \frac{1}{\rho} \left[\frac{\partial p}{\partial r} + \frac{s}{r} \frac{\partial p}{\partial s} \right] - \frac{\partial \overline{uw}}{\partial s} - \frac{\partial \overline{w^2}}{\partial r} - \overline{u^2} \Gamma^2_{11} - \overline{w^2} \Gamma^2_{22} - \overline{uw}\, \Gamma^2_{22} \tag{75}$$

Turbulence Closure Modelling for the Curved Turbulent Flows

The turbulent wakes of a single airfoil and a cascade which develop under the influence of streamline curvature were calculated using three different turbulence closure models. The first model was comprised of transport equations for the turbulent kinetic energy and the rate of energy dissipation. The second model used equations for the rate of turbulent kinetic energy dissipation and Reynolds stresses, but the effects of the convection and diffusion in the Reynolds stress transport equation were handled collectively. The third model utilized equations of turbulent kinetic energy dissipation and Reynolds stresses in nearly exact form. All three of the models were modified for the effects of streamline curvature.

The transport equations for the turbulence closure which make up the three turbulence closure models are as follows:

First model: two-equation model.

$$U^i \frac{\partial k}{\partial x^i} = \frac{\partial}{\partial x^i}\left(\frac{\nu_{eff}}{\sigma_k}\frac{\partial k}{\partial x^i}\right) + P - \varepsilon \tag{76}$$

$$U^i \frac{\partial \varepsilon}{\partial x^i} = \frac{\partial}{\partial x^i}\left(\frac{\nu_{eff}}{\sigma_\varepsilon}\frac{\partial \varepsilon}{\partial x^i}\right) + S - C_{\varepsilon 2}\frac{\varepsilon^2}{k} \tag{77}$$

where

$$\nu_{eff} = C_\mu k^2/\varepsilon \quad , \quad P = -\overline{u_i u_j}\, U^i_{,j}$$

$$k = \frac{1}{2} g_{ij}\, \overline{u^i u^j}$$

$$-\overline{u^i u^j} = \nu_{eff}\left(U^i_{,j} + U^j_{,i}\right) - \frac{2}{3} k\, g^{ij}$$

and S is the source term in the transport equation of the rate of turbulent kinetic energy dissipation. Two forms of S were utilized and the results by each form were analyzed. The two forms of S are:

$$S = C_{\varepsilon 1}\frac{\varepsilon}{k} P \tag{78}$$

and

$$C_\ell \frac{\varepsilon^2}{k}\left(\overline{u^i u^j} - \frac{2}{3} k\delta_{ij}\right)\left(\overline{u^j u^i} - \frac{2}{3} k\delta_{ji}\right) \tag{79}$$

Second and third models: Reynolds stress models.

The second and third models utilize the simplified form of the transport equation of Reynolds stress. The pressure-strain correlation term in the transport equation of Reynolds stress was modelled following the proposals by Rotta [50] and Naot, Savit, and Wolfstein [51]. Furthermore, the rate of turbulence energy production, which appears in the modelling of mean-strain effects in the pressure-strain correlation, was replaced with the rate of turbulent kinetic energy dissipation. The second and third models differ only in the handling of convection and diffusion terms. The convection and diffusion terms are handled collectively in the second model; the effects of

the two terms are assumed to be proportional to the production term and the magnitude of the effects are corrected at each iteration.

The third model includes the individual effects of convection and diffusion and is similar to the equation used by Launder, Reece, and Rodi [20] for straight non-rotating flows. The rotation-originated redistribution term was added in the turbulence closure equations.

Second model: simplified Reynolds stress model. The equation used for this case is given as follows:

$$0 = (1 + C_1)(-u_k\overline{u^j U^i}_{,k} - u_k\overline{u^i U^j}_{,k})(1 - \gamma) - \frac{2}{3} g^{ij}\varepsilon(1 - \gamma) - C_{\phi 1}\frac{\varepsilon}{k}(\overline{u^i u^j} - \frac{2}{3} g^{ij}k) \tag{80}$$

where C_1 relates the collective effects of the convection and diffusion terms to the production terms.

Third model: full Reynolds stress model. The complete Reynolds stress equation (with suitable modelling for pressure-velocity correlation, etc.) is given as follows:

$$U^k\overline{u^i u^j}_{,k} = [C_s\frac{k}{\varepsilon}\overline{u_k u_m}(\overline{u^i u^j})_{,m}]_{,k} + (-\overline{u_k u^j}U^i_{,k} - u\overline{u^i U^j}_{,k})(1 - \gamma) - 2(\varepsilon^{i\ell m}\Omega_\ell\overline{u_m u^j} + \varepsilon^{j\ell m}\Omega_\ell\overline{u_m u^i}) - \frac{2}{3} g^{ij}\varepsilon(1 - \gamma) - C_{\phi 1}\frac{\varepsilon}{k}(\overline{u^i u^j} - \frac{2}{3} g^{ij}k) \tag{81}$$

The values of constants in equations (76) through (81) were not optimized for the present curved wakes; the values used by Pope and Whitelaw [54] were adopted. The value of C_ℓ in equation (79) was 1.8 for the present calculation.

The effect of streamline curvature on a fluid flow has been qualitatively explained with the motion of a disturbed element of fluid. The argument based on incompressible, inviscid fluid is as follows. The effect of streamline curvature is to stabilize the flow field and consequently diminish the turbulent transportation when the angular momentum increases with the radius of streamline curvature and vice versa for the opposite case. Quantitatively, the following expression can be derived for the criterion of stability:

$$\omega^2 = 2\frac{U}{r^2}\frac{d}{dr}(Ur) = 2(\frac{U}{r}\frac{dU}{dr} + \frac{U^2}{r^2}) \tag{82}$$

where ω is the corresponding frequency, U is the circumferential velocity component, and r is the radius of curvature. For most thin shear flow, the first term is dominant. To account for the above effect of curvature, Bradshaw [22] proposed modification of the conventional effective viscosity model and Launder, Pridden, and Sharma [24] modified the two-equation model. Irwin and Smith [64] reported successful calculation by manipulating curvature terms which

appear in the transport equation of Reynolds stress in the special coordinate system. The turbulence closure models with the conventional dissipation equation (with the source term (81)) have been widely applied and criticized for poor prediction of curved flows (e.g., Launder, Pridden, and Sharma, [24], and Bradshaw [22]).

The existing prediction techniques for curved turbulent flow utilizing the turbulence models with the conventional dissipation equation (with the source term (78)) are considered to be inadequate. This is caused by the inappropriate form of the dissipation equation which is based on unproven assumptions and tested with only straight flows.

To represent the effect of streamline curvature properly, the rate of energy dissipation should be increased where the angular momentum increases with the radius of curvature and decreased where the angular momentum decreases with the radius of curvature. For the coordinate system shown in Figure 31, the production term in equation (76) is, neglecting high-order stress terms,

$$\begin{aligned} P &= -\overline{u_i u_j}\, U^i_{,j} \\ &= -\overline{u^2}\left(\frac{\partial U}{\partial s} + U\frac{s}{r^2} + V\frac{s^2}{r^3}\right) - \overline{v^2}\left(\frac{\partial V}{\partial r} + U\frac{s}{r^2} - V\frac{s^2}{r^3}\right) \\ &\quad - \overline{uv}\left(\frac{\partial U}{\partial r} + \frac{\partial V}{\partial s} - \frac{U}{r} + U\frac{s^2}{r^3} + V\frac{s}{r^2} - V\frac{s^3}{r^4}\right) \end{aligned} \tag{83}$$

and if higher order curvature terms including s/r^2 are neglected,

$$P = -\overline{u^2}\frac{\partial U}{\partial s} - \overline{v^2}\frac{\partial V}{\partial r} - \overline{uv}\left(\frac{\partial U}{\partial r} + \frac{\partial V}{\partial s} - \frac{U}{r}\right)$$

and for the first model,

$$P = \nu_{eff}\left[2\left(\frac{\partial U}{\partial s}\right)^2 + 2\left(\frac{\partial V}{\partial r}\right)^2 + \left(\frac{\partial U}{\partial r}\right)^2 + \left(\frac{\partial V}{\partial s}\right)^2 + 2\frac{\partial U}{\partial r}\frac{\partial V}{\partial s} - \frac{U}{r}\frac{\partial V}{\partial s} - \frac{U}{r}\frac{\partial U}{\partial r}\right]$$

The above expression can be further simplified for the thin shear layer with small pressure gradient in the normal direction,

$$P = \nu_{eff}\left[\left(\frac{\partial U}{\partial r}\right)^2 - \frac{U}{r}\frac{\partial U}{\partial r}\right] \tag{84}$$

The second term of the above expression has the same form as the principal term of expression (82) and represents the curvature effect that was discussed qualitatively. As will be shown in the next section, turbulence closure models with the conventional dissipation equation [with the source term (78)] do not predict curved turbulent wakes accurately even though the transport equations are in the curvilinear coordinate system. Referring to equation (76), it is

clear that the turbulent kinetic energy increases with a decrease in angular momentum (rU). However, the dissipation rate also increases when the production of kinetic energy dissipation rate, and the overall effect of curvature is not adequately included in the turbulence modelling.

Chambers and Wilcox [25], proposed modification of the first model for the curvature effect. They suggested adding extra singular terms to the transport equations of turbulent kinetic energy and the rate of energy dissipation. However, these terms increase both the kinetic energy and the rate of energy dissipation where the angular momentum decreases with the radius of curvature, and subsequently do not fully account for the curvature effect for the present set of data.

Two different dissipation equations were tried for better prediction of curved turbulent wakes. As Lumley and Khajeh-Nouri [21] argued, the production term can be used as the source term in the dissipation equation with the assumption that

$$(\overline{u^i u^j} - \frac{2}{3} k\delta_{ij})\alpha(U^i_{,j} + U^j_{,i}) \ . \tag{85}$$

This assumption is not valid when the flow field is affected by streamline curvature and rotation; therefore, the exact source term,

$$(\overline{u^i u^j} - \frac{2}{3} k\delta_{ij})(\overline{u^j u^i} - \frac{2}{3} k\delta_{ji})$$

by Lumley and Khajeh-Nouri [21] was utilized. To make the dimensions correct, the following source term was used for the present calculation:

$$S = C_\ell \frac{\varepsilon^2}{k^3}\left(\overline{u^i u^j} - \frac{2}{3} k\delta_{ij}\right)\left(\overline{u^j u^i} - \frac{2}{3} k\delta_{ji}\right) \tag{86}$$

which is given as the second form of the source term in equation (77).

Also, a modification of the conventional dissipation equation was tried in order to represent the curvature effect more accurately. The coefficient of the source term, which includes production of energy, was modified as follows:

$$S = C_{\varepsilon 1}(1 + C_c R_i)\frac{\varepsilon}{k} P \tag{87}$$

where $R_i = \frac{k}{\varepsilon}\frac{1}{r}\frac{\partial(rU)}{\partial r}$ and can be interpreted as the Richardson number in curved turbulent flow. The constant C_c relates the streamline curvature to the local dissipation rate, and the optimized value with the available data was 0.03.

Nine turbulence closure models used for calculation of the wakes of isolated airfoils and cascades of airfoils are tabulated and shown in Table 2.

Numerical Technique

The numerical scheme for the turbulent wakes of single airfoils and cascades of airfoils is very similar to that used for calculation of the rotor wake. The wakes of single airfoils and cascades of airfoils are two-dimensional, and the numerical scheme developed for the rotor wake can be simplified for the calculation of two-dimensional wakes. The continuity and mean momentum equations (73), (74), and (75), along with the closure equations (76) through (81) were solved in elliptic form. At the near-wake region, the streamwise velocity gradient is of the same order of magnitude as the normal velocity gradient. None of the shear stress components are negligible. Therefore, the conventional boundary-layer assumption cannot be invoked in this region. The parabolic marching technique does not produce accurate predictions. The initial values of unknowns were obtained by parabolic marching technique, then the values were corrected iteratively.

The typical domain of calculation of the wake of an isolated airfoil is shown in Figure 32. The boundary conditions on AB and CD were based on the experimental data. The turbulent kinetic energy on boundaries AD and BC was calculated on the basis of the free-stream turbulence intensity (0.2%). The boundary values of dependent variables except the rate of the turbulent kinetic energy dissipation were directly obtained from the experimental data. As mentioned earlier, the rate of turbulent kinetic energy dissipation was assumed to be equal to the production of the energy. For the first iteration, the origin of the coordinate system in Figure 31 was located on the line which is normal to the camber line and passes the trailing edge of the blade. This distance between the origin of the coordinate system and the trailing edge was assumed to be one chord length for the first calculation. The iteration was performed downstreamwise from the trailing edge. After each sweep of the iteration, the origin of the coordinate system was corrected and the effect of the streamline curvature was more accurately estimated for the next iteration. The turbulent kinetic energy and rate of energy dissipation were handled as diffusion terms in the first and second model. In the second model, the Reynolds stress components were first computed using equation (75) and the values of U^1, k, ε at the previous iteration. The governing equations were solved with these Reynolds stress components. Typical positions of grid nodes are given in Figure 33. In the third model, the shear-stress nodes were located between the adjacent nodes in the normal direction to provide stability in calculation. About 20 iterations gave converged values for all closure models. Figure 34 shows calculated values at different iterations for the wake of a single airfoil with the second turbulence closure model.

About 20 seconds were necessary for each iteration with the first model on IBM 370/3066 at The Pennsylvania State University. The second and third models required about 20 and 50 percent more computing time, respectively.

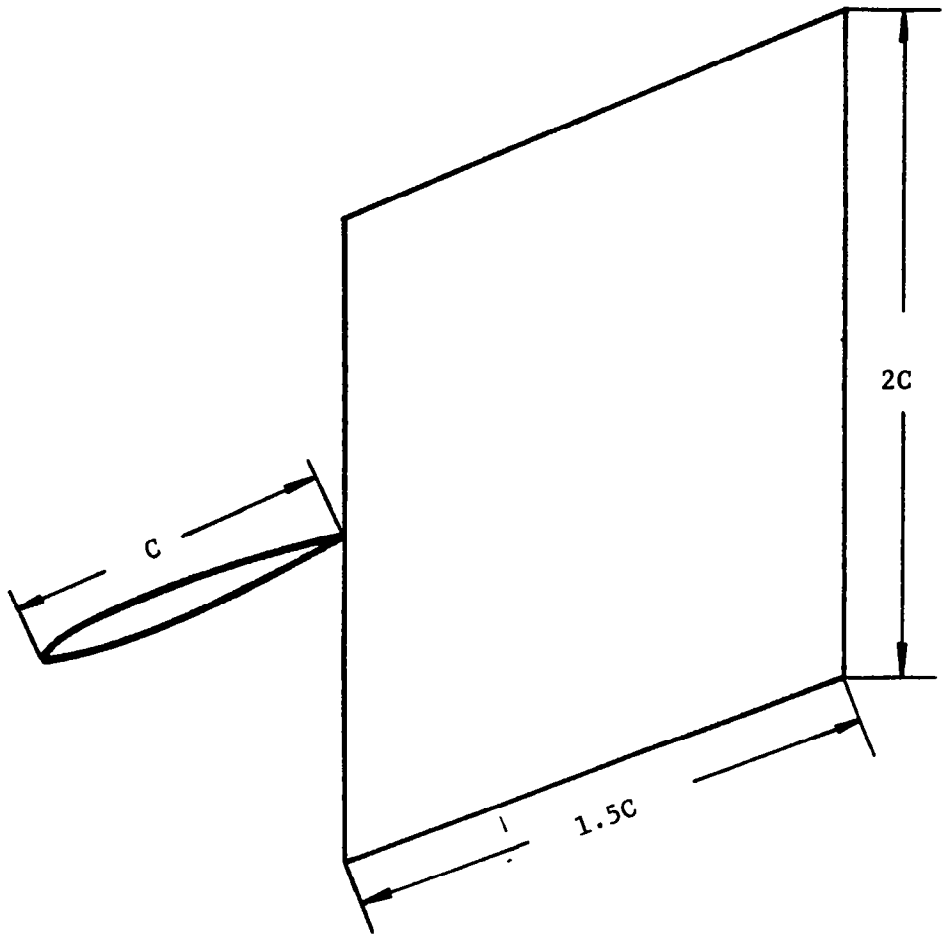

Figure 32. Domain of Calculation for the Single Airfoil Wake

Table 2. Turbulence Closure Models with Different Forms of the Source Term in the Equation for the Rate of Turbulent Kinetic Energy Dissipation

Turbulence Models	Source Term in the Dissipation Equation		
	$S = P = -\overline{u_i u_j}\, U^i_{,j}$	$S = C_e \frac{\varepsilon^2}{k}\left(\overline{u^i u^j} - \frac{2}{3} k \delta_{ij}\right)\left(\overline{u^j u^i} - \frac{2}{3} k \delta_{ji}\right)$	$S = C_{\varepsilon 1}\left(1+C_{\varepsilon} R_i\right) \frac{\varepsilon}{k} P$
k-ε	A1	A2	A3
Modified Reynolds Stress	B1	B2	B3
Reynolds Stress	C1	C2	C3

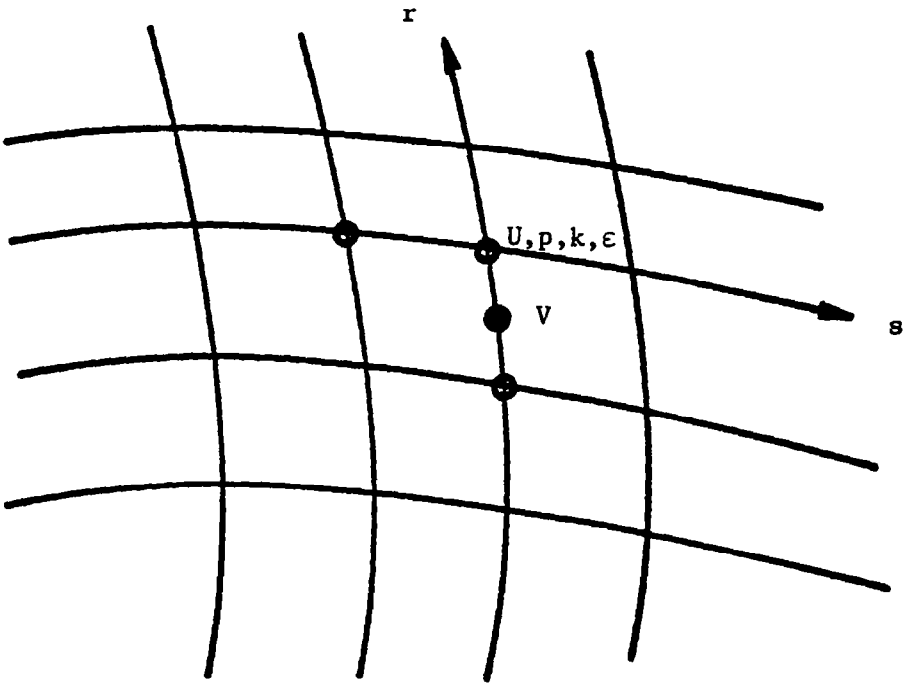

Figure 33. Typical Nodes for the Single Airfoil Wake

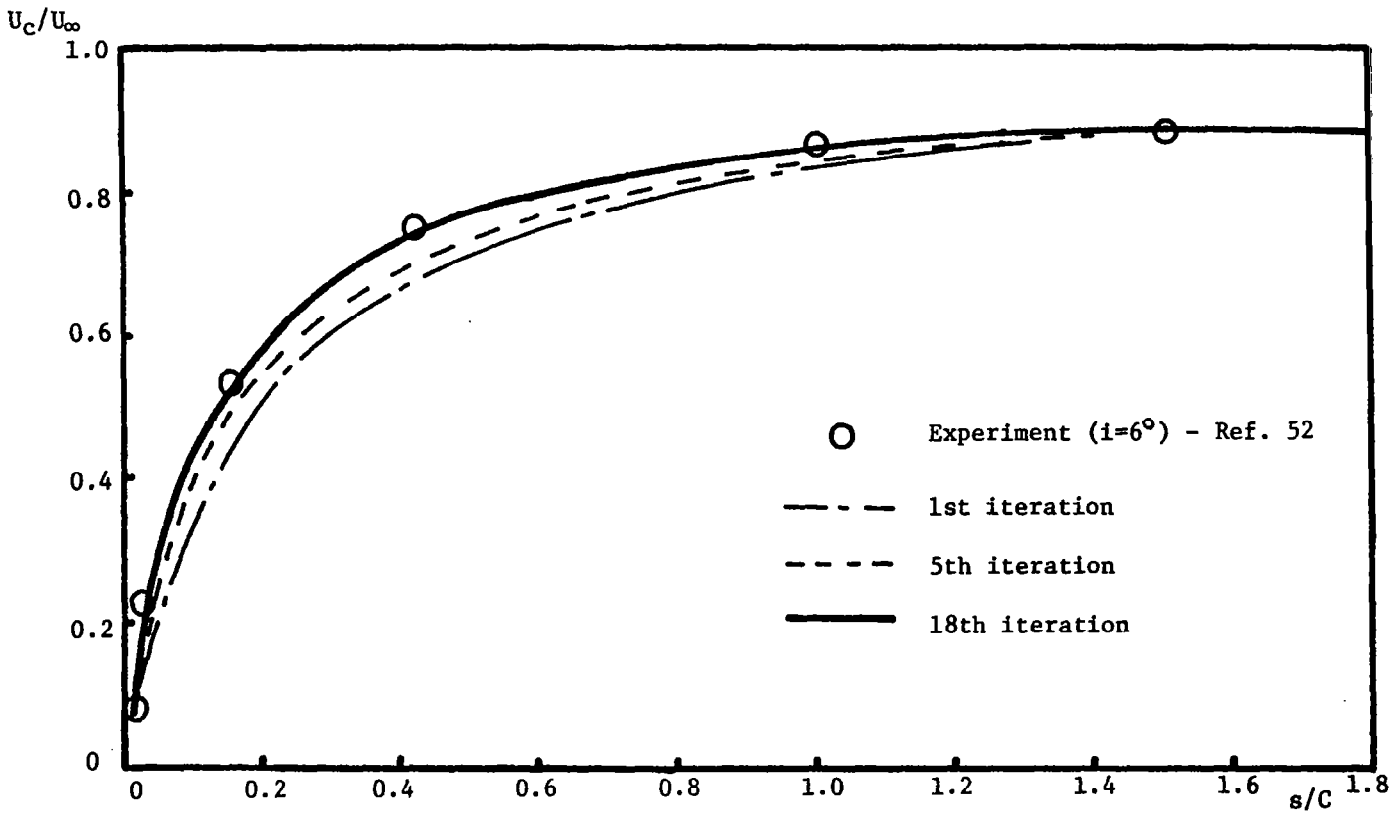

Figure 34. Wake Centerline Velocity Prediction at Various Iterations

A well-documented problem, the turbulent wake of a flat plate was solved to test the present numerical scheme. This symmetric turbulent wake, measured by Chevray and Kovasznay [55] was previously calculated by Launder et al. [20] and Pope and Whitelaw [54]. The predicted variation of the wake centerline velocity is shown in Figure 35, along with the experimental data. The three turbulence closure models predicted almost identical mean velocity profiles. Launder et al. [20] and Pope and Whitelaw [54] also reported almost identical results for this standard problem. Therefore, no additional numerical results for this problem are compared here.

Comparison of the Numerical Predictions of the Isolated Airfoil Wakes with Corresponding Experimental Data

The turbulent wakes of the isolated airfoil were numerically calculated and the results were compared with the experimental data. The three different turbulence closure models, equations (77) and (78), (80), and (81) were used for the calculation, along with three different forms of the source terms in the dissipation equations, equations (78), (86), and (87). Hence, the numerical predictions with nine different sets of turbulence schemes were compared with the experimental data. The turbulence closure models are shown in Table 2. The experimental data by Hah and Lakshminarayana [52] were used for the comparison. The measuring stations for the single airfoil wake are shown in Figure 35.

The calculated profiles of mean velocity and shear stress without curvature modification are given in Figure 36. The experimental data are also provided for comparison. The results with curvature modification are presented in Figures 37 and 38. The figures show that the three turbulence models do not predict the mean velocity and shear stress profiles accurately when the dissipation equation with the conventional source term (78) is used. All three models predict higher shear stress at the suction side than was found from the experimental data. However, this discrepancy disappears by modifying the conventional source term, equation (87) or by adopting the exact source term, equation (86). All three models predicted almost identical results for the mean velocity and the shear stress when the dissipation equation was modified.

The calculated values of turbulence intensity with different closure models are shown in Figures 39 through 47. The first model predicts almost isotropic values for the three intensity components, and the profile is corrected when the modified or exact source term is used in the dissipation equation. The second and third turbulence closure models with the conventional source term in the dissipation equation predict a higher intensity level on the pressure side and lower intensity level on the suction side than was found in the experimental data. However, the discretancy between prediction and experiment is considerably decreased by modifying the coefficient of the conventional source term or by adopting the exact source term. As described earlier, the turbulence level in the wake is not linearly dependent on the mean shear rate. The turbulence level on the pressure side is very low compared to that on the suction side of the wake, even though the mean shear rate on the pressure side is higher than that on the suction side. When the production of turbulent

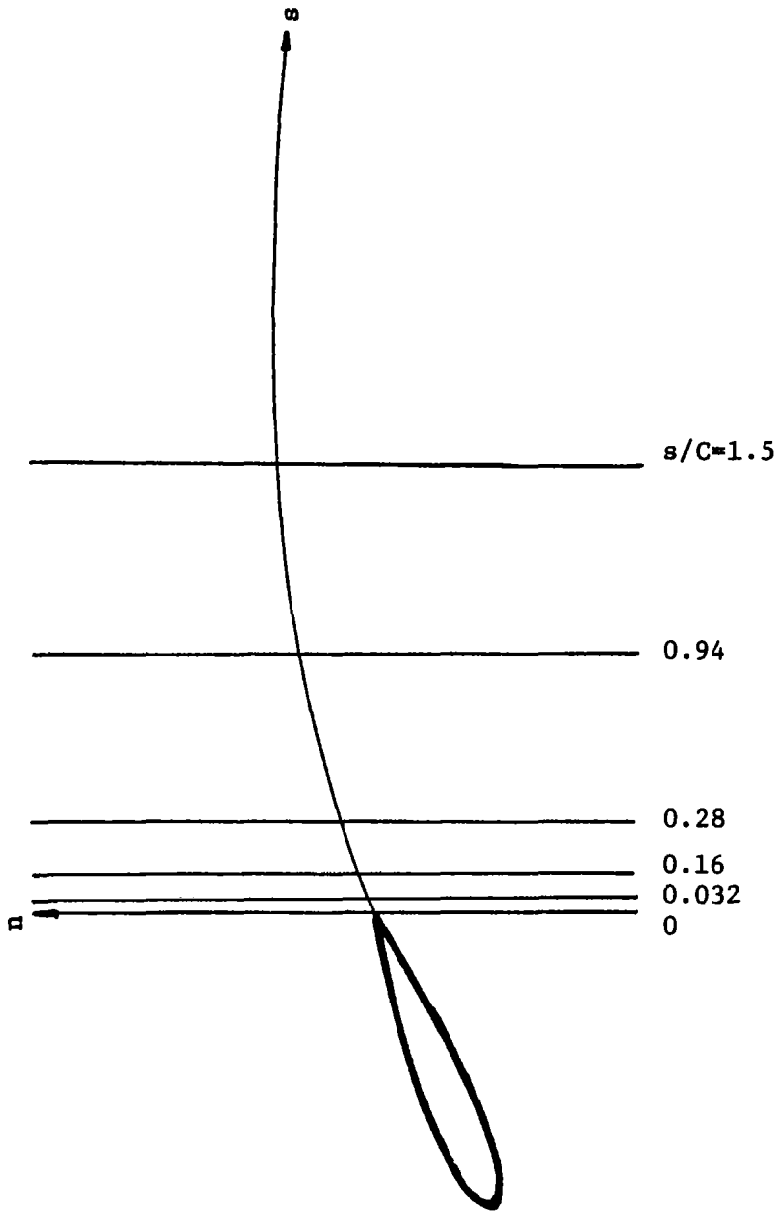

Figure 35. Measuring Stations

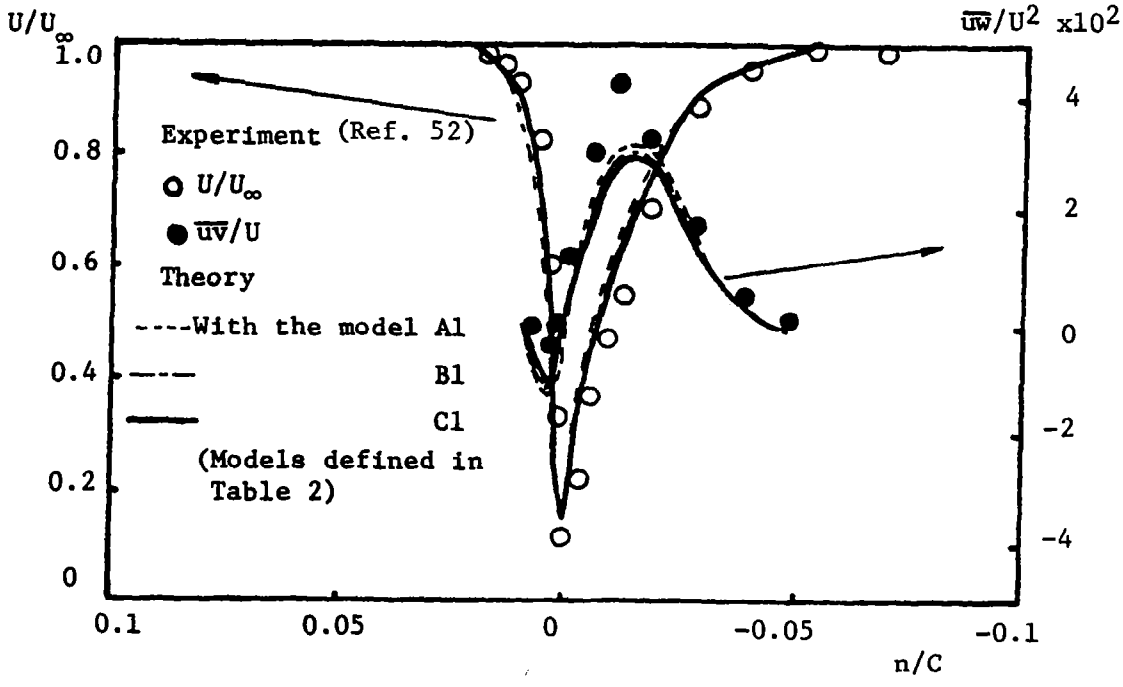

Figure 36. Streamwise Velocity and Shear Stress Profile at s/C=0.032 and i=6°

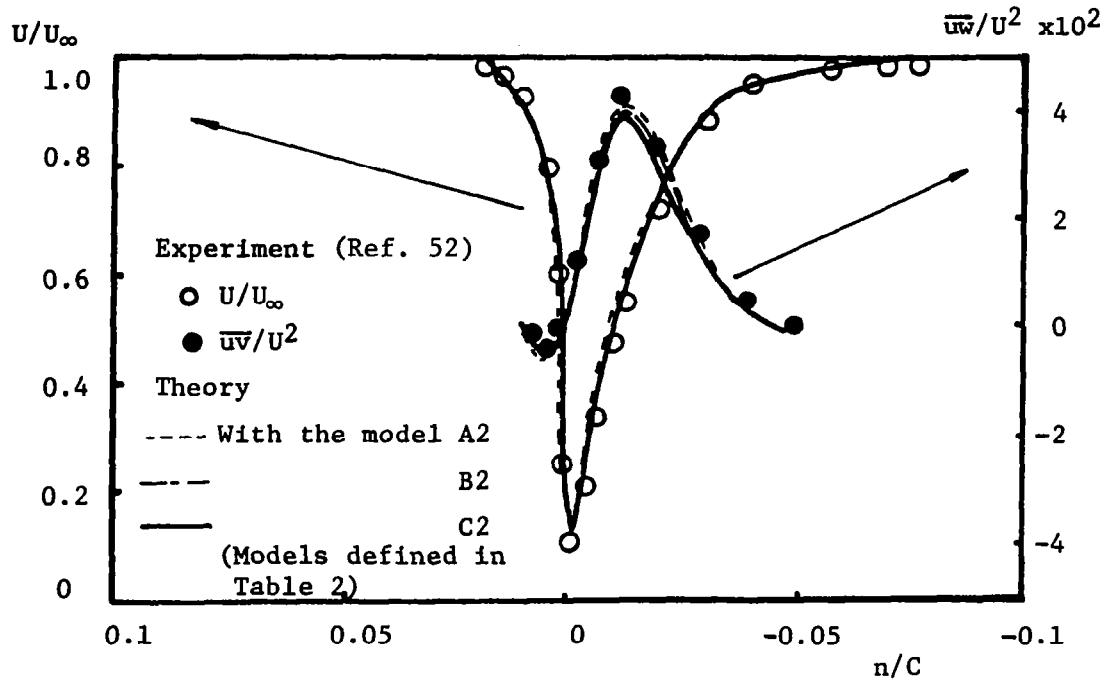

Figure 37. Streamwise Velocity and Shear Stress Profile at s/C=0.032 and i=6°

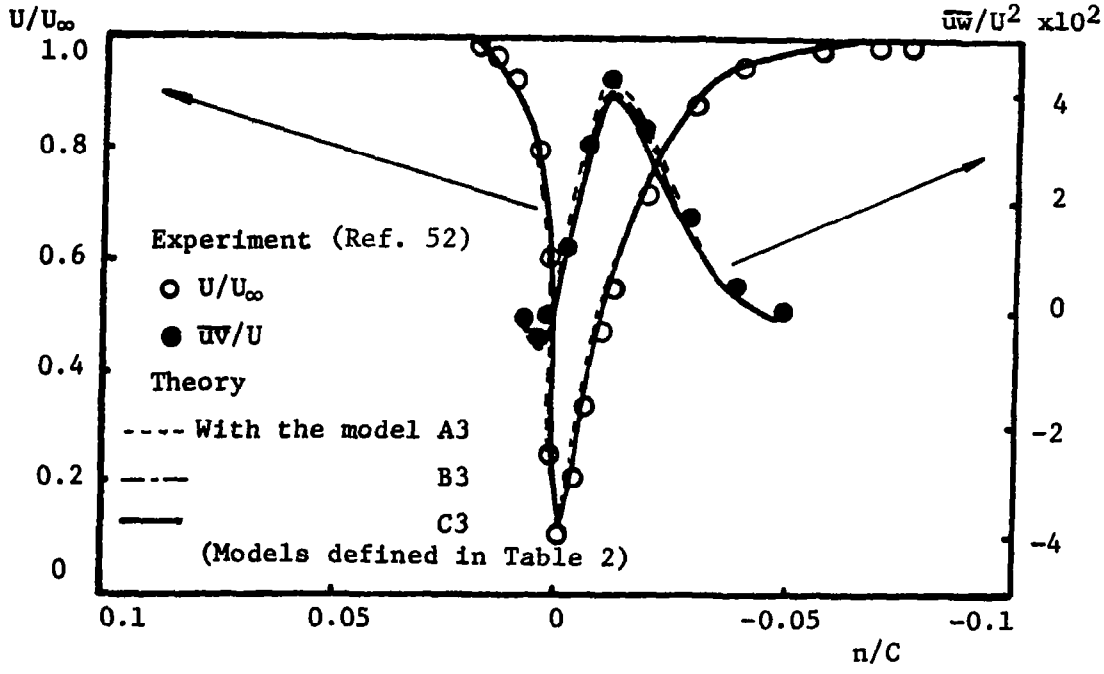

Figure 38. Streamwise Velocity and Shear Stress Profile at s/C=0.032 and i=6°

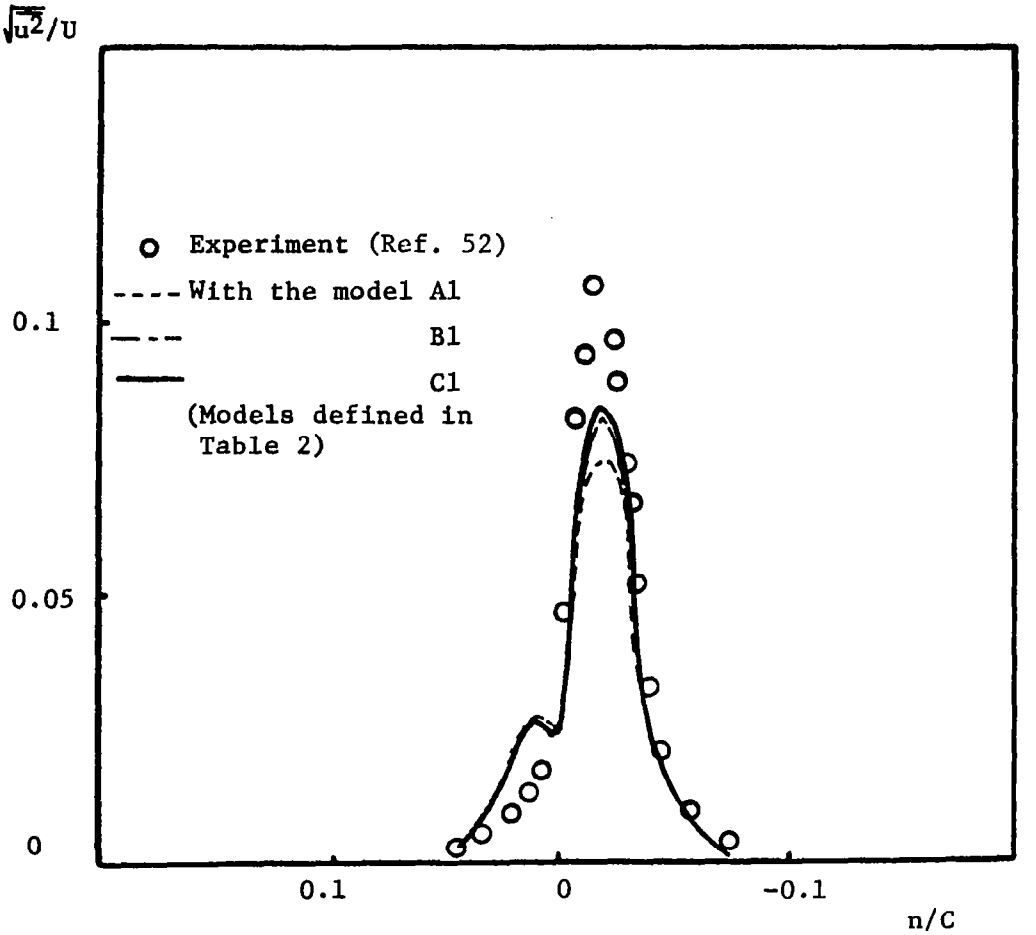

Figure 39. Relative Streamwise Intensity at s/C=0.032 and i=6°

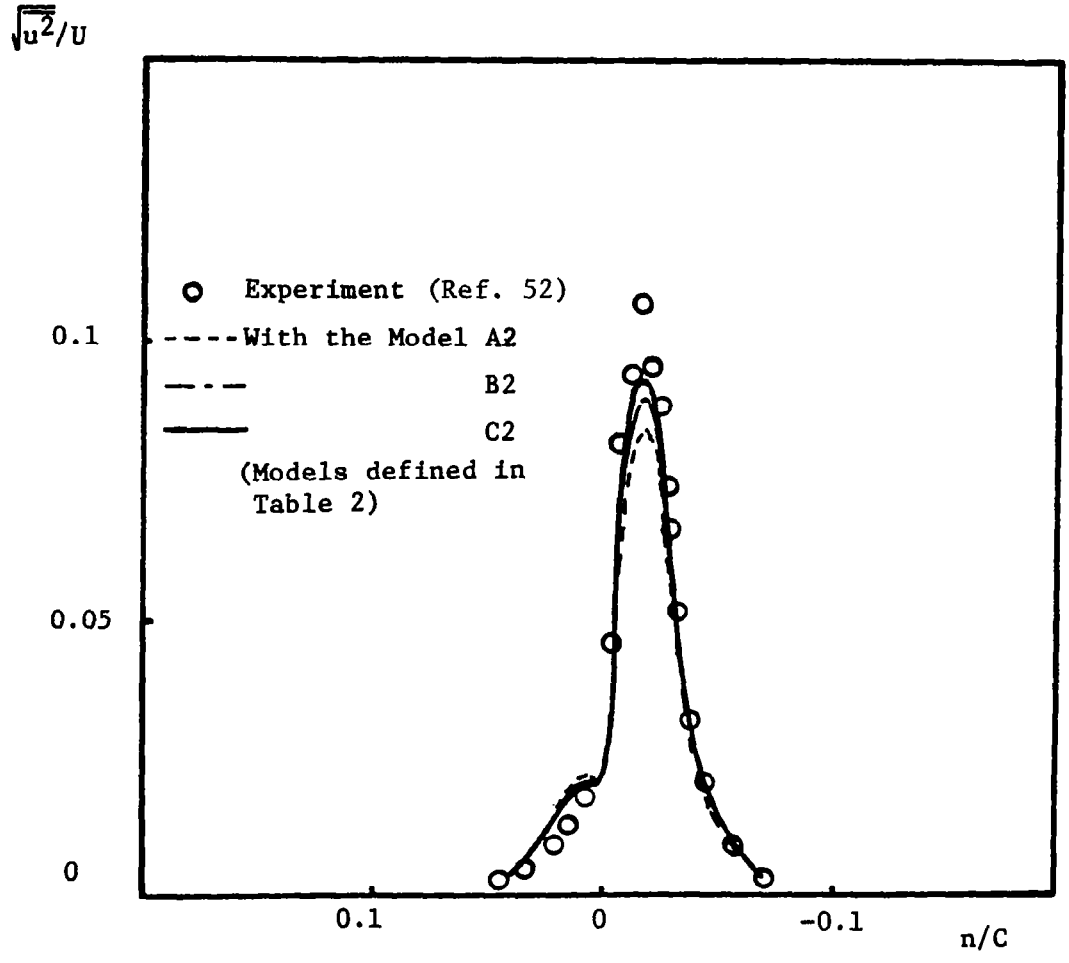

Figure 40. Relative Streamwise Intensity at s/C=0.032 and i=6°

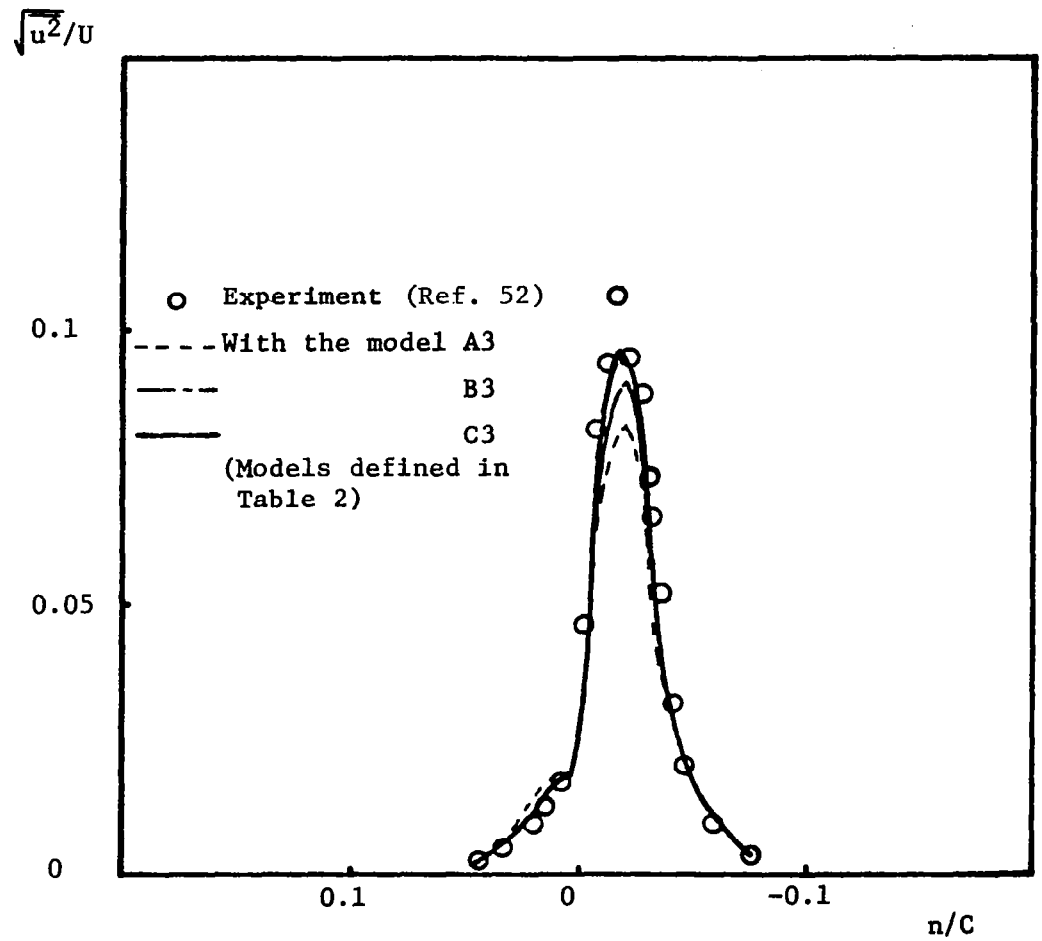

Figure 41. Relative Streamwise Intensity at s/C=0.032 and i=6°

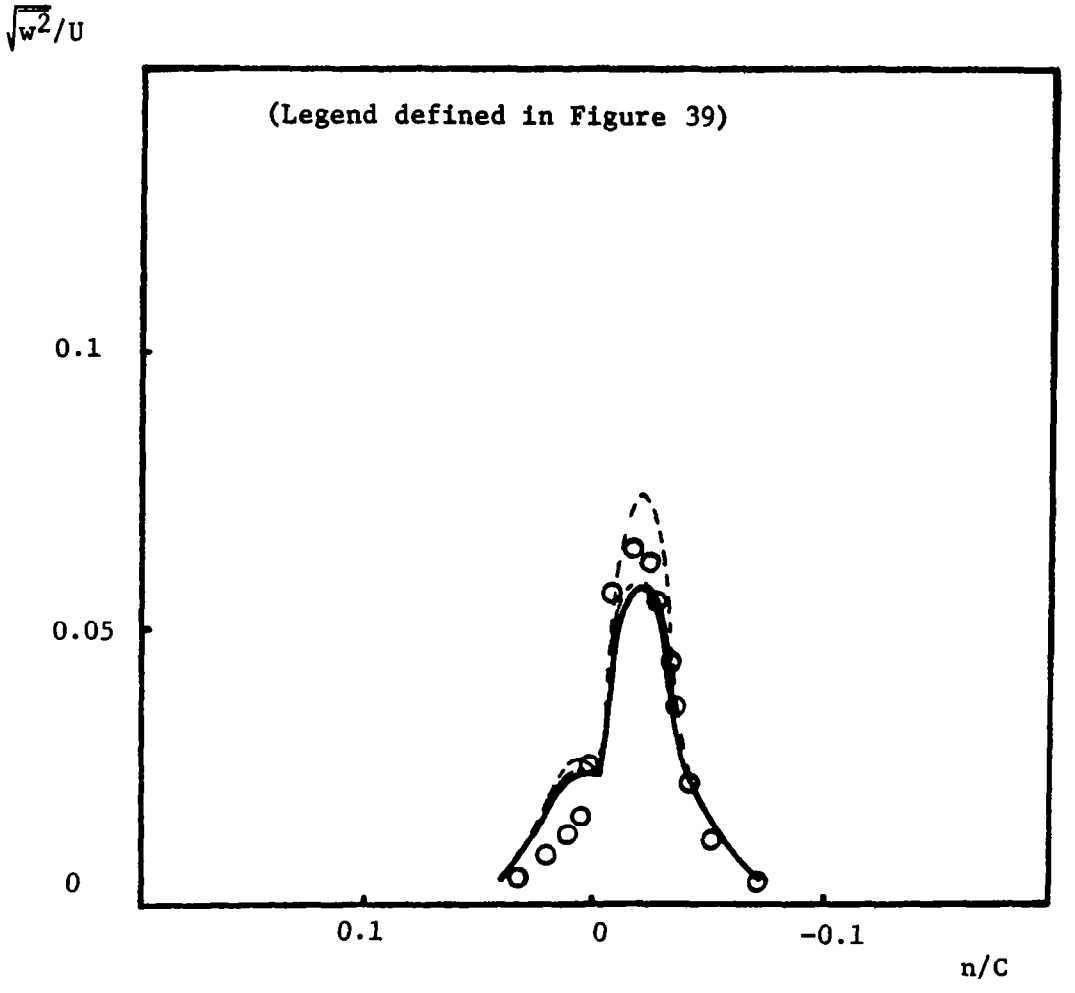

Figure 42. Relative Normal Intensity at s/C=0.032 and i=6°

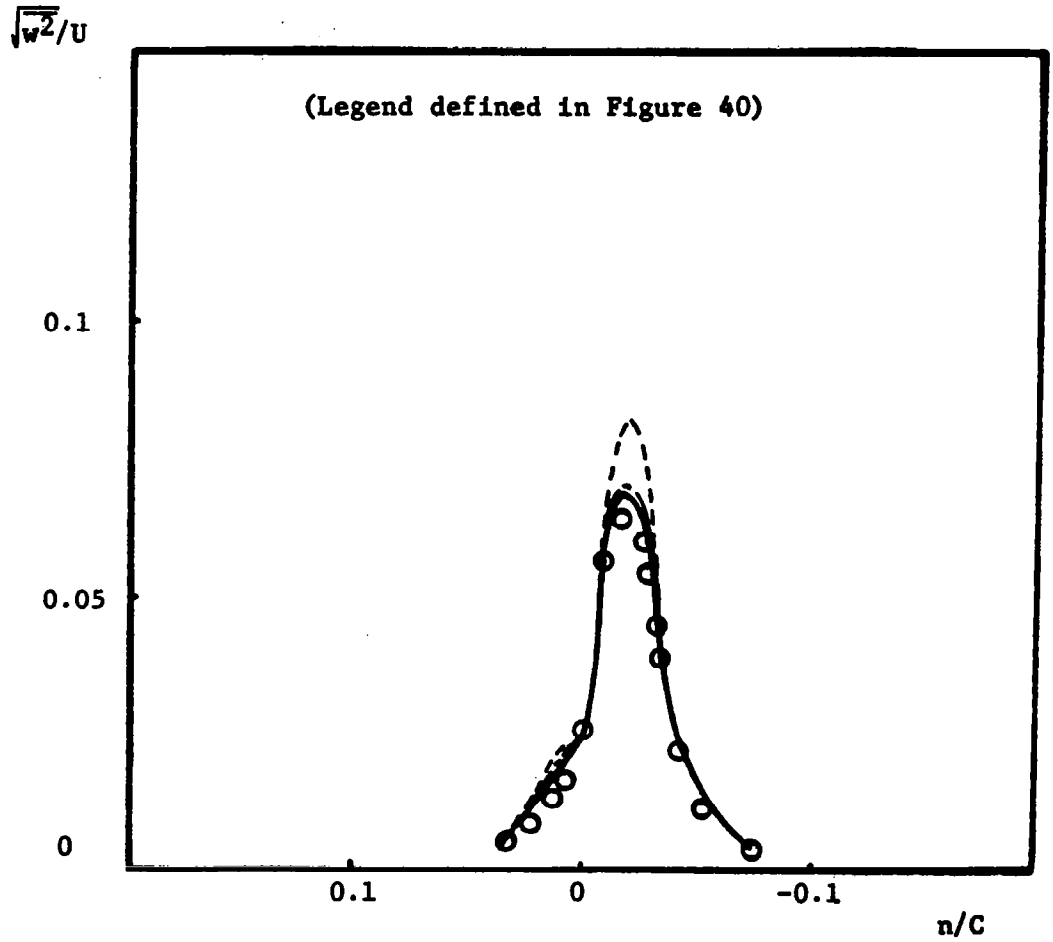

Figure 43. Relative Normal Intensity at s/C=0.032 and i=6°

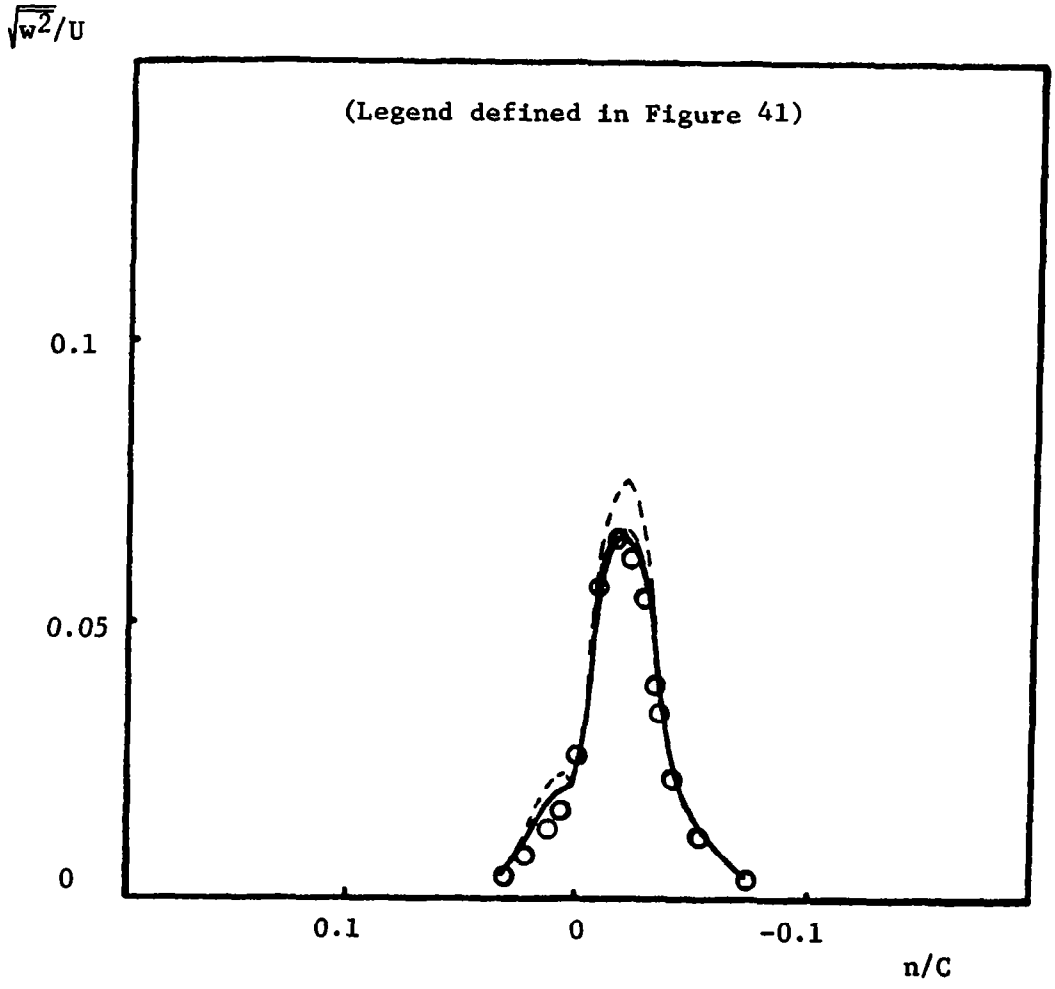

Figure 44. Relative Normal Intensity at s/C=0.032 and i=6

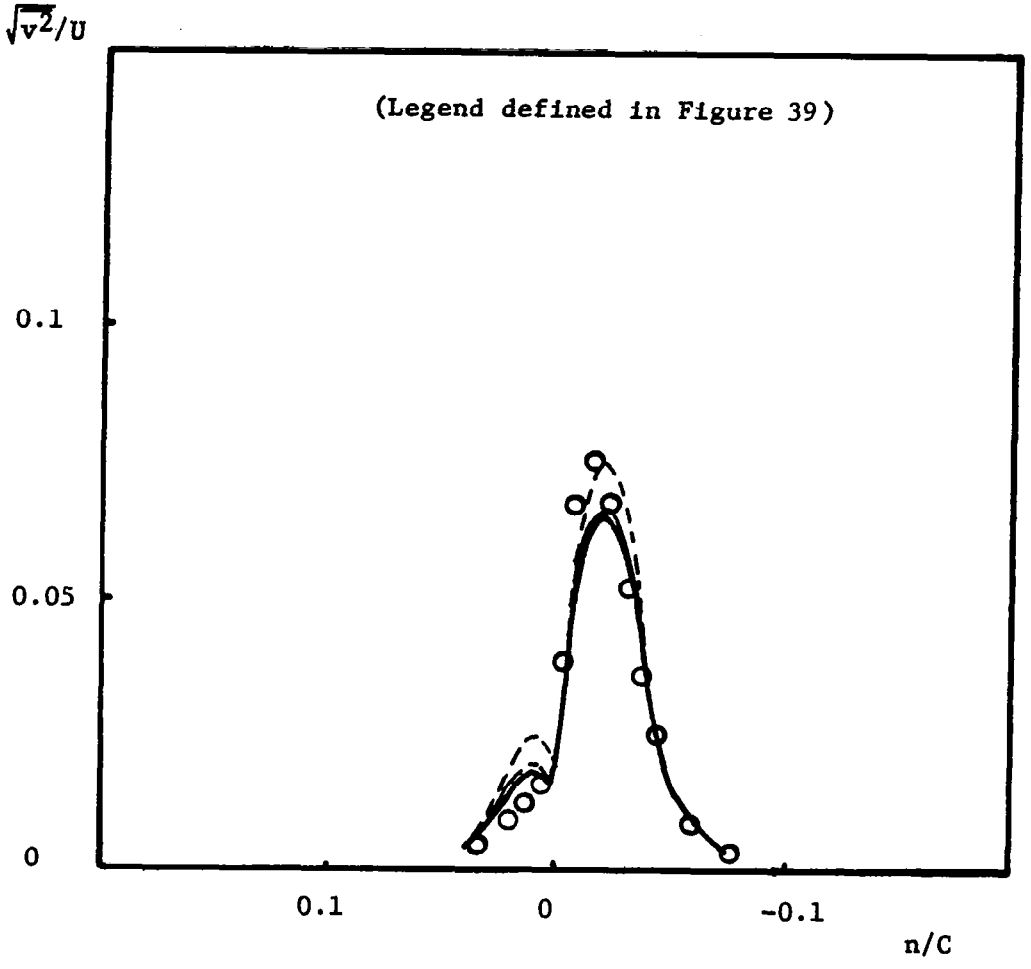

Figure 45. Relative Spanwise Intensity at s/C=0.032 and i=6°

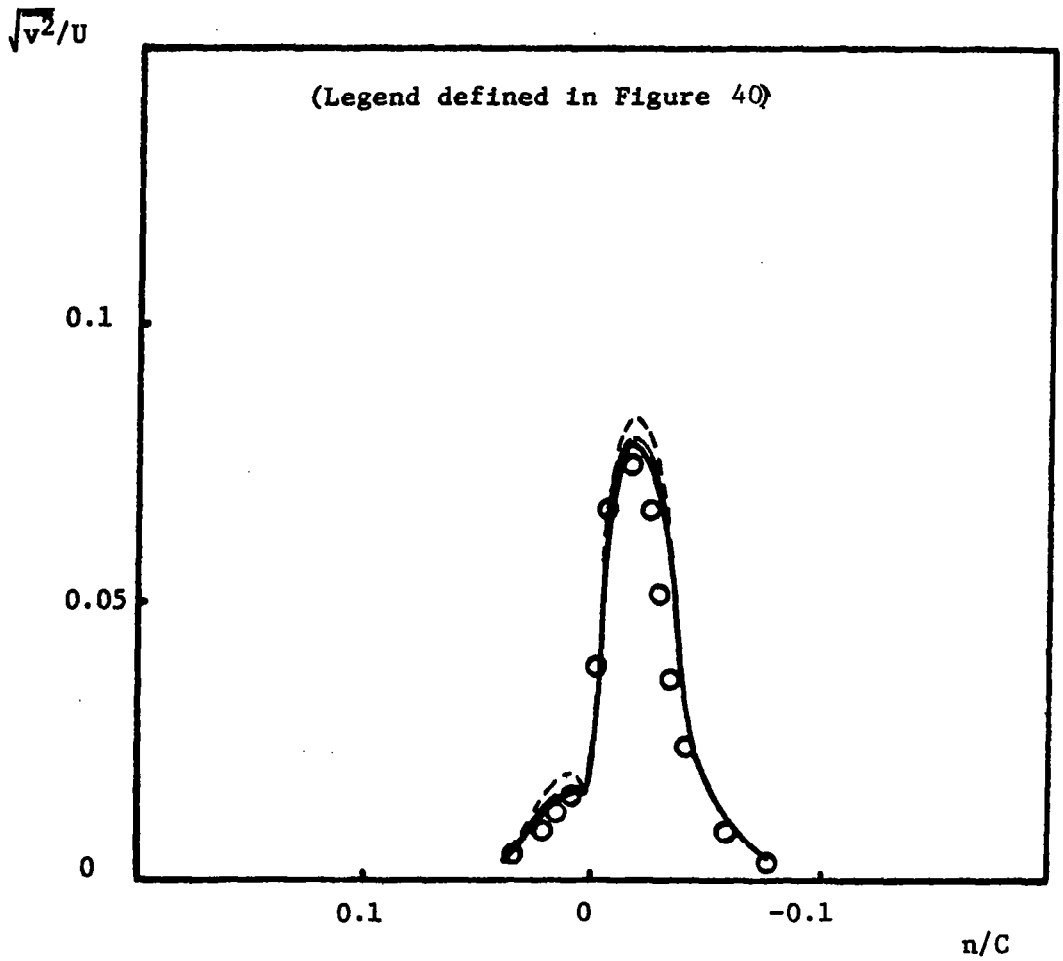

Figure 46. Relative Spanwise Intensity at s/C=0.032 and i=6°

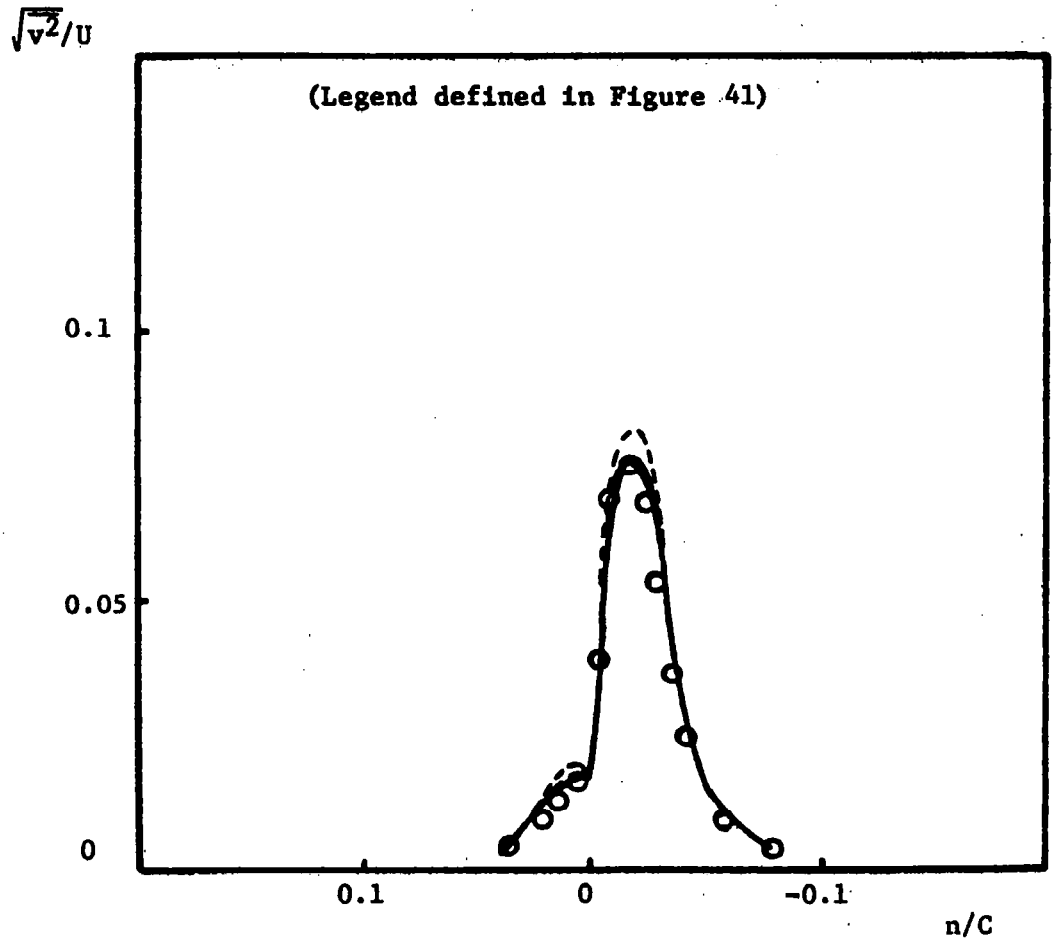

Figure 47. Relative Spanwise Intensity at s/C=0.032 and i=6°

kinetic energy is used as the source term in the dissipation equation, the turbulence quantities become strongly linked to the mean-shear rate and the prediction becomes inaccurate. When the modified or exact source term are adopted in the dissipation equation, this strong link between the mean shear rate and the turbulence quantities no longer exists, and more accurate predictions are obtained. The predicted overall decay rate of mean velocity is shown in Figure 47b.

Cascade Wake Data and Comparison with Predictions

The wakes of a cascade measured by Raj and Lakshminarayana [53] were calculated for further comparison. The blade profiles were similar to the NACA-65 $(8A_2\ I_{86})_{10}$ blade section, and other important parameters are:

solidity C/S = 1.505, inlet angle $\beta_1 = 45°$, incidence i = 2°, 0°, -6°, and Reynolds number based on chord length = 3×10^5.

The upstream velocity and free stream turbulence intensity were 24 ms^{-1} and 0.16 percent. Because the experimental data did not provide spanwise intensity, the energy distribution at the inlet boundary was guessed with available single airfoil wake data. Also, the rate of turbulent kinetic energy dissipation was assumed to be equal to the production of energy. Because of the characteristics of the flow around a cascade, the periodic boundary condition was applied between corresponding points in normal direction. The flow field and coordinate system is shown in Figure 48.

Since the experimental data of i = -6 provides the most detailed information on the boundary conditions, the comparison is made for the experimental data of i = -6°. Figures 49, 50, and 51 show predicted mean velocity and Reynolds stress distribution with three turbulence models. The modified turbulence closure models show substantial improvement in prediction compared to original closure models, and all the three models predict almost identical results if they are properly modified.

The predicted intensity distributions are shown in Figures 52 through 57. The first model predicted only isotropic intensity values, though the trend was improved by modifying the conventional source term for curvature or adopting the exact source term in the dissipation equation. The second and third models provided better predictions for individual components, and improvements were observed when the dissipation equation was modified.

The discrepancy between theory and experiment in the distribution of streamwise intensity near the center of the wake is not explained at this stage. It may be due to scatter in measurements or to improper turbulence modelling. The trajectory of the wake centerline is shown compared with predicted values in Figure 58. Even though the curvature seems moderate, its effect on turbulence structure, as well as mean velocity, is appreciable.

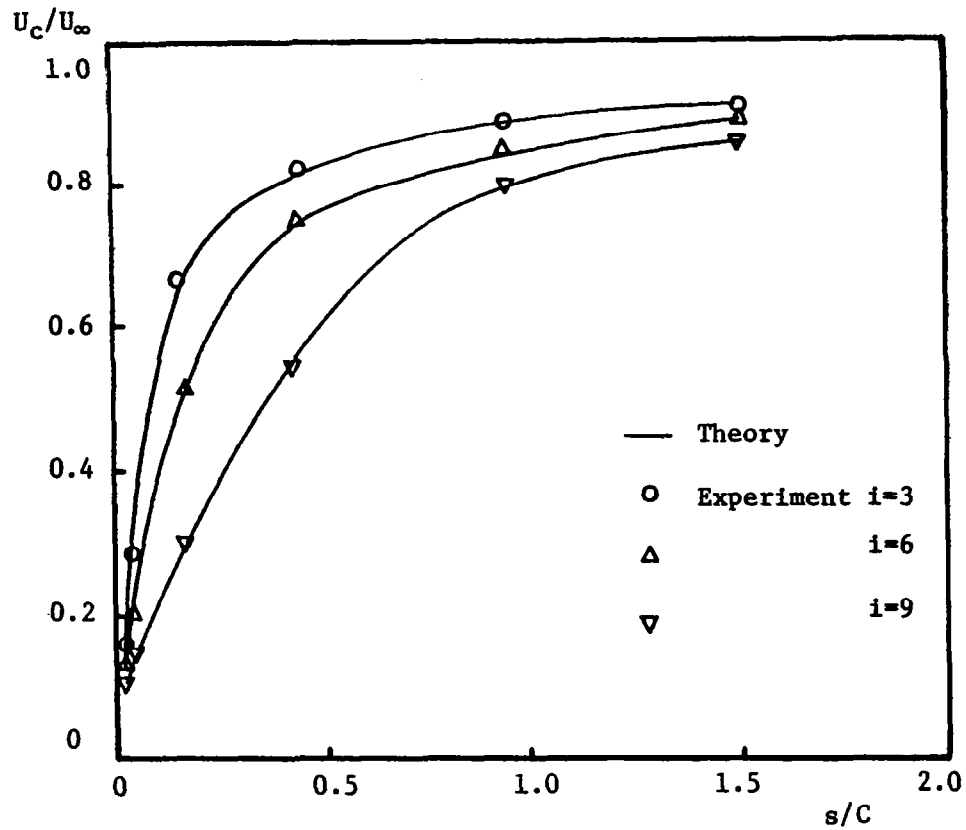

Figure 47b. Decay of Wake Centerline Velocity

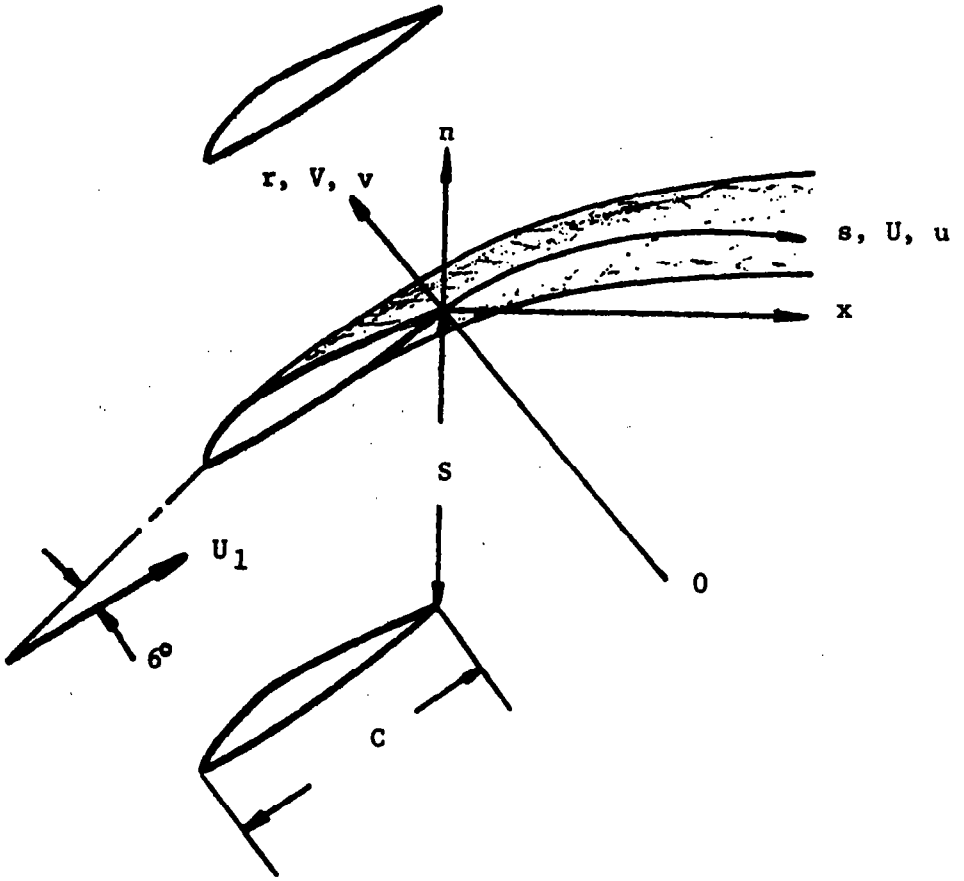

Figure 48. Coordinate System for the Cascade Wake

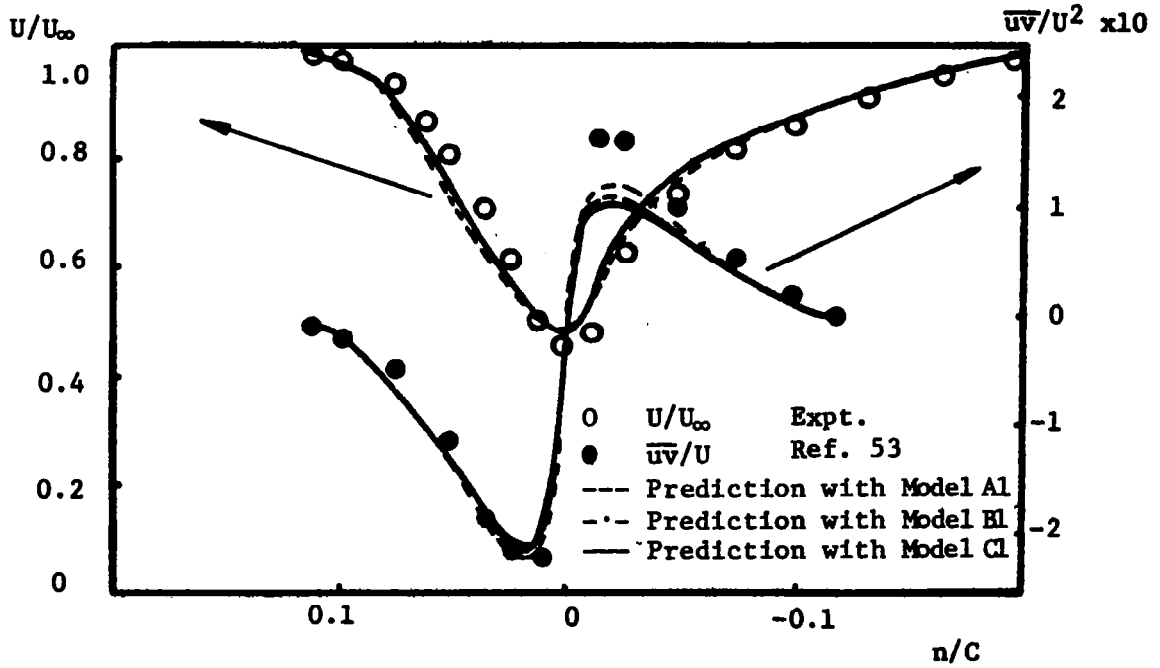

Figure 49. Streamwise Velocity and Shear Stress Profile at s/C=0.08 and i=-6° (Data of Raj and Lakshminarayana, [53])

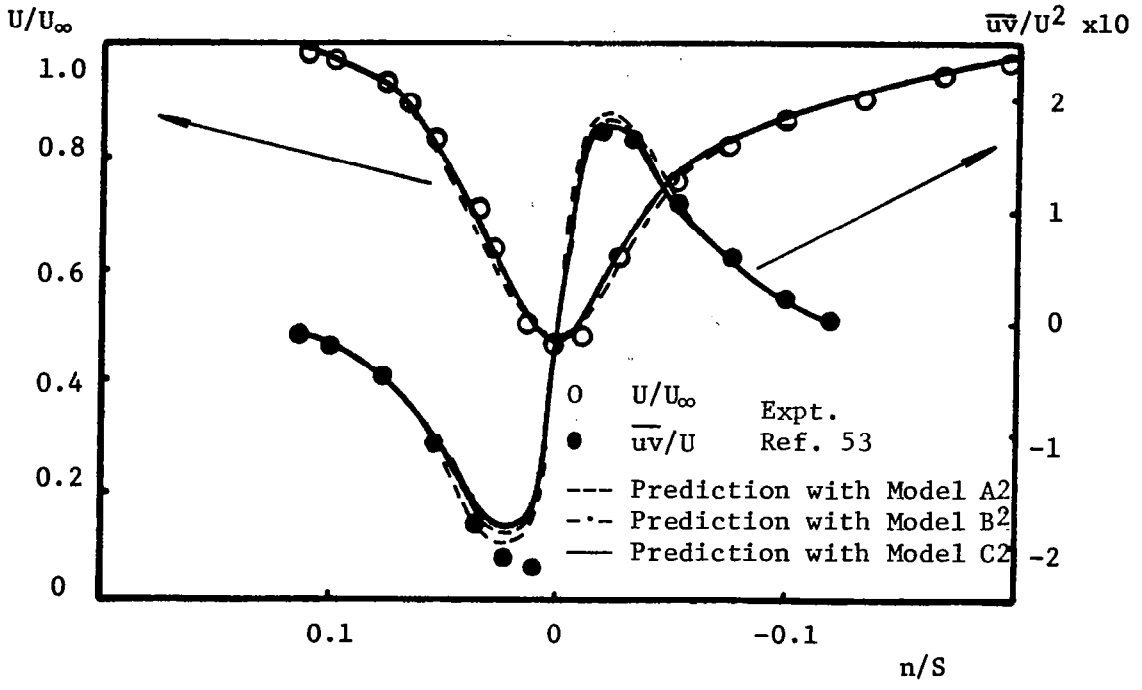

Figure 50. Streamwise Velocity and Shear Stress Profile at s/C=0.08 and i=-6° (Data of Raj and Lakshminarayana, [53])

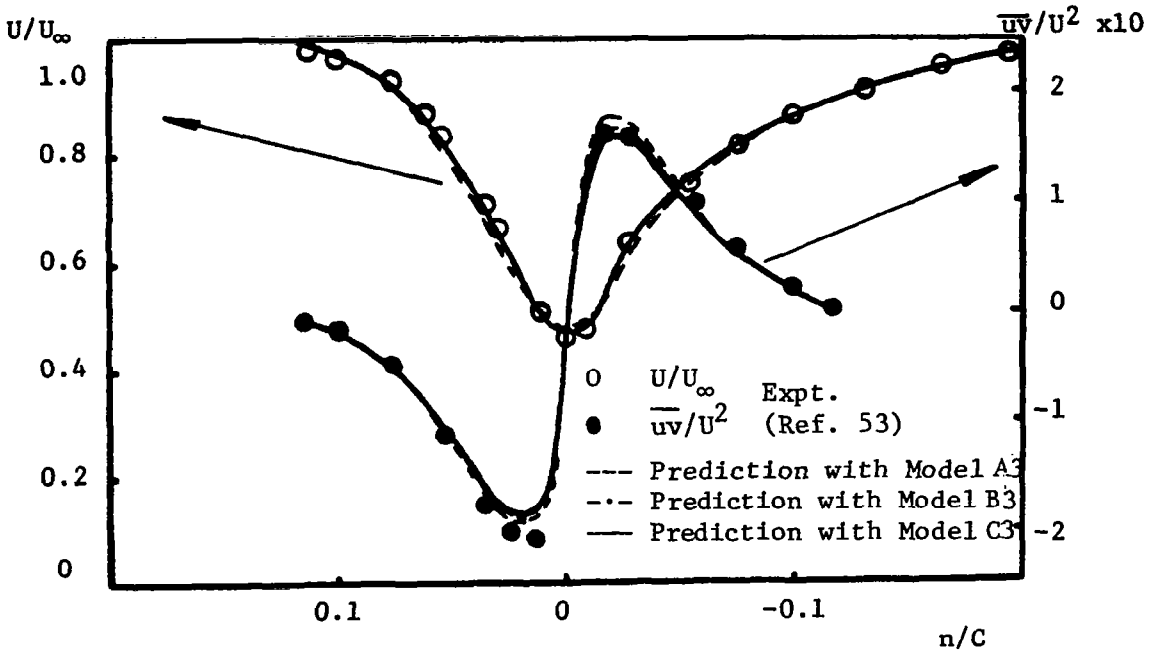

Figure 51. Streamwise Velocity and Shear Stress Profile at s/C=0.08 and i=-6° (Data of Raj and Lakshminarayana, [53])

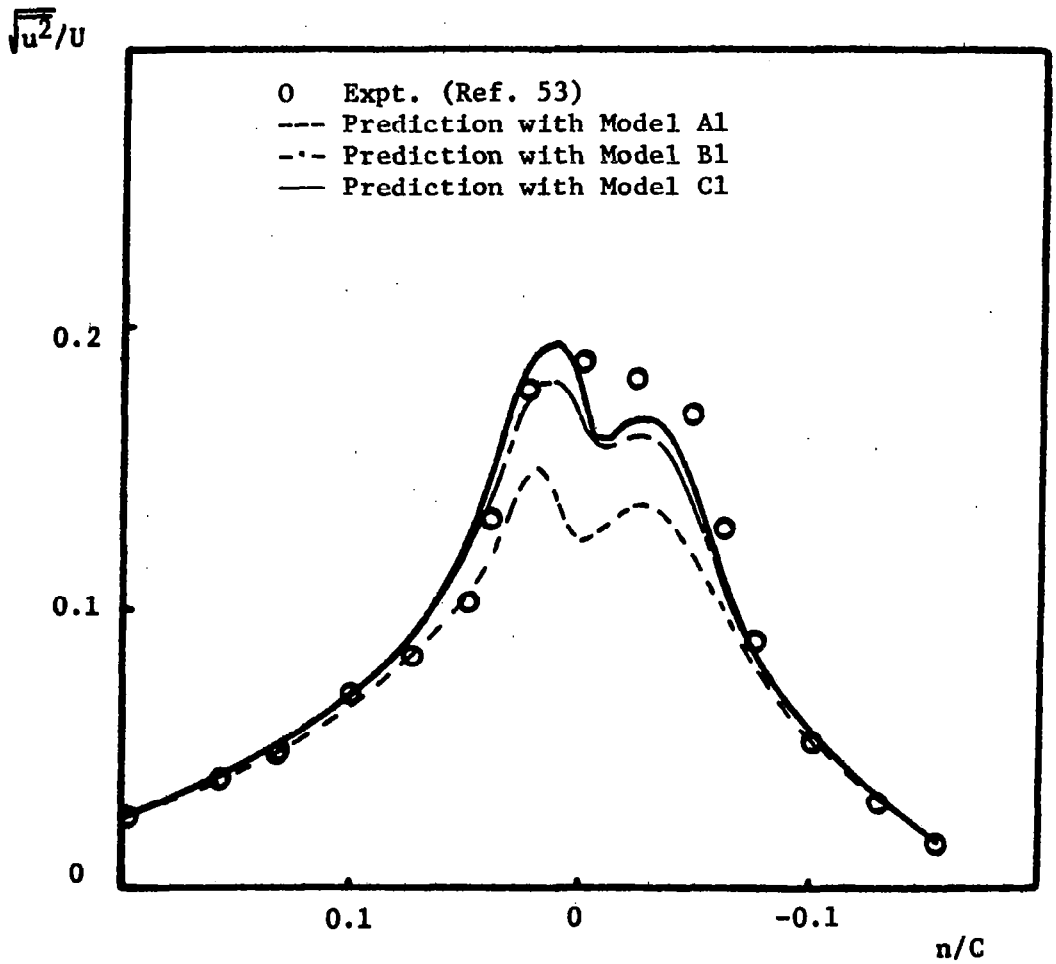

Figure 52. Relative Streamwise Intensity at s/C=0.08 and i=-6° (Data of Raj and Lakshminarayana, [53])

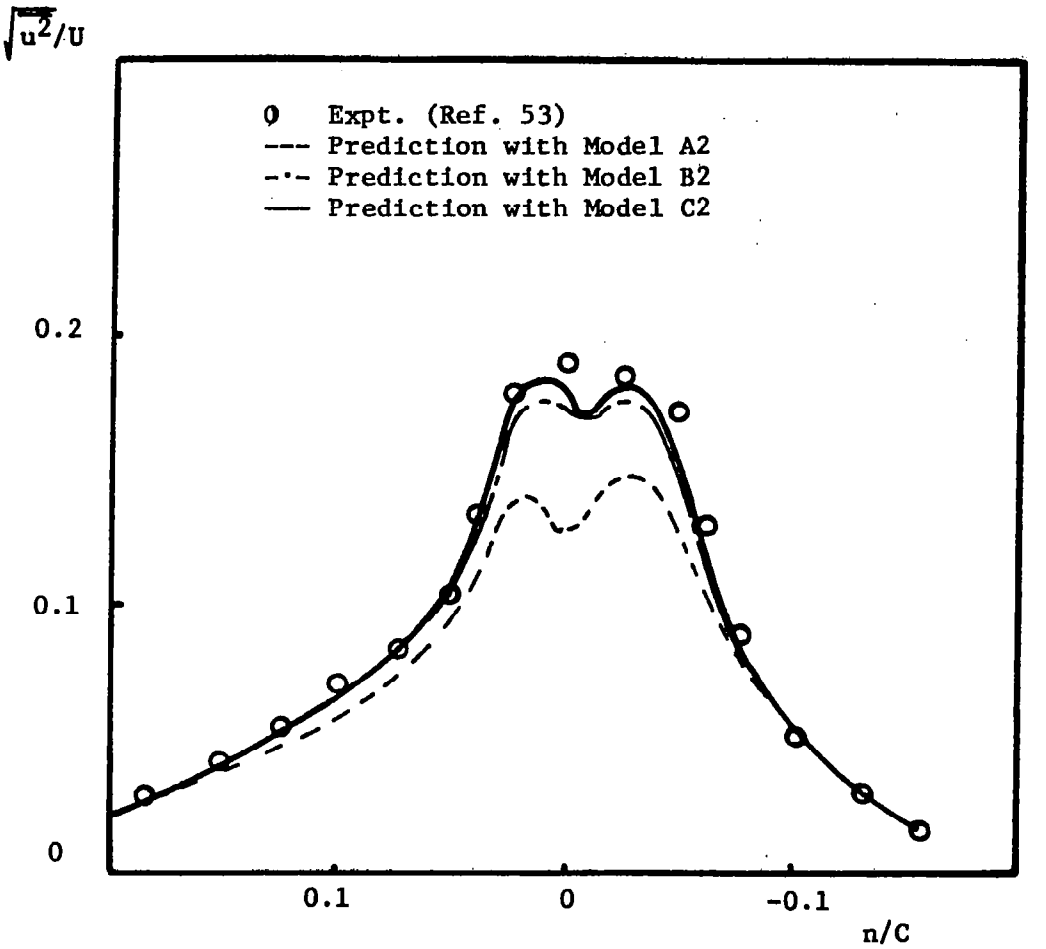

Figure 53. Relative Streamwise Intensity at s/C=0.08 and i=-6° (Data of Raj and Lakshminarayana, [53])

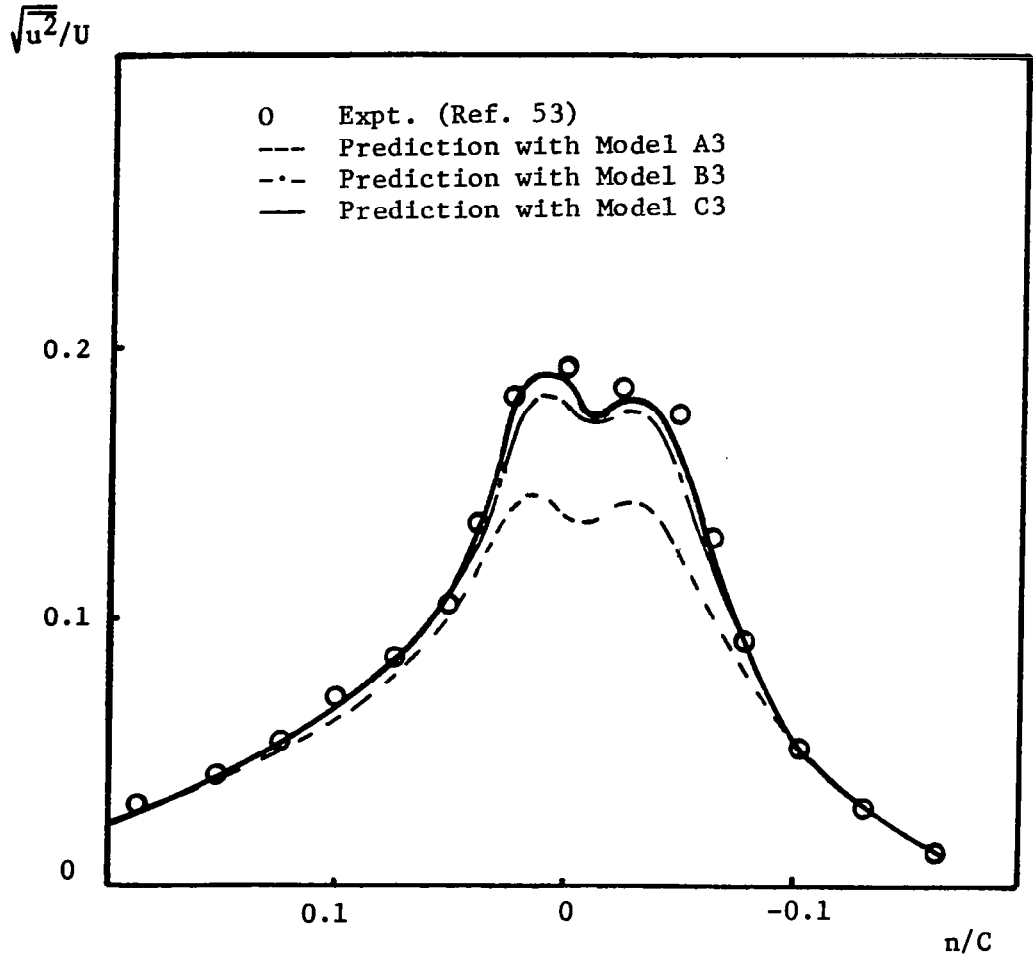

Figure 54. Relative Streamwise Intensity at s/C=0.08 and i=-6° (Data of Raj and Lakshminarayana, [53])

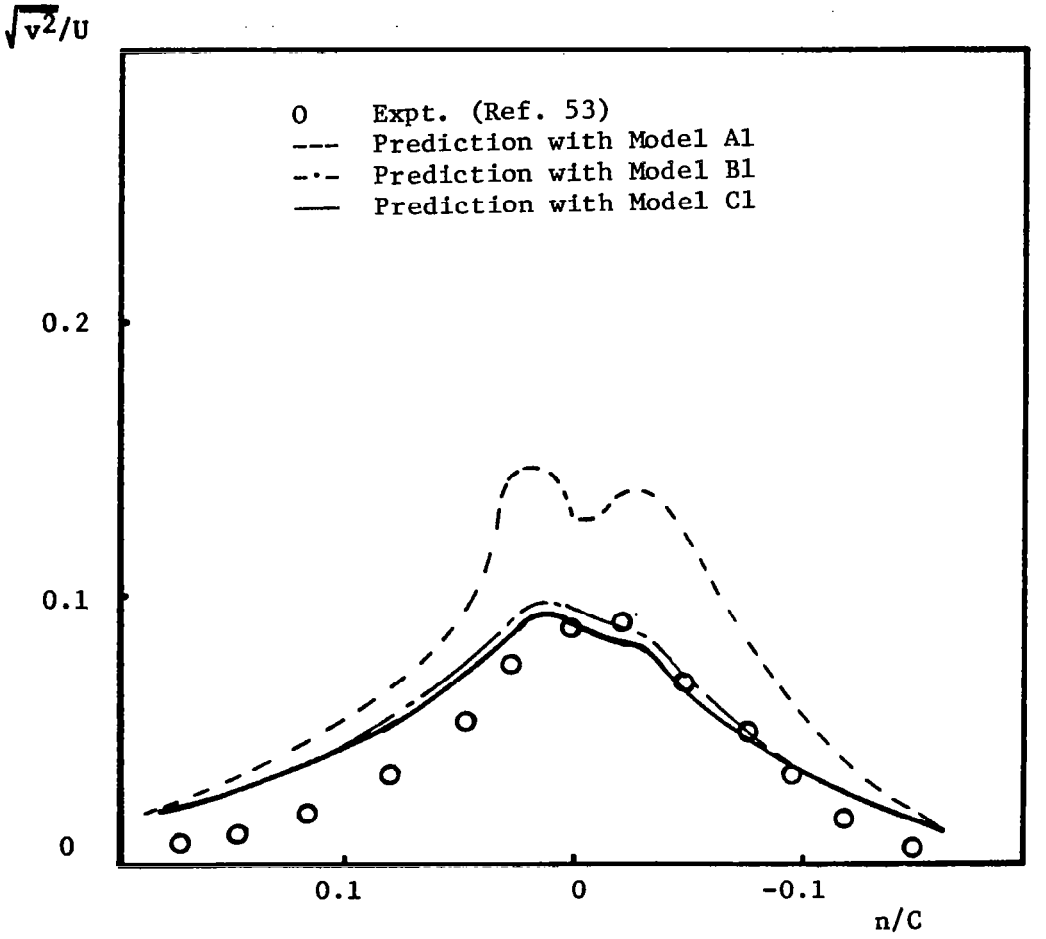

Figure 55. Relative Normal Intensity at s/C=0.08 and i=-6° (Data of Raj and Lakshminarayana, [53])

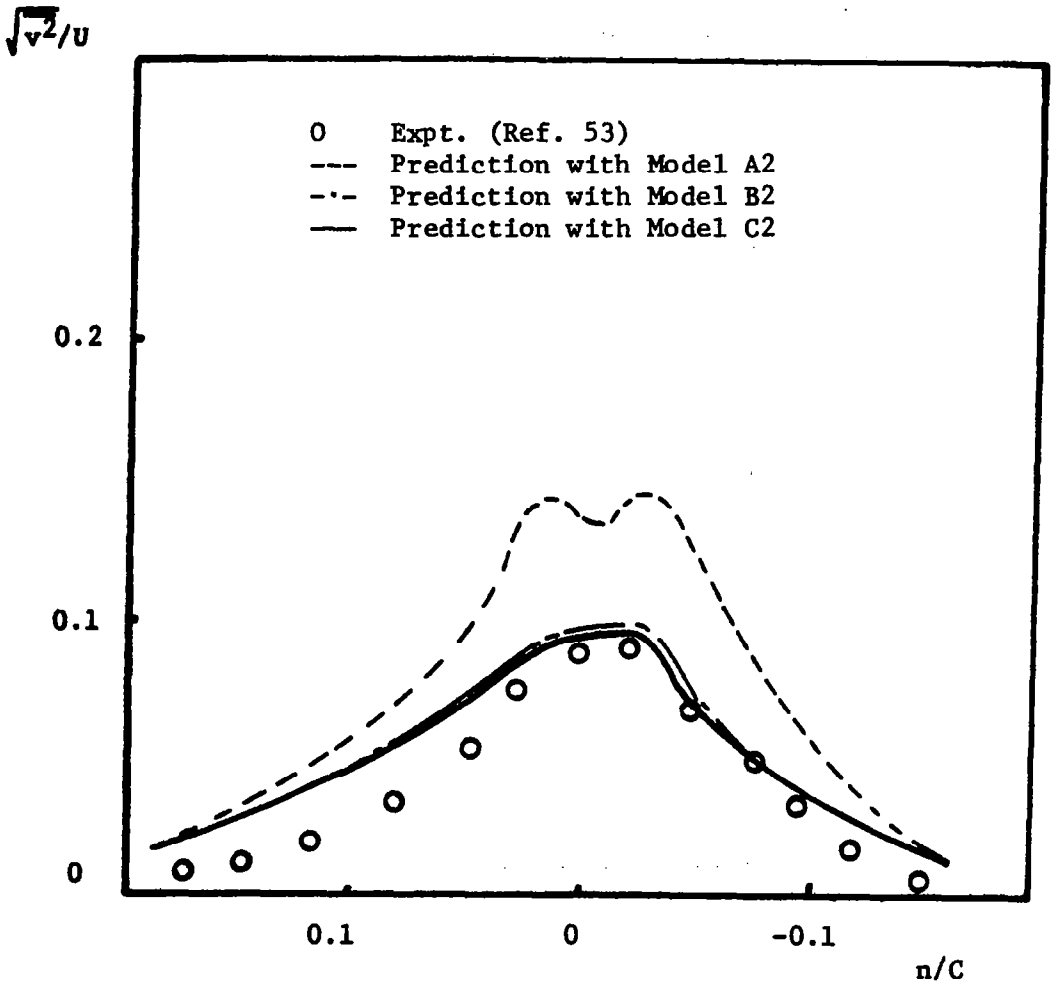

Figure 56. Relative Normal Intensity at s/C=0.08 and i=-6° (Data of Raj and Lakshminarayana, [53])

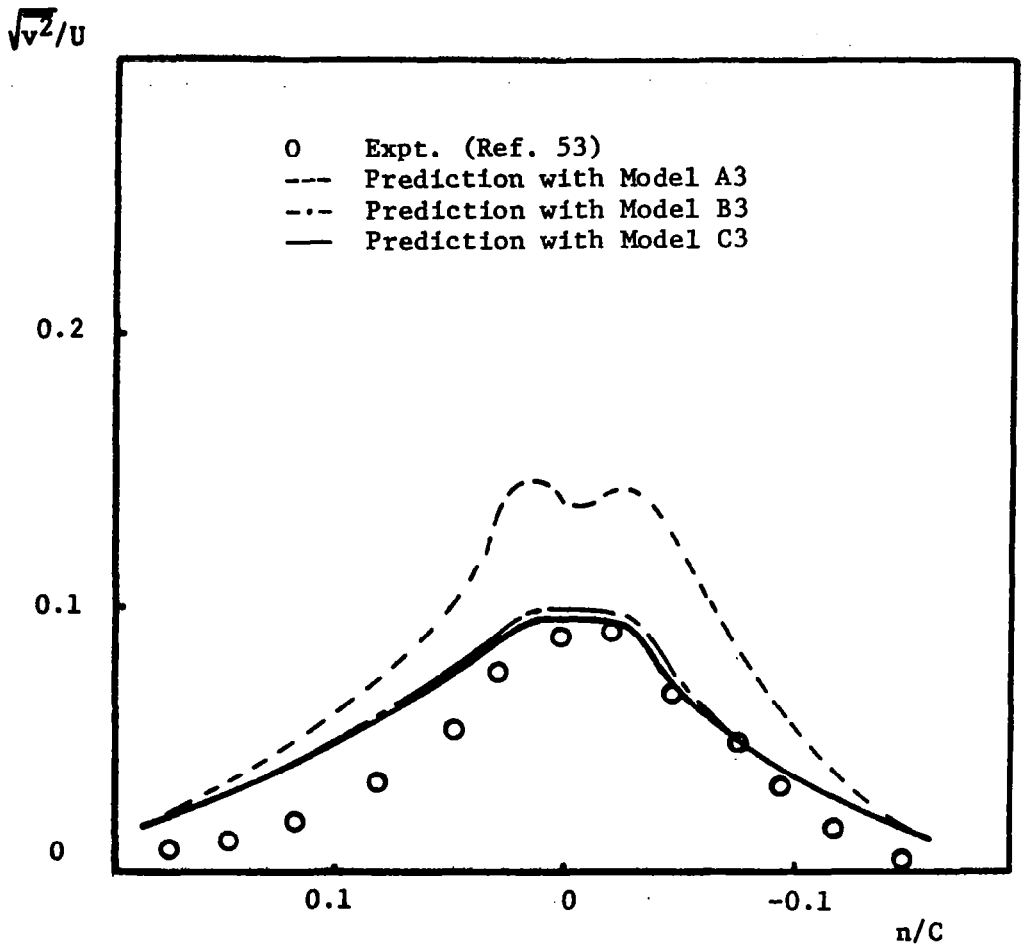

Figure 57. Relative Normal Intensity at s/C=0.08 and i=-6° (Data of Raj and Lakshminarayana, [53])

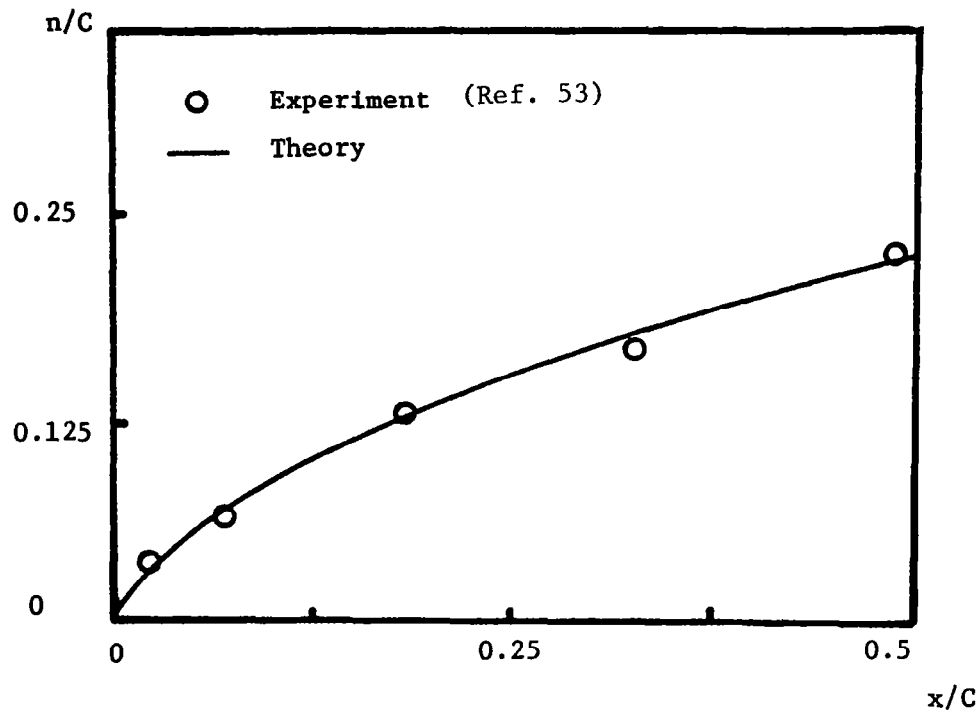

Figure 58. Locus of Minimum Velocity Points Across the Wake (Data of Raj and Lakshminarayana, [53])

FORTRAN PROGRAM FOR THE PREDICTION OF ROTOR WAKE DEVELOPMENT

The Fortran computer program that calculates the development of the turbulent rotor wakes in a compressor is designed to be run on the IBM 370 computer system, but should prove easily adaptable to other installations. It is approximately 1450 cards in length and consists of a main program and one short subroutine. The subroutine ELIM is to solve tri-diagonal matrices and any efficient routine can be used instead of this routine. Various routines to generate curve-fitted data of experimental results are not included in this appendix because any kind of utility subroutines for this kind of mathematical operations can be used. Various subroutines used for plotting the results are not included for the same reason. Some portion of computing time and computer storage may be saved by several modifications in the computer code, but this has not yet been tried.

The development of turbulent wakes of a single airfoil and a cascade of airfoils can be also predicted with the present computer program. The wake of a cascade of airfoils can be considered as a simplified case of rotor wake, when the radial distance is very large and the rotational speed is zero. The single airfoil wake is a further simplification of the rotor wake, with large blade spacing or very small chord length compared to the blade spacing. Therefore the present computer program can be used for the prediction of a cascade and an airfoil wake.

Main Program

The main program first reads input data cards, which are detailed later in this section. As the present numerical scheme is for elliptic calculation, boundary conditions are required for all the boundaries of the calculating domain. The input data includes all these boundary conditions. The geometry of the compressor, the angle β at various radial stations, and other constants are given as input data. The present program is written to receive boundary conditions as a combination of polynomials and Gaussian functions. However, this is quite arbitrary and any kind of curve-fitted distribution of unknowns on the boundary surface can be used. Seven equally spaced radial stations are used for the finite difference calculation. The normal stations vary from 75 at first radial station to 87 at the last radial station. At each radial station, two different spacings between normal station are used. In the 20 nodal points from the central nodal points in both normal directions, the spacing between nodal points are 1/4 of the spacings of outer radial points. Also the present calculation domain contains one complete rotor passage with the blade trailing edge at the center. Therefore, the normal spacing varies in the radial direction to cover the spacing between blades with the given number of radial points. The number of radial stations and normal stations in finite difference calculation is also arbitrary even though it requires some change of constant in the program and can be done without any major effort. Any type of automatic or numerical mesh generation in the surface normal to the streamwise direction can be incorporated in the present computer program

without any difficulty. With the given initial and boundary conditions, the six components of Reynolds stress are calculated and with this Reynolds stress components, the momentum and turbulence closure equations are solved. The detailed operations in the main program are shown in the flow chart (Figure 6). Because the available computer memory storage was quite small (around 200 k with IBM 370/3033 at The Pennsylvania State University), the computed results were stored in the RJE batch files and the unknown quantities stored in the batch files were updated during numerical calculation.

Input Data Cards

Input data cards are as follows. Various formats are also given for each data card.

Card 1 Card 1 contains one integer and two floating point numbers (I5, 2F10.4)

Columns	Name	Description
1 to 5	IAL	Number of iteration
6 to 15	DENS	Density of fluid (kg/m^3)
16 to 25	SOR	Successive over-relaxation factor. A fixed value of 1.55 was used for the present study.

Card 2 Card 2 contains three floating point numbers (3F10.3)

Columns	Name	Description
1 to 10	DR	Radial spacing in finite difference grid (m)
11 to 20	DS	Streamwise spacing in finite difference grid (m)
21 to 30	DN	Normal spacing in finite difference grid (m)

Card 3 Card 3 contains two floating point numbers (3F10.3)

Columns	Name	Description
1 to 10	EF	Turbulence kinetic energy at free stream (m^2/sec^2)
11 to 20	DR	The rate of turbulence kinetic energy dissipation at free stream (m^2/sec^3)

Card 4 Card 4 contains one floating point number in columns 1 to 10, Ω, the angular speed of rotor.

Card 5 Card 5 contains one floating point number in columns 1 to 10, AL, the radial variation of the angle between steramwise direction and machine axis (radian/m).

Card 6 Card 6 contains four floating point numbers for the description of the compressor geometry (4F10.3)

Columns	Name	Description
1 to 10	VNON(1)	Free-stream velocity at hub (m/sec)
11 to 20	B(1)	Outlet angle at hub (Radian)
21 to 30	SA(1)	Blade spacing at hub (m)
31 to 40	R(1)	Hub radius (m)

Card 7 Card 7 contains three floating point numbers to describe radial variation of unknown quantities.

Columns	Name	Description
1 to 10	BC1	Radial variation of outlet angle (radian)
11 to 20	SAC1	Radial variation of spacing (m)
21 to 30	VNONC1	Radial variation of free-stream velocity (m/sec)

Cards 8 to 18 Cards 8 to 18 are used to give coefficients of functions for the distribution of the streamwise velocity on the boundary surfaces. The following function was used for the description of streamwise velocity component

$$U(n) = A_1 U_\infty - A_2 U_\infty \left[e^{-0.693 n/L_s} - 1.0 + A_5 \left(\frac{n}{L_s}\right) + A_6 \left(\frac{n}{L_s}\right)^2 + A_7 \left(\frac{n}{L_s}\right)^3 \right]$$

where U_∞ = free stream velocity

L_s = length scale, the distance from the wake center to the point where the velocity defect is half of that at the wake center. Different length scales are used in the pressure and suction sides of the wake. $L_s = A_3$ in suction side and $L_s = A_4$ in pressure side.

n = normal distance, n = 0, at the wake center

$A_1, A_2 \cdots A_7$ = coefficient of functions

Each card contains seven floating point numbers to describe the seven coefficients used.

Columns	Name	Description
1 to 7	XC(1,1,I)	A_1
8 to 14	XC(1,2,I)	A_2
15 to 21	XC(1,3,I)	A_3
22 to 28	XC(1,4,I)	A_4
29 to 35	XC(1,5,I)	A_5
36 to 42	XC(1,6,I)	A_6
43 to 49	XC(1,7,I)	A_7

Cards 19 to 29

Cards 19 to 29 are used to give coefficients of functions for the distribution of the radial velocity on the boundary surfaces. The following functions were used for the description of the radial velocity component.

$$W(n)/U_\infty = WD4 \quad \text{if} \quad n/S < x_{34}$$

$$W(n)/U_\infty = (WD4 - WD3)x(n/S)/(x_{34} - x_{33}) + WD4 - (WD3 - WD4)x(x_{33})/(x_{34} - x_{33})$$

$$\text{if} \quad +x_{34} \leqq n/S < +x_{33}$$

$$W(n)/U_\infty = +(WD_3 - WC)x(n/S)/x_{33} + WC \quad \text{if} \quad +x_{33} \leqq n/S < 0$$

$$W(n)/U_\infty = (WD_1 - WC)x(n/S)/x_{31} + WC \quad \text{if} \quad 0 \leqq n/S < x_{31}$$

$$W(n)/U_\infty = (WD_2 - WD_1)x(n/S)/(x_{32} - x_{31}) + WD_2 - (WD_2 - WD_1)x(x_{32})/(x_{32} - x_{31})$$

$$\text{if} \quad x_{31} \leqq n/S < x_{32}$$

$$W(n)/U_\infty = WD_2 \quad \text{if} \quad n/S \geqq x_{32}$$

where W(n) = radial velocity
S = spacing of the blade
n = normal distance from the wake center

$WC, WD_1, WD_2, WD_3, WD_4, x_{31}, x_{32}, x_{33}, x_{34}$ = constants

Each card contains nine floating point numbers to describe nine coefficients used.

Columns	Name	Description
1 to 6	XC(3,1,I)	WC
7 to 12	XC(3,2,I)	x_{31}
13 to 18	XC(3,3,I)	WD_1
19 to 24	XC(3,4,I)	x_{32}
25 to 30	XC(3,5,I)	WD_2
31 to 36	XC(3,6,I)	x_{33}
37 to 42	XC(3,7,I)	WD_3
43 to 48	XC(3,8,I)	x_{34}
49 to 54	XC(3,9,I)	WD_4

Cards 30 to 40

Cards 30 to 40 are used to give coefficients of functions for the description of the normal velocity on the boundary surfaces. The following functions were used for the description of the normal velocity component.

$$V(n)/U_\infty = V_4 \quad \text{if} \quad n/S < +x_{24}$$

$$V(n)/U_\infty = +(V_4 - V_3)x(n/S)/(x_{24} - x_{23}) + V_4 - (V_4 - V_3)x(x_{24})/(x_{24} - x_{23}) \quad \text{if} \quad -x_{24} \leq n/S < +x_{23}$$

$$V(n)/U_\infty = +V_3 \times (n/S)/x_{23} \quad \text{if} \quad +x_{23} \leq n/S < 0$$

$$V(n)/U_\infty = V_1 \times (n/S)/x_{21} \quad \text{if} \quad 0 \leq n/S < x_{21}$$

$$V(n)/U_\infty = (V_2 - V_1)x(n/S)/(x_{22} - x_{21}) + V_2 - (V_2 - V_1)x(x_{22})/(x_{22} - x_{21})$$

$$\text{if} \quad x_{21} \leq n/S < x_{22}$$

$$V(n)/U_\infty = V_2 \quad \text{if} \quad x_{22} \leq n/S$$

where U_∞ = free stream velocity
S = spacing of the blade
n = normal distance from the wake center
V = normal velocity
V_1, V_2, V_3, V_4,
x_{21}, x_{22}, x_{23},
x_{24} = constants

Each card contains eight floating point numbers to describe eight coefficients used.

Columns	Name	Description
1 to 6	XC(2,1,I)	x_{21}
7 to 12	XC(2,2,I)	V_1
13 to 18	XC(2,3,I)	x_{22}
19 to 24	XC(2,4,I)	V_2
25 to 30	XC(2,5,I)	x_{23}
31 to 36	XC(2,6,I)	V_3
37 to 42	XC(2,7,I)	x_{24}
43 to 68	XC(2,8,I)	V_4

Cards 41 to 51

Cards 41 to 51 are used to give coefficients of functions for the description of the turbulence kinetic energy on the boundary surfaces. The following functions were used for the description of the turbulence kinetic energy.

$$EN(n)/U_\infty^2 = E4 \quad \text{if} \quad n/S < -x_{44}$$

$$EN(n)/U_\infty^2 = (E4 - E3)x(n/S)/(-x_{44} + x_{43}) + E4 - (E4 - E3)x(-x_{44})/(-x_{44} + x_{43})$$

$$\text{if} \quad -x_{44} \leqq n/S < -x_{43}$$

$$EN(n)/U_\infty^2 = (E3 - E5)x(n/S)/(-x_{43} + x_{45}) + E3 - (E3 - E5)(-x_{43})/(-x_{43} + x_{45})$$

$$\text{if} \quad -x_{43} \leqq n/S \leqq -x_{45}$$

$$EN(n)/U_\infty^2 = (E1 - E5)x(n/S)/(x_{41} + x_{45}) + E1 - (E1 - E5)x(x_{41})/(x_{41} + x_{45})$$

$$\text{if} \quad -x_{45} \leqq n/S < x_{41}$$

$$EN(n)/U_\infty^2 = (E2 - E1)x(n/S)/(x_{42} - x_{41}) + E2 - (E2 - E1)x(x_{42})/(x_{42} - x_{41})$$

$$\text{if} \quad x_{41} \leqq n/S < x_{42}$$

$$EN(n)/U_\infty^2 = E2 \quad \text{if} \quad x_{42} \leqq n/S$$

where U_∞ = free stream velocity
EN = turbulence kinetic energy
n = normal distance from the wake center
E1,E2,E3,E4,E5,
x_{41}, x_{42}, x_{43},
x_{44}, x_{45} = constants

Each card contains ten floating point numbers to describe ten coefficients used.

Columns	Name	Description
1 to 6	XC(4,1,I)	x_{41}
7 to 12	XC(4,2,I)	E1
13 to 18	XC(4,3,I)	x_{42}
19 to 24	XC(4,4,I)	E2
25 to 30	XC(4,5,I)	x_{45}
31 to 36	XC(4,6,I)	E5
37 to 42	XC(4,7,I)	x_{43}
43 to 48	XC(4,8,I)	E3
49 to 54	XC(4,9,I)	x_{44}
55 to 60	XC(4,10,I)	E4

These cards are not utilized in the Fortran program listing attached. The program can be easily modified to include the generalization of the input data mentioned above.

Because many experimental data indicate that the distribution of turbulence kinetic energy can be approximately represented with the mean shear rate when proper coefficients are used. This simple representation of turbulence kinetic energy is used instead of the above multi-functions for the same input data.

Typical Input Data Set

```
    11.1077     1.55
0.015       0.0014     0.002213
2.0         4.0
111.63
1.286
29.6        0.502       0.1018      0.341
0.0225      0.0051      1.7
0.209  0.745  0.003  0.001  -0.00260.00017-0.0001
0.0
0.0
0.0
0.0
0.392  0.481  0.003  0.004  -0.017 0.004  0.0003
0.426  0.349  0.017  0.024  0.0186 -0.007 -0.0349
0.243  0.723  0.003  0.003  -0.01  -0.00000.00004
0.632  0.312  0.003  0.005  -0.0522-0.00130.00036
0.593  0.352  0.022  0.028  0.0162 -0.021 -0.0029
0.573  0.411  0.026  0.04   -0.094 0.006  0.009
-0.2890.062 0.387 0.5    0.043 -0.0620.126 -0.27 0.066
0.0
0.0
0.0
0.0
-0.1270.094 0.333 0.5    0.049 -0.12 0.235 -0.3  0.065
0.016 0.117 0.169 0.882 0.055 -0.1940.234 -0.7140.117
-0.3820.074 0.56  1.0    0.164 -0.1  0.256 -0.5 0.155
0.125 0.1    0.291 1.25   0.127 -0.16 0.2    -0.6  0.163
-0.1870.2    0.096 1.0    0.023 -0.2  -0.141-0.5  -0.037
-0.18 0.2    0.031 1.0    0.02  -0.5  0.062 -1.0  0.222
0.042 -0.1270.1    -0.014-0.03 0.101 -0.33 0.015
0.0
0.0
0.0
0.0
0.105 -0.13 0.5    -0.03 -0.1320.073 -0.55 0.02
0.29  -0.15 0.7    -0.032-0.2540.08  -0.7  0.02
0.052 -0.14 0.12   -0.055-0.0610.137 -0.4   0.1
0.1    -0.1640.3    -0.08 -0.1  0.2    -0.5  0.22
0.26   -0.1  0.72   -0.01 -0.03 0.078 -1.0
0.21   -0.0870.74   -0.004-0.5250.076 -1.0
0.04   0.12  0.13   -0.02 0.011 0.03  0.04  0.06   -0.01 -0.025
0.0
0.0
0.0
0.0
0.065 0.142 0.11   -0.05 0.05  0.021 0.033 0.036 -0.05 -0.001
0.07  0.15    .12   -0.06 0.05  0.02  0.08  0.025 -0.06 -0.001
0.05  0.12  0.128  -0.02 0.03  0.002 0.063 0.024 -0.02 -0.0044
0.05  0.10  0.13   -0.04 0.034 0.002 0.05  0.04  -0.05 -0.004
0.11  0.15  0.11   -0.3  0.03  0.00150.11  0.0187 -0.3 -0.001
0.11  0.12  0.11   -0.3  0.03  0.00150.11  0.0187 -0.3 -0.001
```

CONCLUSIONS

The major conclusions derived from this investigation are as follows:

1. The development of the turbulent wake of rotor blades in a compressor was predicted numerically. The numerical results show excellent agreement with various wake data from different blade geometries. All the components of the mean velocity profile, as well as the turbulence intensity and stress profiles, are predicted accurately.

2. The non-orthogonal curvilinear coordinate system utilized describes the actual streamline closely, and provides simplicity in describing the governing equations and the boundary conditions.

3. The Reynolds stress transport equation was modified for the effects of rotation and the streamline curvature. The modelled Reynolds stress transport equation contains rotation-originated redistribution term for the effect of rotation. The modelled equation of the turbulence kinetic energy dissipation was modified for the effect of streamline curvature.

4. The effects of the convection and the diffusion were handled collectively in the modified Reynolds stress model to save the computer storage and the computing time. The total effect of the convection and the diffusion terms in the Reynolds stress transport equation was assumed to be related to the production of the Reynolds stress. Good agreement between the experimental data and the numerical predictions indicates that the above assumption is valid for the present problem.

5. The development of the rotor wake was also predicted with two-equation model, which does not include the effect of rotation and the streamline curvature. The two-equation model and the modified Reynolds stress model show the following difference in predictions. The modified Reynolds stress model demonstrates substantial improvements in predicting the mean velocity as well as turbulence quantities, compared to the two-equation model. The difference in predictions comes mainly from the effect of rotation. The two-equation model almost predicts isotropic turbulence intensities while the modified Reynolds stress model predicts the components of the intensities. Therefore, the two-equation model cannot accurately predict turbulent flow whose structure is anisotropic. The modified Reynolds stress model predicts turbulence intensity and shear stress components accurately. The increase in radial turbulence intensity, observed experimentally, is also predicted well. The modified Reynolds stress model also predicts more accurate shear stresses than the two-equation model.

6. Two-dimensional asymmetric turbulent wakes from airfoil were also studied numerically in order to investigate the effect of the streamline curvature. Three turbulence closure models were used for the prediction. The three turbulence closure models show the following differences in predicting two-dimensional asymmetric turbulent wakes:

   All three models do not predict the effects of streamline curvature accurately when the existing dissipation equation is used. At near wake, higher turbulence intensity and shear stress are predicted on the pressure side of the wake than are found in the experimental results, while lower turbulence intensity and shear stress are predicted in the suction side of the wake.

   When the dissipation equation is modified, all three models predict mean velocity and shear stress distributions accurately. The two-equation model predicts only isotropic turbulence intensities, while the modified Reynolds stress and Reynolds stress models predict individual turbulence intensities.

   The modified Reynolds stress and Reynolds stress models predict both the mean velocity and turbulence quantities accurately. However, computer time and storage can be significantly reduced by using the second model.

7. The effects of rotation and streamline curvature on the development of the turbulent wake is substantial and these effects should be properly included in the turbulence closure modeling for the accurate numerical prediction.

   The prediction scheme reported in this investigation is part of a program which will provide a full prediction method for the actual flow field inside the turbomachinery. The present prediction scheme, combined with the numerical scheme for the three-dimensional flow fields inside the rotor blade passages will be invaluable in the development of the present status of technology in this field.

REFERENCES

1. Raj, R. and Lakshminarayana, B., "On the Investigation of Cascade and Turbomachinery Rotor Wake Characteristics," NASA Report No. NASA CR 134680, 1974.

2. Reynolds, B. and Lakshminarayana, B., "Characteristics of Lightly Loaded Fan Rotor Blade Wakes," NASA CR 3188, 1979.

3. Ravindranath, A. and Lakshminarayana, B., "Three Dimensional Mean Flow and Turbulence Characteristics of a Compressor Rotor Blade," NASA CR 159518, June 1980.

4. Tennekes, H. and Lumley, J., A First Course in Turbulence, The MIT Press, Cambridge, Massachusetts, 1972.

5. Goldstein, S., "Concerning Some Solutions of the Boundary Layer Equations in Hydrodynamics," Proceedings of the Cambridge Philosophical Society, Vol. 26, Part 1, pp. 3-30, 1930.

6. Stewartson, K., "On the Flow Near the Trailing Edge of a Flat Plate," SIAM, Vol. 18, No. 1, 1970.

7. Robinson, J. L., "Similarity Solutions in Several Turbulent Shear Flows," NPL Report 1242, 1967.

8. Lakshminarayana, B., "The Nature of Flow Distortions by Rotor Blade Wakes," AGARD CP 177, 1976.

9. Raj, R. and Lakshminarayana, B., "Three-Dimensional Characteristics of Turbulent Wakes Behind Rotor of Axial-Flow Turbomachinery," Trans. ASME, J. Engr. for Power 98, 218-228, 1976.

10. Prandtl, L., "Einfluss stabilisierender kräfte auf die turbulenz," Sonderdruck aus Vostrage aus dem Geiete der Aerodynamik und Verwandter Getiete, Aachen, 1929 (Translation N.A.C.A. TM-625).

11. Cebeci, T., Smith, A. M. O., "Analysis of Turbulent Boundary Layers," Applied Mathematics and Mechanics, Vol. 15, New York: Academic, 1974.

12. Norris, L. H. and Reynolds, W. C., "Turbulent Channel Flow with a Moving Wavyboundary," Stanford University, Dept. Mech. Eng. Rep. FM-10, 1975.

13. Wolfshtein, M., "The Velocity and Temperature Distribution in One-Dimensional Flow with Turbulence Augmentation and Pressure Gradient," Int. J. Heat Mass Transfer 12, 301-318, 1969.

14. Jones, W. P. and Launder, B. E., "The Prediction of Laminarization with a Two Equation Model of Turbulence," Int. J. Heat Mass Transfer 5, 1972.

15. Launder, B. E. and Spalding, D. B., "The Numerical Computation of Turbulent Flows," Numerical Methods in Applied Mechanics and Engineering 3, 269-289, 1974.

16. Saffman, P. G. and Wilcox, D. C., "Turbulence-Model Predictions for Turbulent Boundary Layers," AIAA J. 12, 541-546, 1974.

17. Mellor, G. L. and Herring, H. J., "A Survey of the Mean Turbulent Field Closure Methods," AIAA J. 11, 590-599, 1973.

18. Reynolds, W. C., "Computation of Turbulent Flows," Annual Review of Fluid Mechanics, Annual Reviews, Inc., 1976.

19. Hanjalic, K. and Launder, B. E., "A Reynolds Stress Model of Turbulence and its Application to Thin Shear Flows," J. Fluid Mech. 52, Part 4, 609-638, 1972.

20. Launder, B. E., Reece, G. J. and Rodi, W., "Progress in the Development of a Reynolds-Stress Turbulence Closure," J. Fluid Mech. 68, Part 3, 537-566, 1975.

21. Lumley, J. L. and Khajeh-Nouri, B., "Computational Modelling of Turbulent Transport," Adv. in Geophys. A18, 169-192, 1974.

22. Bradshaw, P., "Effects of Streamline Curvature on Turbulent Flow," AGARDgraph No. 169, 1973.

23. So, R. M. C., "A Turbulent Velocity Scale for Curved Shear Flows," J. Fluid Mech. 70, Part 1, 37-58, 1975.

24. Launder, B. E., Pridden, C. H. and Sharma, B. I., "The Calculation of Turbulent Boundary Layers on Spinning and Curved Surfaces," Trans. ASME, J. Fluids Engr., 231-239, 1977.

25. Chambers, T. L. and Wilcox, D. C., "Critical Examination of Two-Equation Turbulence Closure Models for Boundary Layers," AIAA J. 15, No. 6, June 1975.

26. Taylor, G. I., "Stability of a Viscous Liquid Contained Between Two Rotating Cylinders," Phil. Trans. Roy. Soc. (London), Ser. A., Vol. 223, pp. 289-343, 1923.

27. Trefethen, L., "Flow in Rotating Radial Ducts," General Electric Engineering Laboratory, Report 55GL350-A, August 1957.

28. Bradshaw, P., "The Analogy Between Streamline Curvature and Buoyancy in Turbulent Shear Flow," J. Fluid Mech. 36, Part 4, p. 1007, 1969.

29. Johnston, J. P., "The Effects of Rotation on Boundary Layers in Turbomachine Rotors," NASA SP-304, edited by B. Lakshminarayana, et al., pp. 207-242, 1972.

30. Majumdar, A. K., Pratrap, V. S. and Spalding, D. B., "Numerical Computation of Flows in Rotating Ducts," Trans. ASME, J. Fluids Engr., 148-153, 1077.

31. Reynolds, B., Lakshminarayana, B. and Ravindranath, A., "Characteristics of the Near-Wake of a Compressor or Fan Rotor Blade," AIAA J. 17, No. 9, September 1979.

32. Ravindranath, A. and Lakshminarayana, B., "Mean Velocity and Decay Characteristics of the Wake of a Compressor Blade with Moderate Loading," J. Engr. for Power 102, No. 3, 535-548, 1980.

33. Raj, R. and Lumley, J. L., "A Theoretical Investigation on the Structure of Fan Wakes," ASME Paper 76-WA/FE-22, 1976.

34. Lakshminarayana, B. and Reynolds, B., "Turbulence Characteristics in the Near Wake of a Compressor Rotor Blade," AIAA J., 1354-1362, November 1980.

35. Patankar, S. V. and Spalding, D. B., "A Calculation Procedure for Heat, Mass and Momentum Transfer in Three-Dimensional Parabolic Flows," Intern. J. Heat and Mass Transfer 15, 1787-1806, 1973.

36. Ghia, U. and Studerus, C. J., "Three-Dimensional Laminar Incompressible Flow in Straight Polar Ducts," Computers and Fluids, Vol. 5, 1977.

37. Briley, W. R., "Numerical Method for Predicting Three-Dimensional Steady Viscous Flow in Ducts," J. Computational Physics 14, 8028, 1974.

38. Zienkiewicz, O. C., The Finite Element Method in Engineering Science, McGraw-Hill, 1969.

39. Thames, F. C., Thompson, J. F., and Mastin, C. M., "Numerical Solution of the Navier-Stokes Equations for Arbitrary Two-Dimensional Airfoils," NASA SP-347, Part 1, 469-530, March 1975.

40. Sorenson, R. and Steger, J. L., "Simplified Clustering of Nonorthogonal Grids Generated by Elliptic Partial Differential Equations," NASA TM 73252, 1976.

41. Peaceman, D. W. and Rachford, H. H., J. Soc. Indust. Appl. Math, Vol. 3, p. 28, 1955.

42. Spence, D. A., "Growth of Turbulent Wake Close Behind an Airfoil at Incidence," Gr. Brit. Aero. Res. Council, C.P. No. 125, 1952.

43. Evans, R. L., "Turbulence and Unsteadiness Measurement Downstream of a Moving Blade Row," J. Engr. for Power 97, 131-139, 1975.

44. Schmidt, D. P. and Okiishi, T. H., "Multistage Axial Flow Turbomachine Wake Production, Transport and Interaction," AIAA J. 15, 1138, 1977.

45. Gallus, H. E., Private Communication, 1977.

46. Kool, P., DeRuyck, J., and Hirsch, C. H., "The Three-Dimensional Flow and Blade Wake in an Axial Plane Downstream of an Axial Compressor Rotor," ASME Paper No. 78-GT-66, 1978.

47. Horlock, J. H. and Wordsworth, J., "The Three-Dimensional Laminar Boundary Layer on a Rotating Helical Blade," J. Fluid Mech. 23, Part 2, 305, 1965.

48. Miyake, Y. and Fujita, S., "A Laminar Boundary Layer on a Rotating Three-Dimensional Blade," J. Fluid Mech. 65, Part 3, 481, 1974.

49. Daly, B. J. and Harlow, F. H., "Transport Equations of Turbulence," Phys. of Fluids 13, 1970.

50. Rotta, J. C., "Statische Thorie Nichthomogener Turbulenz," J. Physics 129, 1951.

51. Naot, D., Shavit, A., and Wolfshtein, M., "Interactions Between Components of the Turbulent Velocity Correlation Tensor," Israel J. of Tech., 259, 1970.

52. Hah, C. and Lakshminarayana, B., "Prediction and Measurement of Mean Velocity and Turbulence Structure in the Near Wake of an Airfoil," submitted for publication in J. Fluid Mech., 1981.

53. Raj, R. and Lakshminarayana, B., "Characteristics of the Wake Behind a Cascade of Airfoils," J. Fluid Mech. 61, Part 4, 707-730, 1973.

54. Pope, S. B. and Whitelaw, J. H., "The Calculation of Near-Wake Flows," J. Fluid Mech. 73, Part 1, 9-32, 1976.

55. Chevray, R. and Kovasznay, S. G., "Turbulence Measurements in the Wake of a Thin Flat Plate," AIAA J. 7, 1969.

56. Fermin, M. C. P. and Cook, T. A., "Detailed Exploration of the Compressible Viscous Flow Over Two-Dimensional Airfoils at High Reynolds Numbers," T. M. A. 1076, Royal Aircraft Establishment, England, 1968.

57. Silverstein, A. and Katzoff, S., "Design Charts for Predicting Downwash Angles and Wake Characteristics Behind Plain and Flapped Wings," NACA Report No. 648, 1939.

58. Preston, J. H., Sweeting, N. E., and Cox, D. K., "The Experimental Determination of the Boundary Layer and Wake Characteristics of a Piercy Airfoil with Particular Reference to the Trailing Edge Region," Gr. Brit. Aero. Res. Council, R and M 2013, 1945.

59. Mendelsohn, R. A., "Wind Tunnel Investigation of the Boundary Layer and Wake and their Relation to Airfoil Characteristics--NACA 65-012 Airfoil with a True Contour Flap and a Beveled Trailing Edge Flap," NASA TN 1304, 1947.

60. Bradshaw, P., "Prediction of the Turbulent Near-Wake of a Symmetrical Airfoil," AIAA J. 8, 1970.

61. Townsend, A. A., The Structure of Turbulent Shear Flow, Cambridge University Press, 1956.

62. Dennis, S. C. R. and Dunwoody, J., "The Steady Flow of a Viscous Fluid Past a Flat Plate," J. Fluid Mech. 24, 577-595, 1966.

63. Dennis, S. C. R. and Chang, G.-Z., "Numerical Integration of the Navier-Stokes Equations for Steady Two-Dimensional Flows," Phys. Fluids, Supplement II, 88-93, 1969.

64. Irwin, H. P. A. H. and Smith, A., "Prediction of the Effect of Streamline Curvature on Turbulence," Phys. of Fluids 18, No. 6, June 1975.

APPENDIX A

LISTING OF THE ROTOR WAKE CODE

```
C
C     ROTOR WAKE CODE
C
C     NUMERICAL PREDICTION OF TURBULENT ROTOR WAKES BY
C     MODIFIED RSM MODEL WHICH INCLUDES EFFECTS OF
C     STREAMLINE CURVATURE AND ROTATION.
C
C
C     INPUT DATA CARD FORMAT AND BRIEF EXPLANATION ARE
C     AS FOLLOWS.
C
C     1. FIRST CARD - IAL,DENS,SOR(15,2F10.4)
C                     IAL: NUMBER OF ITERATION
C                     DENS:  DENSITY OF FLUID
C                     SOR:  SOR FACTOR
C     2. SECOND CARD-DR,RS,DN(3F10.3)
C                    FINITE DIFFERENCES IN R,S,N
C                    DIRECTIONS
C     3.  THIRD CARD-EF,DF,SF(3F10.3)
C                    EF:  FREE-STREAM TURBULENT
C                         KINETIC ENERGY
C                    DF:  FREE-STREAM TURBULENT
C                         ENERGY DISSIPATION RATE
C                    SF:  DUMMY PARAMETER
C     4.  FOURTH CARD-OM(F10.3)
C                     OM:  ANGULAR SPEED OF ROTOR
C     5   FIFTH CARD-AL(F10.3)
C                    AL:  RADIAL VARIATION OF
C                         FLOW OUTLET ANGLE
C     6   SIXTH CARD-VNON(1),B(1),SA(1),R(1)
C                    (4F10.3)
C                    VNON(1): FREE-STREAM VELOCITY
C                             AT HUB
C                    B(1).  OUTLET ANGLE AT HUB
C                    SA(1):  SPACING AT HUB
C                    R(1):  R-COODINATE OF HUB
C     7   SEVENTH CARD-BC1,SAC1,VNONC1(3F10.3)
C                      BC1:  RADIAL VARIATION OF QUTLET
C                            ANGLE
C                      SAC1:  RADIAL VARIATION OF
C                             SPACING
C                      VNONC1:  RADIAL VARIATION OF
C                               FREE-STREAM VELOCITY
C      8  EIGHTH-51ST CARDS SPECIFY BOUNDARY CONDITIONS
```

```
C          FOR ELLIPTIC CALCULATION AND DEPEND ON
C          CURVE-FITTING.
C
C
C          THE RESULTS ARE PRINTED AND AUTOMATICALLY
C          STORED IN RJE BAT-FILES FOR NEXT ITERATION.
C
C
C
C
C
      DIMENSION U(11,100),V(11,100),W(11,100),UN(7,100)
     X,N10(10,100),VN(7,100),WN(7,100),B(20),A(4,300)
     X,SA(20),UL(7,100),VLL(7,100),WL(7,100),VNON(20)
     X,ENL(7,100),DIL(7,100),P(7,100),PL(7,100),PN(7,100)
     X,N101(20),EN(11,100),DI(11,100),G(4,300)
     X,ENN(7,100),DIN(7,100),U1(100),W1(100),EN1(100),DI1(100)
     X,R(20),IMAX(20),XC(4,10,11),RS(6,100),AR(6,7)
C
C
C
      READ(5,27) IAL,DENS,SOR
   27 FORMAT(I5,2F10.4)
      READ(5,41) DR,DS,DN
   41 FORMAT(3F10.3)
 4991 FORMAT(4F10.3)
      DN0=DN
      READ(5,41) EF,DF,SF
C     ANGULAR VELOCITY
      READ(5,42) OM
   42 FORMAT(F10.3)
C     INVERSE OF ANGLE VARIATION
      READ(5,42) AL
      READ(5,4991) VNON(1),B(1),SA(1),R(1)
      READ(5,41) BC1,SAC1,VNONC1
      DO 61 I=2,7
      B(I)=B(1)+FLOAT(I-1)*BC1
      R(I)=R(1)+FLOAT(I-1)*DR
      SA(I)=SA(1)+FLOAT(I-1)*SAC1
      VNON(I)=VNON(1)-FLOAT(I-1)*VNONC1
   61 CONTINUE
      VNON(8)=VNON(1)
      VNON(9)=VNON(1)
      VNON(10)=VNON(7)
      VNON(11)=VNON(7)
      SA(8)=SA(1)
      SA(9)=SA(1)
      SA(10)=SA(7)
      SA(11)=SA(7)
C     NUMBER OF N
      IMAX(1)=75
      DO 330 I=1,7
      IMAX(I)=IMAX(1)+ 2*(I-1)
  330 CONTINUE
```

```
      IMAX(8)=IMAX(1)
      IMAX(9)=IMAX(1)
      IMAX(10)=IMAX(7)
      IMAX(11)=IMAX(7)
C
C     GETTING INITIAL VELOCITY DISTRIBUTION
C
C     DATA 2  ********
      DO 301 I=1,11
      READ(5,351)XC(1,1,I),XC(1,2,I),XC(1,3,I),XC(1,4,I),
     $XC(1,5,I),XC(1,6,I),XC(1,7,I)
  301 CONTINUE
  351 FORMAT(7F7.4)
      DO 310 I=1,11
      READ(5,352)XC(3,1,I),XC(3,2,I),XC(3,3,I),XC(3,4,I),
     $XC(3,5,I),XC(3,6,I),XC(3,7,I),XC(3,8,I),XC(3,9,I)
  310 CONTINUE
  352 FORMAT(9F6.3)
      DO 320 I=1,11
      READ(5,305)XC(2,1,I),XC(2,2,I),XC(2,3,I),XC(2,4,I),
     $XC(2,5,I),XC(2,6,I),XC(2,7,I),XC(2,8,I)
  320 CONTINUE
  305 FORMAT(8F6.3)
      DO 307 I=1,11
      READ(5,308)XC(4,1,I),XC(4,2,I),XC(4,3,I),XC(4,4,I),
     $XC(4,5,I),XC(4,6,I),XC(4,7,I),XC(4,8,I),XC(4,9,I),
     $XC(4,10,I)
  307 CONTINUE
  308 FORMAT(10F6.3)
      IF(IAL.NE.1) GO TO 3600
      DO 309 I=1,4
      IF(I.EQ.1)J1=7
      IF(I.EQ.2)J1=8
      IF(I.EQ.3)J1=9
      IF(I.EQ.4)J1=10
      DO 209 J=1,J1
      DO 219 K=2,5
      XC(I,J,K)=XC(I,J,1)+FLOAT(K-1)*(XC(I,J,6)-XC(I,J,1))/
     $5.0
  219 CONTINUE
  209 CONTINUE
  309 CONTINUE
C
C     INITIAL DISTRIBUTION OF UNKNOWNS
C
      DO 335 I=1,11
      IMM=IMAX(I)
      IM=(IMM+1)/2
      DO 336 J=1,IMM
      IMM1=IM-20
      IMM2=IM+20
      IF(J.LT.IMM1.OR.J.GT.IMM2)GO TO 361
      SN=FLOAT(J-IM)*DN/4.0
      GO TO 365
```

```
361 IF(J.GT.IM)IMM1=IMM2
    SN=FLOAT(IMM1-IM)*DN/4.0
   X+DN*FLOAT(J-IMM1)
365 Y1PS=XC(1,4,I)
    IF(J.LT.IM)Y1PS=XC(1,3,I)
    E10=-0.6931*(SN/Y1PS)**2
    IF(E10.LT.-10.0)E10=-10.0
    SNS=SN/Y1PS
    U(I,J)=VNON(I)*XC(1,1,I)-VNON(I)*XC(1,2,I)*EXP(E10)
   X-VNON(I)*XC(1,2,I)*(-1.0+SNS*XC(1,5,I)+XC(1,6,I)*SNS**2
   $+XC(1,7,I)*SNS**3)
    Y3=SN/SA(I)*2.0
    IF(J.LT.IM) GO TO 215
    IF(Y3.GE.XC(3,2,I)) GO TO 220
    VL=VNON(I)*(XC(3,3,I)-XC(3,1,I))/XC(3,2,I)
    W(I,J)=VL*Y3+VNON(I)*XC(3,3,I)-VL*XC(3,2,I)
    GO TO 325
220 IF(Y3.GE.XC(3,4,I)) GO TO 225
    VL=VNON(I)*(XC(3,5,I)-XC(3,3,I))/(XC(3,4,I)-XC(3,2,I))
    W(I,J)=VL*Y3+VNON(I)*XC(3,5,I)-VL*XC(3,4,I)
    GO TO 325
225 W(I,J)=VNON(I)*XC(3,5,I)
    GO TO 325
215 IF(Y3.LE.XC(3,6,I)) GO TO 228
    VL=(XC(3,7,I)-XC(3,1,I))*VNON(I)/XC(3,6,I)
    W(I,J)=VL*Y3+VNON(I)*XC(3,7,I)-VL*XC(3,6,I)
    GO TO 325
228 IF(Y3.LE.XC(3,8,I)) GO TO 229
    VL=(XC(3,9,I)-XC(3,7,I))*VNON(I)/(XC(3,8,I)-XC(3,6,I))
    W(I,J)=VL*Y3+VNON(I)*XC(3,9,I)-VL*XC(3,8,I)
    GO TO 325
229 W(I,J)=VNON(I)*XC(3,9,I)
325 IF(J.LT.IM) GO TO 240
    IF(Y3.GT.XC(2,1,I)) GO TO 245
    V(I,J)=XC(2,2,I)/XC(2,1,I)*Y3*VNON(I)
    GO TO 336
245 IF(Y3.GT.XC(2,3,I)) GO TO 247
    VL=VNON(I)*(XC(2,4,I)-XC(2,2,I))/(XC(2,3,I)-XC(2,1,I))
    V(I,J)=VL*Y3+XC(2,4,I)*VNON(I)-VL*XC(2,3,I)
    GO TO 336
247 V(I,J)=VNON(I)*XC(2,4,I)
    GO TO 336
240 IF(Y3.LE. XC(2,5,I)) GO TO 250
    V(I,J)=VNON(I)*XC(2,6,I)/XC(2,5,I)*Y3
    GO TO 336
250 IF(Y3.LE.XC(2,7,I)) GO TO 255
    VL=VNON(I)*(XC(2,8,I)-XC(2,6,I))/(XC(2,7,I)-XC(2,5,I))
    V(I,J)=VL*Y3+VNON(I)*XC(2,8,I)-VL*XC(2,7,I)
    GO TO 336
255 V(I,J)=VNON(I)*XC(2,8,I)
336 CONTINUE
    IMC=IMM-50
    IMC1=IMC+1
    DO 410 J3=1,50
```

```
      U(I,J3)=U(I,51)
  410 CONTINUE
      DO 415 J3=IMC1,IMM
      U(I,J3)=U(I,IMC)
  415 CONTINUE
  335 CONTINUE
      DO 3335 I=1,11
      IMM=IMAX(I)
      IM=(IMM+1)/2
      IMM1=IM-20
      IMM2=IM+20
      DO 3336 J=1,IMM
      IMX=IMM1-30
      IMY=IMM2+30
      IF(J.LT.IMX.OR.J.GT.IMY) GO TO 586
      IF(J.LT.IMM1.OR.J.GT.IMM2) GO TO 3361
      DN=DN0/4.0
      SN=FLOAT(J-IM)*DN
      GO TO 3365
 3361 IF(J.GT.IM) IMM1=IMM2
      DN=DN0
      SN=FLOAT(IMM1-IM)*DN/4.0+DN*FLOAT(J-IMM1)
 3365 Y3=SN/SA(I)*2.0
      IF(J.EQ.1.OR.J.EQ.IMM) GO TO 586
      ECE=0.007
      IF(J.LE.IM) ECE=0.002
      IF(I.EQ.7) ECE=ECE*5.0
      TT=-XC(4,2,I)*VNON(I)**2/(XC(4,1,I)*1.2 )**2
      UG=(U(I,J+1)-U(I,J-1))/2.0/DN
      WG=(W(I,J+1)-W(I,J-1))/2.0/DN
      IF(J.EQ.IMM1)UG=0.5*((U(I,J+1)-U(I,J))/DN+(U(I,J)
     $-U(I,J-1))/4.0/DN)
      IF(J.EQ.IMM1)WG=0.5*((W(I,J+1)-W(I,J))/DN+(W(I,J)
     $-W(I,J-1))/4.0/DN)
      IF(J.EQ.IMM2)UG=0.5*((U(I,J+1)-U(I,J))/4.0/DN+(U(I,J)
     $-U(I,J-1))/DN)
      IF(J.EQ.IMM2)WG=0.5*((W(I,J+1)-W(I,J))/4.0/DN+(W(I,J)
     $-W(I,J-1))/DN)
      EN(I,J)=ECE*(ABS(UG)+0.5*ABS(WG))/3.0
      DIC=0.60-0.075*FLOAT(I-1)
      DIC=DIC*0.8
      IF(I.EQ.6)DIC=0.3
      DI(I,J)=1.0*DIC*EN(I,J)*ABS(UG)
     $+0.3*DIC*EN(I,J)*ABS(WG)
      IF(EN(I,J).GT.EF.AND.DI(I,J).GT.DF) GO TO 3336
  586 DI(I,J)=DF
      EN(I,J)=EF
 3336 CONTINUE
C
C     ***    ***    ***
      IF(I.NE.2) GO TO 3335
      WRITE(6,691)(J,EN(I,J),DI(I,J),J=1,IMM)
  691 FORMAT(4('    ',I3,'  ',2F10.1))
 3335 CONTINUE
```

```
C
C
C
C
C   ***   ***   ***
C
C
      DO 451 I=1,7
      IMM=IMAX(I)
      IM=(IMM+1)/2
      IMM1=IM-20
      IMM2=IM+20
      DO 455 J=2,100
      N10(I,1)=1
      N10(I,J)=N10(I,J-1)+10
      IF(N10(I,J ).GT.IMM1) GO TO 461
  455 CONTINUE
  461 N10(I,J)=IMM1
  462 J=J+1
      N10(I,J)=N10(I,J-1)+2
      IF(N10(I,J).GT.IMM2)GO TO 463
      GO TO 462
  463 N10(I,J)=N10(I,J-1)+10
  464 J=J+1
      N10(I,J)=N10(I,J-1)+10
      IF(N10(I,J).GT.IMM)GO TO 466
      GO TO 464
  466 N101(I)=J-1
      N20=N101(I)
      WRITE(6,1421) I
 1421 FORMAT(1H ,'INITIAL CONDITION AT STATION=',I3)
      WRITE(6,470) (N10(I,J),U(I,N10(I,J)),V(I,N10(I,J)
     X),W(I,N10(I,J)),EN(I,N10(I,J)),DI(I,N10(I,J)),
     $J=1,N20)
  470 FORMAT(I5,5F10.2,5H      ,I5,5F10.2)
  451 CONTINUE
      DO 1820 I=1,7
      KM=IMAX(I)
      DO 2011 J=1,KM
      P(I,J)=-0.5*OM**2*R(I)**2
 2011 CONTINUE
      WRITE(14,830) (U(I,J),V(I,J),W(I,J),P(I,J),EN(I,J
     $),DI(I,J),J=1,KM)
 1820 CONTINUE
C
C  ***   ***   ***
C
C
C
      DO 700 K=1,12
C
C       GET BOUNDARY CONDITION FOR R-SWEEP
C
C
```

```
      IMM=IMAX(1)
      FK=0.0
      IF(K.EQ.1) GO TO 277
      FK=(FLOAT(K-1))
  277 DO 1320 J=1,IMM
      U(1,J)=(U(9,J)-U(8,J))/11.0*FK+U(8,J)
      V(1,J)=(V(9,J)-V(8,J))/11.0*FK+V(8,J)
      W(1,J)=(W(9,J)-W(8,J))/11.0*FK+W(8,J)
      EN(1,J)=(EN(9,J)-EN(8,J))/11.0*FK+EN(8,J)
      DI(1,J)=(DI(9,J)-DI(8,J))/11.0*FK+DI(8,J)
 1320 CONTINUE
      IMM7=IMAX(7)
      DO 71320 J=1,IMM7
      U(7,J)=( U(11,J)- U(10,J))/11.0*FK+U(10,J)
      V(7,J)=( V(11,J)- V(10,J))/11.0*FK+V(10,J)
      W(7,J)=( W(11,J)- W(10,J))/11.0*FK+W(10,J)
      EN(7,J)=(EN(11,J)-EN(10,J))/11.0*FK+EN(10,J)
      DI(7,J)=(DI(11,J)-DI(10,J))/11.0*FK+DI(10,J)
71320 CONTINUE
C
C     STARTING ITERATION
C
C
      SS=DS*FLOAT(K)
      DO 10 I=2,6
      IMM=IMAX(I)
      IMM01=IMM-1
      IM=(IMM+1)/2
      IMML=IMAX(I-1)
      IML=(IMML+1)/2
      IMM1=IM-20
      IMM2=IM+20
      S=SIN(B(I))
      C=COS(B(I))
      ID=IM-IML
      CH1=-SS*S**4/R(I)**2
      CH2=-S**2/R(I)
      CH3=SS**2/2.0/R(I)**3*2.0*S**4-SS**2/R(I)**2/AL*S**3*C
      CH4=SS**2/R(I)**3*S*C-1.0/AL-SS**2/R(I)**2/AL*(S*C)**2
      CH5=-SS*S**3*C/R(I)**2
      CH6=CH5+SS/R(I)/AL*S**2
      CH7=SS**2/R(I)**3*S**3*C+1.0/AL-SS**2/R(I)**2/AL
     X*S**2*(C**2+1.0)
      CH8=-S*C/R(I)
      CH9=SS/R(I)**2*S*C-SS/R(I)/AL*C**2
      CH10=SS/R(I)**2*S**2-SS/R(I)*S*C/AL
      CH11=-SS**3/R(I)**4*S**4-2.0*SS**3/R(I)**3/AL*S**3*C
      CH12=-SS**2/R(I)**3*S**2+2.0*SS**2/R(I)**2/AL*S*C
      CH14=-SS**3/R(I)**4*S**3*C+SS**3/R(I)**3
     $/AL*S**2*(1.0+2.0*C**2)
      CH15=-SS/R(I)**2*(S*C)**2+SS/R(I)/AL*S*C
      CH16=SS**2/R(I)**3*S**2*C**2-SS**2/R(I)**2/AL*S*C
     $*(C**2+1.0)
      AA=-SS*S/R(I)+SS*C/AL
```

```
      DO 3 J=1,IMM
      U1(J )=U(I,J)
      W1(J)=W(I,J)
      EN1(J)=EN(I,J)
      DI1(J)=DI(I,J)
    3 CONTINUE
      DO 905 J=2,IMM01
      DO 910 N=1,6
      DO 915 M=1,6
      AR(N,M)=0.0
  915 CONTINUE
      AR(N,7)=0.0
  910 CONTINUE
      DN=DN0/4.0
      IF(J.LT.IMM1.OR.J.GT.IMM2) DN=DN0
      GUS=0.0
      GU=(U(I,J+1)-U(I,J-1))/2.0/DN
      GW=(W(I,J+1)-W(I,J-1))/2.0/DN
      TE=EN(I,J)
      TD=DI(I,J)
      AR(1,1)=-1.5*TD/TE-4.0*OM*S**3*SS/R(I)-GUS-U(I,J)*CH1
     X-W(I,J)*CH3
      AR(1,4)=-0.8*(-SS/R(I)*S*C+SS/AL)*(GU+U(I,J)*CH5+
     $W(I,J)*CH4
     X)+4.0*OM*S*(1.0+SS**2/R(I)**2*S**2-2.0*SS**2/R(I)
     $**2/AL*S*C)
      AR(1,5)=-0.8*(GU+U(I,J)*CH1+W(I,J)*CH3)-4.0*OM*S
     $**2*C*SS/R(I)
      AR(1,7)=-TD/3.0*2.2*(1.0+SS**2/R(I)**2*S**4)
      AR(2,2)=-1.5*TD/TE+4.0*OM*C*(-SS/R(I)*S*C+SS/AL)
      AR(2,5)=4.0*OM*C*(-SS/R(I)*S**2)
      AR(2,6)=4.0*OM*C*(1.0+SS**2/R(I)**2*S**2-2.0*SS**2
     $/R(I)/AL*S*C)
      AR(2,7)=-TD/3.0*2.2*(1.0+SS**2/R(I)**2*S**2*C**2
     X-2.0*SS**2/R(I)/AL*S*C)
      AR(3,3)=-0.8*(-SS/R(I)*S*C+SS/AL)*(GW+U(I,J)*CH8
     $+W(I,J)*CH9)
     $-0.8*(U(I,J)*CH2+W(I,J)*CH10)*SS/R(I)*S**2+4.0*OM
     $*S**3*SS/R(I)
      AR(3,4)=-4.0*OM*S-0.8*(U(I,J)*CH2+W(I,J)*CH10)
      AR(3,6)=-0.8*(GW+CH8*U(I,J)+W(I,J)*CH9)-4.0*OM*C
      AR(3,7)=-TD*2.2/3.0
      AR(4,1)=-0.4*(U(I,J)*CH2+W(I,J)*CH10)-2.0*OM*S
      AR(4,3)=-0.4*(-SS/R(I)*S*C+SS/AL)*(GU+U(I,J)*CH5
     $+W(I,J)*CH4)
     $+0.4*SS/R(I)*S**2*(GUS+U(I,J)*CH1+W(I,J)*CH3)+2.0
     $*OM*S*(1.0
     $+SS**2/R(I)**2*S**2-2.0*SS**2/R(1)/AL*S*C)
      AR(4,4)=-0.4*(GUS+U(I,J)*CH1+W(I,J)*CH3)-0.4*(-SS/
     $R(I)*S*C
     $+SS/AL)+0.4*SS/R(I)*S**2*(U(I,J)*CH2+W(I,J)*CH10)
     $-2.0*OM*C*(-SS/R(I)*S*C+SS/AL)-1.5*TD/TE
      AR(4,5)=-0.4*(GW+U(I,J)*CH8+W(I,J)*CH9)-2.0*OM*C
      AR(4,6)=-0.4*(GU+U(I,J)*CH5+W(I,J)*CH4)+2.0*OM*S
```

```
     $*(-SS/R(I)*S*C
     $+SS/AL)
      AR(4,7)=2.2/3.0*TD*SS/R(I)*S**2
      AR(5,1)=-2.0*OM*C*SS/R(I)*S**2
      AR(5,2)=-0.4*(GU+U(I,J)*CH5+W(I,J)*CH4)+2.0*OM*S*
     $(-SS/R(I)*S*C
     $+SS/AL)
      AR(5,4)=2.0*OM*C*(1.0+SS**2/R(I)**2*S**2)
      AR(5,5)=-0.4*(GUS+U(I,J)*CH1+W(I,J)*CH3)-2.0*OM
     $*S**3*SS/R(I)
     $+2.0*OM*C*(-SS/R(I)*S*C+SS/AL)-1.5*TD/TE
      AR(5,6)=-0.4*(-SS/R(I)*S*C+SS/AL)*(GU+U(I,J)*CH5
     $+W(I,J)*CH4)
     $+2.0*OM*S*(1.0+SS**2/R(I)**2*S**2-2.0*SS**2/R(I)/
     $AL*S*C)
      AR(5,7)=-TD*2.2/3.0*(SS**2/R(I)**2*C*S**3-SS**2/
     $R(I)/AL*S**2)
      AR(6,2)=-0.4*(GW+U(I,J)*CH8+W(I,J)*CH9)-2.0*OM*C
      AR(6,3)=2.0*OM*C*(1.0+SS**2/R(I)**2*S**2
     $-2.0*SS**2/R(I)/AL*S*C)
      AR(6,4)=-2.0*OM*C*SS/R(I)*S**2
      AR(6,5)=-0.4*(U(I,J)*CH2+W(I,J)*CH10)-2.0*OM*S
      AR(6,6)=-0.4*(-SS/R(I)*S*C+SS/AL)*(GW+U(I,J)*CH8
     $+W(I,J)*CH9)
     $+0.4*SS/R(I)*S**2*(U(I,J)*CH2+W(I,J)*CH10)-2.0*OM
     $*C*(-SS/R(I)
     $*S*C+SS/AL)+2.0*OM*S*SS/R(I)*S**2+2.0*OM*C*(-SS/R
     $(I)*S*C+SS/AL)
     $-1.5*TD/TE
      AR(6,7)=2.2/3.0*TD*SS/R(I)*S**2
      DO 930 II=1,5
      IJ=II+1
      AR(II,II)=1.0/AR(II,II)
      AR(II,7)=AR(II,7)*AR(II,II)
      DO 931 N=IJ,6
      AR(II,N)=AR(II,N)*AR(II,II)
931   CONTINUE
      DO 932 N=IJ,6
      AR(N,7)=AR(N,7)-AR(II,7)*AR(N,II)
932   CONTINUE
      DO 933 N=IJ,6
      DO 934 M=IJ,6
      AR(M,N)=AR(M,N)-AR(M,II)*AR(II,N)
934   CONTINUE
933   CONTINUE
930   CONTINUE
      AR(6,7)=AR(6,7)/AR(6,6)
      NV=6
943   NV=NV-1
      IF(NV.EQ.0) GO TO 944
      NX=NV+1
      DO 936 N=NX,6
      AR(NV,7)=AR(NV,7)-AR(NV,N)*AR(N,7)
936   CONTINUE
```

```
      GO TO 943
  944 RS(1,J)=AR(1,7)
      RS(2,J)=AR(2,7)
      RS(3,J)=AR(3,7)
      RS(4,J)=AR(4,7)
      RS(5,J)=AR(5,7)
      RS(6,J)=AR(6,7)
      PRE=-(GU*RS(5,J)+GW*RS(6,J))-TD
      WRITE(6,6330) I,J,GU,GW,RS(1,J),RS(2,J),RS(3,J),RS
     $(4,J),RS(5,J),RS(6,J),PRE
 6330 FORMAT('  ',2I4,'   ',2F10.2,' ',6F10.4,'  ',F12.1)
  905 CONTINUE
      MM=0
   15 MM=MM+1
C
C     NEW S
C
      PR=2.0*OM*U(I,IMM)*S+R(I)*OM**2-U(I,IMM)**2*CH2
      PR1=U(I,IMM)**2*CH1+2.0*OM*(-SS*S/R(I)+SS*C/AL)*S**2*
     $U(I,IMM)
      DO 20 J=1,IMM
      RUV=0.0
      IMM11=IMM1+1
      IMM22=IMM2-1
      IF(J.LE.IMM11.OR.J.GE.IMM22) GO TO 965
      DN=DN0/4.0
      RUV=(RS(5,J+1)-RS(5,J-1))/2.0/DN
  965 IF((J-ID).LT.1) GO TO 145
      IF((J-ID).GT.IMML) GO TO 146
      UNN=U(I-1,J-ID)
      GO TO 141
  145 UNN=U(I-1,1)
      GO TO 141
  146 UNN=U(I-1,IMML)
  141 DN=DN0
      IF(J.GE.IMM1.AND.J.LE.IMM2)DN=DN0/4.0
      A(1,J)=-V(I,J)/2.0/DN
      A(2,J)=U(I,J)/DS+W(I,J)/DR
      A(3,J)=V(I,J)/2.0/DN
      A(4,J)=PR1-U(I,J)**2*CH1+2.0*OM*(-SS*S/R(I)+SS*C/AL
     X)*U(I,J)*S**2-RUV+U(I,J)*U1(J)/DS
     X+W(I,J)*UNN/DR
      IF(J.EQ.IMM1)GO TO 19
      IF(J.EQ.IMM2)GO TO 18
      GO TO 20
   19 A(1,J)=-V(I,J)/8.0/DN
      A(2,J)=U(I,J)/DS+W(I,J)/DR-3.0/8.0*V(I,J)/DN
      A(3,J)=V(I,J)/2.0/DN
      GO TO 20
   18 A(1,J)=-V(I,J)/2.0/DN
      A(3,J)=V(I,J)/8.0/DN
      A(2,J)=U(I,J)/DS+3.0/8.0*V(I,J)/DN+W(I,J)/DR
   20 CONTINUE
      A(4,1)=A(4,1)-A(1,1)*U(I,1)
```

```
      A(4,IMM)=A(4,IMM)-A(3,IMM)*U(I,IMM)
      CALL ELIM(A,IMM)
      DO 101 J=1,IMM
      UN(I,J)=A(4,J)
  101 CONTINUE
C
C     NEW R
C
      DO 30 J=1,IMM
      RWV=0.0
      IMM11=IMM1+1
      IMM22=IMM2-1
      IF(J.LE.IMM11.OR.J.GE.IMM22) GO TO 966
      DN=DN0/4.0
      RWV=(RS(6,J+1)-RS(6,J-1))/2.0/DN
  966 IF((J-ID).LT.1) GO TO 165
      IF((J-ID).GT.IMML)GO TO 166
      WNN= W(I-1,J-ID)
      GO TO 161
  165 WNN= W(I-1,1)
      GO TO 161
  166 WNN= W(I-1,IMML)
  161 DN=DN0
      IF(J.GE.IMM1.AND.J.LE.IMM2)DN=DN0/4.0
      A(1,J)=-V(I,J)/2.0/DN
      A(2,J)=UN(I,J)/DS+W(I,J)/DR
      A(3,J)=V(I,J)/2.0/DN
      A(4,J)=UN(I,J)*W1( J)/DS+W(I,J)*WNN/DR-UN(I,J)
     X**2*CH2-RWV-2.0*OM*UN(I,J)*S+R(I)*OM**2-PR
      IF(J.EQ.IMM1)GO TO 29
      IF(J.EQ.IMM2)GO TO 28
      GO TO 30
   29 A(1,J)=-V(I,J)/8.0/DN
      A(3,J)=V(I,J)/2.0/DN
      A(2,J)=UN(I,J)/DS+W(I,J)/DR-3.0/8.0*V(I,J)/DN
      GO TO 30
   28 A(1,J)=-V(I,J)/2.0/DN
      A(3,J)=V(I,J)/8.0/DN
      A(2,J)=UN(I,J)/DS+3.0/8.0*V(I,J)/DN+W(I,J)/DR
   30 CONTINUE
      A(4,1)=A(4,1)-A(1,1)*W(I,1)
      A(4,IMM)=A(4,IMM)-A(3,IMM)*W(I,IMM)
      CALL ELIM(A,IMM)
      DO 102 J=1,IMM
      WN(I,J)=A(4,J)
  102 CONTINUE
      UM1=200.0
      DO 103 J=1,IMM
      U(I,J)=UN(I,J)
      W(I,J)=WN(I,J)
      IF(J.LT.IMM1.OR.J.GT.IMM2)GO TO 103
      IF(U(I,J).GE.UM1)GO TO 103
      UM1=U(I,J)
      NT=J
```

```
  103 CONTINUE
      IF(MM.GE.2)GO TO 600
      GO TO 15
C
C     NEW N
C
  600 NT1=NT+1
      VN(I,NT)=0.0
      DO 40 J=NT1,IMM
      DN=DN0
      IF(J.LE.IMM2)DN=DN0/4.0
      IF((J-ID).GT.IMML)GO TO 176
      WNN= W(I-1,J-ID)
      GO TO 171
  176 WNN= W(I-1,IMML)
  171 GM=-( U(I,J)-U1(J))/DS
      VN(I,J)=VN(I,J-1)+GM*DN
   40 CONTINUE
      NT2=NT-1
      DO 640 J=1,NT2
      DN=DN0
      JJ=NT-J
      IF(JJ.GE.IMM1)DN=DN0/4.0
      IF((JJ-ID).LT.1) GO TO 175
      WNN=W(I-1,JJ-ID)
      GO TO 671
  175 WNN=W(I-1,1)
  671 GM=-(U(I,JJ)-U1(JJ))/DS
      VN(I,JJ)=VN(I,JJ+1)-GM*DN
  640 CONTINUE
      DO 46 J=1,IMM
      V(I,J)=VN(I,J)
   46 CONTINUE
      DO 1020 J=1,IMM
      IF((J-ID) .LT.1) GO TO 1145
      IF((J-ID).GT.IMML) GO TO 1146
      ENNN= EN(I-1,J-ID)
      DINN= DI(I-1,J-ID)
      GO TO 1141
 1145 ENNN=EN(I-1,1)
      DINN= DI(I-1,1)
      GO TO 1141
 1146 ENNN=EN(I-1,IMML)
      DINN= DI(I-1,IMML)
 1141 DN=DN0
      IF(J.GE.IMM1.AND.J.LE.IMM2) DN=DN0/4.0
      IF(J.EQ.1) GO TO 73
      IF(J.EQ.IMM) GO TO 74
      IF(J.EQ.IMM1) GO TO 75
      IF(J.EQ.IMM2) GO TO 76
      Q1=(U(I,J+1)-U(I,J-1))/2.0/DN
      Q2=(W(I,J+1)-W(I,J-1))/2.0/DN
      GO TO 77
   73 Q1=(U(I,J+1)-U(I,J))/DN
```

```
      Q2=(W(I,J+1)-W(I,J))/DN
      GO TO 77
   74 Q1=(U(I,J)-U(I,J-1))/DN
      Q2=(W(I,J)-W(I,J-1))/DN
      GO TO 77
   75 Q1=0.5/DN*(U(I,J+1)-0.75*U(I,J)-0.25*U(I,J-1))
      Q2=0.5/DN*(W(I,J+1)-0.75*W(I,J)-0.25*W(I,J-1))
      GO TO 77
   76 Q1=0.5/DN*(0.25*U(I,J+1)+0.75*U(I,J)-U(I,J-1))
      Q2=0.5/DN*(0.25*W(I,J+1)+0.75*W(I,J)-W(I,J-1))
   77 E=0.09*EN(I,J)**2/DI(I,J)
      PR=E*(Q1**2+Q2**2+Q1*(CH5+CH6)+Q2*(CH7+CH8))
      A(1,J)=-VN(I,J)/2.0/DN-E/DN**2
      A(2,J)=UN(I,J)/DS+WN(I,J)/DR+E*2.0/DN**2
      A(3,J)=VN(I,J)/2.0/DN-E/DN**2
      A(4,J)=UN(I,J)*EN1(J)/DS+WN(I,J)*ENNN/DR
     $+PR
     $-DI(I,J)
      G(1,J)=-VN(I,J)/2.0/DN-E/1.3/DN**2
      G(2,J)=UN(I,J)/DS+WN(I,J)/DR+E*2.0/1.3/DN**2
      G(3,J)=VN(I,J)/2.0/DN-E/1.3/DN**2
      G(4,J)=UN(I,J)*DI1(J)/DS+WN(I,J)*DINN/DR
     $+1.44*DI(I,J)/EN(I,J)*PR
     $-1.92*DI(I,J)**2/EN(I,J)
      IF(J.EQ.IMM1) GO TO 1019
      IF(J.EQ.IMM2) GO TO 1018
      GO TO 1020
 1019 A(1,J)=-VN(I,J)/8.0/DN-E/10.0/DN**2
      A(2,J)=UN(I,J)/DS-3.0/8.0*VN(I,J)/DN+WN(I,J)/DR
     $+0.5*E/DN**2
      A(3,J)=VN(I,J)/2.0/DN-E/2.5/DN**2
      A(4,J)=UN(I,J)*EN1(J)/DS+WN(I,J)*ENNN/DR
     $+PR                                        -DI(I,J)
      G(1,J)=-VN(I,J)/8.0/DN-E/13.0/DN**2
      G(2,J)=UN(I,J)/DS-3.0/8.0*VN(I,J)/DN
     $+WN(I,J)/DR+1.0/2.6*E/DN**2
      G(3,J)=VN(I,J)/2.0/DN-E/2.5/1.3/DN**2
      G(4,J)=UN(I,J)*DI1(J)/DS+WN(I,J)*DINN/DR
     $+1.44*DI(I,J)/EN(I,J)*PR
     $          -1.92*DI(I,J)**2/EN(I,J)
      GO TO 1020
 1018 A(1,J)=-VN(I,J)/2.0/DN-E/2.5/DN**2
      A(3,J)=VN(I,J)/8.0/DN-E/10.0/DN**2
      A(2,J)=UN(I,J)/DS+3.0/8.0*VN(I,J)/DN+WN(I,J)/DR
     $+0.5*E/DN**2
      A(4,J)=UN(I,J)*EN1(J)/DS+WN(I,J)*ENNN/DR
     $+PR
     $-DI(I,J)
      G(1,J)=-VN(I,J)/2.0/DN-E/2.5/1.3/DN**2
      G(3,J)=VN(I,J)/8.0/DN-E/13.0/DN**2
      G(2,J)=UN(I,J)/DS+3.0/8.0*VN(I,J)/DN+WN(I,J)/DR
     $+0.5/1.3*E/DN**2
      G(4,J)=UN(I,J)*DI1(J)/DS+WN(I,J)*DINN/DR
     $+1.44*DI(I,J)/EN(I,J)*PR
```

```
     $-1.92*DI(I,J)**2/EN(I,J)
 1020 CONTINUE
      A(4,1)=A(4,1)-A(1,1)*EN(I,1)
      A(4,IMM)=A(4,IMM)-A(3,IMM)*EN(I,IMM)
      G(4,1)=G(4,1)-G(1,1)*DI(I,1)
      G(4,IMM)=G(4,IMM)-G(3,IMM)*DI(I,IMM)
      CALL ELIM(A,IMM)
      DO 1101 J=1,IMM
      ENN(I,J)=A(4,J)
 1101 CONTINUE
      CALL ELIM(G,IMM)
      DO 1107 J=1,IMM
      DIN(I,J)=G(4,J)
 1107 CONTINUE
      DO 106 J=1,IMM
      EN(I,J)=ENN(I,J)
      DI(I,J)=DIN(I,J)
  106 CONTINUE
C
C
C     ***   ***   ***   ***   ***
C
C
      N20=N101(I)
      WRITE(6,2370)K,I
      WRITE(6,2470)     (N10(I,J),U(I,N10(I,J)),V(I,
     $N10(I,J)),W(I,N10
     X(I,J)),EN(I,N10(I,J)),DI(I,N10(I,J)),J=1,N20)
 2470 FORMAT(            I5,5F10.2,5H     ,I5,5F10.2)
 2370 FORMAT(1H ,'***','S-STATION=',I3,'      R-STATION
     $=',I3,'***')
   10 CONTINUE
      DO 820 I=1,7
      KM=IMAX(I)
      DO 5011 J=1,KM
      P(I,J)=-0.5*OM**2*R(I)**2
 5011 CONTINUE
      WRITE(14,830) (U(I,J),V(I,J),W(I,J),P(I,J),
     $EN(I,J),DI(I,J),J=1,KM)
  820 CONTINUE
  830 FORMAT(3F5.1,F7.1,2F9.1,3F5.1,F7.1,2F9.1)
  700 CONTINUE
      GO TO 44444
 3600 DO 4700 K=1,12
      IF(K.NE.1) GO TO 1840
      DO 1830 I=1,7
      KM=IMAX(I)
      READ(5,830) (UL(I,J),VLL(I,J),WL(I,J),PL(I,J),ENL(I,J)
     $,DIL(I,J),J=1,KM)
 1830 CONTINUE
      DO 1835 I=1,7
      KM=IMAX(I)
      READ(5,830) (U(I,J),V(I,J),W(I,J),P(I,J),EN(I,J)
     $DI(I,J),J=1,KM)
```

```
 1835 CONTINUE
 1840 DO 1845 I=1,7
      KM=IMAX(I)
      READ(5,830)(UN(I,J),VN(I,J),WN(I,J),PN(I,J),ENN(I,J)
     $,DIN(I,J),J=1,KM)
 1845 CONTINUE
C
C
      SS=DS*FLOAT(K)
      DO 4010 I=2,6
      IMM=IMAX(I)
      IMMO1=IMM-1
      IM=(IMM+1)/2
      IMML=IMAX(I-1)
      IML=(IMML+1)/2
      IMM1=IM-20
      IMM2=IM+20
      S=SIN(B(I))
      C=COS(B(I))
      ID=IM-IML
      CH1=-SS*S**4/R(I)**2
      CH2=-S**2/R(I)
      CH3=SS**2/2.0/R(I)**3*2.0*S**4-SS**2/R(I)**2/AL*S**3*C
      CH4=SS**2/R(I)**3*S*C-1.0/AL-SS**2/R(I)**2/AL*(S*C)**2
      CH5=-SS*S**3*C/R(I)**2
      CH6=CH5+SS/R(I)/AL*S**2
      CH7=SS**2/R(I)**3*S**3*C+1.0/AL-SS**2/R(I)**2/AL
     X*S**2*(C**2+1.0)
      CH8=-S*C/R(I)
      CH9=SS/R(I)**2*S*C-SS/R(I)/AL*C**2
      CH10=SS/R(I)**2*S**2-SS/R(I)*S*C/AL
      CH11=-SS**3/R(I)**4*S**4-2.0*SS**3/R(I)**3/AL*S**3*C
      CH12=-SS**2/R(I)**3*S**2+2.0*SS**2/R(I)**2/AL*S*C
      CH14=-SS**3/R(I)**4*S**3*C+SS**3/R(I)**3
     $/AL*S**2*(1.0+2.0*C**2)
      CH15=-SS/R(I)**2*(S*C)**2+SS/R(I)/AL*S*C
      CH16=SS**2/R(I)**3*S**2*C**2-SS**2/R(I)**2/AL*S*C
     $*(C**2+1.0)
      DO 4905 J=2,IMMO1
      DO 4910 N=1,6
      DO 4915 M=1,6
      AR(N,M)=0.0
 4915 CONTINUE
      AR(N,7)=0.0
 4910 CONTINUE
      DN=DNO/4.0
      IF(J.LT.IMM1.OR.J.GT.IMM2) DN=DNO
      GUS=(UN(I,J)-UL(I,J))/2.0/DS
      GWS=(WN(I,J)-WL(I,J))/2.0/DS
      GU=(U(I,J+1)-U(I,J-1))/2.0/DN
      GW=(W(I,J+1)-W(I,J-1))/2.0/DN
      TE=EN(I,J)
      TD=DI(I,J)
      AR(1,1)=-1.5*TD/TE-4.0*OM*S**3*SS/R(I)-GUS-U(I,J)*CH1
```

```
X-W(I,J)*CH3
 AR(1,4)=-0.8*(-SS/R(I)*S*C+SS/AL)*(GU+U(I,J)*CH5+
$W(I,J)*CH4
X)+4.0*OM*S*(1.0+SS**2/R(I)**2*S**2-2.0*SS**2/R(I)
$**2/AL*S*C)
 AR(1,5)=-0.8*(GU+U(I,J)*CH1+W(I,J)*CH3)-4.0*OM*S
$**2*C*SS/R(I)
 AR(1,7)=-TD/3.0*2.2*(1.0+SS**2/R(I)**2*S**4)
 AR(2,2)=-1.5*TD/TE+4.0*OM*C*(-SS/R(I)*S*C+SS/AL)
 AR(2,5)=4.0*OM*C*(-SS/R(I)*S**2)
 AR(2,6)=4.0*OM*C*(1.0+SS**2/R(I)**2*S**2-2.0*SS**2
$/R(I)/AL*S*C)
 AR(2,7)=-TD/3.0*2.2*(1.0+SS**2/R(I)**2*S**2*C**2
X-2.0*SS**2/R(I)/AL*S*C)
 AR(3,3)=-0.8*(-SS/R(I)*S*C+SS/AL)*(GW+U(I,J)*CH8
$+W(I,J)*CH9)
$-0.8*(U(I,J)*CH2+W(I,J)*CH10)*SS/R(I)*S**2+4.0*OM
$*S**3*SS/R(I)
 AR(3,4)=-4.0*OM*S-0.8*(U(I,J)*CH2+W(I,J)*CH10)
 AR(3,6)=-0.8*(GW+CH8*U(I,J)+W(I,J)*CH9)-4.0*OM*C
 AR(3,7)=-TD*2.2/3.0
 AR(4,1)=-0.4*(U(I,J)*CH2+W(I,J)*CH10)-2.0*OM*S
 AR(4,3)=-0.4*(-SS/R(I)*S*C+SS/AL)*(GU+U(I,J)*CH5
$+W(I,J)*CH4)
$+0.4*SS/R(I)*S**2*(GUS+U(I,J)*CH1+W(I,J)*CH3)+2.0
$*OM*S*(1.0
$+SS**2/R(I)**2*S**2-2.0*SS**2/R(I)/AL*S*C)
 AR(4,4)=-0.4*(GUS+U(I,J)*CH1+W(I,J)*CH3)-0.4*(-SS/
$R(I)*S*C
$+SS/AL)+0.4*SS/R(I)*S**2*(U(I,J)*CH2+W(I,J)*CH10)
$-2.0*OM*C*(-SS/R(I)*S*C+SS/AL)-1.5*TD/TE
 AR(4,5)=-0.4*(GW+U(I,J)*CH8+W(I,J)*CH9)-2.0*OM*C
 AR(4,6)=-0.4*(GU+U(I,J)*CH5+W(I,J)*CH4)+2.0*OM*S
$*(-SS/R(I)*S*C
$+SS/AL)
 AR(4,7)=2.2/3.0*TD*SS/R(I)*S**2
 AR(5,1)=-2.0*OM*C*SS/R(I)*S**2
 AR(5,2)=-0.4*(GU+U(I,J)*CH5+W(I,J)*CH4)+2.0*OM*S*
$(-SS/R(I)*S*C
$+SS/AL)
 AR(5,4)=2.0*OM*C*(1.0+SS**2/R(I)**2*S**2)
 AR(5,5)=-0.4*(GUS+U(I,J)*CH1+W(I,J)*CH3)-2.0*OM
$*S**3*SS/R(I)
$+2.0*OM*C*(-SS/R(I)*S*C+SS/AL)-1.5*TD/TE
 AR(5,6)=-0.4*(-SS/R(I)*S*C+SS/AL)*(GU+U(I,J)*CH5
$+W(I,J)*CH4)
$+2.0*OM*S*(1.0+SS**2/R(I)**2*S**2-2.0*SS**2/R(I)/
$AL*S*C)
 AR(5,7)=-TD*2.2/3.0*(SS**2/R(I)**2*C*S**3-SS**2/
$R(I)/AL*S**2)
 AR(6,2)=-0.4*(GW+U(I,J)*CH8+W(I,J)*CH9)-2.0*OM*C
 AR(6,3)=2.0*OM*C*(1.0+SS**2/R(I)**2*S**2
$-2.0*SS**2/R(I)/AL*S*C)
 AR(6,4)=-2.0*OM*C*SS/R(I)*S**2
```

```
      AR(6,5)=-0.4*(U(I,J)*CH2+W(I,J)*CH10)-2.0*OM*S
      AR(6,6)=-0.4*(-SS/R(I)*S*C+SS/AL)*(GW+U(I,J)*CH8
     $+W(I,J)*CH9)
     $+0.4*SS/R(I)*S**2*(U(I,J)*CH2+W(I,J)*CH10)-2.0*OM
     $*C*(-SS/R(I)
     $*S*C+SS/AL)+2.0*OM*S*SS/R(I)*S**2+2.0*OM*C*(-SS/R
     $(I)*S*C+SS/AL)
     $-1.5*TD/TE
      AR(6,7)=2.2/3.0*TD*SS/R(I)*S**2
      DO 4930 II=1,5
      IJ=II+1
      AR(II,II)=1.0/AR(II,II)
      AR(II,7)=AR(II,7)*AR(II,II)
      DO 4931 N=IJ,6
      AR(II,N)=AR(II,N)*AR(II,II)
 4931 CONTINUE
      DO 4932 N=IJ,6
      AR(N,7)=AR(N,7)-AR(II,7)*AR(N,II)
 4932 CONTINUE
      DO 4933 N=IJ,6
      DO 4934 M=IJ,6
      AR(M,N)=AR(M,N)-AR(M,II)*AR(II,N)
 4934 CONTINUE
 4933 CONTINUE
 4930 CONTINUE
      AR(6,7)=AR(6,7)/AR(6,6)
      NV=6
 4943 NV=NV-1
      IF(NV.EQ.0) GO TO 4944
      NX=NV+1
      DO 4936 N=NX,6
      AR(NV,7)=AR(NV,7)-AR(NV,N)*AR(N,7)
 4936 CONTINUE
      GO TO 4943
 4944 RS(1,J)=AR(1,7)
      RS(2,J)=AR(2,7)
      RS(3,J)=AR(3,7)
      RS(4,J)=AR(4,7)
      RS(5,J)=AR(5,7)
      RS(6,J)=AR(6,7)
      PRE=-(GU*RS(5,J)+GW*RS(6,J))-TD
      WRITE(6,6330) I,J,GU,GW,RS(1,J),RS(2,J),RS(3,J),RS
     $(4,J),RS(5,J),RS(6,J),PRE
 4905 CONTINUE
      DO 8921 N9=1,6
      RS(N9,1)=RS(N9,2)
      RS(N9,IMM)=RS(N9,2)
 8921 CONTINUE
      MM=0
 4015 MM=MM+1
C
C     NEW S
C
      DO 4020 J=1,IMM
```

```
      RUV=0.0
      DN=DNO/4.0
      IF(J.LT.IMM1.OR.J.GT.IMM2) DN=DNO
      WCOV=-SS/R(I)*S**2*U(I,J)+(-SS/R(I)*S*C+SS/AL)*V(I,J)
     $+(1.0+SS**2/R(I)**2*S**2-2.0*SS**2/R(I)/AL*S*C)*W(I,J)
      UCOV=U(I,J)-SS/R(I)*S**2*W(I,J)
      VCOV=V(I,J)+(-SS/R(I)*S*C+SS/AL)*W(I,J)
      IF((J-ID).LT.1) GO TO 4145
      IF((J-ID).GT.IMML) GO TO 4146
      UNN=U(I-1,J-ID)
      PNN=P(I-1,J-ID)
      GO TO 4141
4145  UNN=U(I-1,1)
      PNN=P(I-1,1)
      GO TO 4141
4146  UNN=U(I-1,IMML)
      PNN=P(I-1,IMML)
4141  DN=DNO
      IF(J.GE.IMM1.AND.J.LE.IMM2)DN=DNO/4.0
      A(1,J)=-V(I,J)/2.0/DN
      A(2,J)=(UN(I,J)-UL(I,J))/2.0/DS
      A(3,J)=V(I,J)/2.0/DN
      IF(J.EQ.1.OR.J.EQ.IMM) GO TO 9011
      PSN=P(I,J+1)-P(I,J-1)
      RSN=RS(5,J+1)-RS(5,J-1)
      GO TO 9012
9011  RSN=0.0
      PSN=0.0
9012  A(4,J)=-U(I,J)**2-W(I,J)*(U(I+1,J)-UNN)/2.0/DR
     $-W(I,J)**2*CH11
     $-2.0*U(I,J)*W(I,J)*CH3-2.0*U(I,J)*V(I,J)*CH5-2.0*V
     $(I,J)*W(I,J)*CH4
     $+2.0*OM*S*WCOV-RSN/2.0/DN
     $+1.0/DENS*((1.0+SS**2/R(I)**2*S**4)*(PN(I,J)
     $-PL(I,J))/2.0/DS
     $+(SS*2/R(I)**2*S**3*C-SS**2/R(I)/AL*S**2)*PSN
     $/2.0/DN+SS/R(I)*S**2*(P(I+1,J)-PNN)/2.0/DR)
      IF(J.EQ.IMM1) GO TO 4019
      IF(J.EQ.IMM2) GO TO 4018
      GO TO 4020
4019  A(1,J)=-V(I,J)/8.0/DN
      A(2,J)=(UN(I,J)-UL(I,J))/2.0/DS-3.0/8.0*V(I,J)/DN
      A(3,J)=V(I,J)/2.0/DN
      GO TO 4020
4018  A(1,J)=-V(I,J)/2.0/DN
      A(3,J)=V(I,J)/8.0/DN
      A(2,J)=3.0/8.0*V(I,J)/DN+(UN(I,J)-UL(I,J))/2.0/DS
4020  CONTINUE
      A(4,1)=A(4,1)-A(1,1)*U(I,1)
      A(4,IMM)=A(4,IMM)-A(3,IMM)*U(I,IMM)
      CALL ELIM(A,IMM)
      DO 4101 J=1,IMM
      U(I,J)=U(I,J)+SOR*(A(4,J)-U(I,J))
4101  CONTINUE
```

```
C
C     NEW R
C
      DO 4030 J=1,IMM
      RWV=0.0
      DN=DN0/4.0
      IF(J.LT.IMM1.OR.J.GT.IMM2) DN=DN0
      WCOV=-SS/R(I)*S**2*U(I,J)+(-SS/R(I)*S*C+SS/AL)*V(I,J)
     $+(1.0+SS**2/R(I)**2*S**2-2.0*SS**2/R(I)/AL*S*C)*W(I,J)
      UCOV=U(I,J)-SS/R(I)*S**2*W(I,J)
      VCOV=V(I,J)+(-SS/R(I)*S*C+SS/AL)*W(I,J)
      IF((J-ID).LT.1) GO TO 4165
      IF((J-ID).GT.IMML)GO TO 4166
      WNN= W(I-1,J-ID)
      PNN=P(I-1,J-ID)
      GO TO 4161
 4165 WNN= W(I-1,1)
      PNN=P(I-1,1)
      GO TO 4161
 4166 WNN= W(I-1,IMML)
      PNN=P(I-1,IMML)
 4161 A(1,J)=-V(I,J)/2.0/DN
      A(2,J)=(W(I+1,J)-WNN)/2.0/DR
      A(3,J)=V(I,J)/2.0/DN
      IF(J.EQ.1.OR.J.EQ.IMM) GO TO 9111
      RSN=RS(6,J+1)-RS(6,J-1)
      PSN=P(I,J+1)-P(I,J-1)
      GO TO 9112
 9111 PSN=0.0
      RSN=0.0
 9112 A(4,J)=-U(I,J)*(WN(I,J)-WL(I,J))/2.0/DS-2.0*OM*C*VCOV
     $-2.0*OM*UCOV*S-W(I,J)**2*CH12-U(2,J)**2*CH2-2.0*
     $U(I,J)*W(I,J)*CH10
     $-2.0*W(I,J)*V(I,J)*CH9-2.0*U(I,J)*V(I,J)*CH8
     $-RSN/2.0/DN-RS(1,J)*CH2-RS(5,J)*CH8
     $-1.0/DENS*(SS/R(I)*S**2*(PN(I,J)-PL(I,J))/2.0/DS
     $+(SS/R(I)
     $*S*C-SS/AL)*PSN/2.0/DN+(P(I+1,J)-PNN)
     $/2.0/DR)
      IF(J.EQ.IMM1) GO TO 4029
      IF(J.EQ.IMM2) GO TO 4028
      GO TO 4030
 4029 A(1,J)=-V(I,J)/8.0/DN
      A(3,J)=V(I,J)/2.0/DN
      A(2,J)=(W(I+1,J)-WNN)/RD/2.0-3.0/8.0*V(I,J)/DN
      GO TO 4030
 4028 A(1,J)=-V(I,J)/2.0/DN
      A(3,J)=V(I,J)/8.0/DN
      A(2,J)=3.0/8.0*V(I,J)/DN+(W(I+1,J)-WNN)/2.0/DR
 4030 CONTINUE
      A(4,1)=A(4,1)-A(1,1)*W(I,1)
      A(4,IMM)=A(4,IMM)-A(3,IMM)*W(I,IMM)
      CALL ELIM(A,IMM)
      DO 4102 J=1,IMM
```

```
      W(I,J)=W(I,J)+SOR*(A(4,J)-W(I,J))
 4102 CONTINUE
      UM1=200.0
      DO 4103 J=1,IMM
      IF(J.LT.IMM1.OR.J.GT.IMM2)GO TO 4103
      IF(U(I,J).GE.UM1)GO TO 4103
      UM1=U(I,J)
      NT=J
 4103 CONTINUE
C
C     NEW N
C
C
      DO 6030 J=1,IMM
      RWV=0.0
      DN=DN0/4.0
      IF(J.LT.IMM1.OR.J.GT.IMM2) DN=DN0
      WCOV=-SS/R(I)*S**2*U(I,J)+(-SS/R(I)*S*C+SS/AL)*V(I,J)
     $+(1.0+SS**2/R(I)**2*S**2-2.0*SS**2/R(I)/AL*S*C)*W(I,J)
      UCOV=U(I,J)-SS/R(I)*S**2*W(I,J)
      VCOV=V(I,J)+(-SS/R(I)*S*C+SS/AL)*W(I,J)
      IF((J-ID).LT.1) GO TO 6165
      IF((J-ID).GT.IMML)GO TO 6166
      VNN= V(I-1,J-ID)
      PNN=P(I-1,J-ID)
      GO TO 6161
 6165 VNN= V(I-1,1)
      PNN=P(I-1,1)
      GO TO 6161
 6166 VNN= V(I-1,IMML)
      PNN=P(I-1,IMML)
 6161 A(1,J)=-V(I,J)/2.0/DN
      A(2,J)=U(I,J)/DS
      A(3,J)=V(I,J)/2.0/DN
      IF(J.EQ.1.OR.J.EQ.IMM) GO TO 9211
      PSN=P(I,J+1)-P(I,J-1)
      GO TO 9212
 9211 PSN=0.0
 9212 A(4,J)=U(I,J)*VLL(I,J)/DS-W(I,J)*(V(I+1,J)-VNN)/2.0/DR
     $-V(I,J)**2*CH6-W(I,J)**2*CH14-2.0*W(I,J)*U(I,J)*CH15
     $-2.0*V(I,J)*W(I,J)*CH16+2.0*OM*WCOV*C
     $-1.0/DENS*((SS**2/R(I)**2*S**3*C-SS**2/R(I)/AL*S**2)
     $*(PN(I,J)-PL(I,J))/2.0/DS+(1.0+SS**2/R(I)**2*(S*C)**2
     $-2.0*SS**2/R(I)/AL*S*C)*PSN/2.0/DN
     $+(SS/R(I)*S*C-SS/AL)*(P(I+1,J)-PNN)/2.0/DR)
      IF(J.EQ.IMM1) GO TO 6029
      IF(J.EQ.IMM2) GO TO 6028
      GO TO 6030
 6029 A(1,J)=-V(I,J)/8.0/DN
      A(3,J)=V(I,J)/2.0/DN
      A(2,J)=U(I,J)/DS-3.0/8.0*V(I,J)/DN
      GO TO 6030
 6028 A(1,J)=-V(I,J)/2.0/DN
      A(3,J)=V(I,J)/8.0/DN
```

```
      A(2,J)=3.0/8.0*V(I,J)/DN+U(I,J)/DS
 6030 CONTINUE
      A(4,1)=A(4,1)-A(1,1)*V(I,1)
      A(4,IMM)=A(4,IMM)-A(3,IMM)*V(I,IMM)
      CALL ELIM(A,IMM)
      DO 6102 J=1,IMM
      V(I,J)=V(I,J)+SOR*(A(4,J)-V(I,J))
 6102 CONTINUE
C
C     NEW P
C
      DO 4520 J=1,IMM
      RUV=0.0
      DN=DN0/4.0
      IF(J.LT.IMM1.OR.J.GT.IMM2) DN=DN0
      WCOV=-SS/R(I)*S**2*U(I,J)+(-SS/R(I)*S*C+SS/AL)*V(I,J)
     $+(1.0+SS**2/R(I)**2*S**2-2.0*SS**2/R(I)/AL*S*C)*W(I,J)
      UCOV=U(I,J)-SS/R(I)*S**2*W(I,J)
      VCOV=V(I,J)+(-SS/R(I)*S*C+SS/AL)*W(I,J)
      IF((J-ID).LT.1) GO TO 4545
      IF((J-ID).GT.IMML) GO TO 4546
      UNN=U(I-1,J-ID)
      PNN=P(I-1,J-ID)
      VNN=V(I-1,J-ID)
      WNN=W(I-1,J-ID)
      UNNL=UL(I-1,J-ID)
      UNNN=UN(I-1,J-ID)
      VNNL=VLL(I-1,J-ID)
      VNNN=VN(I-1,J-ID)
      WNNL=WL(I-1,J-ID)
      WNNN=WN(I-1,J-ID)
      PNNN=PN(I-1,J-ID)
      PNNL=PL(I-1,J-ID)
      GO TO 4541
 4545 UNN=U(I-1,1)
      PNN=P(I-1,1)
      VNN=V(I-1,1)
      WNN=W(I-1,1)
      UNNN=UN(I-1,1)
      UNNL=UL(I-1,1)
      VNNN=VN(I-1,1)
      VNNL=VLL(I-1,1)
      PNNN=PN(I-1,1)
      PNNL=PL(I-1,1)
      WNNN=WN(I-1,1)
      WNNL=WL(I-1,1)
      GO TO 4541
 4546 UNN=U(I-1,IMML)
      PNN=P(I-1,IMML)
      VNN=V(I-1,IMML)
      WNN=W(I-1,IMML)
      UNNN=UN(I-1,IMML)
      UNNL=UL(I-1,IMML)
      VNNN=VN(I-1,IMML)
```

```
      VNNL=VLL(I-1,IMML)
      PNNN=PN(I-1,IMML)
      PNNL=PL(I-1,IMML)
      WNNN=WN(I-1,IMML)
      WNNL=WL(I-1,IMML)
4541  DN=DNO
      PS1=1.0+SS**2/R(I)**2*S**4
      PS2=SS**2/R(I)**2*S**3*C-SS**2/R(I)/AL*S**2
      PS3=SS/R(I)*S**2
      PS4=1.0+SS**2/R(I)**2*(S*C)**2-2.0*SS**2/R(I)/AL*S*C
      PS5=SS/R(I)*S*C-SS/AL
      PS6=1.0
      IF(J.GE.IMM1.AND.J.LE.IMM2)DN=DNO/4.0
      A(1,J)=1.0/DN**2
      A(2,J)=-2.0/DN**2
      A(3,J)=1.0/DN**2
      IF(J.EQ.1.OR.J.EQ.IMM) GO TO 9311
      PSN1=PN(I,J+1)+PL(I,J-1)-PN(I,J-1)-PL(I,J+1)
      PSN2=P(I+1,J+1)-P(I+1,J-1)
      RSN=RS(2,J+1)-RS(2,J-1)
      WSN=W(I,J+1)-W(I,J-1)
      GO TO 9312
9311  PSN1=0.0
      PSN2=0.0
      WSN=0.0
      RSN=0.0
9312  A(4,J)=-PS1*(PN(I,J)+PL(I,J)-2.0*P(I,J))/DS**2
     $-PS6*(P(I+1,J)+PNN-2.0*P(I,J))/DR**2-0.5*PS2*
     $PSN1/DN/DS-0.5*PS3*(PN(I+1,J)
     $+PNNL-PNNN-PL(I+1,J))/DR/DS
      IF((J-ID).LT.1.OR.(J-ID).GT.IMML) GO TO 4707
      PNN1=P(I-1,J-1)-P(I-1,J+1)
      GO TO 4708
4707  PNN1=0.0
4708  A(4,J)=A(4,J)-0.5*PS5*(PSN2+PNN1)/DR/DN
     $+DENS*(((UN(I,J)-UL(I,J))/2.0/DS+U(I,J)*CH1+W(I,
     $J)*CH3*(
     $(W(I+1,J)-WNN)/2.0/DR+U(I,J)*CH3+W(I,J)*CH11)
     $-((U(I,J)-UNN)/2.0/DR+U(I,J)*CH3+W(I,J)*CH11)*((WN(I,J)
     $-WL(I,J))/2.0/DS+U(I,J)*CH2+W(I,J)*CH10)-
     $(RSN-2.0*RS(2,J))/DN**2
     $-2.0*(-OM*S*((WN(I,J)-WL(I,J))/2.0/DS-(U(I+1,J)-UNN
     $)/2.0/DR)+OM*C*((V(I+1,J)-VNN)/2.0/DR-WSN
     $/2.0/DN)))
      IF(J.EQ.IMM1) GO TO 4519
      IF(J.EQ.IMM2) GO TO 4518
      GO TO 4520
4519  A(1,J)=0.10/DN**2
      A(2,J)=-0.50/DN**2
      A(3,J)=0.4/DN**2
      GO TO 4520
4518  A(1,J)=0.4/DN**2
      A(3,J)=0.100/DN**2
      A(2,J)=-0.50/DN**2
```

```
 4520 CONTINUE
      A(4,1)=A(4,1)-A(1,1)*P(I,1)
      A(4,IMM)=A(4,IMM)-A(3,IMM)*P(I,IMM)
      CALL ELIM(A,IMM)
      DO 4501 J=1,IMM
      P(I,J)=P(I,J)+SOR*(A(4,J)-P(I,J))
 4501 CONTINUE
      IF(MM.GE.2) GO TO 4600
      GO TO 4015
 4600 DO 41020 J=1,IMM
      IF((J-ID) .LT.1) GO TO 41145
      IF((J-ID).GT.IMML) GO TO 41146
      ENNN= EN(I-1,J-ID)
      DINN= DI(I-1,J-ID)
      GO TO 41141
41145 ENNN=EN(I-1,1)
      DINN= DI(I-1,1)
      GO TO 41141
41146 ENNN=EN(I-1,IMML)
      DINN= DI(I-1,IMML)
41141 DN=DNO
      IF(J.GE.IMM1.AND.J.LE.IMM2) DN=DNO/4.0
      Q1=0.0
      Q2=0.0
      Q3=0.0
      Q4=0.0
      IF(J.EQ.1.OR.J.EQ.IMM) GO TO 4077
      IF(J.EQ.IMM1) GO TO 4075
      IF(J.EQ.IMM2) GO TO 4076
      Q1=U(I,J)*CH5+W(I,J)*CH4+(U(I,J+1)-U(I,J-1))/2.0/DN
      Q2=U(I,J)*CH8+W(I,J)*CH9+(W(I,J+1)-W(I,J-1))/2.0/DN
      Q3=(UN(I,J)-UL(I,J))/2.0/DS+U(I,J)*CH1+W(I,J)*CH3
      Q4=(WN(I,J)-UL(I,J))/2.0/DS+U(I,J)*CH2+W(I,J)*CH10
      GO TO 4077
 4075 Q1=0.5/DN*(U(I,J+1)-0.75*U(I,J)-0.25*U(I,J-1))
     $+U(I,J)*CH5+W(I,J)*CH9
      Q2=0.5/DN*(W(I,J+1)-0.75*W(I,J)-0.25*W(I,J-1))
     $+U(I,J)*CH8+W(I,J)*CH9
      GO TO 4077
 4076 Q1=0.5/DN*(0.25*U(I,J+1)+0.75*U(I,J)-U(I,J-1))
     $+U(I,J)*CH5+W(I,J)*CH4
      Q2=0.5/DN*(0.25*W(I,J+1)+0.75*W(I,J)-W(I,J-1))
     $+U(I,J)*CH8+W(I,J)*CH9
 4077 E=0.1*RS(2,J)*EN(I,J)/DI(I,J)
      PR=-RS(1,J)*Q3-RS(5,J)*Q1-RS(4,J)*Q4-RS(6,J)*Q2
      IF(J.EQ.IMM1) GO TO 41019
      IF(J.EQ.IMM2) GO TO 41018
      A(1,J)=-V(I,J)/2.0/DN-E/DN**2
      A(2,J)=U(I,J)/DS+W(I,J)/DR  +E*2.0/DN**2
      A(3,J)=V(I,J)/2.0/DN-E/DN**2
      A(4,J)=PR-DI(I,J)+U(I,J)*EN1(J)/DS+W(I,J)*ENNN/DR
      G(1,J)=-V(I,J)/2.0/DN-E/1.3/DN**2
      G(2,J)=U(I,J)/DS+W(  I,J)/DR+E*2.0/1.3/DN**2
      G(3,J)=V(I,J)/2.0/DN-E/1.3/DN**2
```

```
      G(4,J)=U(I,J)*DI1(I)/DS+ W( I,J)*DINN/DR
     $+1.44*DI(I,J)/EN(I,J)*PR
     $-1.92*DI(I,J)**2/EN(I,J)
      GO TO 41020
41019 A(1,J)=-V(I,J)/8.0/DN- E/10.0/DN**2
      A(2,J)=U(I,J)/DS-3.0/8.0*V  (I,J)/DN+WN(I,J)/DR
     $+0.5*E/DN**2
      A(3,J)=V(I,J)/2.0/DN-E/2.5/DN**2
      A(4,J)=PR-DI(I,J)+U(I,J)*EN1(J)/DS+W  (I,J)*ENNN/DR
      G(1,J)=-V(I,J)/8.0/DN-E/13.0/DN**2
      G(2,J)=U(I,J)/DS-3.0/8.0*V(I,J)/DN
     $+W(I,J)/DR+1.0/2.6*E/DN**2
      G(3,J)=V(I,J)/2.0/DN-E/2.5/1.3/DN**2
      G(4,J)=U(I,J)*DI1(J)/DS+W  (I,J)*DINN/DR
     $+1.44*DI(I,J)/EN(I,J)*PR
     $          -1.92*DI(I,J)**2/EN(I,J)
      GO TO 41020
41018 A(1,J)=-V(I,J)/2.0/DN-E/2.5/DN**2
      A(3,J)=V(I,J)/8.0/DN-E/10.0/DN**2
      A(2,J)=U(I,J)/DS+3.0/8.0*V  (I,J)/DN+WN(I,J)/DR
     $+0.5*E/DN**2
      A(4,J)=U(I,J)*EN1(J)/DS+W(I,J)*ENNN/DR+PR-DI(I,J)
      G(1,J)=-V(I,J)/2.0/DN-E/2.5/1.3/DN**2
      G(3,J)=V(I,J)/8.0/DN-E/13.0/DN**2
      G(2,J)=U(I,J)/DS+3.0/8.0*V(I,J)/DN+W(I,J)/DR
     $+0.5/1.3*E/DN**2
      G(4,J)=U(I,J)*DI1(J)/DS+W(I,J)*DINN/DR
     $+1.44*DI(I,J)/EN(I,J)*PR
     $-1.92*DI(I,J)**2/EN(I,J)
41020 CONTINUE
      A(4,1)=A(4,1)-A(1,1)*EN(I,1)
      A(4,IMM)=A(4,IMM)-A(3,IMM)*EN(I,IMM)
      G(4,1)=G(4,1)-G(1,1)*DI(I,1)
      G(4,IMM)=G(4,IMM)-G(3,IMM)*DI(I,IMM)
      CALL ELIM(A,IMM)
      DO 41101 J=1,IMM
      EN(I,J)=EN(I,J)+SOR*(A(4,J)-EN(I,J))
41101 CONTINUE
      CALL ELIM(G,IMM)
      DO 41107 J=1,IMM
      DI(I,J)=DI(I,J)+SOR*(G(4,J)-DI(I,J))
41107 CONTINUE
C
C
C     ***   ***   ***   ***   ***
C
C
      N20=N101(I)
      WRITE(6,2370)K,I
      WRITE(6,2470)     (N10(I,J),U(I,N10(I,J)),V(I,N10
     $(I,J)),W(I,N10
     X(I,J)),EN(I,N10(I,J)),DI(I,N10(I,J)),J=1,N20)
 4010 CONTINUE
      DO 4820 I=1,7
```

```
      KM=IMAX(I)
      WRITE(14,630) (U(I,J),V(I,J),W(I,J),P(I,J),EN(I,J
     $),DI(I,J),J=1,KM)
      UL(I,J)=U(I,J)
      VLL(I,J)=V(I,J)
      WL(I,J)=W(I,J)
      PL(I,J)=P(I,J)
      ENL(I,J)=EN(I,J)
      DIL(I,J)=DI(I,J)
 4820 CONTINUE
 4700 CONTINUE
44444 STOP
      END
      SUBROUTINE ELIM(S,NN)
      DIMENSION S( 4,300)
      NNO1=NN-1
      DO 1 II=1,NNO1
      S(2,II)=1.0/S(2,II)
      S(3,II)=S(3,II)*S(2,II)
      S(4,II)=S(4,II)*S(2,II)
      S(4,II+1)=S(4,II+1)-S(4,II)*S(1,II+1)
      S(2,II+1)=S(2,II+1)-S(1,II+1)*S(3,II)
    1 CONTINUE
      S(4,NN)=S(4,NN)/S(2,NN)
      NV=NN
    3 NV=NV-1
      IF(NV.EQ.0) GO TO 4
      NVA1=NV+1
      S(4,NV)=S(4,NV)-S(3,NV)*S(4,NV+1)
      GO TO 3
    4 RETURN
      END
```


*U.S. GOVERNMENT PRINTING OFFICE: 1982 539-007/31 1-3

1. Report No. NASA CR-3509	2. Government Accession No.	3. Recipient's Catalog No.
4. Title and Subtitle NUMERICAL ANALYSIS AND FORTRAN PROGRAM FOR THE COMPUTATION OF THE TURBULENT WAKES OF TURBOMACHINERY ROTOR BLADES, ISOLATED AIRFOILS AND CASCADE OF AIRFOILS		5. Report Date February 1982 6. Performing Organization Code
7. Author(s) C. Hah and B. Lakshminarayana		8. Performing Organization Report No. PSU-TURBO-81-4 10. Work Unit No.
9. Performing Organization Name and Address The Pennsylvania State University Department of Aerospace Engineering 233 Hammond Building University Park, Pennsylvania 16802		11. Contract or Grant No. NSG-3012 13. Type of Report and Period Covered Contract Report
12. Sponsoring Agency Name and Address National Aeronautics and Space Administration Washington, D.C. 20546		14. Sponsoring Agency Code 505-32-02

15. Supplementary Notes
Final report. Project Manager, Loretta M. Shaw, Fluid Mechanics and Acoustics Division, NASA Lewis Research Center, Cleveland, Ohio 44135. Based in part on a dissertation by C. Hah submitted in partial fulfillment of the requirements for the degree Doctor of Philosophy at The Pennsylvania State University in March 1980.

16. Abstract
Turbulent wakes of turbomachinery rotor blades, isolated airfoils, and a cascade of airfoils were investigated both numerically and experimentally. The study was confined to low subsonic and incompressible wake flows. A finite difference procedure was employed in the numerical analysis utilizing the continuity, momentum, and turbulence closure equations in the rotating, curvilinear, and nonorthogonal coordinate system. A nonorthogonal curvilinear coordinate system was developed to improve the accuracy and efficiency of the numerical calculation. Three turbulence models were employed to obtain closure of the governing equations. The first model was comprised to transport equations for the turbulent kinetic energy and the rate of energy dissipation, and the second and third models were comprised of equations for the rate of turbulent kinetic energy dissipation and Reynolds stresses, respectively. The second model handles the convection and diffusion terms in the Reynolds stress transport equation collectively, while the third model handles them individually. All three models were modified for the effect of Reynolds stresses of the second and third models. This is the first reported attempt to modify Reynolds stress model for the effect of the streamline curvature and rotation. The turbulent wakes of an isolated airfoil and a cascade of airfoils are handled as simpler cases of the general rotating three-dimensional wake. The numerical results demonstrate that the second and third models provide accurate predictions, but the computer time and memory storage can be considerably saved with the second model. The experimental data are utilized to compare various turbulence closure models for the effect of streamline curvature.

17. Key Words (Suggested by Author(s))	18. Distribution Statement
Three-dimensional wake; Turbomachinery; Rotor wake; Axial flow compressor	Unclassified - unlimited STAR Category 02

19. Security Classif. (of this report)	20. Security Classif. (of this page)	21. No. of Pages	22. Price*
Unclassified	Unclassified	170	A08

*For sale by the National Technical Information Service, Springfield, Virginia 22161